TECHNISCHE UNIVERSITÄT MÜNCHEN

TUM School of Life Sciences

The Role of the Peripheral Intestinal Clock in Microbiome Regulation and Host Metabolism

Marjolein Heddes

Vollständiger Abdruck der von der TUM School of Life Sciences der Technischen Universität München zur Erlangung des akademischen Grades einer

Doktorin der Naturwissenschaften (Dr. rer. nat.)

genehmigten Dissertation.

Vorsitz: Prof. Dr. Nina Henriette Uhlenhaut

Prüfende der Dissertation:

1. Prof. Dr. Dirk Haller
2. Prof. Dr. Martin Klingenspor
3. Priv.-Doz. Dr. Olga Ramich

Die Dissertation wurde am 02.08.2023 bei der Technischen Universität München eingereicht und durch die TUM School of Life Sciences am 26.02.2024 angenommen.

Abstract

Both circadian rhythms and the gut microbiome play integral roles in host metabolism, and their reciprocal interactions are crucial for metabolic homeostasis. Disruption of either system can lead to physiological changes that contribute to chronic metabolic diseases, such as obesity. The intestine, in particular, plays an essential role in nutrient metabolism and maintaining gut microbial homeostasis. In this study, the aim was to investigate the impact of the intestinal circadian clock on host physiology, focusing on its interactions with the gut microbiome and macronutrient metabolism.

To examine the role of the intestinal clock, a mouse model with specific loss of the core clock gene *Bmal1* in intestinal epithelial cells (*Bmal1*$^{IEC-/-}$) was generated. Disruption of the intestinal clock resulted in minor morphological alterations in intestinal parameters, including reduced mucus production. Importantly, it was identified that the peripheral intestinal epithelial cell (IEC) clock plays a vital role in regulating the circadian composition and functioning of both fecal and cecal bacteria. Specifically, it was observed that genera such as *Ruminococcus, Alistipes, Clostridium*, *Desulfovibrio, Odoribacter, Eubacterium,* and *Oscillibacter,* which are predominantly involved in carbohydrate- and amino acid metabolism, are under the control of the intestinal clock. Consequently, microbial-metabolic profiles were altered in *Bmal1*$^{IEC-/-}$ mice, revealing changes in branched-chain fatty acids, hyodeoxycholic acid, and taurine-conjugated bile acids. Additionally, intestinal clock deficiency disrupted the rhythmicity of 30% of the measured cecal metabolites. To investigate the causal relationship between the intestinal clock-regulated microbiome and metabolism, *Bmal1*$^{IEC-/-}$ derived microbiota was transferred to germ-free wild-type hosts. Recipient mice receiving an arrhythmic microbiome displayed an obese phenotype, with a 15% increase in body weight and increased fat mass.

Bulk RNA-sequencing analyses further uncovered the regulatory role of IEC-specific *Bmal1* in the rhythmic expression of genes involved in carbohydrate and lipid absorption and transportation. *Bmal1*$^{IEC-/-}$ mice fed a high-fat, high-sugar western diet (WD) showed a disrupted metabolic phenotype, including significant weight gain and impaired carbohydrate metabolism compared to controls. Remarkably, these effects were independent of changes in microbial rhythmicity, as both genotypes exhibited equally suppressed microbial rhythmicity upon low-fermentable-fiber purified WD intake. The depletion of fiber within purified diets was accompanied by altered intestinal clock-gene expression in control mice. Nevertheless, dietary supplementation with a mixture of fermentable fibers significantly elevated clock-gene expression and microbial oscillations. However, supplementation with the fermentable fiber inulin alone was insufficient to target the intestinal clock and ameliorate metabolic abnormalities in control mice fed a high-fat diet. This highlights the need for a mixture of fermentable fiber to improve the intestinal clock and modulate microbial composition.

In summary, our study highlights the critical role of the intestinal peripheral clock in circadian microbial functioning and host metabolism. Given the impact of circadian desynchrony on health, interventions targeting the intestinal circadian clock, such as dietary modification, prebiotics, probiotics, and microbiota transplantation, hold promise in benefiting individuals with metabolic disorders.

Zusammenfassung

Sowohl die zirkadianen Rhythmen als auch das Darmmikrobiom spielen eine wesentliche Rolle im Stoffwechsel des Wirtes, und ihre gegenseitigen Wechselwirkungen sind für die metabolische Homöostase entscheidend. Eine Störung beider Systeme kann zu physiologischen Veränderungen führen, die zu chronischen Stoffwechselkrankheiten wie Adipositas beitragen. Insbesondere der Darm spielt eine wesentliche Rolle im Nährstoffstoffstoffwechsel und bei der Aufrechterhaltung der mikrobiellen Homöostase im Darm. In dieser Studie sollten die Auswirkungen der zirkadianen Uhr des Darms auf die Wirtsphysiologie untersucht werden, wobei der Schwerpunkt auf den Wechselwirkungen mit dem Darmmikrobiom und dem Makronährstoffmetabolismus lag.

Um die Rolle der intestinalen Uhr zu untersuchen, wurde ein Mausmodell mit spezifischem Verlust des zentralen Uhrengens *Bmal1* in intestinale Epithelzellen (*Bmal1*$^{IEC-/-}$) erzeugt. Die Unterbrechung der intestinalen Uhr führte zu geringfügigen morphologischen Veränderungen der intestinalen Parameter, einschließlich einer verminderten Schleimproduktion. Es wurde festgestellt, dass die Uhr der peripheren intestinalen Epithelzellen (IEC) eine wichtige Rolle bei der Regulierung der zirkadianen Zusammensetzung und Funktion von Fäkal- und Zäkalbakterien spielt. Insbesondere wurde festgestellt, dass Gattungen wie *Ruminococcus, Alistipes, Clostridium, Desulfovibrio, Odoribacter, Eubacterium* und *Oscillibacter*, die vorwiegend am Kohlenhydrat- und Aminosäurestoffwechsel beteiligt sind, unter der Kontrolle der Darmuhr stehen. Folglich waren die mikrobiell-metabolischen Profile in *Bmal1*$^{IEC-/-}$ Mäusen verändert, was sich unter anderem in verzweigtkettigen Fettsäuren, Hyodeoxycholsäure und Taurin-konjugierten Gallensäuren zeigte. Darüber hinaus wurde durch das Fehlen der Darmuhr die Rhythmik von 30 % der gemessenen Metaboliten im Zäkum gestört. Um den kausalen Zusammenhang zwischen dem durch die Darmuhr regulierten Mikrobiom und dem Stoffwechsel zu untersuchen, wurden die von *Bmal1*$^{IEC-/-}$ abgeleitete Mikrobiota auf keimfreien Wildtyp-Wirte übertragen. Empfängermäuse, die ein arrhythmisches Mikrobiom erhielten, zeigten einen fettleibigen Phänotyp mit einem um 15-prozentigen höheren Körpergewicht und einer erhöhten Fettmasse.

RNA-Sequenzierungsanalysen deckten außerdem die regulatorische Rolle des IEC-spezifischen *Bmal1* bei der rhythmischen Expression von Genen auf, die an der Aufnahme und dem Transport von Kohlenhydraten und Lipiden beteiligt sind. *Bmal1*$^{IEC-/-}$ Mäuse, die mit einer fett- und zuckerreichen westlichen Diät (WD) gefüttert wurden, wiesen einen gestörten Stoffwechselphänotyp auf, einschließlich einer signifikanten Gewichtszunahme und eines gestörten Kohlenhydratstoffwechsels im Vergleich zu den Kontrollen. Bemerkenswerterweise waren diese Effekte unabhängig von Veränderungen der mikrobiellen Rhythmizität, da beide Genotypen bei der Aufnahme von gereinigter

WD mit wenig fermentierbaren Fasern eine gleichermaßen unterdrückte mikrobielle Rhythmizität aufwiesen. Der Mangel an Ballaststoffen in der gereinigten Nahrung ging bei den Kontrollmäusen mit einer veränderten Expression von Uhren-Gene im Darm einher. Eine Nahrungsergänzung mit einer Mischung fermentierbaren Fasern erhöhte jedoch die Expression von Uhren-Gene und mikrobiellen Oszillationen signifikant. Die Supplementierung mit dem fermentierbaren Ballaststoff Inulin allein reichte jedoch nicht aus, um die intestinale Uhr zu beeinflussen und metabolische Anomalien bei Kontrollmäusen, die mit einer fettreichen Diät gefüttert wurden, zu bessern. Dies unterstreicht die Notwendigkeit einer Mischung aus fermentierbaren Ballaststoffen, um die intestinale Uhr zu verbessern und die mikrobielle Zusammensetzung zu modulieren.

Zusammenfassend unterstreicht unsere Studie die entscheidende Rolle der peripheren Uhr des Darms für die zirkadiane mikrobielle Funktion und den Stoffwechsel des Wirts. Angesichts der Auswirkungen der zirkadianen Desynchronität auf die Gesundheit versprechen Interventionen, die auf die zirkadiane Uhr des Darms abzielen, wie z. B. Ernährungsumstellung, Präbiotika, Probiotika und Mikrobiota-Transplantation, Vorteile für Menschen mit Stoffwechselstörungen

Table of contents

Abstract ii

Zusammenfassung v

1. Introduction 1

1.1 The biological clock 1

1.2 The molecular clock 2

1.3 Organization of the circadian system 3

1.4 The impact of circadian misalignment on host metabolism 4

1.4.1 Genetic modification of core clock-genes 4

1.4.2 Circadian environmental disruption 5

1.4.3 Dietary composition 6

1.5 Intestinal diurnal rhythms 6

1.5.1 Intestinal cell proliferation 7

1.5.2 Intestinal barrier 9

1.5.3 Intestinal motility 10

1.5.4 Nutrient intake, absorption and digestion 10

1.5.5 Gut microbial composition 12

1.5.6 Gut microbial functioning 14

1.6 Proposed mechanisms regulating microbial rhythmicity 15

1.6.1 Food timing and intake 15

1.6.2 Circadian clocks 16

1.6.3 Host circadian clock and microbial crosstalk 17

1.7 Importance of dietary fiber in modulating microbiota composition and functioning 19

1.8 The role of gut microbial rhythmicity in host metabolism 20

1.9 Intestinal epithelial cell specific *Bmal1* knockout studies 21

2. Aim 23

3. Material and methods 24

3.1 Animal experiments 24

3.1.1 Ethical statement 24
3.1.2 Mouse models 24
3.1.3 Long-term dietary interventions 24
3.1.4 Fiber dietary intervention paradigm 26
3.1.5 Tissue collection 26
3.1.6 Body composition measurements 26
3.1.7 Food intake 27
3.1.8 Complete gastrointestinal transit time 27
3.1.9 Oral glucose tolerance test (OGTT) 27
3.1.10 Germ free experiments 28
3.1.11 Antibiotic treatments 28
3.2 Energy assimilation 28
3.3 Behavior analyses 29
3.4 Tissue processing, H&E staining and histological scoring 29
3.5 Alcian blue / Periodic acid-Schiff (AB/PAS) staining 31
3.6 RNA isolation and qPCR 31
3.7 RNA-sequencing 32
3.8 Gut permeability measurements 33
3.9 Glucose uptake experiments 34
3.10 High-throughput 16S Ribosomal RNA (rRNA) gene sequencing and microbial analysis 34
3.11 Fluorescence–activated cell sorting (FACS) 35
3.11.1 Intestinal epithelial cell isolation 35
3.11.2 Immune cell isolation 35
3.11.3 Staining and FACS measurements 36
3.12 Complement 3 ELISA 37
3.13 Untargeted metabolite measurements 37
3.14 Targeted metabolite analyses 39

3.15 PICRUST 2.0 41

3.16 Statistical Analyses 41

4. Results 42

4.1 Loss of intestinal *Bmal1* does not alter circadian behavior 42

4.2 The intestinal clock regulates fecal microbial rhythmicity. 46

4.3 Targeted fecal metabolomics reveals intestinal clock regulation of microbial metabolite production 50

4.4 The intestinal clock regulates the rhythmic cecal microbiota 54

4.5 Untargeted metabolomics reveals intestinal clock regulation of cecal metabolite rhythmicity 57

4.6 The intestinal clock regulates transcripts involved in nutrient metabolism 59

4.7 Disruption of host metabolism and immunity by transfer of intestinal clock-deficient derived microbiota 64

4.8 Westernized dietary feeding results in metabolic abnormalities in intestinal clock-deficient mice 72

4.9 Westernized dietary feeding results in genotype-dependent alterations in microbial community but not rhythmicity. 75

4.10 Lack of fermentable fiber suppresses microbial rhythmicity 80

5. Discussion 87

5.1 The role of the intestinal clock in regulating microbial rhythmicity and function 87

5.2 Implications of intestinal clock-controlled microbiota on metabolic and immune health. 92

5.3 Impact of the intestinal clock on host metabolism under western diet conditions 93

5.4 Modulation of microbial rhythmicity by dietary fiber and implications for metabolic health 94

6. Conclusion and perspective 97

Supplements 98

List of Figures x

List of Tables xii

List of Supplementary Figures xiii

List of Supplementary Tables xiv

Abbreviations xv

References xix

Acknowledgements xxxviii

Publications and Presentations xxxix

List of cited publications xli

Curriculum Vitae xlii

1. Introduction

1.1 The biological clock

The Earth's daily cycle of light and dark prompts adjustments in behavior and physiology across nearly all life forms, including animals, plants, and bacteria. The first indications of programmed daily rhythms were observed by Jean Jacques d'Ortous De Mairan in 1729, showing continues (nearly 24-h) leaf movements in *Mimosa pudica* plants under constant darkness (DD) (de Mairan, 1729). Halberg was the first to describe these endogenous 24-hour rhythms under constant conditions in the absence of any environmental input as circadian (circa, "about"; dies "a day") in 1959 (Chandrashekaran, 1998). Although it was not until the 20th century that the existence of the endogenous biological clocks in animals and humans was discovered, the study of biological rhythms is now widely studied in nearly all living organisms (Aschoff, 1965; Aschoff & Wever, 1962; Richter, 1922).

Within mammals, the circadian pacemaker resides in the suprachiasmatic nucleus (SCN) within the ventrolateral hypothalamus, consisting of thousands of neurons (Wever, 1975). SCN lesion studies within rats resulted in complete arrhythmic activity, eating behavior and body temperature, therefore defining the SCN as the central clock (Stephan & Zucker, 1972). Environmental input signals, known as *Zeitgebers* (German for "time-giver"), can entrain the pacemaker to the 24-hour day (Aschoff, 1951, 1954). One of the strongest *Zeitgeber* is light, which signals to the SCN via retinal cells (Moore, 1996). However, temperature, social interaction, food, and exercise can also act as *Zeitgebers* (Heyde & Oster, 2019; Mistlberger & Skene, 2004; Rensing & Ruoff, 2002; Zbidi et al., 2016).

In the chronobiology field, it is essential to differentiate between circadian rhythms and diurnal rhythms. Circadian rhythms are (1) endogenously generated and persist under constant conditions in the absence of a *Zeitgeber* (Aschoff, 1965; Menaker & Wisner, 1983). Additionally, circadian rhythms are (2) temperature compensated and (3) entrainable to *Zeitgebers*. A diurnal rhythm does not have to be circadian; it may be a simple response to environmental cues such as temperature changes, so-called 'masking' (Pittendrigh, 1954). Although daily life is continuously exposed to entraining *Zeitgebers* like light and temperature, investigating the circadian clock in free-running conditions (constant darkness/light) is necessary to comprehend the underlying mechanisms of how a rhythm is generated.

1.2 The molecular clock

Cell-autonomous clocks have been found in almost all mammalian tissues (Welsh et al., 2004). On a molecular level, the cell-autonomous clocks are composed of transcriptional–translational autoregulatory feedback loop (TTL), driving approximately 24-hour rhythms in RNA and protein expression and translation of core clock components (Takahashi, 2017). In mammals, the TTL consists of several key components, including the transcription factors Circadian Locomotor Output Cycles Kaput (CLOCK) and brain and muscle aryl hydrocarbon receptor nuclear translocator-like protein 1 (BMAL1), the negative regulators Period (PER) and Cryptochrome (CRY), and the accessory feedback regulators nuclear factors REV-ERB and retinoic acid receptor related orphan receptors (ROR). The CLOCK and BMAL1 proteins dimerize and bind to E-box elements of the *Per* (*Per1, Per2,* and *Per3*) and *Cry* (*Cry1* and *Cry2*) promoter regions, activating their transcription. After translation, PER and CRY proteins accumulate within the cytoplasm, heterodimerize, and then translocate back to the nucleus, where they inhibit their own transcription by binding to the CLOCK-BMAL1 complex and preventing its activity **(Figure 1)**. The proteasome continuously degrades the CRY-PER heterodimers, allowing the CLOCK-BMAL1 complex to resume its activity and initiate another round of transcription and translation (Takahashi, 2017).

In addition to the primary feedback loop, the CLOCK-BMAL1 complex also activates the transcription of *Rev-Erb-α,-β* and *Ror-α,-β,-γ.* Consequently, their protein transcription competes within the *Bmal1* promotor region for RORE elements, mediating *Bmal1* expression. REV-ERB inhibits *Bmal1* transcription, while ROR promotes it (Takahashi, 2017). Together, the interconnection of both loops generates robust rhythms in mammals with a period of ∼24 hours (Takahashi, 2017).

These core circadian clock genes regulate the transcription of clock-controlled genes (CCGs) by binding to ROREs, D-boxes, or E-boxes in their promotor regions (Takahashi, 2017). In mammals, up to 10% of all genes exhibit circadian rhythms, indicating that the circadian system plays a fundamental role in regulating a wide range of physiological processes, including key genes involved in immune regulation, metabolism, hormone regulation, and many more (Hughes et al., 2009; Panda et al., 2002).

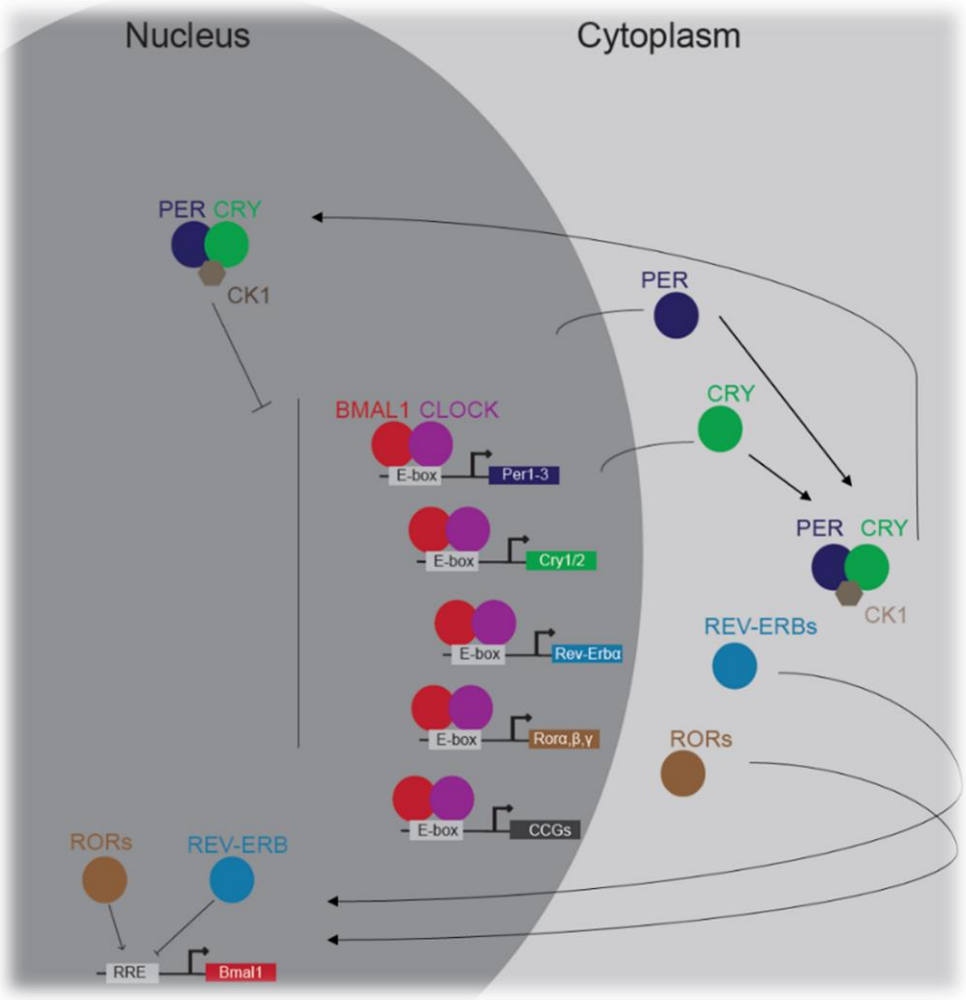

Figure 1 Mammalian circadian clock mechanism.
BMAL1 (red) and CLOCK (purple) bind to the E-box of indicated genes, including *Per1-3* (blue), *Cry1/2* (green), *Rev-Erbα* (light blue), and *Rorα,β,γ* (brown). PERs and CRYs locate back to the nucleus after binding casein kinase 1 (CK1δ/ϵ), repressing the expression of the previously mentioned genes. In an accessory loop, the by CLOCK and BMAL1 regulated transcription of REV-ERBs and RORs compete for binding to rev-responsive elements (RRE) on the *Bmal1* gene promotor. Where ROR positively regulates BMAL1 transcription and REV-ERB negatively. In addition, CLOCK/BMAL1 regulates the transcription of clock-controlled genes (CCGs) (grey box). BMAL; brain and muscle ARNT-like 1, CLOCK; circadian locomotor output cycles kaput, PER; period, CRY; cryptochrome, ROR; retinoic acid receptor-related orphan receptors, REV-ERB; nuclear receptor subfamily 1 group D (adjusted from (Mohawk et al., 2012)).

1.3 Organization of the circadian system

Circadian clocks are not limited to the SCN but have been discovered in various organs, tissues, and cells throughout the body. These peripheral clocks exist in organs such as the liver, pancreas, lung, skin, muscle, gastrointestinal (GI) tract, and adipose tissue (Zhang et al., 2020). Similar to the SCN, peripheral clocks rely on the TTL molecular mechanism described earlier, regulating cell-specific functions (Balsalobre et al., 1998; Schibler, 2003). Studies utilizing primary cell culture models and tissue explant cultures have proven sustained peripheral clock gene rhythms, highlighting the intrinsic characteristics of these peripheral clocks (Yoo et al., 2004).

For all clocks to function as a coordinated circadian system, the SCN synchronizes peripheral clocks through various modes of communication, including humoral signaling, temperature, activity/rest cycle, and the autonomic nervous system (Mohawk et al., 2012). Additionally, apart from SCN synchronization, food intake patterns serve as a prominent *Zeitgeber* for peripheral tissues, influencing the phase of their circadian gene expression independent of the SCN (Damiola et al., 2000; Deota et al., 2023; Stokkan et al., 2001). For instance, altering the timing of food intake, such as restricting feeding to the daytime (6 a.m. till 6 p.m.) instead of the nighttime (6 p.m till 6 a.m.), can shift the phase of circadian genes by 12 hours in rodent-derived liver cells, while the SCN remains entrained to the light/dark cycle (Damiola et al., 2000; Stokkan et al., 2001). Time-restricted feeding, where food intake is limited to certain hours of the day, is therefore a commonly used method to rescue peripheral clock regulation, especially in metabolic-relevant organs such as the liver and kidney (Izumo et al., 2014).

Misalignment or desynchronization of the circadian system, where peripheral clocks become uncoupled from the SCN, can occur due to factors such as shift work, frequent travel across time zones (jetlag), sleep disturbances, or irregular eating schedules. This misalignment has been implicated as a significant factor in various diseases like obesity, cancer, type 2 diabetes (T2D), and depression, emphasizing the significance of circadian clock mechanisms in maintaining host health (Bray et al., 2013; Grosjean et al., 2023; Kervezee et al., 2020; Mota et al., 2017; Papantoniou et al., 2018; Scheer et al., 2009; Walker et al., 2020).

1.4 The impact of circadian misalignment on host metabolism

1.4.1 Genetic modification of core clock-genes

Research focusing on the ablation of core clock genes in mice has provided valuable insights into the intricate relationship between circadian rhythms and physiological processes, particularly in relation to host metabolism. Notably, whole-body Clock-mutant mice ($Clock^{\Delta 19/\Delta 19}$) exhibit a wide array of metabolic changes, such as increased body weight and adiposity, as well as symptoms reminiscent of metabolic syndrome (Turek et al., 2005). Additionally, these mutant mice exhibit a loss of diurnal gene expression in key metabolic genes involved in protein and lipid metabolism, suggesting a potential mechanism underpinning the observed metabolic alterations (McCarthy et al., 2007). Similarly, whole-body *Bmal1* mutations render mice more susceptible to diet-induced obesity, along with reduced glucose tolerance and impaired adipogenesis and adipocyte differentiation (Lamia et al., 2008; Rudic et al., 2004; Shimba et al., 2005). Furthermore, studies employing *Per2* knockout and *Cry1/Cry2* double knockout mice have revealed that these animals exhibit reduced body weight and glucose intolerance

under normal chow conditions. However, intriguingly, under high-fat diet (HFD) conditions, they experience significant increases in body weight and adiposity, underscoring the complex interaction between core clock genes and metabolic responses (Barclay et al., 2013; Grimaldi et al., 2010; Yang et al., 2009).

Investigations into tissue-specific ablation of core clock genes have further elucidated their distinct effects on metabolic processes. For instance, specific deletion of *Bmal1* in the pancreas results in impaired glucose homeostasis, while liver-specific *Bmal1* deletion leads to elevated triglyceride and cholesterol levels (Marcheva et al., 2010; Pan et al., 2016). Similarly, *Bmal1* deletion in adipocytes is associated with reduced energy expenditure and subsequent weight gain (Paschos et al., 2012), while in skeletal muscle, it impairs glucose uptake and oxidation (Harfmann et al., 2016). These findings underscore the significance of tissue-specific circadian clocks in regulating diverse aspects of metabolism.

Research involving humans has also provided valuable evidence linking core clock genes to metabolic disorders. Polymorphisms in clock genes, including CLOCK and BMAL1, have been associated with obesity and T2D (Corella et al., 2016; Sookoian et al., 2008; Woon et al., 2007).

1.4.2 Circadian environmental disruption

An alternative approach to exploring the interplay between internal circadian rhythms and host metabolism is through studies using controlled lab settings that mimic circadian disruptions. In humans, such controlled settings include forced desynchrony protocols, which force subjects to follow a different day-night cycle that is substantially shorter or longer than the endogenous 24-hour rhythm. Individuals undergoing forced desynchrony protocols have exhibited hyperglycemia, hyperinsulinemia, and decreased leptin levels (Scheer et al., 2009). Similarly, shifting rodent activity to the rest phase leads to increased body fat and glucose intolerance (Salgado-Delgado et al., 2010). Moreover, exposure to dim light at night has been found to promote weight gain, insulin resistance, and disrupts the circadian clock in peripheral tissues and the SCN (Fonken et al., 2013; Fonken et al., 2010). In addition, altering the timing of food intake from the active phase to the rest phase results in desynchronization between peripheral clocks and the SCN clock, leading to increased body fat, reduced glucose tolerance, and altered lipid metabolism (Arble et al., 2009; Bray et al., 2013; Damiola et al., 2000; Stunkard & Allison, 2003). Conversely, feeding mice an HFD restricted to their active phase has been shown to improve diet-induced metabolic syndrome (Hatori et al., 2012).

1.4.3 Dietary composition

The diet's nutrient composition also plays a crucial role in host metabolism through its crosstalk with circadian clocks. For example, HFD (45% kcal) consumption in rodents leads to changes in rhythmic behavior, with active food consumption occurring during the light phase. Although core-clock genes maintain their rhythmicity, CCGs in metabolic-related tissues such as the liver and adipose tissue exhibit reduced rhythmicity, resulting in disruption of metabolic homeostasis (Eckel-Mahan et al., 2013; Kohsaka et al., 2007; Pendergast et al., 2013). Interestingly, apart from the desynchronization between the SCN and peripheral clocks caused by altered feeding patterns, peripheral clocks themselves can also become misaligned under HFD conditions. For example, the liver shows a direct phase shift after just one week of HFD, while other organs, like white adipose tissue, spleen, and lung, may require more time to respond or may not be as responsive to HFD (Pendergast et al., 2013). It is important to note that these studies compared HFD to chow diet conditions, suggesting that the observed effects may be attributed to alterations in nutrient components other than dietary fat.

In vitro studies examining the effects of carbohydrates on clock remodeling and metabolic homeostasis have shown that both glucose and fructose can alter the expression of core clock genes in cell cultures (Chapnik et al., 2016; Hirota et al., 2002). Moreover, excessive sucrose intake (65%) in rats has been associated with the development of metabolic syndrome and changes in the oscillations of core clock and metabolic-related genes, such as hexose transporter genes, in the small intestine. Notably, liver core clock genes remained unaffected by sucrose intake, indicating tissue-specific variations in the response to nutrient intake (Sun, Hanzawa, Kim, et al., 2019; Sun, Hanzawa, Umeki, et al., 2019).

These collective studies underscore the importance of both central and peripheral circadian clocks in host metabolism. Further research using animal models is necessary to gain a better understanding of how nutrients and meal timing affect peripheral clock function and circadian host metabolism in vivo.

1.5 Intestinal diurnal rhythms

One important peripheral organ involved in host metabolism is the GI tract, playing a key role in nutrient uptake and supply. The presence of clock genes throughout the entire GI tract has been well-documented in rodent models and humans (Davidson et al., 2003; Hoogerwerf et al., 2007; Pan & Hussain, 2009; Pardini et al., 2005; Polidarova et al., 2011; Sladek et al., 2007; Yamamoto et al., 2004). The stomach, duodenum, jejunum, ileum, and colon exhibit endogenous circadian rhythms, with each of these organs slightly differing in phase (Hoogerwerf et al., 2007; Moore et al., 2014; Polidarova et al., 2009; Sladek et al., 2007; Yamamoto et al., 2004). For instance, duodenal circadian rhythms

precede those in the colon, aligning with the progression of food through the digestive system (Polidarova et al., 2009). Further evidence for an intrinsic endogenous GI peripheral clock derives from the study of Moore et al., showing robust clock gene rhythmicity in intestinal explants and organoids (Moore et al., 2014).

Apart from the intestinal epithelial cells (IECs) having their own core clock machinery, the GI tract exhibits a range of physiological rhythmic functions, including nutrient absorption and digestion, gut motility, gastric acid output, hormone release, epithelial barrier function, and microbial composition and activity **(Figure 2).** Subsequent subchapters will delve into these functions in greater detail. Of note, the precise control mechanisms behind most rhythmic processes, whether they are governed by the central clock or the peripheral intestinal clock or if they arise from other systemic influences, are still largely unknown.

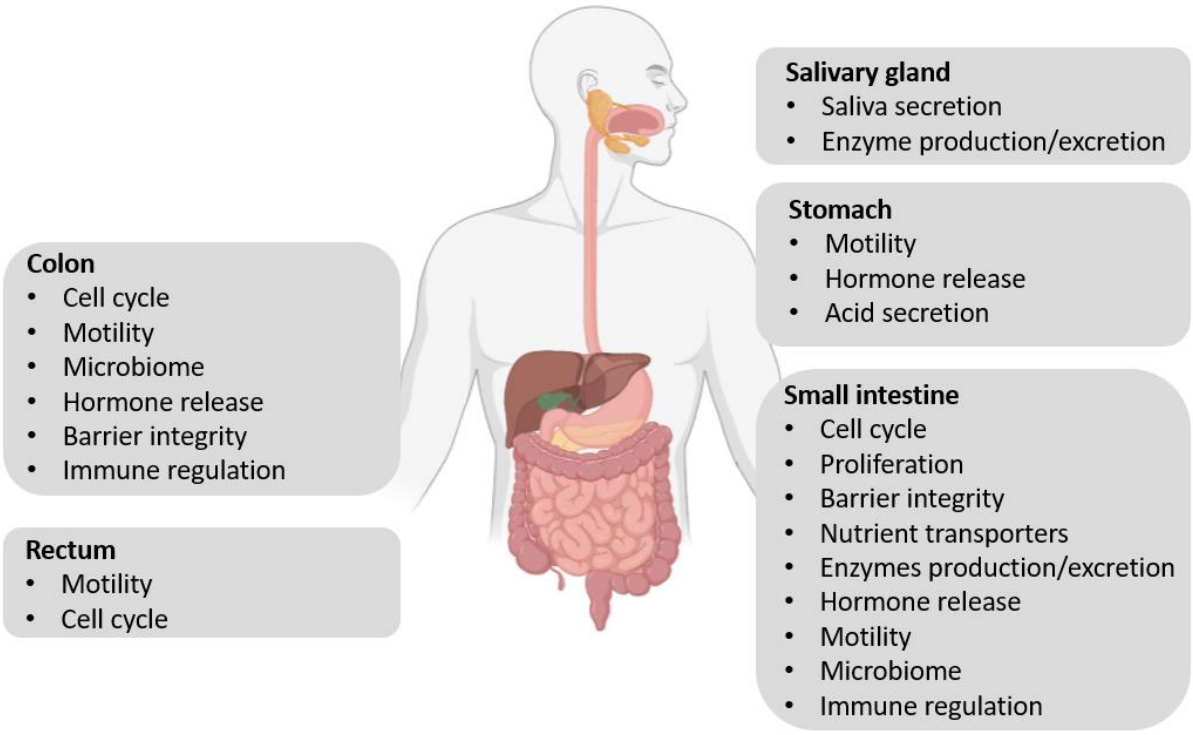

Figure 2 Rhythmic gastrointestinal functions.
Summary of diurnal/circadian rhythms discovered throughout the gastrointestinal tract (adjusted from (Segers & Depoortere, 2021)).

1.5.1 Intestinal cell proliferation

The GI tract consists of several layers, including the *Serosa, Muscularis externa, Submucosa,* and *Mucosa* (Young, 2006). The epithelium (part of the mucosa) comes in contact with the nutrients first and consists of several cell types responsible for nutrient absorption and digestion, mucus secretion, and hormonal release. The intestinal epithelium is one of the most rapidly renewing tissues in the

body, with a turnover time of 3-5 days, to maintain homeostasis of the GI. This turnover is regulated by a population of intestinal stem cells located in the crypts of Lieberkühn, which give rise to proliferative transit amplifying cells that differentiate into various cell types, including enterocytes, goblet cells, Paneth cells, and enteroendocrine cells (Cheng & Leblond, 1974).

Studies have demonstrated that the circadian clock is a critical regulator of intestinal stem cell proliferation by governing DNA synthesis (Scheving et al., 1980). Diurnal variations in the cell cycle have been observed throughout the murine gastrointestinal tract, with DNA synthesis displaying a phase difference of 6-8 hours along its length from the tongue to the rectum. This temporal pattern commences approximately one hour before the onset of light in the esophagus, followed by the stomach, duodenum, jejunum, ileum, and ultimately the rectum (Scheving et al., 1980). These findings suggest a diurnal rhythm associated with nutrient intake, as alterations in feeding schedules can synchronize the proliferation rhythms to the time of food consumption (Burholt et al., 1985; Yoshida et al., 2015). However, even during fasting conditions, these rhythmic fluctuations persist in humans and mice, albeit with a slightly reduced amplitude, indicating its inherent circadian origin (Scheving, 2000; Scheving et al., 1984).

Interestingly, studies investigating diurnal rhythms in intestinal stem cell proliferation are scarce and inconclusive. The initial investigations into the regeneration of intestinal tissue reported that the proliferation of intestinal progenitor cells remained constant and did not exhibit any variation with respect to time of day (Bertalanffy, 1960; Leblond & Stevens, 1948; Pilgrim et al., 1963). Recent research tackled this inconsistency by revealing that proliferation rhythms are feeble before stress but become more apparent during regenerative phases with increased inflammation (Karpowicz et al., 2013; Stokes et al., 2017; Stokes et al., 2021). The *Wingless* signaling pathways play a critical role in intestinal stem cell renewal. In the mouse intestine, *Wingless* signaling is boosted by R-spondins and their Leucine-rich repeat-containing G-protein coupled receptor 5 (*Lgr5)* to promote self-renewal of *Lgr+* stem cells and intestinal crypt growth and proliferation. The circadian clock regulates the production of *Wingless3A* ligand by Paneth cells, resulting in 24-hour oscillations of signaling activity that couple circadian rhythms to proliferation (Matsu-Ura et al., 2016). Downstream components of the *Wingless* signaling pathway, including target genes such as *c-Myc*, have also been shown to be regulated by the circadian clock (Repouskou & Prombona, 2016). The bidirectional interaction between the circadian clock and *c-Myc* may enable a balance between circadian clock control and stem cell-driven processes to coordinate environmental signals with intestinal epithelial tissue renewal.

1.5.2 Intestinal barrier

The intestinal epithelium forms a physical and immunological barrier that separates the gut lumen from the host's internal environment. This protective barrier is maintained through the presence of intercellular tight junctions that connect adjacent epithelial cells, effectively restricting the paracellular diffusion of harmful microorganisms and antigens (Groschwitz & Hogan, 2009). Notably, the expression of tight junction proteins, such as occludin and claudins, follows diurnal patterns within the colon and is directly regulated by the binding of CLOCK-BMAL1 to the E-boxes in the promotor region of these tight junction genes (Kyoko et al., 2014; A. Martchenko et al., 2020; Summa et al., 2013). Studies involving mice with disrupted global circadian clocks, through either genetic mutation or light cycle disruption, have demonstrated increased permeability in the intestines (Eum et al., 2023; Kyoko et al., 2014; Summa et al., 2013; Voigt et al., 2016). This increased permeability allows the movement of pro-inflammatory substances from the gut into the body, predisposing the mice to metabolic and inflammatory diseases. Furthermore, mice with IEC-specific deletion of *RORα* or *Bmal1*, as well as those experiencing circadian disruption by shifting the light-dark phase, display an increased susceptibility to induced colitis by dextran sulfate sodium (Amara et al., 2019; Jochum et al., 2022; Liu et al., 2017; Pagel et al., 2017; Preuss et al., 2008). These observations are accompanied by the downregulation of tight-junction proteins and the upregulation of systemic pro-inflammatory cytokines, such as IL-6 and TNF-*α* (Jochum et al., 2022). Those studies suggest that disruption of intestinal rhythms might be involved in intestinal inflammatory diseases.

Apart from the mechanical barrier provided by the tight junctions, the intestinal immune barrier also exhibits diurnal rhythmicity. Most immune cells harbor a molecular clock (Labrecque & Cermakian, 2015). For instance, the group 3 innate lymphoid cells (ILC3s), which act as a first line of defense within the innate immune system, contain clock genes. Disruption of these clock genes in ILC3s leads to intestinal dysbiosis and increased susceptibility to inflammation (Godinho-Silva et al., 2019; Teng et al., 2019). Specifically, clock-gene deletion within ILC3s results in disrupted expression of IL22 and IL17, as well as impaired lipid uptake (Godinho-Silva et al., 2019; Teng et al., 2019; Wang et al., 2019; Yu et al., 2013). Moreover, T-helper 17 cells (Th17), key players in the adaptive immune response, also exhibit daytime-dependent variations in the small intestine (SI) (Thu Le et al., 2017; Yu et al., 2013). The differentiation of Th17 cells derived from CD4+ T lymphocytes plays a crucial role in controlling bacterial infections and is regulated by RORγt, a circadian clock mediator (Korn et al., 2009; Yu et al., 2013). In addition, deletion of the core-clock gene *Rev-Erbα* resulted in suppressed Th17 cell recruitment (Amir et al., 2018).

In summary, disrupting circadian rhythmicity is suggested to impair immune response and barrier integrity within the intestines, which, in turn, can promote inflammation and the onset of metabolic disorders.

1.5.3 Intestinal motility

Intestinal motility, a critical aspect of digestive function, displays diurnal patterns in the stomach, SI, colon, and rectum in both rodents and humans (Auwerda et al., 2001; Goo et al., 1987; Kellow et al., 1986; Kumar et al., 1986; Lindberg et al., 1996; Rao et al., 2001). Electric rhythm measurements, which are indicative of motility and colonic pressure changes, have revealed that colonic movements are more prominent during the active phase following a meal, while activity during the rest phase is minimal. Interestingly, individuals with CLOCK/PER3 polymorphisms, as well as those who work night shift or travel across time zones, experience alterations in gut motility, leading to symptoms such as constipation and diarrhea (Vener et al., 1989; Yamaguchi et al., 2015). Studies on rodents have further demonstrated that mice lacking *Per1* or *Per2* genes display disrupted colonic motility and changes in fecal output (Hoogerwerf et al., 2010; Saito et al., 1976). The consistent presence of rhythmicity in stool output, intracolonic pressure changes, and tissue contractility, even under constant conditions, indicates that these measures of colonic motility are circadian in nature (Hoogerwerf et al., 2010; Saito et al., 1976).

1.5.4 Nutrient intake, absorption and digestion

The circadian system plays a crucial role in regulating metabolism, particularly in response to the 24-hour variations in nutrient availability. The GI tract, as the primary organ responsible for processing nutrients, is of great importance in this regard. Enteroendocrine cells, present throughout the entire GI tract, have a significant influence on energy intake and glucose metabolism. Enteroendocrine cells exhibit diurnal rhythms in hormone production, including cholecystokinin, glucagon-like peptide 1 (GLP-1), glucose–dependent inotropic polypeptide (GIP), and peptide YY (PYY) (Elliott et al., 1993; Martchenko, 2021). GIP and GLP-1, for instance, stimulate insulin secretion and slow gastric emptying, thereby regulating glucose and lipid metabolism as well as energy intake (Deane et al., 2010; Nauck et al., 1997). Remarkably, rats on a westernized diet (high-fat + high-sugar) exhibit disrupted diurnal GLP-1 response, potentially due to the suppression of the L-cell clock within enteroendocrine cells induced by HFD (Gil-Lozano et al., 2016; Martchenko et al., 2018; S. E. Martchenko et al., 2020).

The SI is particularly crucial in the digestion and absorption of nutrients. Early research has demonstrated the existence of diurnal rhythms in intestinal nutrient absorption, which synchronizes with feeding time (Furuya & Yugari, 1974). Further investigations have revealed that many more SI metabolic functions, including enzyme activity, exhibit diurnal oscillations. Enzymes responsible for the degradation of carbohydrates (amylase, disaccharidase), proteins (protease pepsin), and fats (lipase) exhibit diurnal oscillations in rodents, peaking shortly before the active feeding phase (Barattini et al., 1993; Furukawa et al., 2005; Oishi et al., 2006; Saito et al., 1976). Rhythmic transport of monosaccharides and the activity of disaccharidases persist even in the absence of nutrient delivery (Stevenson et al., 1980).

Furthermore, nearly all macronutrient transporters, including those responsible for lipid, carbohydrate, and protein transport, exhibit fluctuations over the 24-hour day. Glucose absorption entails both active transportation from the SI lumen to the enterocytes through sodium-glucose cotransporter 1 (SGLT1), as well as facilitated diffusion across the basolateral membrane of the enterocytes with the assistance of glucose transporter 2 (GLUT2). In contrast, fructose is primarily absorbed via GLUT5, expressed in the jejunum and ileum **(Figure 3).** The expression of these hexose transporter genes in the jejunum follows diurnal rhythms, with peak expression occurring at the onset of the active phase (Pan & Hussain, 2009; Rhoads et al., 1998). These genes are potentially regulated directly by BMAL1, as E-box sites on their promoter regions exhibit peak BMAL1 binding coinciding with peak expression levels (Iwashina et al., 2011).

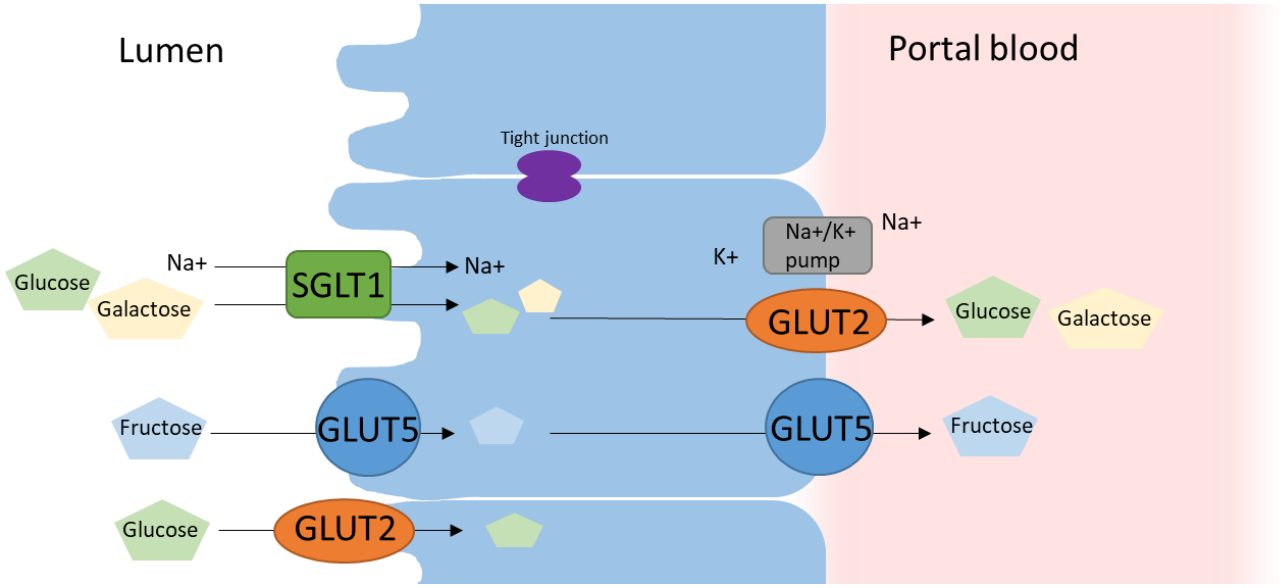

Figure 3 Diurnal carbohydrate absorption in the intestine.
Glucose, galactose and fructose are absorbed across the intestinal epithelial cells of the small intestine through active transport (SGLT1) or facilitated diffusion (GLUT5/2) to enter the bloodstream and go to the liver. Undigested carbohydrates will further pass to the large intestine. *SGLT1:* sodium/glucose co-transporter 1, *GLUT2/5;* glucose transporter 2/5, Na+ sodium, K+ potassium.

As mentioned earlier, food acts as a potent *Zeitgeber* for the intestinal peripheral clock. Daytime-restricted feeding in rodents can entrain nutrient transporters to the food intake patterns (Hoogerwerf et al., 2007; Polidarova et al., 2011; Sladek et al., 2007). Interestingly, whole-body CLOCK mutant mice fail to exhibit this entrainment to food and lose the rhythmicity of transporter genes (Pan & Hussain, 2009). Moreover, after vagotomy in mice, hexose transporters *Sglt1* and *Glut5,* as well as intestinal clock genes, continue to display diurnal rhythmicity with peak levels during the active phase (Hoogerwerf et al., 2007; Houghton et al., 2006; Tavakkolizadeh et al., 2005). These results indicate that food entrainment can only occur in the presence of a functional clock that can act independently of autonomic nervous system input

The circadian system also controls other macronutrient transport systems involved in lipid and protein absorption. In rodents, cholesterol and triglycerides absorption is upregulated during the active phase, and several lipid-related transport genes, including apolipoprotein B (*ApoB*), microsomal triglyceride transporter protein (*Mtp*), apolipoprotein AIV, and intestinal fatty acid binding protein (*Fabp*), exhibit diurnal rhythmicity (Pan & Hussain, 2007, 2009; Wang et al., 2001). Studies using a Nocturnin knockout mouse model, a CCG involved in post-transcriptional regulation of circadian genes, have shown alterations in lipid digestion and absorption, leading to resistance to diet-induced obesity (Douris et al., 2011).

The protein transport gene PEPT1 (H+/oligopeptide cotransporter 1) has also been found to oscillate in rats, with peak expression during the active phase, and is capable of entraining to the feeding schedule (Pan & Hussain, 2007, 2009; Pan et al., 2002; Pan et al., 2004). PEPT1 is directly regulated by the clock gene *Dbp*, which binds to the D-box on the *Pept1* promotor region (Saito et al., 2008). Once again, a functional core clock mechanism is necessary, as CLOCK-mutant mice exhibit arrhythmic expression of *ApoB* and *Mtp* (Pan & Hussain, 2007, 2009).

Together, these highlight the close contact of the circadian system with the diurnal oscillation of macronutrient transporter genes. However, whether they are regulated by the circadian clock, global or peripherally (e.g., the intestinal clock), remains to be elucidated.

1.5.5 Gut microbial composition

The GI microbiota comprises a complex community of microorganisms, including bacteria, viruses, fungi, archaea, and bacteriophages, all playing crucial roles in regulating host physiology (Thursby & Juge, 2017). Among these microorganisms, bacteria are currently recognized as the most diverse and dominant group in the GI tract. Bacterial composition varies substantially throughout the GI tract, with

the highest abundance found in the large intestine (10^{12} colony forming units/g of luminal content) (Backhed et al., 2005).

Bacteria can be classified into various taxonomic levels, starting from phylum, which is further split into class, order, family, genus, and species. The most abundant phyla within the human and murine bacterial community are Firmicutes, Bacteroidetes, Actinobacteria, and Proteobacteria, with the first two making up about 95% of the total bacterial abundance (Arumugam et al., 2011). The importance of the GI microbiome in maintaining intestinal homeostasis has been widely studied, showing the involvement of bacteria in energy extraction, digestion and absorption of nutrients, mucosal maturation, and defense against pathogens (Thursby & Juge, 2017).

Studies investigating diurnal microbial rhythmicity have mainly focused on bacterial composition, with less attention given to other microbiota members. Nevertheless, studies on fecal, cecal, and ileal bacterial composition have demonstrated clear compositional and functional diurnal rhythms throughout the GI tract (Kaczmarek et al., 2017; Liang et al., 2015; Mukherji et al., 2013; Thaiss et al., 2016; Thaiss et al., 2014; Voigt et al., 2014; Zarrinpar et al., 2014). In rodents, 16S rRNA gene sequencing of the fecal microbiota showed that around 20% of taxa oscillate in relative abundance (Leone et al., 2015; Thaiss et al., 2014). Microbial rhythms have also been found in humans, albeit to a lesser extent (Kaczmarek et al., 2017; Reitmeier et al., 2020; Thaiss et al., 2014).

Commonly observed trends across different studies include high bacterial richness (total number of bacterial species measured) during feeding or the active phase and low richness during the rest phase (Leone et al., 2015; Thaiss et al., 2014). Richness is often used as an indicator of microbial eubiosis, with a more diverse microbiota associated with a healthy state, whereas lower diversity is often an indication of pathophysiology (Levy et al., 2017). The major phyla, Firmicutes and Bacteroidetes, have been found to oscillate in antiphase, with Firmicutes peaking during the active feeding phase and Bacteroidetes during fasting in the light phase (Zarrinpar et al., 2014). This is to no surprise since members of the Bacteroidetes are capable of digesting mucus in the absence of nutrients and, therefore, can bloom during the fasting phase (Liang et al., 2015). In addition, several genera, including *Clostridium, Lactobacillus,* and *Bacteroides,* have been found in multiple studies to oscillate diurnally within fecal content (Liang et al., 2015; Thaiss et al., 2014; Zarrinpar et al., 2014).

Of note, most studies have investigated bacterial diurnal rhythmicity and not circadian rhythms. In the absence of external timing cues, the endogenous origin of bacterial circadian rhythms can be observed (Wu et al., 2018). Additionally, it is essential to note that relative abundance is often used to analyze microbiota composition rather than quantitative (absolute) abundance, which may exaggerate microbial rhythmicity due to the masking of highly abundant rhythmic taxa. Indeed, a study that

investigated both quantitative and relative abundance of microbiota found the absence of rhythmicity in several taxa analyzed in quantitative abundance (Liang et al., 2015). Further research investigating bacterial oscillations in quantitative abundance under constant conditions is needed to prove their circadian origin.

1.5.6 Gut microbial functioning

In addition to their composition, microbial-produced metabolites exhibit diurnal rhythmicity, playing a crucial role in maintaining gut health. The gut microbiota is responsible for digesting dietary components such as fibers, oligosaccharides, sugars, starches, amino acids, and lipids. Bacterial dietary carbohydrate metabolism results in the production of short-chain fatty acids (SCFAs), including butyrate (C4), acetate (C2), and propionate (C3) (den Besten et al., 2013). SCFAs play a vital role in maintaining gut health by providing energy to intestinal epithelial cells, mainly through butyrate production by Firmicutes (den Besten et al., 2013). In addition, SCFA contributes to gut barrier integrity, mucus production, glucose metabolism, and protection against inflammation (Cherbut et al., 1998; Gaudier et al., 2009; Lewis et al., 2010; Peng et al., 2009). They exert their local effects by activating SCFA receptors, such as free fatty acid receptors 2 and 3 (FFAR2/FFAR3), which stimulate the release of GLP-1 and PYY, thereby regulating food intake and host metabolism (Cherbut et al., 1998). Additionally, SCFAs modulate histone deacetylase (HDAC) activity and the function of immune cells, such as CD8+ T cells, ILC3s, and macrophages, contributing to immune homeostasis (Bachem et al., 2019; Fawad et al., 2022; Kim et al., 2017; Sanchez et al., 2020).

Studies have demonstrated the diurnal rhythmicity of SCFAs (butyrate, acetate, and propionate) in fecal, cecal, and plasma samples (Leone et al., 2015; Segers et al., 2020; Segers et al., 2019; Tahara et al., 2018). Whole-body knockout of the circadian clock gene *Bmal1* resulted in the loss of cecal SCFA rhythmicity, but this disruption could be restored through restricted feeding (Segers et al., 2020). Conversely, butyrate and acetate have been found to influence the expression of clock genes in the liver and intestines, indicating the crosstalk of peripheral circadian clocks and SCFAs (Leone et al., 2015; Luzader et al., 2018; Tahara et al., 2018).

Another important group of microbial-derived metabolites is secondary bile acids (BAs), which are produced by bacterial-specific transformations within the intestine of primary BAs derived from cholesterol. Primary BAs emanating from the liver can be converted through either deconjugation, dihydroxylation, or isomerization. Deconjugation of BAs requires bile salt hydrolase, which is produced by specific bacteria, including the genera *Lactobacillus* and *Bacteroides* (Song et al., 2019). The fluctuation of primary and secondary BA concentrations within the GI tract and serum follows diurnal

patterns in humans and mice (Duane et al., 1983; Gälman et al., 2005; Ma et al., 2009; Zhang et al., 2011). Primary BAs measured in the serum of mice peak during feeding, while secondary unconjugated BAs, including deoxycholic acid (DCA) and chenodeoxycholic acid (CDCA), peak during the light phase (Zhang et al., 2011). Circadian disruption through genetic ablation of core clock genes or restricted feeding during the day in mice disrupted bile acid metabolism (Ma et al., 2009). In addition, bacterial bile salt hydrolase activity shows diurnal rhythmicity, which can be phase-shifted by feeding patterns (Kombala et al., 2023). Similar to SCFAs, unconjugated BAs, including DCA and CDCA, are capable of altering liver, ileum, and colon clock gene expression (Fawad et al., 2022; Govindarajan et al., 2016; Leone et al., 2015; Parkar et al., 2019; Tahara et al., 2018). Of note, other microbial-derived metabolites, including threonine, serotonin, methionine, choline, lysine, biotin, trimethylamine N-oxide, and lactate, have been found to oscillate in either serum, cecal, or fecal content (Liu et al., 2023; Schugar et al., 2022; Thaiss et al., 2016).

Together these studies highlight the bi-directional relationship between microbial-produced metabolites and circadian clocks. Results imply microbial-produced metabolites as essential mediators for gut microbiota-host circadian communication, however, this requires further investigation.

1.6 Proposed mechanisms regulating microbial rhythmicity

The mechanism behind microbial rhythmicity remains to be elucidated, however, several factors were found to alter its diurnal dynamics, including timing and components of food intake, gender, light cycles, and host circadian clocks (Frazier et al., 2022; Liang et al., 2015; Thaiss et al., 2014; Zarrinpar et al., 2014).

1.6.1 Food timing and intake

Similar to how the gut microbiota is configured, microbial rhythmicity is influenced by various factors, including diet. Multiple studies indicate timing of food intake as a major regulator of diurnal microbial oscillations. For example, restricted feeding (RF) during the light-phase reversed rhythms of a few microbial taxa compared to nighttime RF (Brooks et al., 2021; Thaiss et al., 2016; Thaiss et al., 2014). In addition, ablation of *Per1/Per2* clock gene expression, resulting in loss of microbial rhythmicity, can be restored by RF (Thaiss et al., 2014), highlighting food intake as one of the mediators in diurnal microbial rhythmicity. However, mice submitted to continuous intravenous parenteral nutrition, which eliminates the feeding time effect, showed persistent microbial rhythmicity (Leone et al., 2015). The major phyla Bacteroidetes continued to exhibit diurnal rhythmicity, and mice fasted for 24 hours

showed continued microbial fecal rhythmicity (Pickel et al., 2022). These findings indicate that besides food intake, other mechanisms should be involved in regulating bacterial circadian fluctuation.

Apart from food timing, nutrient content can also influence microbial rhythms. HFD and westernized diets (WD; high-fat, high-sugar) have been shown to attenuate diurnal microbial fluctuations, resulting in arrhythmicity in specific butyrate-producing bacteria from the *Lachnospiraceae* family, even when feeding time remained unaltered (Leone et al., 2015; Zarrinpar et al., 2014). Of note, in both studies, a low-fiber high-fat diet feeding has been compared to a regular high-fiber chow diet. The level of fiber, a critical regulator of microbial homeostasis, could play a substantial role in alternating microbial rhythmicity, as further elaborated in the subchapter entitled "Importance of dietary fiber in modulating microbiota composition and functioning".

1.6.2 Circadian clocks

Another essential factor in maintaining microbial rhythmicity is the host circadian clock. Whole-body *Bmal1* knockout mice show reduced overall microbial rhythmicity, as well as alterations in amplitude and phase of bacterial relative and absolute abundance, including Firmicutes and Bacteroidetes (Liang et al., 2015). Furthermore, rhythmicity in microbial metabolite production, including SCFAs, was also attenuated (Segers et al., 2020; Segers et al., 2019). In addition, Clock-mutant mice exhibited reduced microbial diversity, though rhythmicity was not directly assessed (Voigt et al., 2016). Moreover, the loss of key circadian genes *Per1* and *Per2* also results in the disruption of diurnal fecal and mucosal microbial abundance and microbial-genes oscillations (Liang et al., 2015; Thaiss et al., 2016; Thaiss et al., 2014). Consistent with these findings, environmental circadian disruption in mice induced by simulated jet lag (8-h light shift every three days) for four weeks, capable of altering core clock gene expression, was shown to suppress microbial rhythmicity (Thaiss et al., 2014). Similar observations were made in mouse models subjected to abnormal light exposure, further emphasizing the influence of the circadian clock on gut microbial rhythmicity (Godinho-Silva et al., 2019; Lee et al., 2022; Wu et al., 2018).

Several molecular mechanisms have been proposed to explain how the circadian clock regulates microbial oscillations. For example, the circadian-clock-regulated molecule melatonin can reprogram the composition and diurnal rhythms of the gut microbiota in HFD-fed mice (Xia et al., 2023; Yin et al., 2020). In addition, host control of mucosal immunity was shown to influence microbial rhythmicity (Godinho-Silva et al., 2019; Thaiss et al., 2016). Specifically, ILC-3-derived IL-22 release was found to activate STAT3 on IECs, resulting in the production of anti-microbial peptides and mucus, which supports the growth of commensal bacteria and out-competes pathogens. ILC-3 specific *Bmal1*

knockout resulted in reduced mucus and anti-microbial peptide production and disrupted rhythmicity in Proteobacteria and Bacteroidetes relative abundance (Godinho-Silva et al., 2019; Teng et al., 2019; Wang et al., 2019).

Interestingly, in vitro data reveals that specific non-photosynthetic bacterial strains, including *Klebsiella aerogens* and *Bacillus subtilis*, exhibit endogenous and temperature-compensated rhythms in swarming motility, gene expression, and biofilm formation (Eelderink-Chen et al., 2021; Paulose et al., 2016). Moreover, K*. aerogens* demonstrated synchronization to melatonin, a common metabolite secreted in the GI tract, indicating the ability of this species to entrain to host cues (Paulose et al., 2016). Both species have been found in the mammalian gut, therefore, these studies suggest that gut microbes have their intrinsic circadian rhythms. However, it is worth noting that only 31-44% of the cultures of *K. Aerogens* exhibit circadian rhythmicity, highlighting the need for further research to fully comprehend circadian rhythms in non-photosynthesizing bacteria and their potential influence on community-wide rhythmicity within the intestine.

Whether the rhythmicity of the gut microbiota arises from endogenous bacterial clocks or as a response to the host's circadian process remains uncertain. There is a possibility that circadian clocks in specific gut bacteria may govern the rhythmicity of the entire gut microbial community through bacterial crosstalk. Therefore, further investigations into the rhythmicity of bacterial species in the presence and absence of a host are warranted to shed light on this intriguing phenomenon.

1.6.3 Host circadian clock and microbial crosstalk

In addition to the circadian clock's influence on microbial rhythmicity, the microbiome can also affect the host's circadian function. A mono-colonization study revealed that rhythmic bacterial adherence can program the rhythmic liver transcriptome (Thaiss et al., 2016). In addition, in the absence of microbiota, the expression of rhythmic intestinal genes is reduced compared to microbial-rich specific pathogen-free (SPF) mouse models (Mukherji et al., 2013). Of note, in germ-free (GF) mice, core circadian clock genes remain rhythmic, showing only little alterations in amplitude and phase, indicating mainly the effect of gut microbiota on CCGs but not circadian core clock genes. Although the exact mechanism by which the microbiota induces these gene expression changes is largely unknown, several potential explanations are described in the following paragraphs.

One possible explanation is that IECs can recognize microbial molecules through pattern recognition receptors, such as toll-like receptors (TLR), thereby influencing rhythmic gene expression (Mukherji et al., 2013). For instance, the attachment of segmented filamentous bacteria to the epithelium induces

diurnal IEC gene expression, including the expression of antimicrobial peptides like REG3y (Brooks et al., 2021). This process is mediated by rhythmic segmented filamentous bacteria-induced TLR signaling via Myd88, leading to the release of IL-23 by dendritic cells, followed by ILC3 IL-22 production, ultimately resulting in rhythmic Reg3y expression. Antimicrobial peptide expression is completely arrhythmic in GF mice, emphasizing the importance of microbiota in rhythmic host antimicrobial activity (Brooks et al., 2021). Microbial rhythmicity also specifically regulates the rhythmic metabolic transcriptome, including lipid metabolism, through activation of the IL-23-ILC3-IL22 pathway. This, in turn, upregulates STAT3 signaling within the IECs, which can bind to *Rev-Erba* and thereby regulates the rhythmic *Nfil3* (a leucine-zipper protein) expression, which controls the rhythmic expression of lipid absorption and transport genes, including *Scd1, Fabp4*, and *Cd36* (Wang et al., 2017). Consequently, the absence of intestinal *Nfil3* results in reduced body weight gain under HFD.

Furthermore, several studies have highlighted the impact of the microbiota on circadian IEC gene expression through acetylation. For instance, in SI-IECs, microbiota induces rhythmic histone deacetylase 3 (HDAC3) expression, thereby regulating diurnal oscillations in metabolic gene expression, particularly those involved in lipid metabolism (e.g., Cd36) (Fawad et al., 2022). Mice lacking HDAC3 in their IECs have reduced body fat content, similar to GF and NFIL3-deficient mice under HFD conditions.

Finally, as indicated before, microbial-produced metabolites, such as unconjugated BAs and SCFAs, can alter liver and intestinal clock gene expression (Fawad et al., 2022; Govindarajan et al., 2016; Leone et al., 2015; Parkar et al., 2019; Tahara et al., 2018). For example, butyrate, acetate, isovaleric acid, and propionate have been shown to change the phase and amplitude of *Per2* through the inhibition of HDAC within intestinal enteroids (Fawad et al., 2022).

Although several factors capable of influencing microbial rhythmicity have been identified, there remains a requirement for further investigation to comprehensively understand the underlying mechanisms governing the rhythmicity of gut microbiota. It is crucial to ascertain whether the rhythmicity is self-sustained through microbial cellular clocks, influenced by peripheral circadian clocks, or affected by other external factors. Furthermore, investigating the potential contribution of nutritional dynamics in regulating gut microbial rhythmicity presents a significant and promising area for future research.

1.7 Importance of dietary fiber in modulating microbiota composition and functioning

Laboratory animal models are extensively utilized in research due to their ability to provide controlled conditions, ensuring high comparability between experimental groups. However, it is crucial to acknowledge that the interpretation of data is significantly influenced by the selection of appropriate control conditions, particularly when studying the impact of nutrition. Unfortunately, the choice of control diet is often insufficiently addressed, despite its importance (Dalby et al., 2017; Pellizzon & Ricci, 2018; Warden & Fisler, 2008).

In many animal studies investigating host and microbial physiology, unrefined chow diets composed of plant-based ingredients such as wheat, oat, soybean, and corn are commonly used. However, the nutritional composition of these diets can vary due to seasonal and locational changes in harvested plant materials, making them less well-defined (Pellizzon & Ricci, 2018). On the other hand, purified diets consist of precisely defined ingredients and can be easily modified, allowing for reproducible data (Pellizzon & Ricci, 2018).

One of the most common differences between purified and chow diets is the concentration and type of fibers. Chow diets typically have four times higher fiber levels than purified diets, containing both soluble and insoluble fibers. In contrast, purified diets usually contain only 5% cellulose, which is an insoluble fiber resistant to microbial fermentation (Gonzalez-Blazquez et al., 2020). The solubility of dietary fibers plays a crucial role in regulating microbiota composition and subsequently affects the host. Studies in rodents and humans have shown that a low-fiber diet results in reduced microbial diversity and an increase in microbiota capable of using amino acids and lipids as energy sources, which is associated with adverse metabolic outcomes such as increased weight gain and insulin resistance (Chassaing et al., 2015). Conversely, the presence of soluble fiber promotes the growth of beneficial bacteria and the production of metabolites like SCFAs, leading to improved gut and metabolic host health (Gentile, 2018).

Considering the lack of soluble fibers in most purified diets used in literature, significant differences in host health and microbial composition between laboratory animals fed purified diets and chow diets can be expected. It is essential to mention that purified diets cannot be directly compared to chow diets. However, in the field of circadian research discussed before, studies investigating the effects of diets on microbial composition and gut health often use chow diets as controls for purified high-caloric dietary interventions (Leone et al., 2015; Yu et al., 2021; Zarrinpar et al., 2014). Consequently, the results obtained in those studies, including dampened microbial rhythmicity in response to an HFD, could be attributed to the lack of fermentable fiber. In vitro studies have shown that the addition of

fermentable fibers increases the amplitude of bacterial rhythms (Silva et al., 2022). Moreover, inulin has been found to regulate the expression and phase of circadian clock genes in the liver and hypothalamus of mice (Cheng et al., 2020). Additionally, previous reports have demonstrated phase shifts in *Per2* clock gene expression in mice fed rapidly fermentable cellobiose fibers compared to cellulose (Tahara et al., 2018). Therefore, further research is necessary to elucidate the effect of fat and fiber on microbial oscillations and circadian clocks. Purified dietary alternatives enriched with fiber, such as pectin, inulin, or lignocellulose, may provide a viable option for maintaining murine health and improving the reproducibility of animal experiments.

1.8 The role of gut microbial rhythmicity in host metabolism

The gut microbiome plays a crucial role in maintaining host health, and disruptions of a balanced gut microbiome have been linked to metabolic diseases such as obesity and T2D (Janssen & Kersten, 2017; Li et al., 2017; Yassour et al., 2016). In mice, HFD-induced obesity dampened microbial oscillation and circadian metabolite production (Frazier et al., 2022; Leone et al., 2015; Zarrinpar et al., 2014). For instance, the rhythmicity of major phyla, Firmicutes and Bacteroidetes, is lost compared to a chow diet. Additionally, in a mouse model of T2D, remaining functional host circadian rhythmicity, diurnal gut microbial rhythmicity is disrupted, along with several metabolic pathways involved in protein metabolism, including histidine and methionine biosynthesis (Beli et al., 2019). Furthermore, simulated jet lag, accompanied by suppressed microbial rhythmicity and downregulation of butyrate-producing bacteria, leads to increased body weight and impaired glucose tolerance (Altaha, 2022; Thaiss et al., 2014). Fecal microbial transplantation obtained from jet-lagged mice into GF wild-type recipient mice results in significant weight gain and glucose intolerance compared to fecal microbial transfer obtained from normal light-dark (LD) housed mice (Thaiss et al., 2014).

Recent research highlights the disruption of microbial oscillation in humans with obesity or T2D, including the major phyla Bacteroidetes and Firmicutes (Reitmeier et al., 2020). Reitmeier et al. even identified the arrhythmicity of six bacterial species as a biomarker of T2D in humans (Reitmeier et al., 2020). These species include *Bifidobacterium longum, Clostridium celatum, Intestinibacter bartletti, Romboutsia ilealis, Fecalibacterium prausnitzii,* and *Escherichia coli*. It is important to note that the average abundance of these species is also altered between healthy individuals and those with T2D, indicating potential compositional differences as a disease mediator. Nevertheless, this study supports the hypothesis that diurnal oscillations in microbiota composition and function may contribute to human metabolic health.

Collectively, these findings suggest that the interaction between gut bacteria oscillation and the host circadian clock is crucial for maintaining host health and may play an essential role in the development

of metabolic diseases. Understanding this host-microbiota relationship will be essential for developing effective treatments for metabolic diseases.

1.9 Intestinal epithelial cell-specific *Bmal1* knockout studies

While systemic ablation of the core clock genes has been extensively studied, research on the effects of peripheral circadian clocks is limited. It is well established that the contributions of individual molecular clock components can vary depending on the specific tissue being. Notably, the role of *Bmal1* varies significantly across tissues, as highlighted in the previous paragraph, with tissue-specific ablation of *Bmal1* resulting in several phenotypes, including disrupted behavior, altered glucose and lipid metabolism, arthropathy, shortened lifespan, and infertility (Bunger et al., 2005; Costello et al., 2023; Laposky et al., 2005; Rudic et al., 2004; Shimba et al., 2005). Research on *Bmal1* is explicitly of high interest in the circadian field, as it is the only core clock gene that, upon disruption, exhibits complete arrhythmicity (Bunger et al., 2000)

In the context of gut-microbiome interactions and host metabolism discussed within this introduction, the peripheral clock in the intestine is hypothesized to play a crucial role. **Table 1** summarizes the evidence found thus far in mouse models using intestinal-specific *Bmal1* ablation. Two recent studies have specifically investigated the role of the IEC clock in host metabolism. Yu et al. demonstrated that mice lacking IEC-specific *Bmal1*, under an HFD (60% kJ), exhibited reduced body weight gain and decreased lipid absorption compared to mice with intact *Bmal1*. The authors propose that the arrhythmic and downregulated expression of *Dgat2*, encoding for an enzyme regulating triacylglycerol synthesis, could be a potential mechanism underlying these observations (Yu et al., 2021). Additionally, in the same study, the knockout of *Rev-Erbα* in IECs increased fat absorption and diet-induced obesity (Yu et al., 2021). Another study published in 2022 showed that IEC-specific deletion of *Bmal1* led to arrhythmic expression levels of *Sglt1* and *Glut2,* transporters involved in glucose absorption, accompanied by reduced serum glucose levels after an oral glucose tolerance test (Onuma et al., 2022).

These findings highlight the importance of circadian rhythms in intestinal functionality and the specific role of the peripheral intestinal clock in host metabolism. It is reasonable to speculate that the gut microbiome influences host metabolic homeostasis, and microbial dysbiosis, often induced by dietary factors, may contribute to disease development. While it is evident that IECs play a crucial role in controlling the gut microbiota, it remains to be elucidated whether the IEC clock regulates circadian microbial rhythmicity, thereby influencing host health. Thus, more studies are required to investigate the role of the peripheral intestinal clock in host metabolism and host-microbe interactions, as current research in this area remains limited.

Table 1 Overview of papers using intestinal specific *Bmal1* deficient mouse models

Reference	Journal	Main findings
(Kawai et al., 2019)	JCI insight	• *Bmal1*$^{IEC-/-}$ mice show reduced bone volume through arrhythmic VDR expression resulting in impaired Ca absorption
(Yu et al., 2019)	Theranostics	• *Bmal1*$^{IEC-/-}$ mice show arrhythmic *Mrp2* (multidrug resistance protein) gene expression • *Dbp* direct regulates *Mrp2* through D-box • *Bmal1* regulates *Dbp* direct through E-box
(Tuganbaev et al., 2020)	Cell	• Loss of intestine specific Bmal1 does not affect MHCII frequencies in Small-intestinal epithelial cells
(Stokes et al., 2021)	Cell Mol Gastroenterol Hepatol	• Loss of intestine specific *Bmal1* in an *Apc* (colorectal cancer) mouse model increased number of tumors • *Apc*^{min}*xBmal1*$^{IEC-/-}$ mice show upregulation of *Yap/Tead* genes involved in Hippo signaling pathway
(Chen et al., 2021)	JPP	• *Bmal1*$^{IEC-/-}$ mice show arrhythmic and reduced intestinal *Ces1d*/CES1 levels
(Yu et al., 2021)	Nature comm.	• *Bmal1*$^{IEC-/-}$ mice are protected against diet-induced obesity (60% kJ HFD) • *Bmal1*$^{IEC-/-}$ mice show impaired lipid resynthesis • Circadian controlled *Dgat2* promotes fat absorption
(Penny et al., 2022)	Science immunology	• *Bmal1*$^{IEC-/-}$ mice show slightly elevated but rhythmic IgA concentrations
(Onuma et al., 2022)	Endocrinology	• *Bmal1*$^{IEC-/-}$ mice show arrhythmic *Sglt1/Glut2* expression
(Jochum et al., 2022)	Inflammatory Bowel Disease	• *Bmal1*$^{IEC-/-}$ mice show worsened DSS induced colitis • DSS increased intestinal permeability in *Bmal1*$^{IEC-/-}$ mice • *Bmal1*$^{IEC-/-}$ show decreased SCFA levels
(Ko et al., 2023)	Bone	• Colonic specific *Bmal1*$^{IEC-/-}$ male, not female, mice show reduced bone volume

2. Aim

The circadian clock has been shown to play a crucial role in host metabolism and gut microbial homeostasis. Despite a growing body of evidence, it remains unclear whether specific peripheral tissue clocks play a substantial role in this. Given the significant crosstalk between intestinal epithelial cells (IECs) and bacteria within the gastrointestinal (GI) tract, it is hypothesized that the peripheral clocks within the GI tract may be instrumental in regulating microbial composition. Furthermore, as the GI tract serves as the primary point of nutrient entry, IEC-specific clocks are likely to be involved in nutrient absorption and transportation, potentially influencing host metabolism.

The aim of this study is to investigate the role of the peripheral intestinal clock in microbiome regulation and host metabolism. Toward this aim, the experimental setup of dietary interventions in a mouse model with an IEC-specific deletion of *Bmal1*, one of the core clock genes, was used.

Circadian phenotyping of the newly generated *Bmal1*$^{IEC-/-}$ mice was conducted to assess potential alterations in feeding and activity patterns under the exposure to normal light-dark conditions and constant darkness. Additionally, through the application of 16S rRNA sequencing and (un)targeted metabolomics, the rhythmicity of bacterial composition and functionality in the feces and cecal content was investigated. To elucidate the functional role of intestinal clock-driven bacteria on the host, germ-free mouse transfer experiments were conducted.

Furthermore, transcriptomic analyses of the small intestine (SI), a vital metabolic organ, were performed to gain insights into the control exerted by the intestinal clock on SI oscillating genes. Through several dietary interventions, including a high-fat diet (HFD), western diet (WD), purified control diet (CD), control diet enriched with fiber (CFI), and standard chow, the impact of diet on microbial rhythmicity, as well as the influence of the peripheral IEC clock on metabolic homeostasis, were explored.

In summary, by dissecting the role of the peripheral intestinal clock, this study aims to enhance our understanding of the intricate interplay between circadian rhythms, gut microbiota, and metabolic health.

3. Material and methods

3.1 Animal experiments

3.1.1 Ethical statement

All mouse experiments were conducted at the Technical University of Munich in accordance with Upper Bavarian Animal Health Care and Use Committee (Regierung von Oberbayern; TVA ROB-55.2Vet-2532.Vet_02-18-14).

3.1.2 Mouse models

Mice with specific intestinal epithelial cell deletion of *Bmal1* (*Bmal1*$^{fl/fl}$ *x Villin*$^{CRE/wt}$; referred to as *Bmal1*$^{IEC-/-}$) were generated by crossing *Bmal1*$^{flox/flox}$ *x Villin*$^{CRE/wt}$ with *Bmal1*$^{fl/fl}$ *xVillin*$^{wt/wt}$ (referred to as control) on a C57Bl/6 N/J background. Several generations of mice were used to minimize littermate biases. Only male mice have been used in this study to avoid result variability due to hormonal cycle influences. Unless otherwise indicated, mice received *ad libitum* water and regular chow (V1124-300, Ssniff, Soest, Germany) and were kept in a 12:12 light/dark cycle (300lux, lights on; 5 a.m. (ZT0)- 5 p.m. (ZT12)). At the age of 8 weeks, mice were single-housed under specific-pathogen-free (SPF) conditions unless otherwise stated (22 ± 1°C), according to the recommendations of FELASA.

3.1.3 Long-term dietary interventions

For the diet interventions, mice received chow diet till the age of 8 weeks and were then switched to a purified control diet (y-irradiated) (CD; S5745-E902, Sniff, Soest, Germany) till the age of 12 weeks. At the age of 12 weeks, mice either remained on CD till the age of 20 weeks or got a high-fat diet (HFD, 20% palm oil-based, S5745-E912, Ssniff, Soest, Germany), high-fiber HFD (HFD^{inulin}, 10% inulin, Sniff, Soest, Germany), or a western diet (WD, 30% sucrose in drinking water + HFD) **(Table 2).**

Table 2 Dietary composition

Ingredients	Chow	Control diet (CD)	Fiber-enriched Control diet (CFi))	High-fat diet (HFD)	High-fat high fiber diet (inulin) (HFD^{inulin})
Casein		24.0	24.0	24.0	24.0
Corn starch		47.8	35.8	27.8	22.8
Maltodextrin		5.6	5.6	5.6	5.6
Sucrose		5.0	5.0	5.0	5.0
Cellulose	U	5.0	5.0	5.0	-
Oat Fiber 0F90	N	-	8.0	-	-
Lignocellulose	K	-	2.0	-	-
Inulin (chicory)	N	-	1.0	-	10
Pectin (apple)	O	-	1.0	-	-
L-Cystine	W	0.2	0.2	0.2	0.2
Vitamin premixture	N	1.2	1.2	1.2	1.2
Mineral & trace element mix	*	6.0	6.0	6.0	6.0
Choline Cl		0.2	0.2	0.2	0.2
Soybean oil		5.0	5.0	5.0	5.0
Palm oil		-	-	20.0	20.0
Cholesterol		-	-	-	-
Butter fat		-	-	-	-
Proximate contents					
Crude protein	22.0	21.1	21.1	21.1	21.1
Crude fat	4.5	5.1	5.1	25.1	25.1
Crude fiber	3.9	5	13.6	5.0	9.4
NDF	13.1	(4.1)	13.1	(4.1)	Unknown
ADF	6.0	-	-	-	-
Crude ash	6.5	5.4	5.4	5.4	5.4
Starch	34.2	45.9	34.4	26.7	21.9
Sugar	5.1	6.1	6.2	6.1	6.1

Fatty acids % in the diet					
C12:0	-	0.01	0.01	0.01	0.01
C14:0	0.01	0.02	0.02	0.02	0.21
C16:0	0.54	0.61	0.61	9.41	9.41
C18:0	0.14	0.19	0.19	1.11	1.11
C20:0	0.02	0.02	0.02	0.10	0.10
C16:1	0.02	0.01	0.01	0.04	0.04
C18:1	1.03	1.28	1.28	9.18	9.18
C18:2	2.42	2.63	2.63	4.46	4.46
C18:3	0.28	0.29	0.29	0.32	0.32
ME (Atwater) [A] **MJ/kg**	14.0	15.3	13.9	19.7	18.9
Protein kcal%	27	23	26	18	19
Fat kcal%	12	13	14	48	50
Carbohydrates kcal%	61	64	60	34	31

* Chow dietary composition: Wheat and wheat products, soybean products, corn (maize), minerals, soybean oil, brewer's yeast, vitamins & trace elements, L-lysine HCl, DL-methionine. Exact content is variable between batches. [A] physiological fuel value.

3.1.4 Fiber dietary intervention paradigm

Single-housed *Bmal1*$^{IEC-/-}$ and control mice received ad libitum standard chow until the age of 12 weeks. After, all mice were switched to a fiber-depleted purified control diet (CD; S5745-E902, Sniff, Soest, Germany) for two weeks, followed by a high-fiber CD (CFi; S5745-E918, Sniff, Soest, Germany) for two weeks. Finally, mice received two more weeks of chow diet before sacrifice. Fecal pellets were collected over a 24-hour day at the end of every second week of dietary intervention.

3.1.5 Tissue collection

All animals were sacrificed by cervical dislocation at the age of 16-20 weeks during the second day of darkness (DD), unless otherwise specified. Eyes were removed prior to dissection, and tissues were collected in RNA stabilizer overnight and stored at -80°C until further processing. Fecal pellets, cecal content as well as blood plasma were snap-frozen using dry ice.

3.1.6 Body composition measurements

Fat mass, lean mass, and free fluid were measured with the use of an NMR (Minispec, Bruker). Mice were put alive into the NMR in a restrainer tube. Mice were measured before and after dietary interventions.

3.1.7 Food intake

Average daily food intake was measured over five consecutive days by weighing the remaining food of single-housed mice. Food intake over the 24h day was measured with the use of an automated food monitor system (TSE LabMaster Home Cage Activity, Bad Homburg, Germany) at the age of 10-12 weeks. After a 3-day habilitation, data was collected for a full 24-hour in an LD cycle. Food basket weights were summed up in 1 min intervals. Total food intake was calculated as first derivative of cumulative food intake, and intake was summed up at intervals of 1 hour. A similar record of food basket weight gain as weight loss within a 3-minute period was excluded.

3.1.8 Complete gastrointestinal transit time

Complete gastrointestinal transit time (GITT) was measured by gavaging six hour starved mice natural carmine red (6%, Sigma Aldrich) dissolved in 0.5% methylcellulose (Sigma-Aldrich). T0 indicates the time of gavage. Every 10 minutes, fecal pellets were checked for a red color. If a red color was visible, the time was registered as GITT. GITT was measured at CT1, CT13, and ZT13.

3.1.9 Oral glucose tolerance test (OGTT)

Baseline glucose measurements (either at ZT1 or ZT13) were performed after six hour starvation from tail blood, with the use of a glucometer (FreeStyle, Abbott) and glucose measuring stripes (FreeStyle, Abbott). Directly afterward, 2 mg glucose/g body weight (G-40% glucose concentrate, B. Braun, Melsungen, Germany) was orally administered to the mice. Blood glucose levels (mmol/L) were measured after 15, 30, 60, and 120 min of gavage. The area under the curve (AUC) was measured in mg/dl as described in **Table 3.**

Table 3 OGTT area under the curve analyses

	Time	**Formula**
A	0-15 min:	AUC = 0,5 *(t0 + t15) *15
B	15-30 min:	AUC = 0,5 *(t15 + t30)*15
C	30-60 min:	AUC = 0,5 *(t30 + t60)*30
D	60-120 min:	AUC = 0,5 *(t60 + t120)*60
E	total AUC:	sum of all AUCs (A-E)
F	Incremental AUC:	total AUC (E) – t0*120

3.1.10 Germ free experiments

3.1.10.1 Housing conditions

Germ-free (GF) mice on a C57Bl6 background were held at the Technical University of Munich in the gnotobiotic facility. Mice were located in isolators equipped with HEPA filters (LD 12:12, 24-26°C) and were fed ad libitum autoclaved chow (V1124-300, Ssniff, Soest, Germany) and had ad libitum access to autoclaved water. Before microbial transfer, germ-free status was confirmed by gram staining of fecal suspension as well as by cultivation of feces in Wilkins-Chalgren Anaerobe (WCA) agar plates (OXOID, UK) under aerobe and anaerobe conditions. Presence of fungus was checked by fungi-traps.

3.1.10.2 Colonization of germ-free mice

Fresh cecal content of *Bmal1*$^{IEC-/-}$ or their controls (*Bmal1*$^{fl/fl}$) was suspended in glycerol (40% glycerol/PBS), followed by snap freezing (-80°C). Gavage was prepared by centrifugation of glycerol aliquot, followed by supernatant transfer under anaerobic conditions to exclude the presence of residual matter. The supernatant was transferred to Hungate anaerobic tubes. Cecal content was orally gavaged at ZT13 (100µl, of 7×10^6 bacteria/µl) with the use of a 20 Gauge gavage needle (Fine Science Tool). The body weight of mice was monitored weekly, and feces was sampled after week 5 of gavage in DNA stabilizer. Native fecal samples were taken at ZT4 and ZT16 for metabolic measurements. Mice were sacrificed at the second day of darkness by cervical dislocation after 6 weeks of gavage. Prior to dissection, eyes were removed.

3.1.11 Antibiotic treatments

Mice were treated at the age of 8 weeks with a mixture of vancomycin (0.25 g/l)/metronidazole (1.0 g/l) in their drinking water for a total duration of 4 weeks. At the age of 12 weeks, mice were gavaged (100µl, of 7×10^6 bacteria/µl) with either a mixture of control or *Bmal1*$^{IEC-/-}$ derived cecal microbiota. Body weight was measured weekly. Mice were sacrificed after five weeks of colonization by cervical dislocation. Prior to dissection, eyes were removed.

3.2 Energy assimilation

Fecal samples were collected from individual mice over 5 days and dried at 55 °C for another 5 days. Dried fecal pellets were ground using the TissueLyserII (Qiagen, Retsch, Haan, Germany) and pressed into two pellets of 1 gram (technical duplicates). Gross fecal energy content was measured using a 6400 bomb calorimeter (Parr Instrument Company, Moline, IL, USA). Total fecal caloric value was measured by incorporating the energy equivalence value of the bomb calorimeter (EE), the increase in combustion temperature (ΔT), energy released by the ignition thread (E_{thread}=20 kJ), weight and energy

released by combustion aid (if used, $E_{combustion\ aid}$=26.45 kJ/g) and the weight of the sample (see formula below).

$$Caloric\ value\ [J * g^{-1}] = \frac{(\mathrm{EE}*\Delta\mathrm{T}) - E_{thread} - (E_{combustion\ aid} * M_{combustion\ aid})}{M_{sample}}$$

Assimilation efficiency was calculated by recording the food intake and feces production over the fecal collection days, as indicated in the formula below.

$$Assimilation\ efficiency\ (\%) = \frac{(\text{Food intake [g]} * \text{Efood [kJ*g-1]}) - (\text{Feces production [g]} * \text{Efeces [kJ*g-1]})}{\text{Food intake [g]} * \text{Efood [kJ*g-1]}} * 100$$

3.3 Behavior analyses

Mice were individually housed in cages equipped with running wheels. Handling and activity measurements during experiments were performed as described (Jud et al., 2005). The wheel-running activity was analyzed using ClockLab software (v6.0.52, Actimetrics). The last days of each condition were used to determine the period (tau, calculated using an X^2 periodogram and confirmed by fitting a line to the onsets of activity), the duration of the active period (alpha), the amount of activity, and the subjective day/night activity ratio (where the subjective day under DD conditions is the inactive period between the offset of activity and the onset of activity and the subjective night is the active period between the onset of activity and the offset of activity).

3.4 Tissue processing, H&E staining, and histological scoring

Intestinal tissue cross-sections, as well as gonadal fat, were collected directly after sacrifice. Tissue sections were 4% formaldehyde fixed for 48h, followed by dehydration (Leica TP1020) and paraffin embedding (**Table 4**, each step 60min) (VWR, Ismaning, Germany). Paraffin-embedded tissues were cut into five µM slices (Leica RM2255, Soest, Germany) and stained with hematoxylin and 0.2% eosin (H&E, Leica ST5020, Leica Microsystems, **Table 5**). DPX's new mounting media (Merck, Darmstadt, Germany) was added to preserve the tissues with a glass coverslip (VWR, Ismaning, Germany). Histological scores were assessed blindly based on the degree of immune cell infiltration of all colonic wall layers (*mucosa, submucosa* and *muscularis*), crypt hyperplasia, goblet cell depletion and mucosal damage, resulting in a score from 0 (not inflamed) to 12 (severely inflamed) according to Katakura method (Katakura et al., 2005). For adipocyte quantifications, sections were scanned (PreciPoint M8, Freising, Germany), and the average surface area of adipocytes was measured with the help of the Adiposoft program (ImageJ). The crypt depth and villus length were measured in 20 well-oriented crypts/villi. The length from crypt/villus base to the top was measured using the ViewPoint Light software (Precipoint, Freising, Germany), and the average length was calculated for each section.

Table 4 Dehydrating and paraffin embedding

Step	Reagent	Step	Reagent
1	70% EtOH	7	100% EtOH
2	70% EtOH	8	100% EtOH
3	80% EtOH	9	Xylene
4	96% EtOH	10	Xylene
5	96% EtOH	11	Paraffin
6	100% EtOH	12	Paraffin

Table 5 Deparaffinization, rehydration and H&E staining

Deparaffinization and rehydration		
Step	Reagent	Time
1	Xylene	5 min
2	Xylene	5 min
3	100% EtOH	5 min
4	100% EtOH	5 min
5	96% EtOH	2 min
6	96% EtOH	2 min
7	70% EtOH	2 min
8	70% EtOH	2 min
9	dH_2O	30 sec
H&E staining		
1	Hematoxylin	2 min
2	Tab H_20	15 sec
3	Bluing reagent	30 sec
4	dH_2O	30 sec
5	96% EtOH	30 sec
6	Eosin	2 min
7	96% EtOH	30 sec
8	96% EtOH	30 sec
9	100% EtOH	30 sec
10	100% EtOH	30 sec
11	Xylene	1.5 min
12	Xylene	end

3.5 Alcian blue / Periodic acid-Schiff (AB/PAS) staining

Formaldehyde-fixed small intestinal (jejunum) sections were deparaffinized, rehydrated, and stained with alcian blue (Fisher, Dreieich, Germany) solution of 1% v.v. in 3% acetic acid at a pH 2.5 for 5 minutes to detect acidic mucins in goblet cells. Following that, the sections were treated with periodic acid (1% v/v) for 10 minutes and co-stained with Schiff's reagent (Sigma-Aldrich, Taufkirchen, Germany) for 15 minutes (dark) to stain for neutral mucins. Hematoxylin was used to counterstain the nuclei, and the tissue sections were dehydrated and mounted using DPX new (Merck KGaA, Darmstadt, Germany). The slides were scanned and analyzed further using a PreciPoint M8 microscope (Precipoint, Freising, Germany). For quantification, 50 well-oriented crypts were selected, and PAS+ cells were counted. The number of PAS+ cells was calculated as a total number per 100 μm^2.

3.6 RNA isolation and qPCR

RNA was extracted from snap-frozen tissue samples in RNAlater (Sigma Aldrich) with the use of RA1 buffer (Macherey Nagel) and the NucleoSpin RNAII kit (Macherey-Nagel) following the manufacturer's protocol. RNA quality and quantity were measured using a NanoDrop (ND-10000 spectrophotometer, Thermo Fisher Scientific). cDNA was synthesized from 1000ng RNA using the cDNA synthesis kit Multiscribe RT (Thermofischer Scientific) **(Table 6)**. Samples were incubated in the thermocycler for 5 min 25°C, 10 min 25°C, 120 min 37°C, 5 sec °C. Quantitative real-time PCR (qPCR) was performed in a Light Cycler 480 system (Roche Diagnostics, Mannheim, Germany) using the Universal Probe Library system according to the manufacturer's instructions. In short, 10 µM UPL-Probe, 20 µM forward and reverse primer, 1000 ng/µl cDNA, and 2x Master Mix were used. The primers and probes used are described in **Table 7**. RNA abundance was normalized to the housekeeping gene *Ef1α*. Relative expression values were determined using the 2-ΔΔCt method (Livak & Schmittgen, 2001).

Table 6 cDNA synthesis protocol

cDNA synthesis component	Volume per sample [µl]
10x Reaction buffer	2
RIboLock RNAse inhibitor (20u/µl)	1
10x Random hexamer primers	2
dNTP mix 10mM	0.8
M-MulV Reverse Transcriptase (20u/µl)	1
PCR grade H_20	3.2

Table 7 Primer sequences and UPL probe numbers used for qRT-PCR analysis

Gene	F 5'-3'	R 5'-3'	Probe
Bmal1	ATTCCAGGGGGAACCAGA	GGCGATGACCCTCTTATCC	15
Per2	TCCGAGTATATCGTGAAGAACG	CAGGATCTTCCCAGAAACCA	5
Rev-Erbα	AGGAGCTGGGCCTATTCAC	CGGTTCTTCAGCACCAGAG	1
Cry1	ATCGTGCGCATTTCACATAC	TCCGCCATTGAGTTCTATGAT	85
Fabp2	ACGGAACGGAGCTCACTG	TGGATTAGTTCATTACCAGAAACCT	56
Sglt1	CTGGCAGGCCGAAGTATG	TTCCAATGTTACTGGCAAAGAG	49
Glut2	TTACCGACAGCCCATCCT	TGAAAAATGCTGGTTGAATAGTAAAA	3
Glut5	TGGTTGGAACCTTGGTGAATA	TGGTTGGAACCTTGGTGAATA	58
Ef1a	GCCAAT TTCTGGTTGGAATG	GGTGACTTTCCATCCCTTGA	67
Ocln	CACGACAGGTGGGGAGTC	TTGATCTGAAGTGATAGGTGGATATT	17
Cdh1	ATCCTCGCCCTGCTGATT	ACCACCGTTCTCCTCCGTA	18

3.7 RNA-sequencing

RNA quality was verified using an Agilent2100 Bioanalyzer (Agilent) with RNA 6000Nano Reagents (Agilent). Library preparation and rRNA depletion was performed using the TruSeq Stranded mRNA Library Prep Kit. After the final quality control, the libraries were sequenced in a paired-end mode (2x150 bases) in the Novaseq6000 sequencer (Illumina) with a depth of ≥ 12 Million paired reads per sample.

3.7.1 Pre-processing

The quality of Next Generation Sequencing data was assessed with FastQC v0.11.5. Adapter content and low-quality reads were removed using Trimmomatic v0.39 (Bolger et al., 2014). Trimmed FASTQ files were then mapped against the mouse mm10 genome with the STAR v2.7.5c aligner (Dobin et al., 2013). Format conversions were performed using samtools v1.3.1 (Li et al., 2009). The featureCounts program v1.4.6 (Liao et al., 2014) was used to count reads located within an exon that do not overlap multiple features, with a threshold of mapping quality (MAPQ) > = 4, and are not chimeric.

3.7.2 Normalization and differentially expressed genes analysis

DESeq2 version 1.22.0 (Love et al., 2014) was used to normalize the read count matrix and perform differential expression analysis. Bioconductor package ''biomaRt'' version 2.38 (Durinck et al., 2009)

was used to map mouse genome informatics (MGI) symbols to Ensembl gene IDs. Gene ontology enrichment analyses were carried out using GOnet (qvalue<0.05) (Pomaznoy et al., 2018).

3.7.3 Circadian analysis

The (differential) rhythmicity of normalized transcripts was measured through both JTK_cycle and CompareRhythms R packages. JTK_cycle (Hughes et al., 2010) was used through the MetaCycle R package (Wu et al., 2016) with a period of 24h and adj. p-value < 0.05 to identify significant oscillating transcripts. CompareRhythms (Pelikan et al., 2022) was used to find altered rhythms between genotypes with the method Deseq2 and just_classify=FALSE.

3.8 Gut permeability measurements

Intestinal tissues were directly isolated after sacrifice and put in ice-cold carbonated (95% O_2 - 5% CO_2) Krebs buffer (113.6 mM NaCl, 2.4 mM Na_2HPO_4, 0.66 mM NaH_2PO_4, 21 mM $NaHCO_3$, 5.4 mM KCL, 1.2 mM $CaCl_2$, 1.2 mM $MgCl_2x6H_2O$, 10 mM glucose, pH 7.4). Intestinal tissue of ~1.5 cm segments was longitudinally opened along the mesenteric border, washed, and mounted in 0.44635 cm^2 ussing chambers (Mund, Scientific Instruments, Aachen, Germany). Mucosal and serosal sides were filled with 3ml of 37°C Krebs buffer, continuously carbonated, and maintained at 37°C. After 30min of equilibrating, transepithelial electrical resistance (RT, Ohm cm2) was measured in open circuit mode, followed by the mucosal addition of 250µl 1.8mM fluorescein sodium salt (FITC) to measure permeability. Serosal samples were taken after 45 min and 60 min of FITC addition and consequently measured by a Fluoroskan Ascent FL (Thermo labsystem, Waltham, USA) fluorometer with λexc 485nm and λem 538nm. Data was collected with the use of the software package Clamp (version 2.14, Mund Scientific instruments).

Permeability (P) was calculated using the following equations:

(1) $$\text{J(flux)}\frac{uM}{h\ x\ cm^2} = \frac{(Conc.1 - Conc.2)\ x\ Volume\ (ml)}{(timepoint\ 1 - timepoint\ 2)\ x\ tissue\ area\ (cm^2)}$$

(2) $$P\frac{cm}{s} = \frac{J\ (flux)}{c}$$

c= Concentration (µM) of FITC at the serosal site at time point 0.

3.9 Glucose uptake experiments

Intestinal tissue was prepared as mentioned above, modified by the addition of 10 mM mannitol Krebs buffer instead of 10 mM glucose at the serosal side. Tissues were kept in a short-circuited state. To measure Na+-dependent glucose transport, 100 mM of glucose was added to the mucosal side and osmotically balanced by equimolar amounts of mannitol on the serosal side. The change in Δ Isc was measured over a 20 min period. Overall glucose transport was measured using a fluorescent-labeled glucose tracer 2-NBDG ([2-(N-(7-Nitrobenz-2-oxa-1,3-diazol-4-yl)Amino)-2-Deoxyglucose]-glucose, Sigma) in a 100 mM glucose solution. After adding 2-NBDG to the mucosal side, samples were taken over a 20 min period and measured at 488 nm/540 nm emission using Multiskan® spectrophotometer (Thermo Scientific).

3.10 High-throughput 16S Ribosomal RNA (rRNA) gene sequencing and microbial analysis

The genomic DNA was extracted from snap-frozen fecal pellets and cecal content using a modified protocol based on Godon et al. (Godon et al., 1997). In short, samples were put in stool stabilizer (Stratec) with 400 mg of 0.1 mm silica beads and 200 µl of Guanidinethiocyanat (protein denaturation), and 500µl of N-laurolylsarcosine (surfactant). Samples were incubated for one hour at 70°C (700rpm). Next, bacteria were lysed using a FastPrep (40 sec 6.5 m/s, 3x). Polyvinylpyrrolidone (PVPP, 15mg) was added to remove polyphenols, and samples were centrifuged for 3 min (15000g 4°C). The clear supernatant was transferred to a new 2mL tube, and 1:100 RNase (10mg/ml) was added, followed by 30min incubation at 37°C (700 rpm). Purification of DNA was carried out using DNA NucleoSpin gDNA columns (Machery-Nagel, No. 740230.250). To amplify the V3-V4 region of the 16S rRNA gene, a two-step PCR was performed with the primers 341F-ovh and 785r-ov, using 24 ng of DNA. The resulting PCR products were sequenced on an Illumina HiSeq using the Rapid v2 chemistry in paired-end mode (2x250 bp), following the procedure described in Reitmeier et al. (Reitmeier et al., 2020). To control for artifacts and ensure reproducibility, two negative controls containing DNA stabilizer without stool or cecal sample were included for every 45 samples. Only high-quality sequences with read counts exceeding 5000 were used for the analysis of the 16S rRNA data. The reads in the FASTQ files were processed using an in-house NGSToolkit (Version Toolkit 3.5.2_64) based on USEARCH 11 (Edgar, 2010). Trimming with a score of 5 was performed on both ends of the R1 and R2 reads, followed by chimera removal using the FASTQ mergepair script of USEARCH (Edgar, 2010; Edgar et al., 2011). The quality-filtered reads were then merged, deduplicated, and clustered using a denoised clustering

approach to generate zero-radius operational taxonomic units (zOTUs) (Edgar, 2016). The use of zOTUs allows for higher resolution in 16S rRNA sequencing analysis by correcting sequencing errors (denoising) and identifying each unique sequence (with 100% similarity) as a distinct microbial strain. In contrast, the previous approach used operational taxonomic unit (OTU) analysis, which merges different strains with more than 97% similarity into a single OTU and assigns it to one microbial strain (Edgar, 2018). Taxonomic assignment was performed using the EZBiocloud database (Yoon et al., 2017). The data were further analyzed using the R-based pipeline RHEA (Lagkouvardos et al., 2017). Phylogenetic trees were constructed using a maximum likelihood approach, with alignments generated by MUSCLE and MegaX software (Kumar et al., 2018). The trees were visualized and annotated using the online tool EvolView (Subramanian et al., 2019). In order to determine the quantitative copy numbers of 16S rRNA genes per gram of fecal sample, 12 artificial DNA standards mimicking 16S rRNA genes were added to each weighted fecal sample before DNA extraction. The same amount of artificial DNA (6 ng) was added to each sample. After sequencing, the FASTQ files were mapped against the spike FASTA sequences using bowtie2 (Langmead & Salzberg, 2012), resulting in the removal of the spike reads and the generation of a new FASTQ file. By comparing the spike sequencing reads to the fecal bacterial reads, the quantitative number of 16S rRNA gene copies per gram of sample was calculated. The copy number of the 16S rRNA gene is proportional to the number of bacteria present in the sample. This approach allows for the estimation of microbial abundances relative to each other, making it suitable for comparative analysis (Tourlousse et al., 2017).

3.11 Fluorescence–activated cell sorting (FACS)

3.11.1 Intestinal epithelial cell isolation

Freshly isolated tissue was used for immune cell isolation. Intestinal tissues were flipped, washed out with PBS, and cut into 1cm segments. Epithelial cells were removed by incubation in Dulbecco's modified Eagle's medium (DMEM, Gibbco) supplemented with 10% fetal calf serum, 1% antibiotics/antimycotics, 0.8% L-glutamine and 20 µL of 1 M DTT while shaking for 15 minutes at 37 °C. The remaining sections were incubated at 37°C for 10 min in 200 µL of 150 mM EDTA in PBS. The cell suspension was pelleted by centrifugation. Using a 40%/20% (PBS/DMEM) percoll gradient, intestinal epithelial cells were purified by centrifugation at 600g for 30 min, followed by washing with PBS. Purified IECs were lysed in RA1 RNA lysis buffer (Machery-Nagel) for further processing.

3.11.2 Immune cell isolation

Leftover intestinal tissues after DTT/EDTA previously described steps were washed three times in Hanks buffer and digested for 15 min in Thermoshake (200 rpm) with 0.6 mg/ml type VIII collagenase

(Sigma-Aldrich) for jejunum. Colonic tissues were digested with Collagenase D (1.25 mg/ml, Sigma-Aldrich), Collagenase V (0.85 mg/ml, Sigma-Aldrich), Dispase II (1mg/ml), DNAse-V (10U/µl, Sigma) and Amphotericin (100x). Gonadal fat was isolated with the use of Collagenase II (4mg/ml), followed by erythrocytes lysis with ACK buffer (150 mM NH4CL, 10 mM KHCOO3, 0.1mM Na2EDTA). Following digestion, cells were passed through a 40 µm strainer. The spleen and mesenteric lymph nodes were directly passed through a 40 µm strainer. Cells were fixed with 2% PFA, washed, and stored in RPMI at 4 °C until further processing.

3.11.3 Staining and FACS measurements

Surface stainings were performed for 30 minutes with conjugated antibodies, depicted in **Table 8**. Cells were analyzed on a Flow Cytometer (Invitrogen™ Attune™ NxT), and analysis was performed using FlowJo software (FlowJo, LLC, version 10.7.2). Gating strategies are illustrated in **Figure 4.**

Table 8 FACS antibodies

Target	Fluorophore	Dilution	Source
CD8	PE	1/100	Bioscience
CD3	PerCP/Cy5.5	1/50	Biolegend
CD4	FITC	1/100	Bioscience

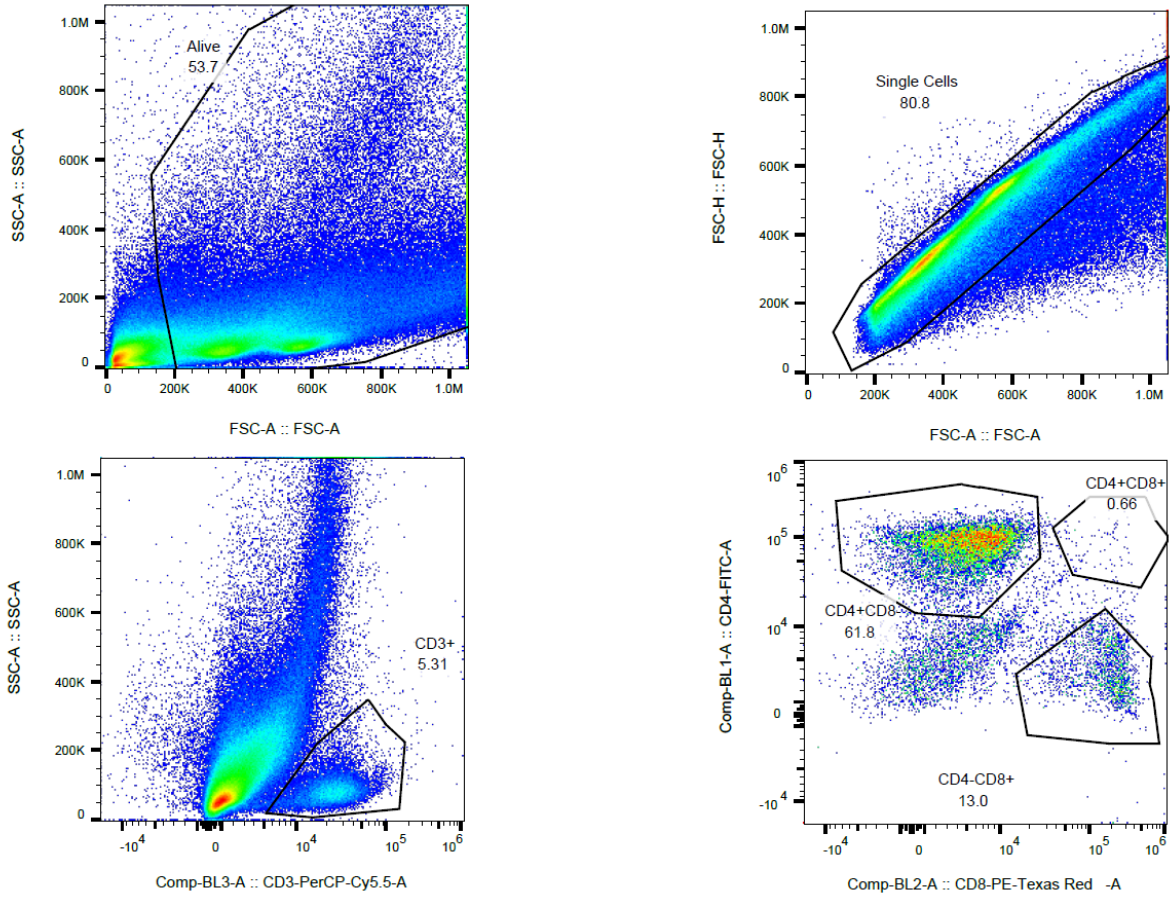

Figure 4 FACS gating strategy
Gating strategy of CD3+CD4+, CD3+CD8+. Plots are shown from a representative sample. The numbers in the plots indicate percentage of cells within each gate.

3.12 Complement 3 ELISA

Concentrations of complement 3 (C3) in fecal supernatant were measured with the use of an ELISA kit (Immunology Consultants Laboratory) according to manufactures protocol and determined by absorbance at 450/620 nm using Multiskan® spectrophotometer (Thermo Scientific).

3.13 Untargeted metabolite measurements

Cecal samples were collected from *Bmal1*$^{IEC-/-}$ mice and their controls every 4 hours over the course of a 24h day. Samples were directly snap-frozen and stored at -80 °C upon metabolite extraction. The untargeted analysis was performed using a Nexera UHPLC system (Shimadzu, Duisburg, Germany) coupled to a Q-TOF mass spectrometer (TripleTOF 6600, AB Sciex, Darmstadt, Germany) as previously

described (Weiss et al., 2022). Separation of the fecal samples was performed either using a UPLC BEH Amide 2.1 × 100 mm, 1.7 µm analytic column (Waters, Eschborn, Germany) with a 400 µL/min flow rate or with a Kinetex XB18 2.1 x 100 mm, 1.7 µm (Phenomenex, Aschaffenburg, Germany) with a 300 µL/min flow rate. For the HILIC-separation, the settings were as follows: The mobile phase was 5 mM ammonium acetate in water (eluent A) and 5 mM ammonium acetate in acetonitrile/water (95/5, v/v) (eluent B). The gradient profile was 100% B from 0 to 1.5 min, 60% B at 8 min and 20% B at 10 min to 11.5 min, and 100% B at 12 to 15 min. For the reversed-phase separation, eluent A was 0.1% formic acid, and eluent B was 0.1% formic acid in acetonitrile. The gradient profile started with 0.2% B, which was held for 0.5 min. Afterwards, the concentration of eluent B was increased to 100% until 10 min, which was held for 3.25 min. Afterwards, the column was equilibrated at starting conditions. A volume of 5 µL per sample was injected. The autosampler was cooled to 10 °C, and the column oven heated to 40 °C. Every tenth run, a quality control sample which was pooled from all samples, was injected. The samples were measured in a randomized order and in the Information Dependent Acquisition (IDA) mode. MS settings in the positive mode were as follows: Gas 1 55, Gas 2 65, Curtain gas 35, Temperature 500 °C, Ion Spray Voltage 5500, declustering potential 80. The mass range of the TOF MS and MS/MS scans were 50–2000 m/z, and the collision energy was ramped from 15–55 V. MS settings in the negative mode were as follows: Gas 1 55, Gas 2 65, Cur 35, Temperature 500 °C, Ion Spray Voltage –4500, declustering potential –80. The mass range of the TOF MS and MS/MS scans were 50–2000 m/z and the collision energy was ramped from –15–55 V.

The “msconvert” from ProteoWizard (Adusumilli & Mallick, 2017) was used to convert raw files to mzXML (de-noised by centroid peaks). The bioconductor/R package XCMS (Smith et al., 2006) was used for data processing and feature identification. More specifically, the matched filter algorithm was used to identify peaks (full width at half maximum set to 7.5 s). Then the peaks were grouped into features using the “peak density” method (Smith et al., 2006). The area under the peaks was integrated to represent the abundance of features. The retention time was adjusted based on the peak groups presented in most of the samples. To annotate possible metabolites to identified features, the exact mass and MS2 fragmentation pattern of the measured features were compared to the records in HMBD (Wishart et al., 2007) and the public MS/MS database in MSDIAL (Tsugawa et al., 2015), referred to as MS1 and MS2 annotation, respectively. The quality control samples were used to control and remove the potential batch effect, t-test was used to compare the features’ intensity between the groups.

JTK_cycle (Hughes et al., 2010) was used to identify metabolite circadian oscillations. Lists of statistically significant differential (rhythmic) metabolites were uploaded on the MetaboloAnalyst 5.0 (Pang et al., 2021) platform for pathway annotation and enrichment analysis.

3.14 Targeted metabolite analyses

3.14.1 Sample preparation for targeted metabolite analyses

Approximately 20 mg of mouse cecal content was weighed in a 2 mL bead beater tube (CKMix 2 mL, Bertin Technologies, Montigny-le-Bretonneux, France) filled with 2.8 mm ceramic beads. 1 mL of methanol-based dehydrocholic acid extraction solvent (c=1.3 µmol/L) was added as an internal standard for work-up losses. The samples were extracted with a bead beater FastPep-24TM 5G, MP Biomedicals Germany GmbH, Eschwege, Germany) supplied with a CoolPrepTM (MP Biomedicals Germany, cooled with dry ice) for 3 times each for 20 seconds of beating at a speed of 6 m/sec and followed by a 30 seconds break.

3.14.2 Targeted bile acid measurement

20 µL of isotopically labeled bile acids (ca. 7 µM each) were added to 100 µL of sample extract. Targeted bile acid measurement was performed using a QTRAP 5500 triple quadrupole mass spectrometer (Sciex, Darmstadt, Germany) coupled to an ExionLC AD (Sciex, Darmstadt, Germany) ultrahigh performance liquid chromatography system. A multiple reaction monitoring (MRM) method was used for the detection and quantification of the bile acids. An electrospray ion voltage of −4500 V and the following ion source parameters were used: curtain gas (35 psi), temperature (450 °C), gas 1 (55 psi), gas 2 (65 psi), and entrance potential (−10 V). The MS parameters and LC conditions were optimized using commercially available standards of endogenous bile acids and deuterated bile acids for the simultaneous quantification of selected 27 analytes. For separation of the analytes a 100 × 2.1 mm, 100 Å, 1.7 µm, Kinetex C18 column (Phenomenex, Aschaffenburg, Germany) was used. Chromatographic separation was performed with a constant flow rate of 0.4 mL/min using a mobile phase consisting of water (eluent A) and acetonitrile/water (95/5, v/v, eluent B), both containing 5 mM ammonium acetate and 0.1% formic acid. The gradient elution started with 25% B for 2 min, increased at 3.5 min to 27% B, in 2 min to 35% B, which was held until 10 min, increased in 1 min to 43% B, held for 1 min, increased in 2 min to 58% B; held 3 min isocratically at 58% B, then the concentration was increased to 65% at 17.5 min, with another increase to 80% B at 18 min, following an increase at 19 min to 100% B which was hold for 1 min, at 20.5 min the column was equilibrated for 4.5 min at starting. The injection volume for all samples was 1 µL, the column oven temperature was set to 40 °C, and the auto-sampler was kept at 15 °C. Data acquisition and instrumental control were performed with Analyst 1.7 software (Sciex, Darmstadt, Germany) (Reiter et al., 2021).

BAs measured are Cholic acid (CA), chenodeoxycholic acid (CDCA), a-Muricholic acid (aMCA), b-Muricholic acid (bMCA), Taurocholic acid (TCA), Taurochenodeoxycholic acid (TCDCA),

Tauroursodeoxycholic acid (TUDCA), Taurohyodeoxycholic acid (THDCA), Taurolithocholic acid (TLCA), Taurodeoxycholic acid (TDCA), Tauro-a-Muricholic acid (TaMCA), Glycochenodeoxycholic acid (GCDCA), Glycocholic acid (GCA), Deoxycholic acid (DCA), Lithocholic acid (LCA), y-Muricholic acid (y-MCA), 12-Dehydrocholic acid (12-DHCA), 12-Ketolithocholic acid (12-keto-LCA), 3-Dehydrocholic acid (3-DHCA), 6-Ketolithocholic acid (6-keto-LCA), 7-Dehydrocholic acid (7-DHCA), 7-Sulfocholic acid (7-sulfo-CA), Allocholic acid (ACA), Cholic acid-7ol-3one (CA-7ol-3one), Ursocholic acid (UCA), Dehydrolithocholic acid (DHLCA), Hyodeoxycholic acid (HDCA), Murideoxycholic acid (MDCA), Ursodeoxycholic acid (UDCA).

3.14.3 Targeted short-chain fatty acid measurement

The 3-NPH method was used for the quantitation of SCFAs (Han, Lin et al. 2015). Briefly, 40 µL of the fecal extract and 15 µL of isotopically labeled standards (ca 50 µM) were mixed with 20 µL 120 mM EDC HCl-6% pyridine-solution and 20 µL of 200 mM 3-NPH HCL solution. After 30 min at 40°C and shaking at 1000 rpm using an Eppendorf Thermomix (Eppendorf, Hamburg, Germany), 900 µL acetonitrile/water (50/50, v/v) was added. After centrifugation at 13000 U/min for 2 min, the clear supernatant was used for analysis. The same system as described above was used. The electrospray voltage was set to -4500 V, curtain gas to 35 psi, ion source gas 1 to 55, ion source gas 2 to 65, and the temperature to 500°C. The MRM-parameters were optimized using commercially available standards for the SCFAs. The chromatographic separation was performed on a 100 × 2.1 mm, 100 Å, 1.7 µm, Kinetex C18 column (Phenomenex, Aschaffenburg, Germany) with 0.1% formic acid (eluent A) and 0.1% formic acid in acetonitrile (eluent B) as elution solvents. An injection volume of 1 µL and a flow rate of 0.4 mL/min was used. The gradient elution started at 23% B, which was held for 3 min, afterwards the concentration was increased to 30% B at 4 min, with another increase to 40%B at 6.5 min, at 7 min 100% B was used, which was held for 1 min, at 8.5 min the column was equilibrated at starting conditions. The column oven was set to 40°C and the autosampler to 15°C. Data acquisition and instrumental control were performed with Analyst 1.7 software (Sciex, Darmstadt, Germany).

3.14.4 Targeted metabolite analyses

MultiQuant 3.0.3 Software (AB Sciex) was used to integrate the data and calculate the concentration. Isotopically labeled standards were used for SCFA quantitation. For bile acid quantitation, we used Dehydrocholic acid as an internal standard to correct for losses during sample preparation and isotopically labeled references to correct for ionization effects during measurement, according to the paper of Reiter et al. 2021 (Reiter et al., 2021). For comparison between the two groups, Mann-Whitney U test was used to test for statistical significance. Metabolite-microbiota correlation analyses were performed on relative abundance zOTU level within the rhythmic in male control (*Bmal1*$^{fl/fl}$), but not *Bmal1*$^{IEC-/-}$ samples with at least a 30% prevalence. Spearman correlation and adjusted p-values

between targeted metabolomics and zOTUs were calculated using the *rcor()* function in R. Correlation matrixes were visualized within the R package "corrplot" (Wei, 2021). Only correlations were plotted with a P-value of <0.05 and coefficient values R ≤ −0.5 and ≥0.5. Furthermore, M2IA online platform (Ni et al., 2020) was used for the global similarity analyses (PA plot) between metabolome and microbiota data.

3.15 PICRUST 2.0

For the prediction of metagenomics functionality, the sequences of the intestinal clock-controlled zOTUs, captured as described above, were used to construct the metagenome using PICRUST2.0 (Douglas et al., 2020). The corrected zOTU 16 s rRNA gene copy number was multiplied by the predicted functionality to predict the metagenome. Resulted enzymatic genes classified according to Enzyme Commission (EC) numbers were mapped to Metacyc pathways. Superclasses were removed, and Metacyc pathway abundance was used for rhythmicity analyses over time with the use of JTK_analyses (Hughes et al., 2010).

3.16 Statistical Analyses

Statistical analyses were performed with the use of R and GraphPad Prism (GraphPad Software V8). Rhythmicity analyses and differential rhythm analyses were done with the use of JTK_cycle and CompareRhythm R scripts (Hughes et al., 2010; Pelikan et al., 2022). In addition, the circadian phase was calculated with the use of the cosine-wave equation: y=baseline+(amplitude·cos(2·π·((x-[phase shift)/24))), with a fixed 24-h period. Connected straight lines of individual 24h period graphs within the figures indicate significant rhythmicity based on cosine analyses, whereas dashed lines indicate non-significant cosine fit. Analysis between two groups were performed using the non-parametric Mann-Whitney U test. Statistics of more than two groups and dietary conditions was performed with a two-way ANOVA. A p-value ≤ 0.05 was assumed as statistically significant. Rhea pipeline (Lagkouvardos et al., 2017) was used for microbial diversity calculations using generalized UniFrac v1.1. distances and illustrated with MDS. Heatmaps were generated using the heatmap.2 R script. Heatmaps were sorted based on the peak phase of controls. Abundance plots and fold change plots were generated using SIAMCAT package in R using the "check.associations() function". Polargraphs were made with the use of ggplot R package. Visualisation of zOTUs and sample trees were conducted using the online platform "evolgenius.info". Spearman correlation and adjusted p-values between targeted metabolomics and zOTUs were calculated using the *rcor()* function in R. Correlation matrixes were visualized within the R package "corrplot" (Wei, 2021).

4. Results

4.1 Loss of intestinal *Bmal1* does not alter circadian behavior

The circadian clock plays a vital role in regulating the rhythmic functions of the host's physiological processes, thereby contributing to overall host health. In mouse models, system-wide and tissue-specific loss of brain and muscle ARNT-Like 1 *(Bmal1)*, an essential circadian clock gene, leads to disruptions in glucose and lipid metabolism, adipocyte differentiation, and arrhythmic production of microbial metabolites (Lamia et al., 2008; Rudic et al., 2004; Shimba et al., 2005). These studies emphasize the significance of maintaining a functional circadian clock for proper host metabolism. Notably, the gastrointestinal (GI) tract plays an essential role in metabolic homeostasis, as it is the first organ to encounter nutrients. Previous studies have indicated several rhythmic intestinal processes related to metabolism. However, whether the circadian clock regulates them remains to be elucidated (Hoogerwerf et al., 2008; Sladek et al., 2007). In this study, the aim was to investigate whether the peripheral intestinal clock controls rhythmic intestinal processes that are important for metabolism. To achieve this, a mouse model with a specific knockout of the core clock gene *Bmal1* in intestinal epithelial cells (IECs) was generated.

To create the mouse model, transgenic Villin-Cre mice were crossed with mice carrying *Bmal1* exon 8 floxed allele ($Bmal1^{fl/fl}$). This breeding strategy allowed us to selectively delete the core clock gene *Bmal1* in IECs, referred to as $Bmal1^{IEC-/-}$ mice. Mice were sampled at six different time points (CT1, CT5, CT9, CT13, CT17, CT21) over the circadian day in constant darkness (DD). In DD, endogenous rhythms can be measured as entrainment by light is eliminated. As expected, *Bmal1* circadian core clock gene expression was both arrhythmic and downregulated in all tissue sections of the intestine, including the jejunum, cecum, and proximal colon in $Bmal1^{IEC-/-}$ mice **(Figure 5A)**. The residual *Bmal1* expression was likely derived from (non)intestinal cells in which Villin-Cre is not expressed, such as tuft cells, vascular epithelial cells, and muscle or immune cells (Esmaeilniakooshkghazi et al., 2020; Madison et al., 2002). Additionally, the circadian rhythms of the clock gene expression of the nuclear receptor subfamily 1 group D member 1 *(Rev-Erbα)* were abolished in the jejunum and proximal colon, while they were dampened in the cecum **(Figure 5B)**. Importantly, the peripheral clock gene expression in the liver remained rhythmic, confirming the specific ablation of the circadian clock in the intestine of $Bmal1^{IEC-/-}$ mice **(Figure 5A, B).**

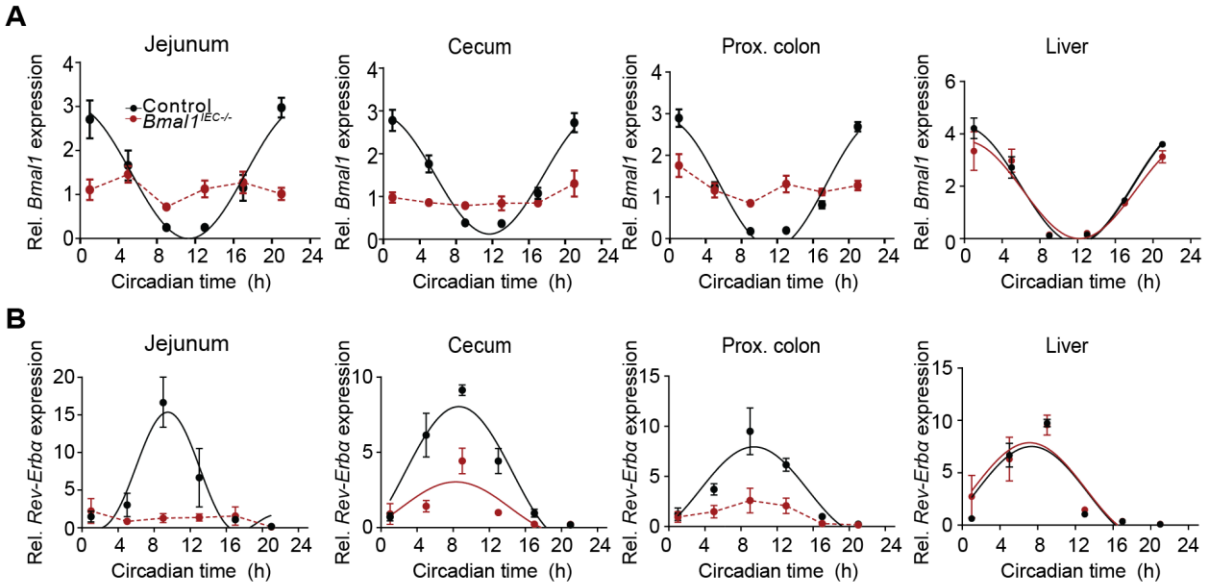

Figure 5 Confirmed deletion of *Bmal1* in intestinal tissue sections of *Bmal1*$^{IEC-/-}$ mice.
(A) Core *Bmal1* and **(B)** *Rev-Erbα* clock gene expression profiles within intestinal tissues and liver measured in constant darkness every 4 hours. Data are presented as mean ± SEM. Significant rhythms (cosine-wave regression, p-value ≤ 0.05) are illustrated with fitted cosine-wave curves; data points connected by dotted lines indicate no significant cosine fit curves (p-value > 0.05) and thus no rhythmicity.

Deletion of core clock genes can have a significant impact on circadian behavior, including locomotor and feeding activity, as observed in studies with whole-body *Bmal1* knockout mice (Bunger et al., 2000). In this study, circadian locomotor activity in *Bmal1*$^{IEC-/-}$ mice was investigated using running-wheel cages under different light conditions. Under a 12-hour light: 12-hour dark paradigm (LD), *Bmal1*$^{IEC-/-}$ mice exhibited rhythmic activity primarily during the dark phase, similar to their control counterparts **(Figure 6A, B)**. To examine the endogenous rhythms, *Bmal1*$^{IEC-/-}$ mice were subsequently exposed to constant darkness (DD) after two weeks in the LD cycle. Notably, the *Bmal1*$^{IEC-/-}$ mice maintained intact circadian locomotor activity **(Figure 6A-B),** indicating that the function of the suprachiasmatic nucleus (SCN), the central pacemaker, remained unaffected. In addition, food intake patterns, total food intake, and fecal output remained unaltered in the absence of a functional intestinal clock **(Figure 6C-E)**. These findings highlight the presence of a functional central pacemaker in intestinal clock-deficient mice, allowing further investigations of the intestinal clock in isolation from other clocks while considering regular circadian feeding and locomotor activity.

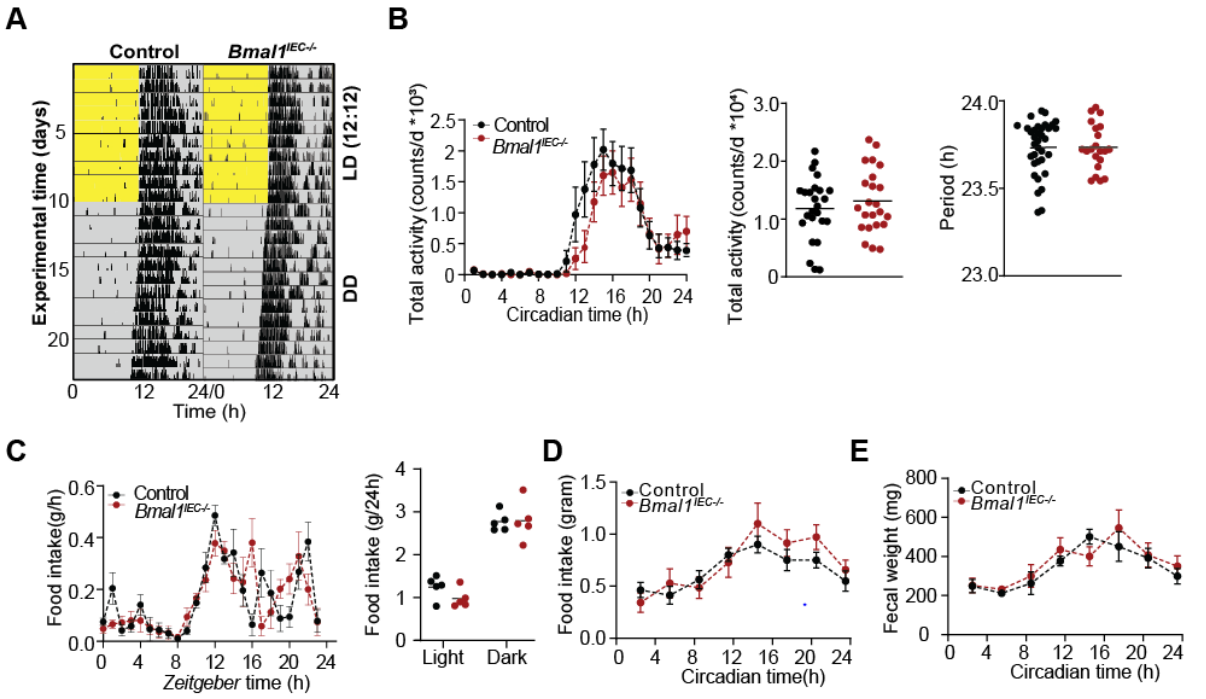

Figure 6 Mice with intestinal specific *Bmal1* deletion do not exhibit a circadian phenotype.
(A) Actogram depicting wheel running activity of *Bmal1*$^{IEC-/-}$ and control (*Bmal1*$^{fl/fl}$) mice in light-dark (12:12) (LD) and continuous darkness (DD). **(B)** Total activity (wheel counts) over the 24-hour day (left) and total circadian activity over the full day (middle) as well as the period (τ) (right). **(C)** Total food intake over 24-hours in LD conditions and their quantification summed up over the light phase (ZT1-12) and dark phase (ZT13-24). **(D)** Total food intake over 24-hours in DD conditions. **(E)** Total fecal weight measured over 24-hour in DD conditions.

Further characterization of *Bmal1*$^{IEC-/-}$ mice revealed no significant changes in the weight of dissected organs, including the liver, cecum, stomach, gonadal fat (eWAT), subcutaneous fat (sWAT), pancreas, spleen, and mesenteric lymph nodes (mLN), when compared to control mice **(Supplementary Figure 1A, B)**. However, the total length of the jejunum and the colon density (weight per cm) exhibited a significant increase in *Bmal1*$^{IEC-/-}$ mice **(Figure 7A, B)**. Nonetheless, morphological analysis of the jejunum revealed no alterations in the length of crypts or villi **(Figure 7C)**. Interestingly, intestinal *Bmal1* ablation led to a significant phase shift of 6.3 hours (p=0.016) in jejunal permeability, as evidenced by fluorescein translocation **(Figure 7D)**. Despite this shift, the total jejunal permeability, gastrointestinal transit time (GITT), as well as the expression of the tight-junction marker *Occludin* and adherens junction *E-cadherin* remained similar between the genotypes **(Figure 7D, Supplementary Figure 1C, D)**.

Alterations in jejunum permeability and length could potentially influence the interactions between luminal content and intestinal epithelial cells. Of particular interest, goblet cells play a pivotal role in producing mucus, which forms a protective barrier on the luminal surface of the intestinal epithelium. This mucus layer acts as a first-line defense against harmful pathogens and toxins present in the gut lumen and is crucial for mediating the cross-talk between gut microbes and the host. Specifically, cross-

feeding interactions, where microbial metabolism of mucin glycans influences the abundance of other microbial taxa, have been implicated in shaping the gut microbiome composition (Fang et al., 2021). To assess the status of mucin production, staining of mucin was performed with Periodic acid Schiff-alcian blue (PAS-AB) on jejunal tissue from *Bmal1*$^{IEC-/-}$ mice and their controls. The results demonstrated a significant loss of mucus-filled goblet cells in the jejunal epithelium of *Bmal1*$^{IEC-/-}$ mice **(Figure 7F)**.

Collectively, these findings demonstrate that the specific loss of *Bmal1* in the intestine leads to minor alterations in intestinal parameters, including increased colon density, altered permeability, and reduced mucus production. These changes suggest potential implications for intestinal function and microbial interactions in the absence of a functional intestinal clock.

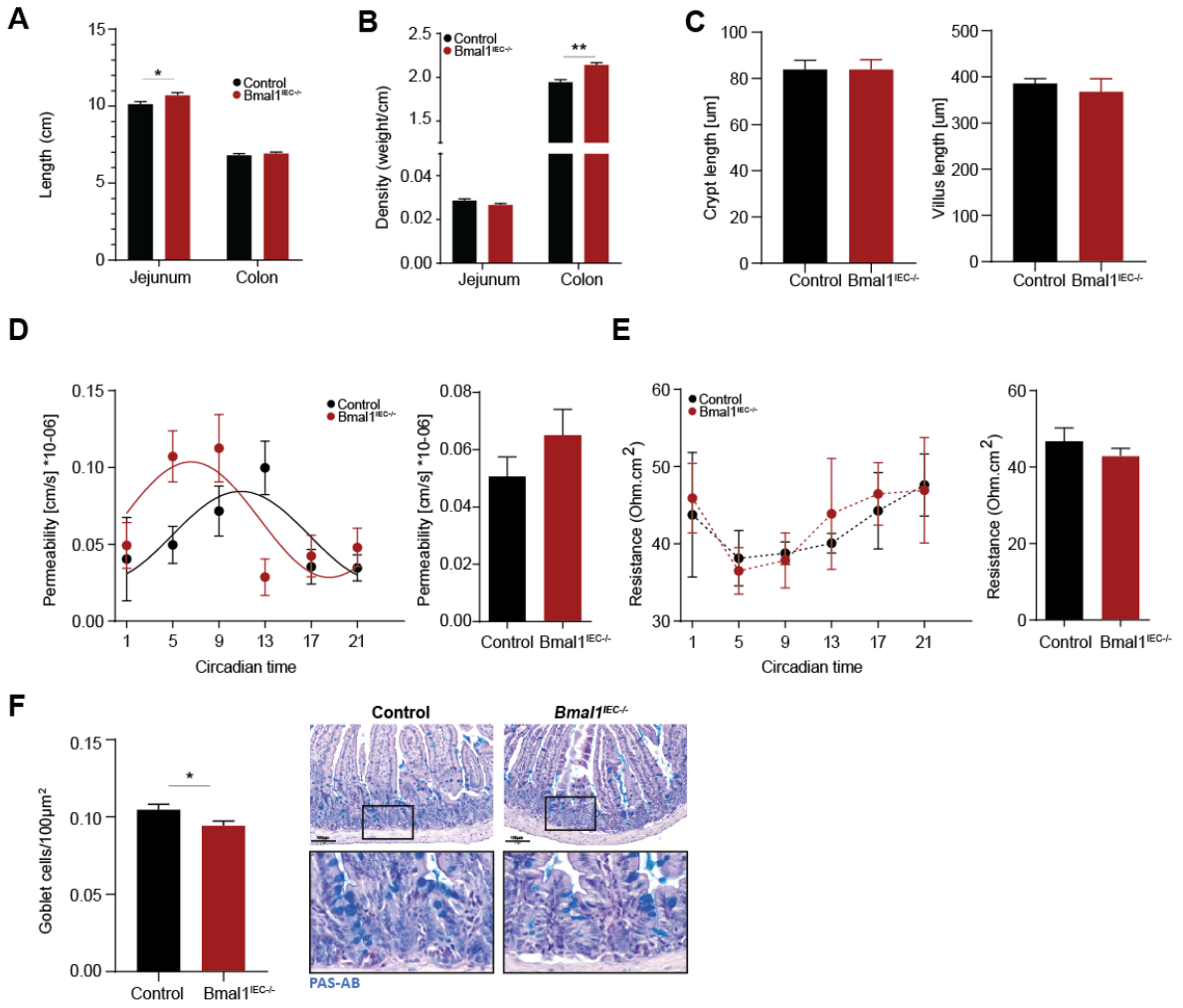

Figure 7 Slight alterations in jejunal parameters in *Bmal1*$^{IEC-/-}$ mice.
(A) Total intestinal segment length (cm). **(B)** Intestinal segment density (weight/cm). **(C)** Jejunum crypt and villus length. **(D)** Permeability measured by Ussing chamber over time in constant darkness (left) and total permeability quantified (right). **(E)** Resistance measured by Ussing chamber over time (left) and quantified (right). **(F)** PAS-AB staining for mucus-filled goblet cells. Asterisks indicate significant differences * p<0.05, ** p<0.01. Significant rhythms (cosine-wave regression, p-value ≤ 0.05) are illustrated with fitted cosine-wave curves; data points connected by dotted lines indicate no significant cosine fit curves (p-value > 0.05) and thus no rhythmicity.

4.2 The intestinal clock regulates fecal microbial rhythmicity.

The alterations in intestinal morphology and functioning observed in *Bmal1*$^{IEC-/-}$ mice raise intriguing questions regarding the potential impact on circadian microbial dynamics within the gut. The circadian clock has been shown to play a crucial role in shaping the rhythmic composition and activity of the gut microbiota (Liang et al., 2015; Thaiss et al., 2014). To investigate the consequences of intestinal clock deficiency on the circadian microbial landscape, 16S rRNA sequencing was performed targeting the V3/V4 variable regions using fecal samples obtained from mice kept under constant darkness.

The analyses of microbial profiling unveiled a clear separation in β-diversity, indicating a dissimilarity of the fecal microbiota between control and *Bmal1*$^{IEC-/-}$ mice **(Figure 8A)**. In control mice, distinct rhythmic patterns in alpha-diversity (richness) were observed over the circadian day, with the lowest richness occurring at CT9, a few hours prior to the onset of activity **(Figure 8B).** Intriguingly, intestinal ablation of *Bmal1* resulted in complete arrhythmicity in alpha-diversity **(Figure 8B).** To further investigate the microbial composition, the relative abundance over time was analyzed, as well as the relative quantification of the copy number of 16S rRNA genes using synthetic DNA spikes, a technique known as "quantitative abundance" analysis (Tourlousse et al., 2017). This approach prevents the masking of rhythmic microbial communities based on the presence of highly abundant taxa.

Quantitative abundance analyses revealed a loss in rhythmicity of the highly abundant phylum Firmicutes in *Bmal1*$^{IEC-/-}$ mice, despite observing comparable rhythmicity in relative abundance between genotypes (**Figure 8C**). In control mice, Firmicutes and Bacteroidetes oscillated in antiphase, with Bacteroidetes peaking at CT12, corresponding to the day-night transition, and Firmicutes peaking during the early night (CT1) (**Figure 8C**). This rhythmic pattern was consistent across both relative and quantitative abundance analyses (**Figure 8C**). Furthermore, *Bmal1*$^{IEC-/-}$ mice exhibited a significant downregulation of total bacterial abundance and quantitative abundance of both Firmicutes and Bacteroidetes compared to their controls **(Figure 8C, Supplement Figure 2)**.

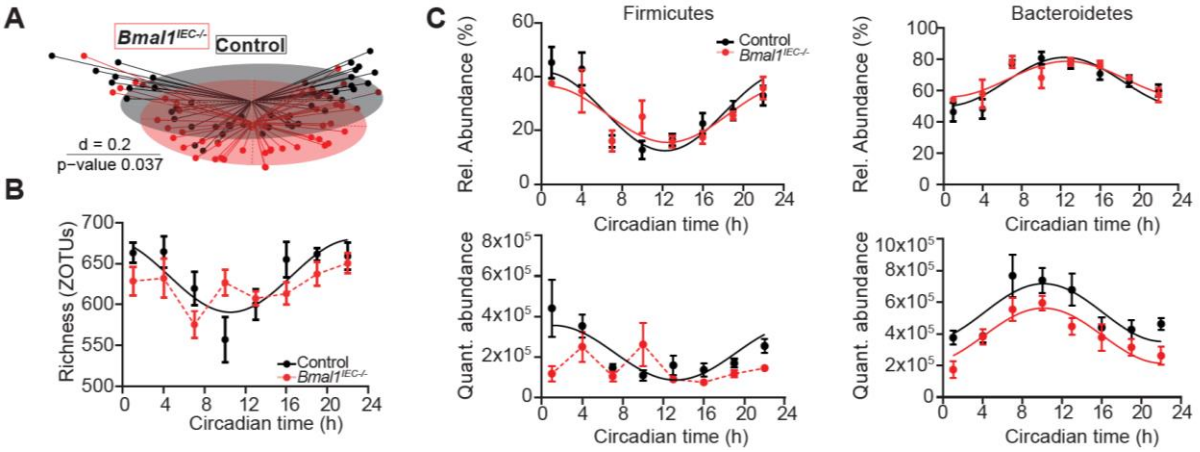

Figure 8 Intestinal *Bmal1* deletion results in arrhythmicity of major phyla.
(A) Beta-diversity (MDS plot) of fecal microbiota analyzed by generalized UniFrac distances stratified by genotype **(B)** Circadian (DD) profile of richness **(C)** Circadian rhythms of major phyla measured by relative (top) and quantitative (bottom) abundance. Significant rhythms (cosine-wave regression, p-value ≤ 0.05) are illustrated with fitted cosine-wave curves; data points connected by dotted lines indicate no significant cosine fit curves (p-value > 0.05) and thus no rhythmicity.

To investigate the rhythmicity of individual bacterial taxa, a subset of 580 prevalent (>10%) and abundant (>0.1%) zero-radius operational taxonomic units (zOTUs) was focused on and subjected to analysis using the JTK_CYCLE algorithm (Hughes et al., 2010). Approximately 60% of all zOTUs exhibited circadian rhythmicity, as demonstrated by both quantitative and relative analyses **(Figure 9A-F).** Notably, visualized by heatmaps ordered on the phase of zOTUs abundance in control mice, as well as in phase vs. amplitude plots, there was an apparent time clustering of zOTUs during the onset and end of the active phase, indicating distinct temporal patterns of specific bacteria **(Figure 9A,C,D,F)**. However, in the absence of a functional intestinal clock, approximately two-thirds of the total zOTUs lost their rhythmicity **(Figure 9B, E)**.

Further examination of specific bacterial taxa that lost rhythmicity in *Bmal1*$^{IEC-/-}$ mice highlighted the families *Lachnospiraceae, Muribaculacea,* and *Ruminococcaceae* as being predominantly under the influence of the intestinal clock **(Figure 10)**. Within these families, the genera *Oscillibacter, Fusimonas, Lactobacillus, Muribaculum, Pseudoflavonifractor, Roseburia* and *Ruminococcus* were significantly altered in rhythmicity **(Figure 10).** Of note, it was observed that the overall abundance of zOTUs, including *Lactobacillus, Oscillibacter, Ruminococcus,* and *Muribaculum,* was significantly decreased in *Bmal1*$^{IEC-/-}$ mice. Conversely, *Bmal1*$^{IEC-/-}$ mice exhibited an upregulation of zOTUs belonging to *Parasutterella,* and *Roseburia* **(Supplementary Figure 3).**

Together, these findings highlight the extensive impact of the intestinal clock on the rhythmicity and abundance of several bacterial taxa within the fecal microbiota.

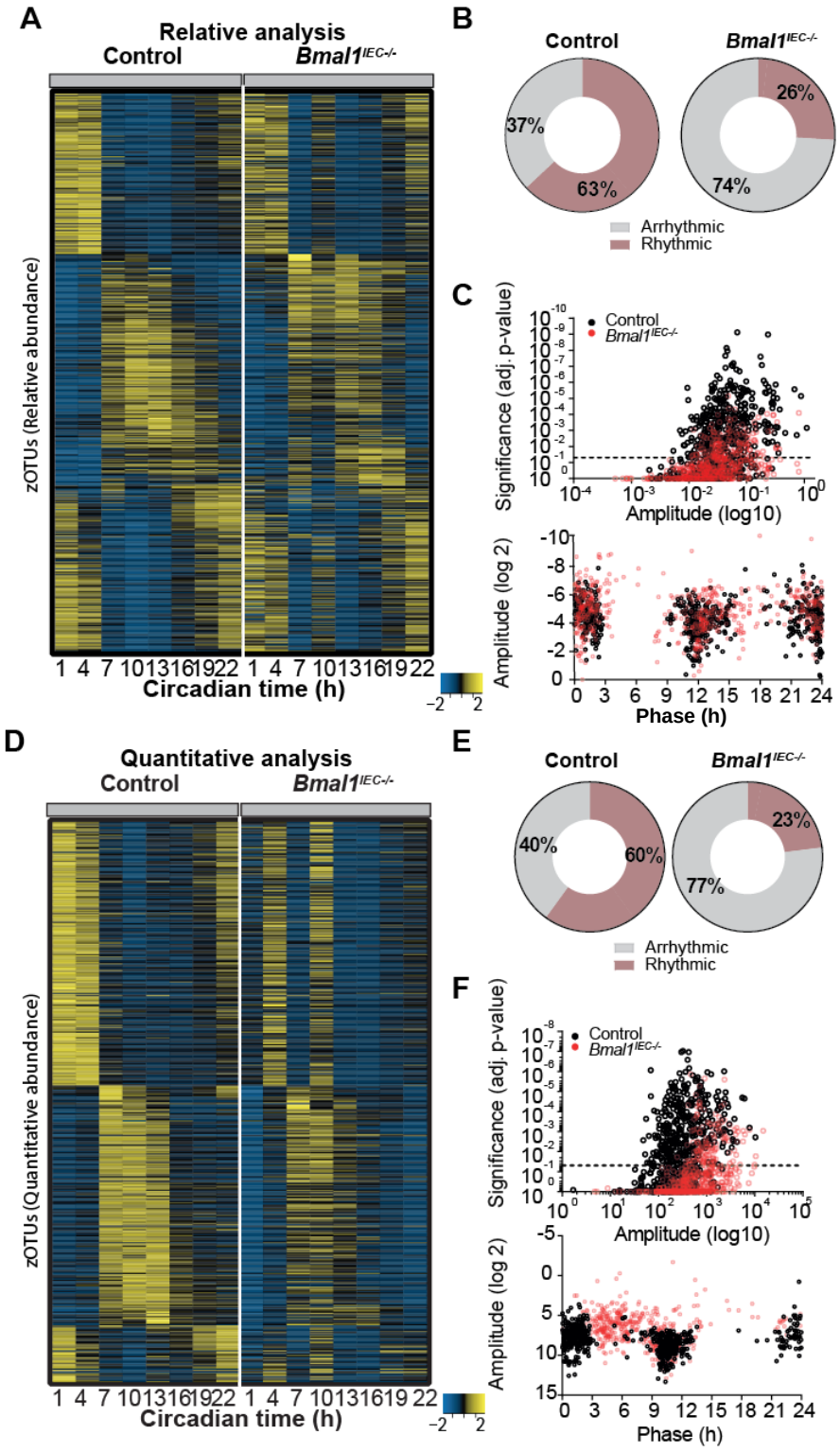

Figure 9 The intestinal clock regulates fecal microbial rhythmicity.
(A) Heatmap showing the relative abundance of 580 fecal zOTUs (mean relative abundance > 0.1%; prevalence > 10%). Every row represents one zOTU and every column one circadian time point. zOTUs are ordered based on the phase of control mice. **(B)** Pie-charts indicating the amount of rhythmic and arrhythmic zOTUs based on relative analyses. **(C)** Significance, amplitude and phase of oscillation of rhythmic and arrhythmic zOTUs based on relative analyses. **(D)** Heatmap, as described in (A), showing the quantitative abundance of 580 zOTUs. **(E)** Pie-charts indicating the amount of rhythmic and arrhythmic zOTUs based on quantitative analyses. **(F)** Significance, amplitude and phase of rhythmic and arrhythmic zOTUs based on quantitative analyses.

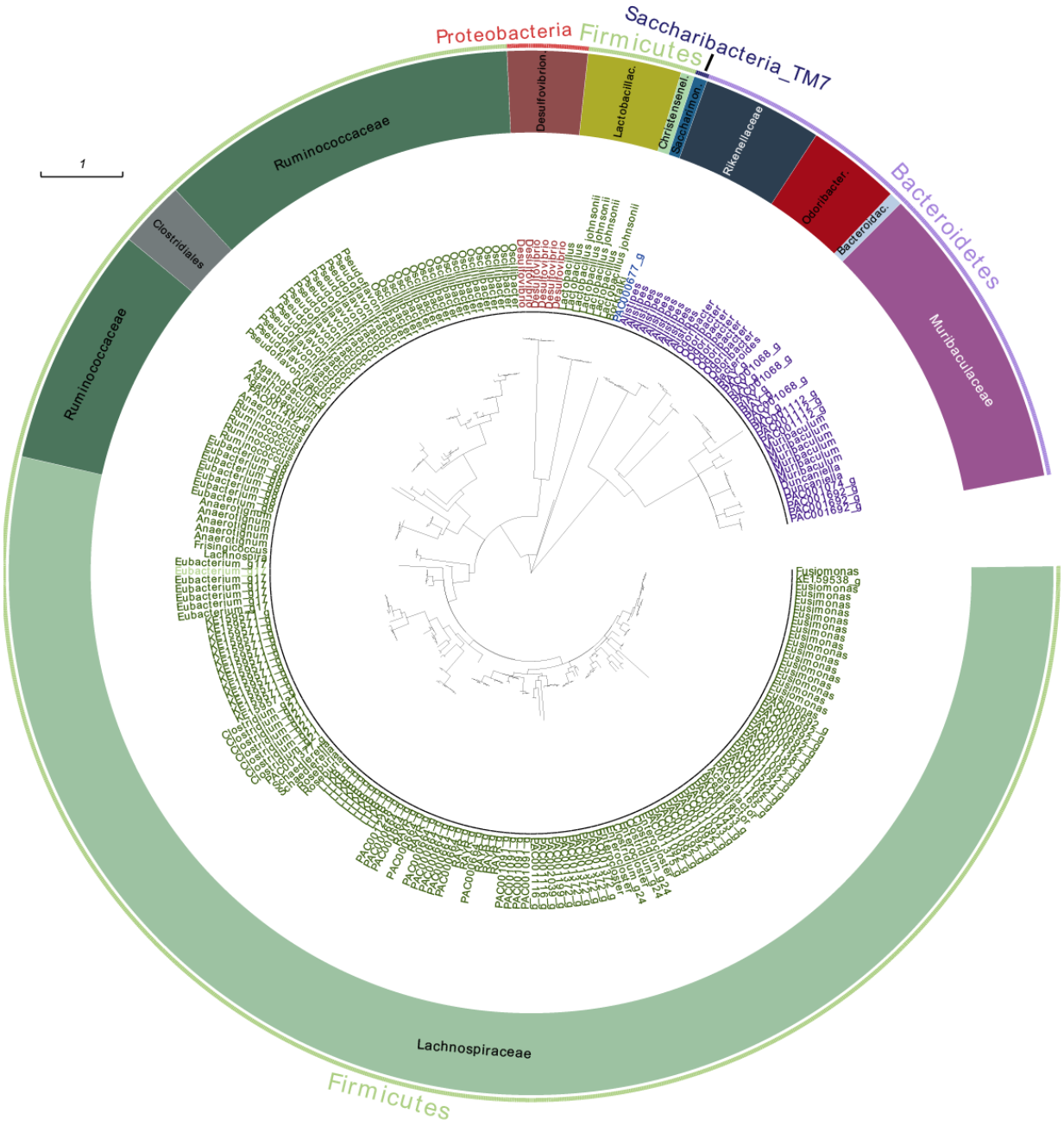

Figure 10 The intestinal clock mainly regulates the rhythmicity of the families *Lachnospiraceae, Ruminococcaceae,* and *Muribaculaceae*.

Taxonomic tree of fecal microbiota rhythmic in control mice but not in *Bmal1*$^{IEC-/-}$ mice. Rhythmicity calculations were performed on the quantitative abundance of zOTUs with the use of JTK_CYCLE. The outer dashed ring indicates phylum taxonomic rank, followed by family name (middle ring) and genera (inner ring, indicated by the individual branches).

4.3 Targeted fecal metabolomics reveals intestinal clock regulation of microbial metabolite production

Intestinal clock-controlled bacterial genera, including *Lactobacillus, Eubacterium, Clostridium,* and *Bacteroides* **(Figure 10)**, are capable of metabolizing bile acids (BAs) and carbohydrates (Yntema et al., 2023). To investigate the functional aspects of the intestinal clock-controlled microbiota, targeted measurements of short-chain fatty acids (SCFAs) and BAs in fecal samples were performed using a mass spectrometer coupled to liquid chromatography (LC-MS).

Procrustes analyses (PA) identified a significant association between intestinal clock-controlled zOTUs and SCFA concentrations (**Figure 11A**). When considering all time points, the total levels of SCFAs were comparable between genotypes. However, the level of valeric acid and low-abundant branched-chain fatty acids (BCFAs), including isovaleric acid, isobutyric acid, and 2-methylbutyric acid, were significantly upregulated in intestinal clock-deficient mice (**Figure 11B)**.

Positive significant correlations were observed between acetate, butyrate, BCFAs, and zOTUs belonging to the phylum Firmicutes, including the well-known SCFA-producing families *Lachnospiraceae* and *Ruminococcaceae* **(Figure 11C)**. Conversely, concentrations of SCFAs negatively correlated with the relative abundance of intestinal clock-driven taxa mainly belonging to the family *Muribaculaceae* of the phylum Bacteroidetes **(Figure 11C)**. Despite overall concentrations being altered, circadian rhythms in SCFAs, valeric acid, and BCFAs persisted in both genotypes, with significantly increased amplitudes for all BCFAs in *Bmal1*$^{IEC-/-}$ mice **(Figure 11D).** Notably, propionate did not exhibit oscillations in either control or *Bmal1*$^{IEC-/-}$ mice **(Figure 11D).**

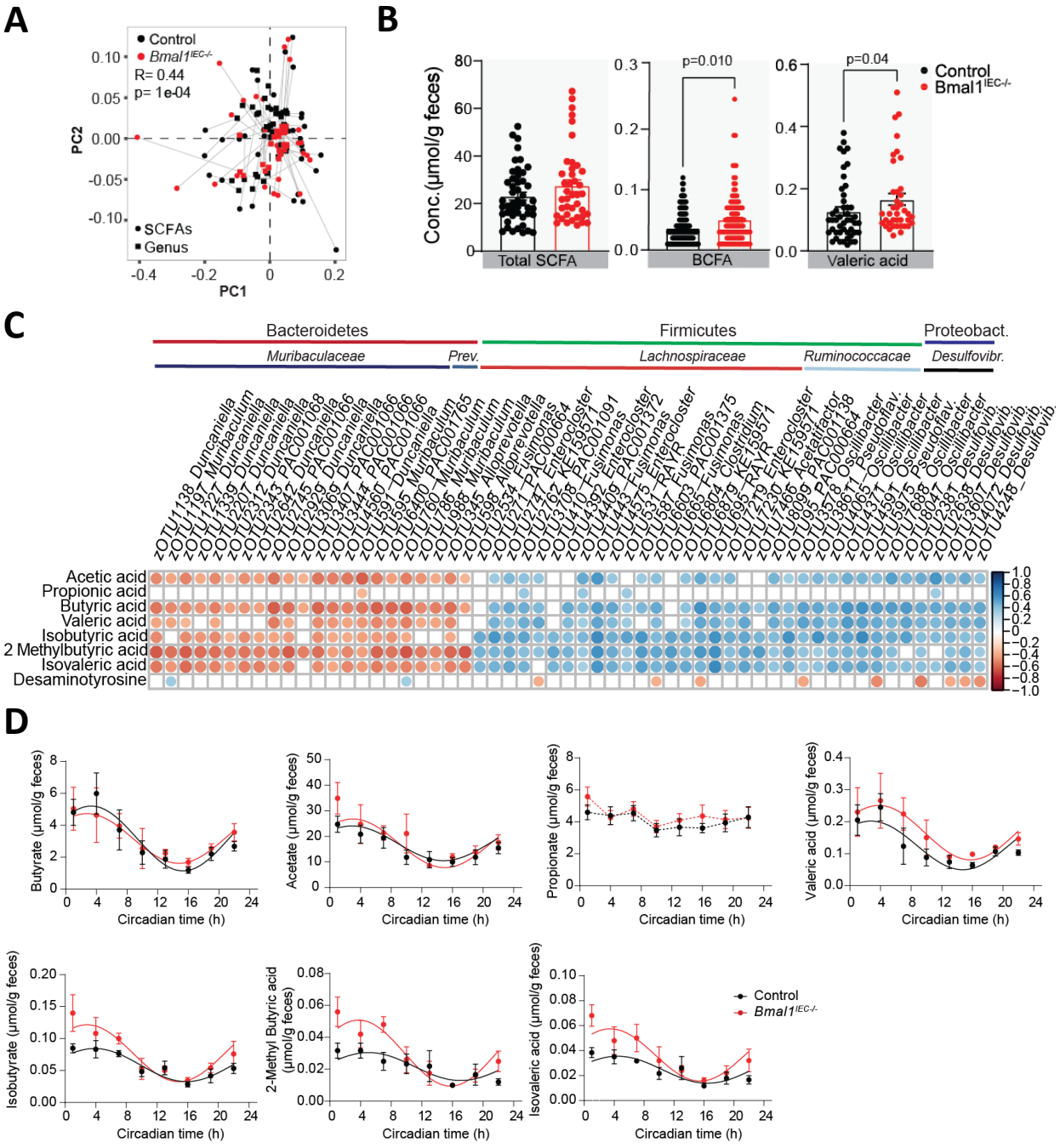

Figure 11 Bacterial alterations in intestinal clock-deficient mice results in altered fecal branched-chain fatty acids and valeric acid concentrations.

(A) Procrustes analyses (PA) of fecal microbiota and SCFA levels. The length of the line is proportional to the divergence between the data from the same mouse. **(B)** Total SFCA, BCFA and Valeric acid levels in feces. **(C)** Spearman correlation (p-value ≤ 0.05 and R ≤ − 0.5; red or R ≥ 0.5; blue) between SCFA and taxa that lost rhythmicity in *Bmal1*$^{IEC-/-}$ mice. **(D)** Circadian profiles of short-chain fatty acids, branched-chain fatty acids and valeric acid. Significant rhythms are illustrated with fitted cosine-regression (solid line); data points connected by dotted lines indicate no significant cosine fit curves (p-value > 0.05) and thus no rhythmicity.

Similar to SCFAs, there were significant associations between intestinal clock-controlled zOTUs and BA levels (**Figure 12A**). Nearly half of the measured BAs differed between genotypes, with most of the alterations observed in microbial-derived secondary BAs **(Figure 12B,C)**. BAs that were significantly upregulated in *Bmal1*$^{IEC-/-}$ mice included DCA, 6- and 12-keto-lithocholic acid (keto-LCA), murideoxycholic acid (MDCA), glycinecholic acid (GCA), cholic acid-7ol-3one (CA-7ol-3one), and hyodeoxycholic acid (HDCA). On the other hand, the BAs 7-Sulfocholic acid (7-sulfo-CA) and taurochenodeoxycholic acid (TCDCA) were downregulated in the absence of a functional intestinal clock (**Figure 12B,C**).

It is worth noting that not all BAs exhibited circadian rhythmicity in fecal samples obtained from control mice. For example, most of the conjugated BAs, DCA, and its derivatives were found to be arrhythmic **(Supplementary Figure 4)**. However, the taurine-conjugated primary BA taurourso-DCA (TUDCA), tauro-α-muricholic acid (TαMCA), taurine-DCA (TDCA) and the secondary BA 7-sulfo-CA acid were rhythmic in control mice and lost rhythmicity in *Bmal1*$^{IEC-/-}$ mice **(Figure 12D)**. In addition, TCDCA significantly reduced its amplitude in intestinal clock-deficient mice **(Figure 12D).**

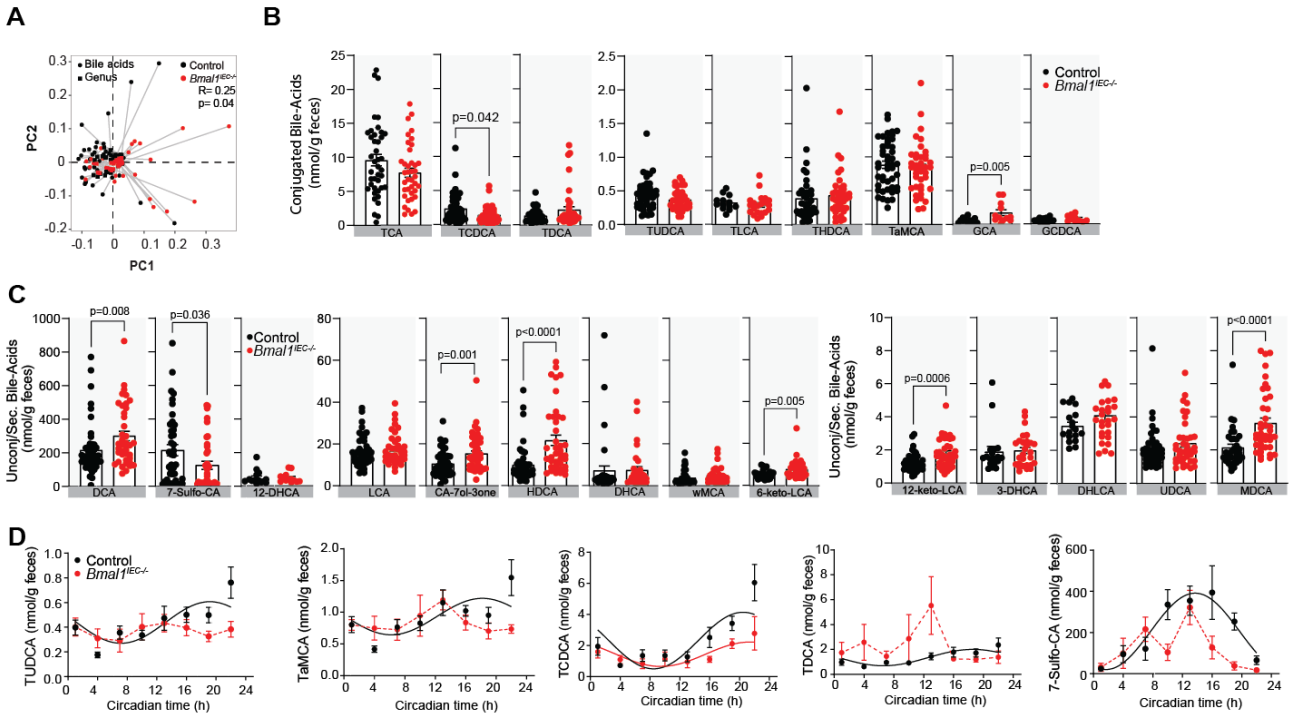

Figure 12 Bacterial alterations in intestinal clock-deficient mice results in altered fecal secondary bile acid concentrations. **(A)** Procrustes analyses (PA) of fecal microbiota and bile acid levels. **(B)** Conjugated and secondary **(C)** fecal bile acid levels combining all time points. **(D)** Circadian profiles of bile acids. Significant rhythms are illustrated with fitted cosine-regression (solid line); data points connected by dotted lines indicate no significant cosine fit curves (p-value > 0.05) and thus no rhythmicity. P-values were calculated with the use of Mann-Whitney U test

Taurine-conjugated BAs exhibited positive association with various intestinal clock-controlled taxonomic members, while secondary BAs showed negative associations with taxa from the Firmicutes phyla **(Figure 13A,B)**. For example, 7-sulfo-CA negatively correlated with *Oscillibacter, Enterocloster,* and *Eubacterium* **(Figure 13A,B),** whereas taurine-conjugated BAs positively correlated with *Alistipes, Odoribacter*, and multiple zOTUs belonging to the *Lachnospiraceae* family **(Figure 13A,B).**

In summary, our findings demonstrate that the intestinal clock-controlled microbiota plays a role in modulating microbial-related metabolites, particularly BCFAs, secondary BAs, and taurine-conjugated BAs, suggesting its involvement in host metabolism.

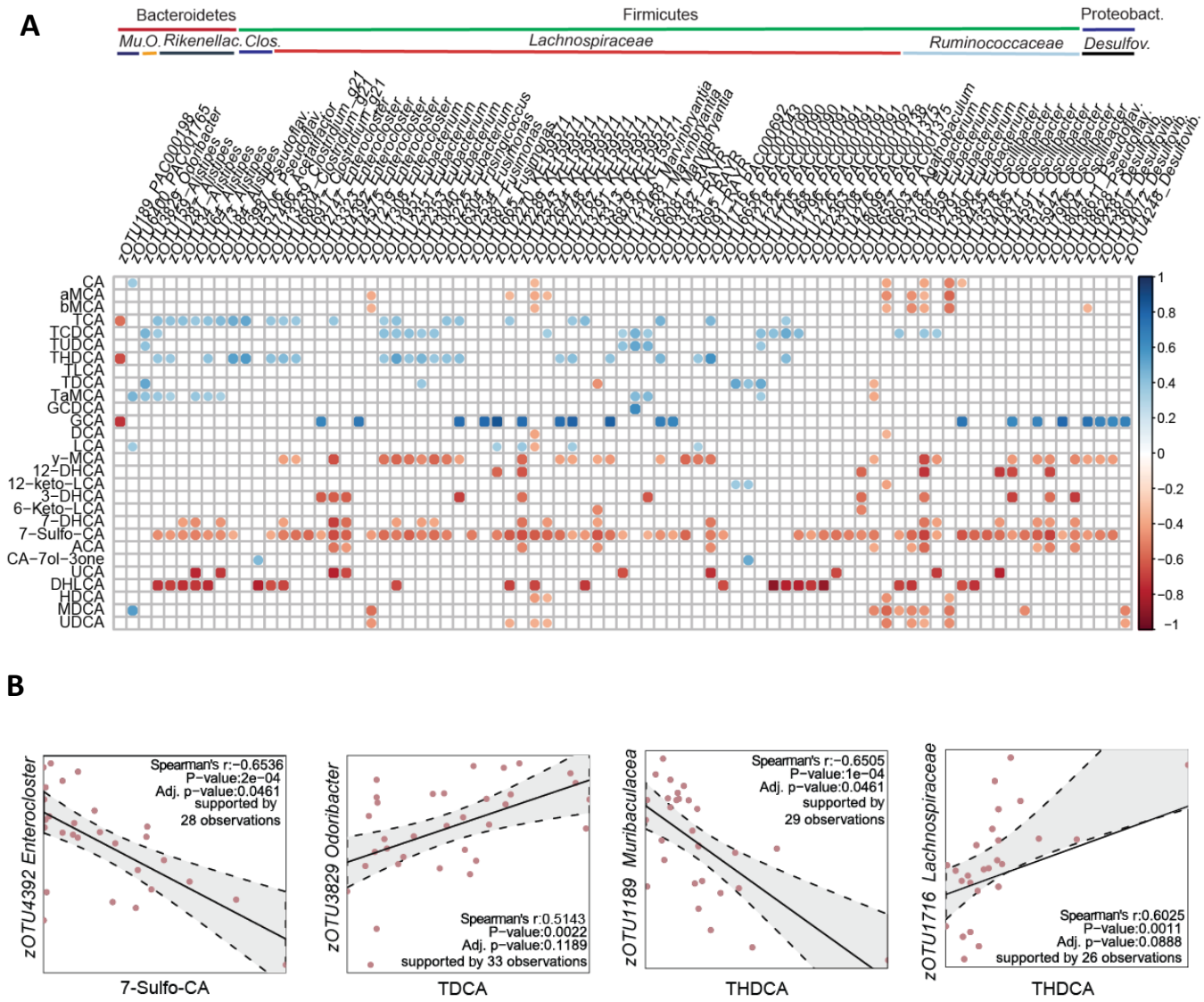

Figure 13 Intestinal clock controlled bacteria show significant correlations with bile acid concentrations.
(A) Spearman correlation of bile acids (p-value ≤ 0.05 and R ≤-0.5 (red) or R ≥ 0.5 (blue)) with gut-clock controlled bacterial taxa **(B)** and their examples.

4.4 The intestinal clock regulates the rhythmic cecal microbiota

It is widely recognized that microbial communities vary across different gastrointestinal sites. The cecum, in particular, possesses unique properties important for host immune functioning, nutrient absorption, and carbohydrate fermentation (Brown et al., 2018; Chambers et al., 2018; Laurin et al., 2011). Additionally, due to its isolation from direct fecal stream exposure, the cecal microbiota is relatively more homogenous and consistent compared to the fecal microbiota. Here, the aim was to investigate whether the intestinal clock also influences the composition of the more homogenous cecal microbiome.

Irrespective of the genotype, significant differences in microbial beta-diversity were observed between cecal and fecal samples, indicating distinct microbial community compositions **(Figure 14A).** In terms of cecal microbial characteristics between genotypes, both beta-diversity and total bacterial abundance did not exhibit significant differences **(Figure 14B,C)**. However, alpha-diversity was found to be arrhythmic in *Bmal1*$^{IEC-/-}$ mice **(Figure 14C)**. Furthermore, the major phyla Bacteroidetes and Proteobacteria displayed loss of rhythmicity in quantitative abundance upon intestinal *Bmal1* deletion (**Figure 14D)**. On the other hand, relative data demonstrated sustained microbial rhythmicity of these phyla in both genotypes **(Supplement Figure 5A)**.

Approximately 30% of the total cecal zOTUs displayed rhythmicity in both relative and quantitative analyses in control mice **(Figure 14E, Supplementary Figure 5B)**, which was notably lower compared to the rhythmicity observed in the fecal microbiota. Of note, upon intestinal clock deficiency, there was a significant loss of zOTU rhythmicity, with approximately 50% of the zOTUs showing disrupted rhythmic quantitative abundance patterns **(Figure 14E,F)**. Relative abundance analyses uncovered a total of 50 cecal zOTUs to be arrhythmic in *Bmal1*$^{IEC-/-}$ mice compared to controls **(Supplementary Figure 5B,C).**

Consistent with the fecal data, the cecal microbial taxa under the control of the intestinal clock included genera such as *Pseudoflavonifractor, Desulfovibrio, Odoribacter, Oscillibacter, Agathobaculum, Eubacterium, Clostridium,* and *Ruminococcus* **(Figure 14G,H, Supplementary Table 1)**. Notably, within the cecal microbiota, a higher number of taxa belonging to the *Muribaculacea* family were found to be regulated by the intestinal clock compared to fecal data **(Figure 14G,H, Supplementary Table 2)**. On the contrary, genera such as *Roseburia, Anaerotignum,* and *Lactobacillus* exhibited unique intestinal clock control in fecal content **(Supplementary Table 3).** Overall abundance analyses within cecal content revealed an upregulation of *Parasuterella* and *Turicibacter* in mice with intestinal clock deficiency **(Supplementary Figure 5D)**.

To profile the putative microbial functions from intestinal clock-controlled zOTUs, PICRUSt2 (Douglas et al., 2020) was used. PICRUSt2 is capable of predicting the functional potential of microbial communities based on their 16S rRNA gene sequencing data. Arrhythmic taxa were found to play essential roles in the regulation of carbohydrate and amino acid metabolism, vitamin and nucleotide biosynthesis, as well as fermentation, identified by MetaCyc pathway abundances **(Figure 15)**.

Taken together, these findings underscore the significance of the intestinal clock in governing the composition and dynamics of both the fecal and cecal microbiota. The observed differences in rhythmicity and taxonomic control between these two sites highlight the distinct functional roles and interactions of the gut microbiota across different gastrointestinal compartments.

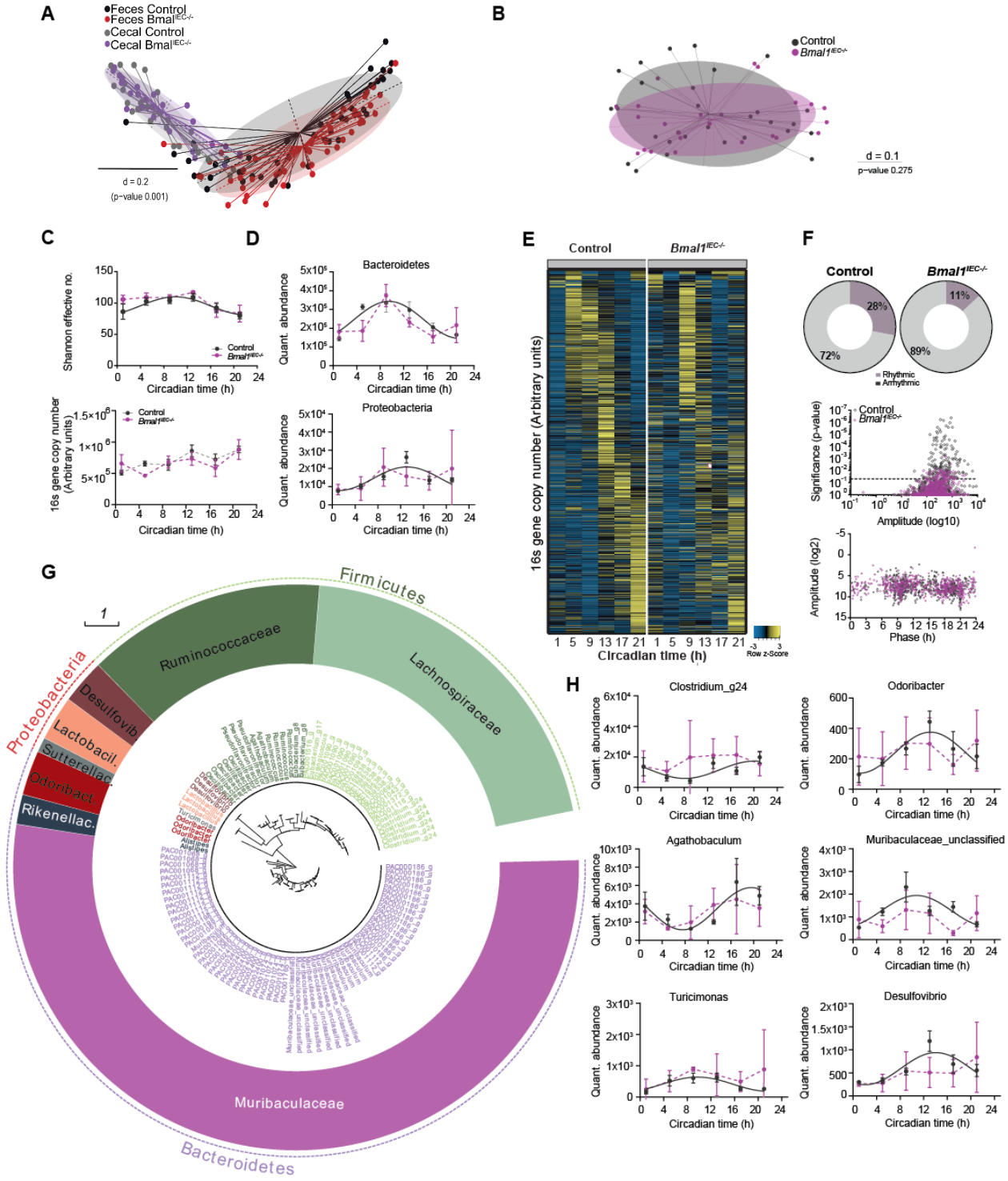

Figure 14 The intestinal clock controls the rhythmicity of the cecal microbiota.
(A) Beta-diversity MDS plot of cecal and fecal content based on generalized UniFrac distances stratified by genotype and location. **(B)** Beta-diversity MDS plot of cecal microbiota based on generalized UniFrac distances stratified by genotype. **(C)** Circadian profile of alpha-diversity and total 16s copy numbers. **(D)** Circadian profiles of Bacteroidetes and Proteobacteria. **(E)** Heatmap showing the quantitative abundance of 580 zOTUs. **(F)** Pie-charts indicating the amount of rhythmic and arrhythmic zOTUs based on quantitative analyses (top). Significance, amplitude and phase of rhythmic and arrhythmic zOTUs (bottom). **(G)** Taxonomic tree of cecal microbiota uniquely rhythmic in control mice but not in *Bmal1*$^{IEC-/-}$ mice identified by quantitative analyses. The outer dashed ring indicates phylum taxonomic rank, followed by family, and genera in the inner ring. **(H)** Circadian profiles of zOTUs losing rhythmicity in *Bmal1*$^{IEC-/-}$ mice. Significant rhythms are illustrated with fitted cosine regression (solid line); data points connected by dotted lines indicate no significant cosine fit curves (p-value > 0.05) and thus no rhythmicity.

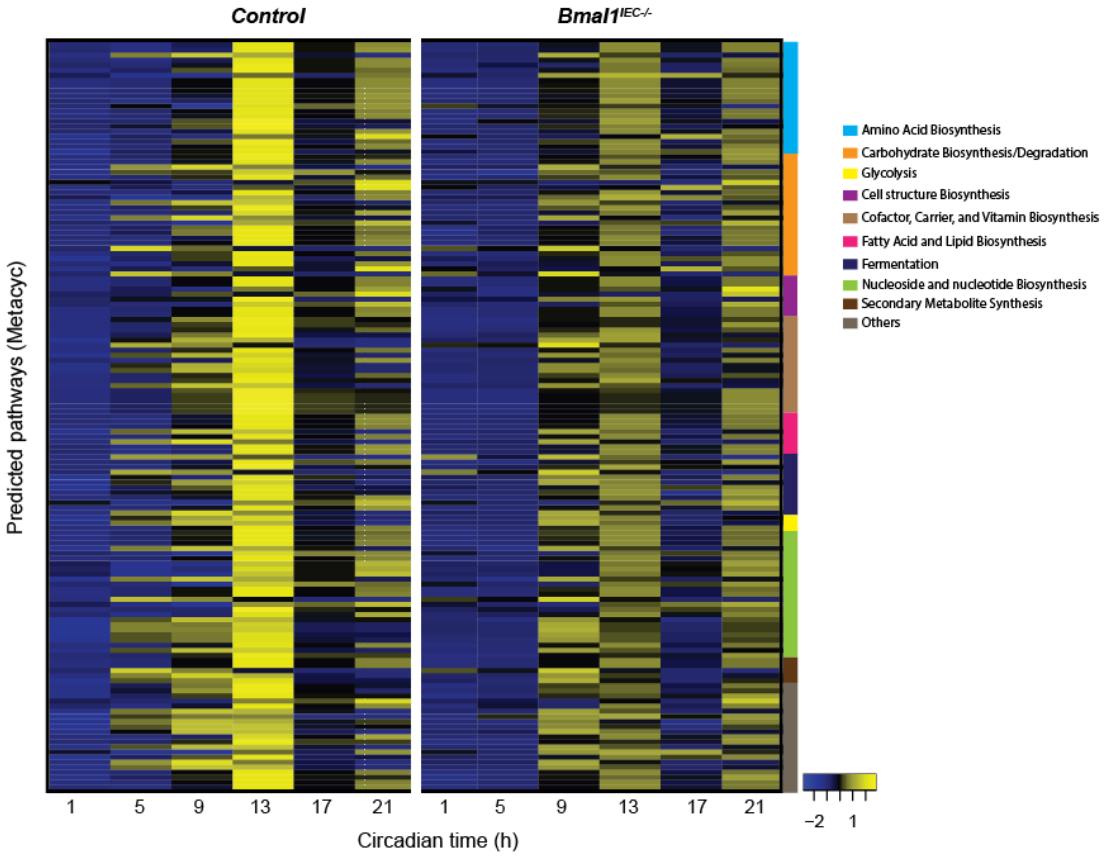

Figure 15 Functional pathways in the cecal microbiota controlled by the intestinal clock.
Heatmap of MetaCyc Pathways predicted using PICRUST2.0 on intestine clock-controlled zOTUs rhythmic in control (left) and arrhythmic in *Bmal1*$^{IEC-/-}$ (right) mice within cecal content. Pathways are colored according to their subclass depicted in the legend. Abundance is color coded with high abundance (yellow) or low abundance (blue) values.

4.5 Untargeted metabolomics reveals intestinal clock regulation of cecal metabolite rhythmicity

To further elucidate the impact of the intestinal clock on host and bacterial-derived metabolites, untargeted metabolomics was conducted using liquid chromatography-mass spectrometry (LC-MS) on cecal content collected from control and *Bmal1*$^{IEC-/-}$ mice at 4-hour intervals over a 24-hour period (DD). Both positive and negative ionization modes were employed of hydrophilic interaction ultra-high performance liquid chromatography (HILIC-UPLC) and reverse-phase UPLC (RP-UPLC) techniques to measure polar and non-polar metabolites.

Principal component analysis (PCA) did not display clear genotype separation; however, clustering within time points was evident in control samples but absent in *Bmal1*$^{IEC-/-}$ samples, particularly during the subjective daytime points of CT1 and CT5 **(Figure 16A)**. Combining data from all time points, *Bmal1*$^{IEC-/-}$ mice exhibited significant alterations in metabolites involved in taurine-, tryptophan-,

vitamin B6 metabolism, bile acid biosynthesis, and lysine- and valine/leucine/isoleucine degradation when compared to control mice **(Figure 16B)**.

Using JTK_CYCLE analyses (Hughes et al., 2010), 3686 rhythmic metabolites in the control group were identified. Strikingly, over 30% of these rhythmic metabolites lost their rhythmicity in *Bmal1*$^{IEC-/-}$ mice, as visualized in the heatmap **(Figure 16C)**. Enrichment analyses of annotated metabolites further revealed that intestinal clock-controlled metabolites are involved in various metabolic pathways, including amino acid metabolism (valine, leucine, and isoleucine biosynthesis, pantothenate and CoA biosynthesis, aminoacyl-tRNA biosynthesis), nucleotide metabolism (pyrimidine metabolism), phenylalanine metabolism, cofactors and vitamins metabolism (riboflavin metabolism, nicotinate and nicotinamide metabolism), and lipid metabolism (biosynthesis of unsaturated fatty acids, sphingolipid metabolism) **(Figure 16D)**. Notably, the intestinal clock predominantly controls metabolites related to carbohydrate metabolism, including galactose, amino sugar, nucleotide sugar, and starch and sucrose metabolism, suggesting impaired carbohydrate utilization upon intestinal clock deficiency **(Figure 16D)**.

Collectively, these results indicate that disruption of the intestinal clock results in significant alterations in host and microbial-derived metabolites, particularly related to the digestion and utilization of lipids and carbohydrates, highlighting the intricate interplay between the gut microbiota, host metabolism, and intestinal-specific circadian regulation.

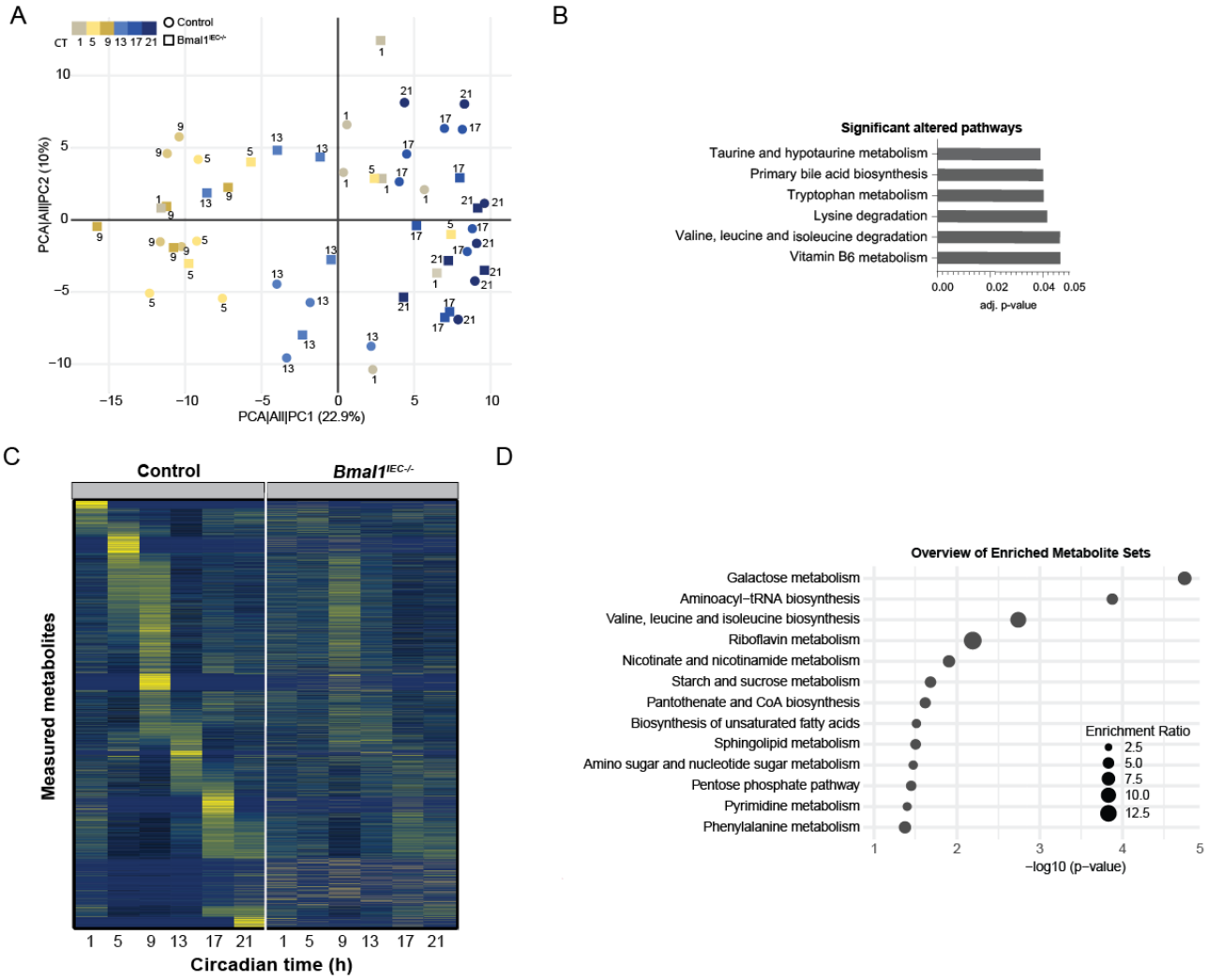

Figure 16 Untargeted metabolomics reveals the role of the intestinal clock in host metabolism.
(A) PCA plots of metabolite profiles, colors indicate time point while shape indicates genotype. **(B)** Significant different pathways between genotypes. **(C)** Heatmap of measured metabolites (rows) over the circadian time (columns). Yellow=high abundant, blue=low abundant. **(D)** Enrichment analyses of intestinal clock-controlled metabolites.

4.6 The intestinal clock regulates transcripts involved in nutrient metabolism

To shed light on the underlying genetic pathways and regulatory networks that contribute to the observed metabolic alterations upon intestinal clock disruption, transcriptional profiling was conducted using bulk RNA-sequencing of jejunal tissue sections collected over the circadian cycle (24 hours) from control and *Bmal1*$^{IEC-/-}$ mice **(Figure 17A)**. The absence of rhythmic expression in *Bmal1* and *Cry1* genes, as well as the significantly reduced amplitude of *Rev-Erbα* and *Per2* normalized gene counts confirmed jejunal clock dysfunction **(Figure 17B)**.

By analyzing all collected samples (CT1-21), more than 350 genes were identified to be differentially expressed (fold change >1, adj. p<0.05) between genotypes **(Figure 17C).** Upregulated genes in

Bmal1$^{IEC-/-}$ jejunum included Succinate Receptor 1 (*Sucnr1*), which is involved in microbiota-induced type 2 immunity (Lei et al., 2018), and transmembrane and immunoglobulin domain containing 1 (*Tmigd1*), implicated in intestinal cell differentiation (Thuring et al., 2023) **(Figure 17C).** On the other hand, downregulated genes in *Bmal1*$^{IEC-/-}$ jejunum included the metabolic-related genes Beta-Carotene Oxygenase 1 *(Bco1),* carboxylesterase 1D (*Ces1d*), Na+-sulfate cotransporter (Scl13a1) and Cytochrome P450 3A44 (*Cyp3a44*), among others **(Figure 17C).** In addition, immune-relevant genes like T-cell surface glycoprotein cd3 delta (*Cd3d*) & cd3 epsilon (*Cd3e*) chain were downregulated **(Figure 17C)**.

Gene set enrichment analysis (GSEA) of the downregulated genes in intestinal clock-deficient mice revealed significant perturbations in pathways associated with immunoregulation and cell adhesion, suggesting potential disruptions in immune function and cellular interactions **(Figure 17D).** No significant altered pathways were found in the GSEA of the upregulated genes.

Moreover, the investigation of the jejunum transcriptome over time yielded intriguing findings. PCA demonstrated distinct clustering based on the time of day (CT1-9: day; CT13-21: night) in control mice, while this effect was less pronounced in *Bmal1*$^{IEC-/-}$ mice **(Figure 17E).** Notably, employing JTK_CYCLE (Hughes et al., 2010) for circadian analyses identified 4448 genes with oscillatory expression patterns, while this number diminished by 60% in intestinal clock-deficient mice. These results highlight the substantial disruption in rhythmic intestinal gene expression patterns associated with the loss of intestinal clock function.

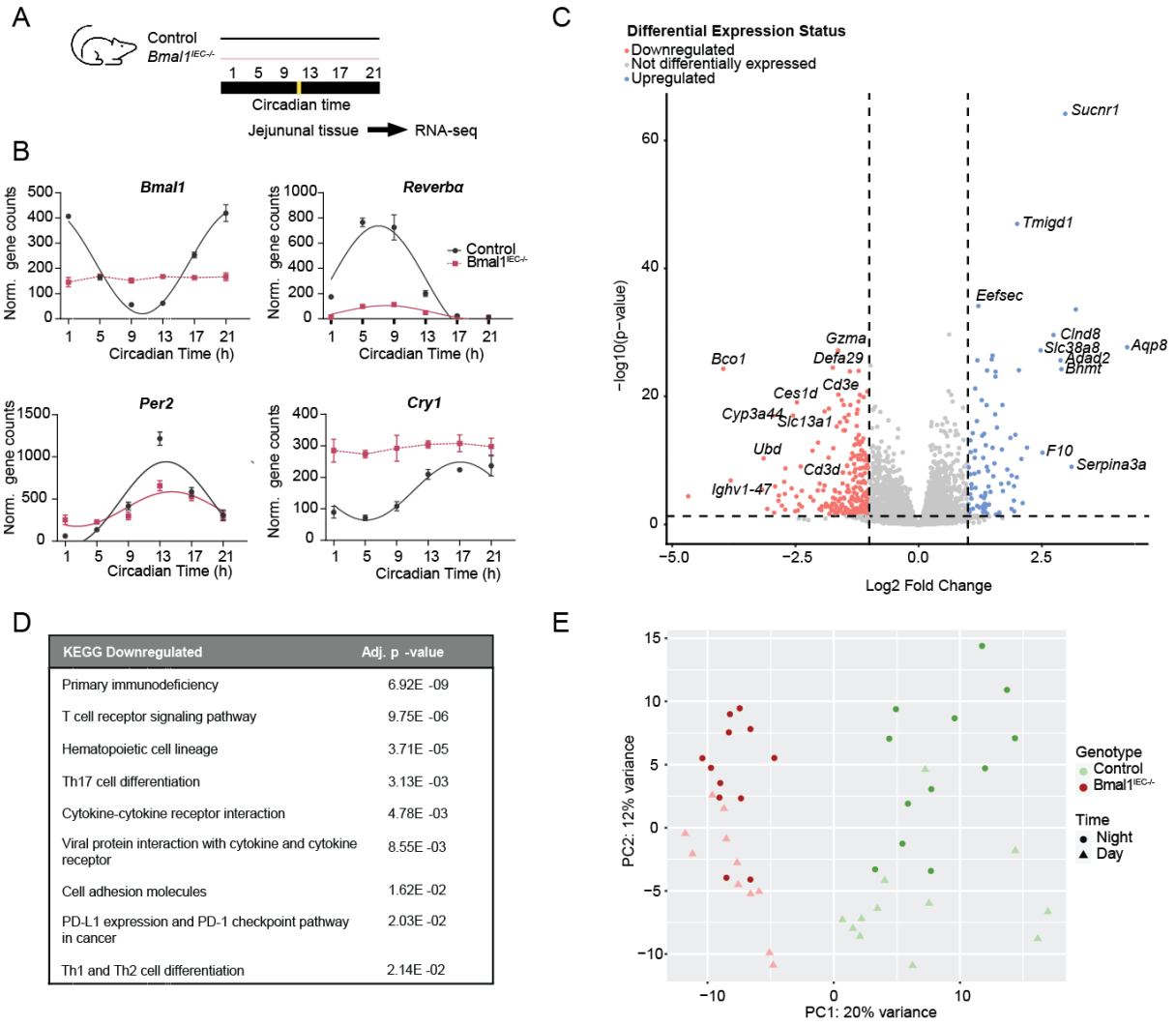

KEGG Downregulated	Adj. p -value
Primary immunodeficiency	6.92E -09
T cell receptor signaling pathway	9.75E -06
Hematopoietic cell lineage	3.71E -05
Th17 cell differentiation	3.13E -03
Cytokine-cytokine receptor interaction	4.78E -03
Viral protein interaction with cytokine and cytokine receptor	8.55E -03
Cell adhesion molecules	1.62E -02
PD-L1 expression and PD-1 checkpoint pathway in cancer	2.03E -02
Th1 and Th2 cell differentiation	2.14E -02

Figure 17 Intestinal clock-regulated genes are involved in metabolic and immune homeostasis.
(A) Experimental paradigm of jejunal tissue sampling every 4 hours over the circadian day (constant darkness), used for RNA-sequencing. **(B)** Normalized gene count profiles for circadian clock genes. **(C)** Volcano plot indicating significant (adjusted p-value <0.05) differential (Fold change >1) genes comparing *Bmal1*$^{IEC-/-}$ mice to controls. Upregulated genes are indicated in blue while downregulated genes are marked in red. **(D)** Gene set enrichment analyses of downregulated genes using KEGG pathway annotation. **(E)** Principal Component Analyses of jejunal samples obtained from control (green) and *Bmal1*$^{IEC-/-}$ (red), split by day (CT1-9, triangle) and night (CT13-21, circle) time points. Significant rhythms (cosine-wave regression, p-value ≤ 0.05) are illustrated with fitted cosine-wave curves; data points connected by dotted lines indicate no significant cosine fit curves (p-value > 0.05) and thus no rhythmicity.

In-depth analyses using CompareRhythms (Pelikan et al., 2022), a tool capable of identifying alterations in rhythmicity, including amplitude and phase shifts, further demonstrated substantial changes in *Bmal1*$^{IEC-/-}$ mice compared to their controls. Specifically, more than 400 transcripts exhibited disrupted or altered rhythmicity patterns in intestinal clock-deficient mice **(Figure 18A)**. The majority of these transcripts displayed significantly reduced amplitudes, indicative of compromised rhythmic gene expression, while some exhibited phase shifts **(Figure 18B)**. Notably, a subset of 41 transcripts related

to oxidative phosphorylation gained rhythmicity in *Bmal1*$^{IEC-/-}$ mice, while their expression remained blunted in control mice **(Supplementary Figure 6A,B).**

GSEA of the transcripts that lost rhythmicity in *Bmal1*$^{IEC-/-}$ mice showed an overrepresentation of genes primarily associated with the digestive system **(Figure 18C, Supplementary Figure 6C).** Notable KEGG pathways included 'selenocompound metabolism', 'carbohydrate digestion and absorption', 'fat digestion and absorption', and 'bile secretion' **(Figure 18C).** Specifically, key genes involved in fat absorption, such as *Fabp2*, *ApoB*, and ATP-binding cassette transporter (*Abca1*), displayed downregulation or altered rhythmicity **(Figure 18C,D)**. Similarly, genes involved in fat digestion, including Acylglycerol-3-Phosphate O-Acyltransferase (*Agpat1/2),* Diacylglycerol O-acyltransferase 2 *(Dgat2),* and Acetyl-Coenzyme A acetyltransferase 2 *(Acat2)*, exhibited arrhythmicity or reduced amplitudes in *Bmal1*$^{IEC-/-}$ **(Figure 18D).** Additionally, genes involved in carbohydrate macronutrient metabolism displayed loss of rhythmicity or highly suppressed amplitudes upon intestinal clock disruption **(Figure 18C,E).** This included the pathways 'glycolysis/gluconeogenesis' and 'fructose and mannose metabolism'. Strikingly, all hexose transporter genes responsible for intestinal glucose, galactose, and fructose transport to the bloodstream, such as *Slc5a1 (Sglt1), Slc2a5 (Glut5),* and *Slc2a2 (Glut2),* exhibited severely reduced amplitude or arrhythmicity in *Bmal1*$^{IEC-/-}$ mice compared to control mice **(Figure 18E).**

Collectively, these findings underscore the importance of the jejunal clock in regulating the circadian transcriptional profiles of key metabolic genes involved in macronutrient absorption and transportation, with a particular focus on carbohydrate and lipid metabolism.

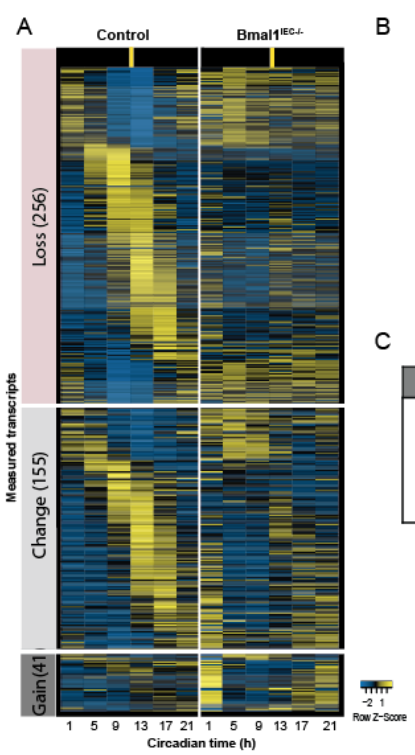

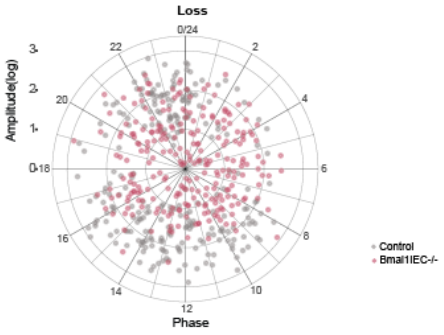

C

KEGG	Adj. p -value
Circadian rhythm	3.27E -08
Selenocompound metabolism	5.62E -06
Cysteine and methionine metabolism	4.44E -04
Carbohydrate digestion and absorption	1.12E -03

KEGG	Adj. p -value
Fat digestion and absorption	4.15E -06
Bile secretion	3.57E -04
Vitamin digestion and absorption	1.28E -03
PPAR signaling pathway	7.96E -03
Carbohydrate digestion and absorption	1.13E -02
Mineral absorption	2.38E -02
Circadian rhythm	2.69E -02
Glycolysis/Gluconeogenesis	2.69E -02
Fructose and mannose metabolism	2.80E -02

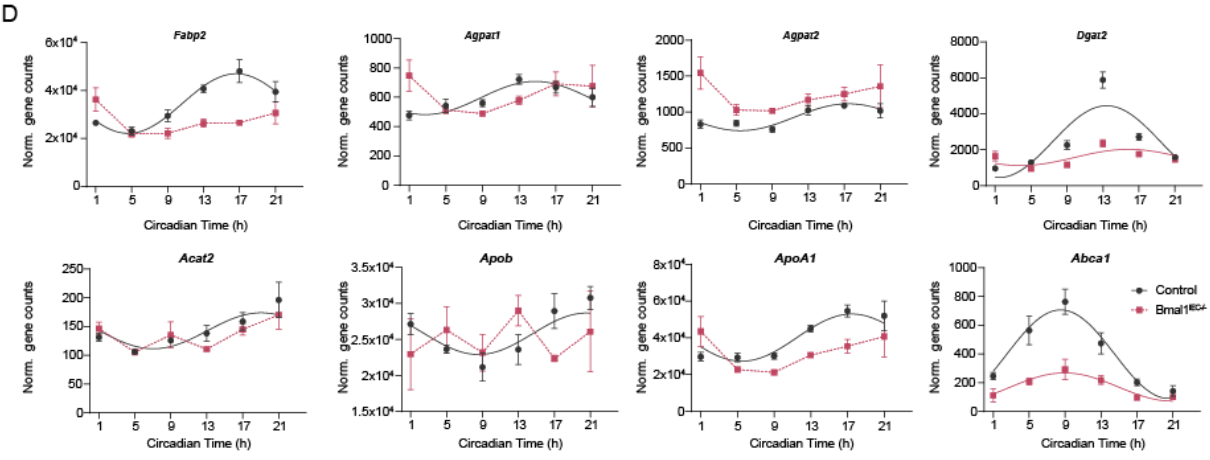

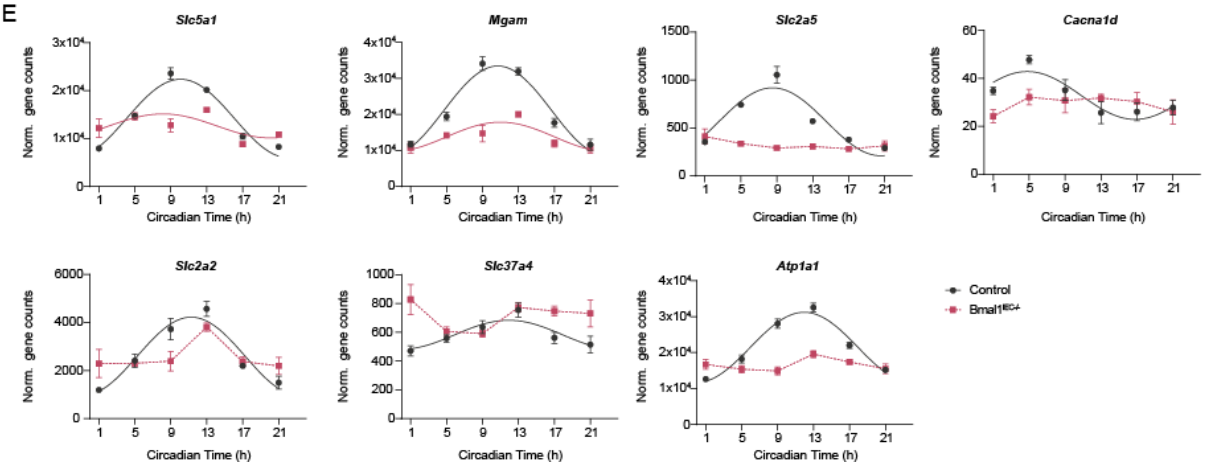

Figure 18 The intestinal clock regulates the rhythmic transcriptome relevant for carbohydrate and lipid metabolism.
(A) Heatmap depicting altered rhythmicity (CompareRhythm) in transcripts detected by RNA-seq between control and *Bmal1*$^{IEC-/-}$ mice. Each gene (row) is organized by the phase of control mice. **(B)** Polarplot depicting phase and amplitude of genes losing rhythmicity (left) and changed rhythmicity (right) in *Bmal1*$^{IEC-/-}$ mice compared to controls. **(C)** KEGG Pathway enrichment analyses using genes that lost rhythmicity (left) or changed rhythmicity (right) in *Bmal1*$^{IEC-/-}$ mice compared to controls. Circadian profiles of lipid **(D)** and carbohydrate **(E)** related metabolic genes measured with RNA-seq that changed or lost rhythmicity in *Bmal1*$^{IEC-/-}$ mice. Significant rhythms (cosine-wave regression, p-value ≤ 0.05) are illustrated with fitted cosine-wave curves; data points connected by dotted lines indicate no significant cosine fit curves (p-value > 0.05) and thus no rhythmicity. Data are represented by mean ± SEM.

4.7 Disruption of host metabolism and immunity by transfer of intestinal clock-deficient derived microbiota

The comprehensive analyses of targeted and untargeted metabolomics, as well as transcriptomic profiling, highlighted the crucial role of the intestinal clock in regulating host metabolism. This is supported by the observed increased body weight in *Bmal1*$^{IEC-/-}$ mice under chow conditions (Facility A (p=0.001)) **(Figure 19A).** Intriguingly, this alteration in body weight was not observed in a separate cohort housed in a different animal facility (Facility B (p=0.15)) nor germ-free (GF) mice lacking microbiota **(Figure 19B,C)**, which underscores the significance of specific intestinal clock-controlled bacteria in regulating host metabolism. It is noteworthy that other metabolic parameters, such as fat mass, glucose clearance, and intestinal sugar transportation, did not exhibit significant differences between genotypes under SPF chow conditions **(Supplementary Figure 7).**

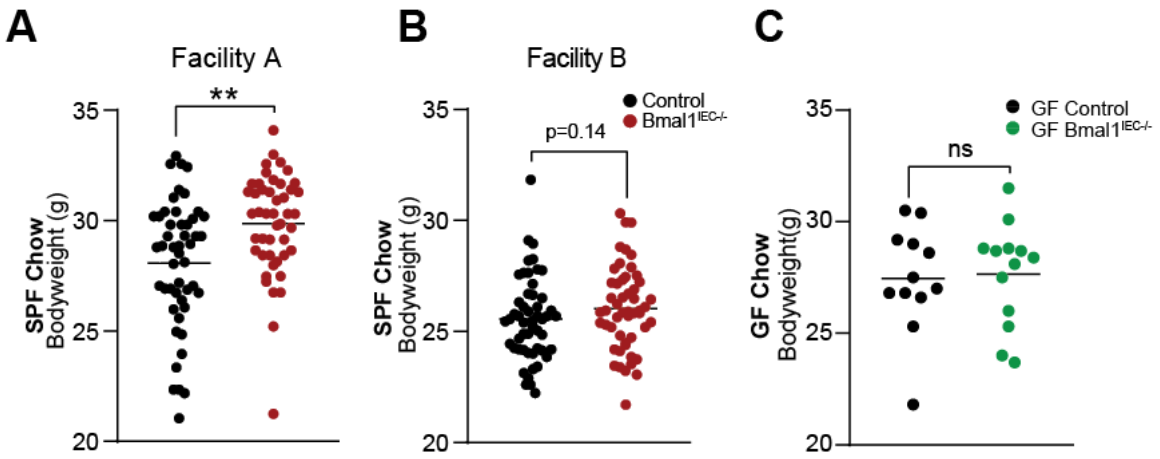

Figure 19 Body weight elevation upon intestinal clock-deficiency is microbiota dependent.
Body weight (gram) of control and *Bmal1*$^{IEC-/-}$ mice under chow diet, measured in **(A)** SPF facility A or **(B)** SPF facility B (Age; 17-21 weeks). **(C)** Body weight (gram) measured in germ-free control and *Bmal1*$^{IEC-/-}$ mice (Age; 13-16 weeks). ** p<0.01 (Mann-Whitney U test).

To further investigate the physiological relevance of the rhythmic microbial composition driven by the intestinal clock on host physiology, GF C57BL/6 mice were colonized with cecal content obtained from either *Bmal1*$^{IEC-/-}$ mice or their controls for a duration of 5 weeks, allowing for the establishment of the cecal microbiome **(Figure 20A).** Beta-diversity analyses of fecal microbial profiles clearly distinguished recipient mice based on the genotypes of the donors **(Figure 20B).** More than 75% of zOTUs identified in the donors of both genotypes were successfully transferred to the recipient mice, indicating a high overall transfer efficiency **(Supplement Figure 8A).** However, the transfer of bacteria to recipients was less efficient for Desulfobacterota, *Muribaculacea,* and *Erysipelotrichaceae,* depending on the donor. In contrast, families like *Oscillospiraceae*, *Lachnospiracea,* and *Ruminococcaceae* exhibited consistent relative abundance patterns compared to their respective donors **(Figure 20C,D).**

Comparing microbiota composition of recipient mice, a significant decrease in *Muribaculaceae* and *Lactobacillaceae* were observed in *Bmal1*$^{IEC-/-}$ recipients, while families such as *Lachnospiraceae, Marinifilaceae, Ruminococcaceae* and *Oscillospiraceae* were enriched **(Figure 20C,D).** Additionally, taxonomic difference analyses revealed 20 zOTUs with a > 2-fold change in relative abundance between recipients **(Supplementary Figure 8C).** Notably, *Enterohabdus, Lactobacillus,* and *Alistipes* were reduced in abundance in *Bmal1*$^{IEC-/-}$ recipients compared to control recipients. Highly abundant zOTUs in *Bmal1*$^{IEC-/-}$ recipients were predominantly associated with the *Oscillospiraceae* and *Lachnospiraceae* families, including the genus *Roseburia* **(Supplementary Figure 8B).**

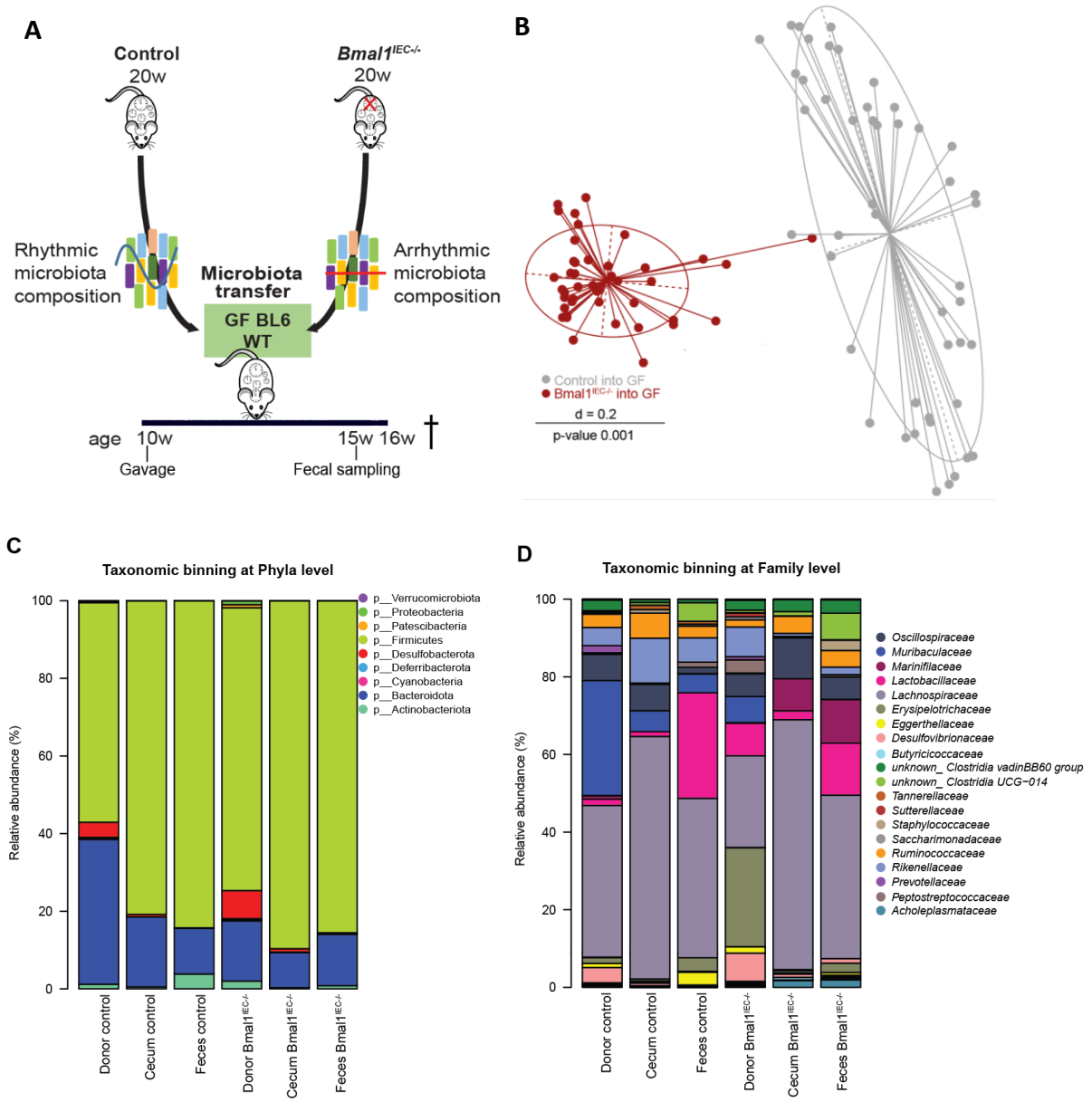

Figure 20 Significant difference in Beta-diversity between recipient mice.
(A) Transfer was performed at CT13 with a mixture of cecal microbiota obtained from controls and *Bmal1*$^{IEC-/-}$ donors (derived at CT13) into 10 weeks old germ-free BL6 wild-type recipient mice. Mice were kept for 6 weeks after gavage until sacrifice at the age of 16 weeks (16w). Fecal profiles were collected 5 weeks after gavage at the age of 15 weeks (15w). **(B)** MDS plot of GUniFrac distances of recipient mice after 5 weeks of transfer. Significance was calculated by PERMANOVA with Bonferroni correction. **(C)** Average relative abundance of donor and recipient mice at phyla and **(D)** family level.

Importantly, the lack of rhythmicity was successfully transferred to recipient mice receiving microbiota from *Bmal1*$^{IEC-/-}$ mice, with a substantial reduction in rhythmicity at all taxonomic levels **(Figure 21A,B)**. Alpha-diversity, although arrhythmic, was significantly higher in *Bmal1*$^{IEC-/-}$ recipients **(Figure 22A).** The rhythmicity of the phyla Proteobacteria and Firmicutes was lost, while Bacteroidetes remained arrhythmic in both control and *Bmal1*$^{IEC-/-}$ recipients (**Figure 22A).** Furthermore, the highly abundant family *Muribaculaceae* exhibited rhythmicity in control mice but was absent in *Bmal1*$^{IEC-/-}$ recipients

(**Figure 22A)**. Additionally, *Lachnospiraceae, Rikenellaceae,* and *Clostridia* maintained circadian rhythmicity in the host after transfer from control donors but lost their rhythmicity in *Bmal1*$^{IEC-/-}$ recipient mice, as observed in their respective donors **(Figure 22C)**.

Following the transfer of arrhythmic microbiota from *Bmal1*$^{IEC-/-}$ mice, elevated levels of both fecal and cecal SCFAs, particularly acetate and butyrate, as well as BCFAs like isobutyrate, were observed **(Figure 22 B,D)**. Additionally, both fecal and cecal levels of the secondary BA 7-ketolitocholic acid were completely absent in control recipient mice but highly abundant in *Bmal1*$^{IEC-/-}$ recipients **(Figure 22 C,E)**. The BAs cholic acid and β-muricholic acid were significantly downregulated **(Figure 22 C,E)**, consistent with observations made in donor mice. Of note, intestinal clock gene and CCG expression at CT13 remained unaltered between recipient mice **(Figure 22 F,G).**

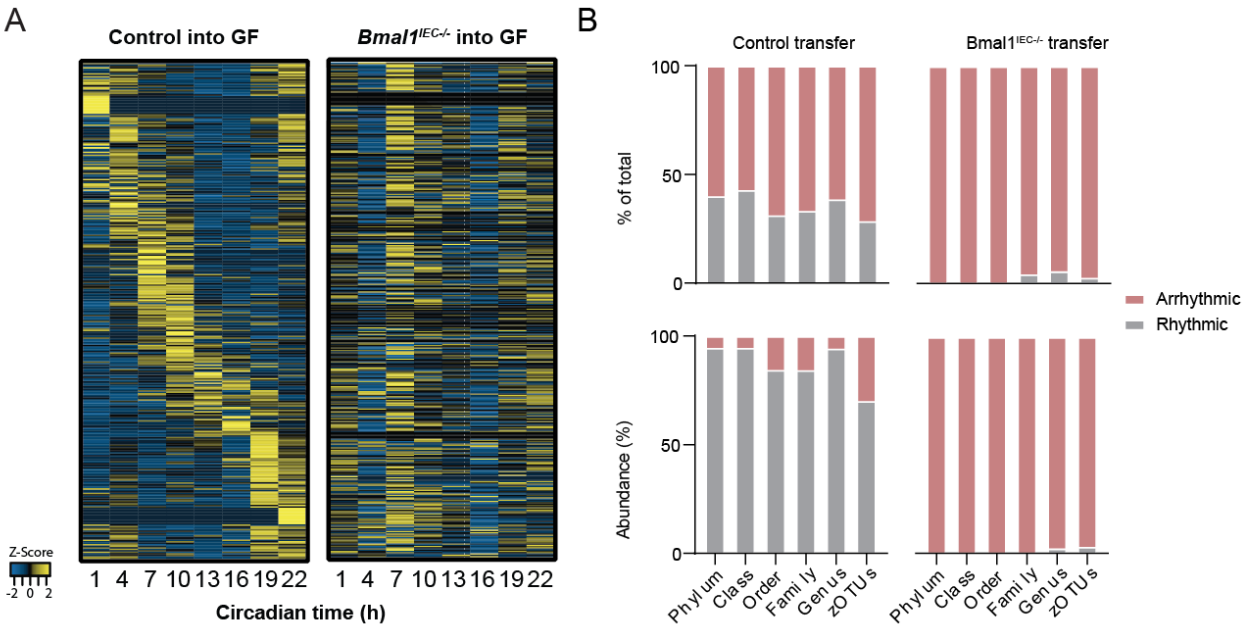

Figure 21 Maintained arrhythmicity upon transfer of *Bmal1*$^{IEC-/-}$ derived microbiota into a germfree host.
(A) Heatmap depicting the relative abundance of zOTUs ordered by their cosine-regression peak phase according to the recipient controls. **(B)** Bar graphs indicating the percentage (top) and abundance (bottom) of rhythmic and arrhythmic taxonomies in control and *Bmal1*$^{IEC-/-}$ recipients.

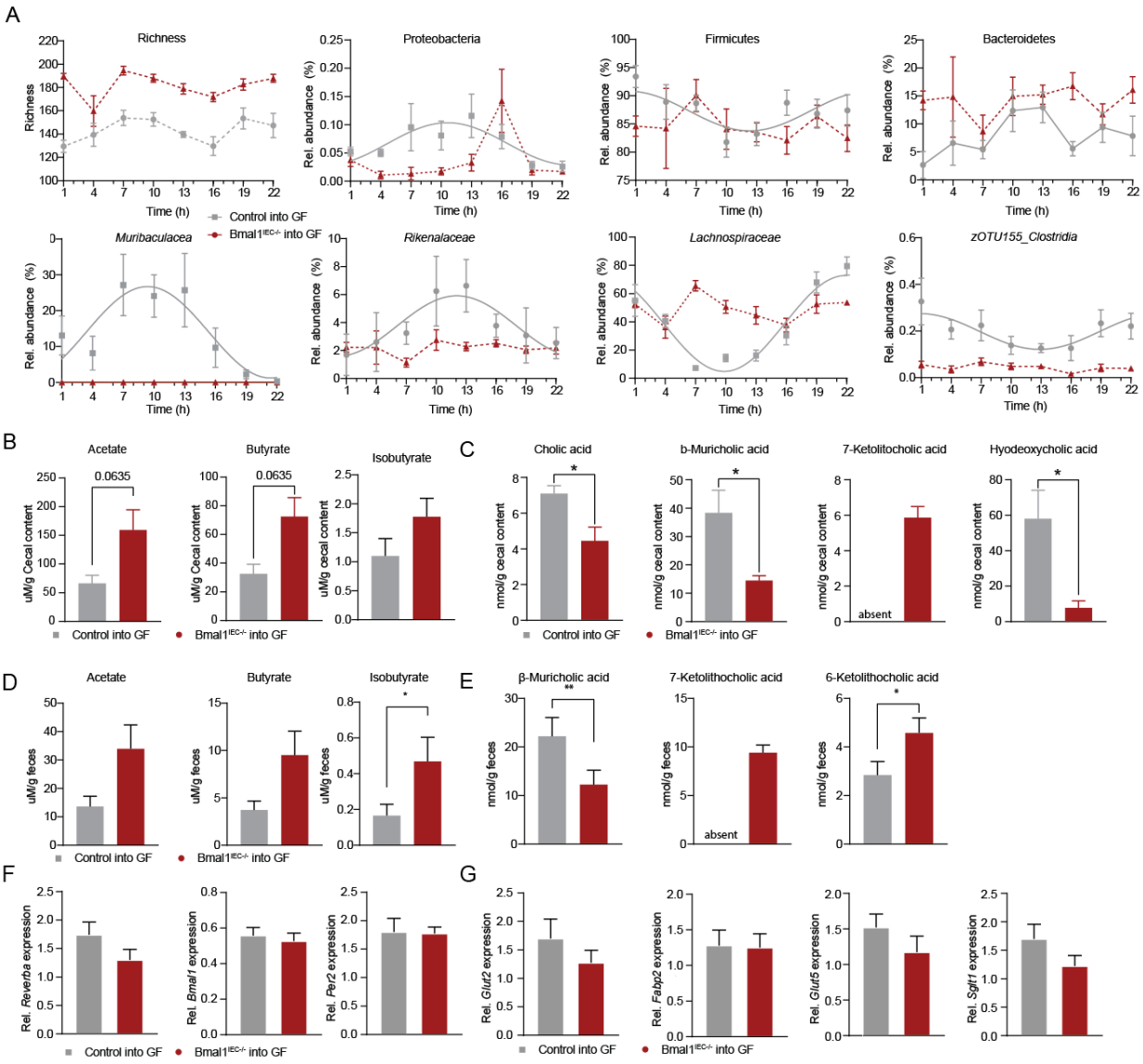

Figure 22 Arrhythmic microbial patterns and metabolite alterations upon *Bmal1*$^{IEC-/-}$ microbial transfer
(A) Diurnal profiles of fecal microbial richness and taxa. **(B)** SCFA concentrations in cecum and **(D)** feces as well as bile acid concentrations in **(C)** cecum and **(E)** fecal content of control and *Bmal1*$^{IEC-/-}$ recipient mice measured by targeted metabolomics. **(F)** Metabolic gene expression and **(G)** Clock gene expression at CT13 measured by qPCR in control and *Bmal1*$^{IEC-/-}$ recipients. Significant rhythms (cosine-wave regression, p-value ≤ 0.05) are illustrated with fitted cosine-wave curves; data points connected by dotted lines indicate no significant cosine fit curves (p-value > 0.05) and thus no rhythmicity. * p<0.05, ** p<0.01.

Notably, mice colonized with *Bmal1*$^{IEC-/-}$ derived microbiota exhibited significant weight gain compared to recipient mice receiving control microbiota **(Figure 23 A,B)**. This weight gain was accompanied by an increase in dissected fat mass, specifically in eWAT and sWAT **(Figure 23C)**. Nuclear magnetic resonance (NMR) further confirmed these findings by revealing a significant increase in total fat mass and a decrease in lean mass among mice that received intestinal clock-deficient microbiota **(Figure 23C)**. These outcomes were independent of any alterations in food intake or total energy assimilation between the recipient mice **(Supplementary Figure 9).** Although less pronounced, similar tendencies

of weight gain were observed in vancomycin-metronidazole antibiotic-treated mice following *Bmal1*$^{IEC-/-}$ microbial gavage (p=0.06, week 5) **(Supplementary Figure 10)**.

Specific taxa, mainly belonging to the *Lachnospiraceae* family, including the genera *Enterocloster, Eubacterium*, and *Lachnoclostridia*, showed a positive correlation with body weight alterations. Conversely, *Roseburia* and Proteobacteria displayed a strong negative correlation with body weight **(Figure 23D)**.

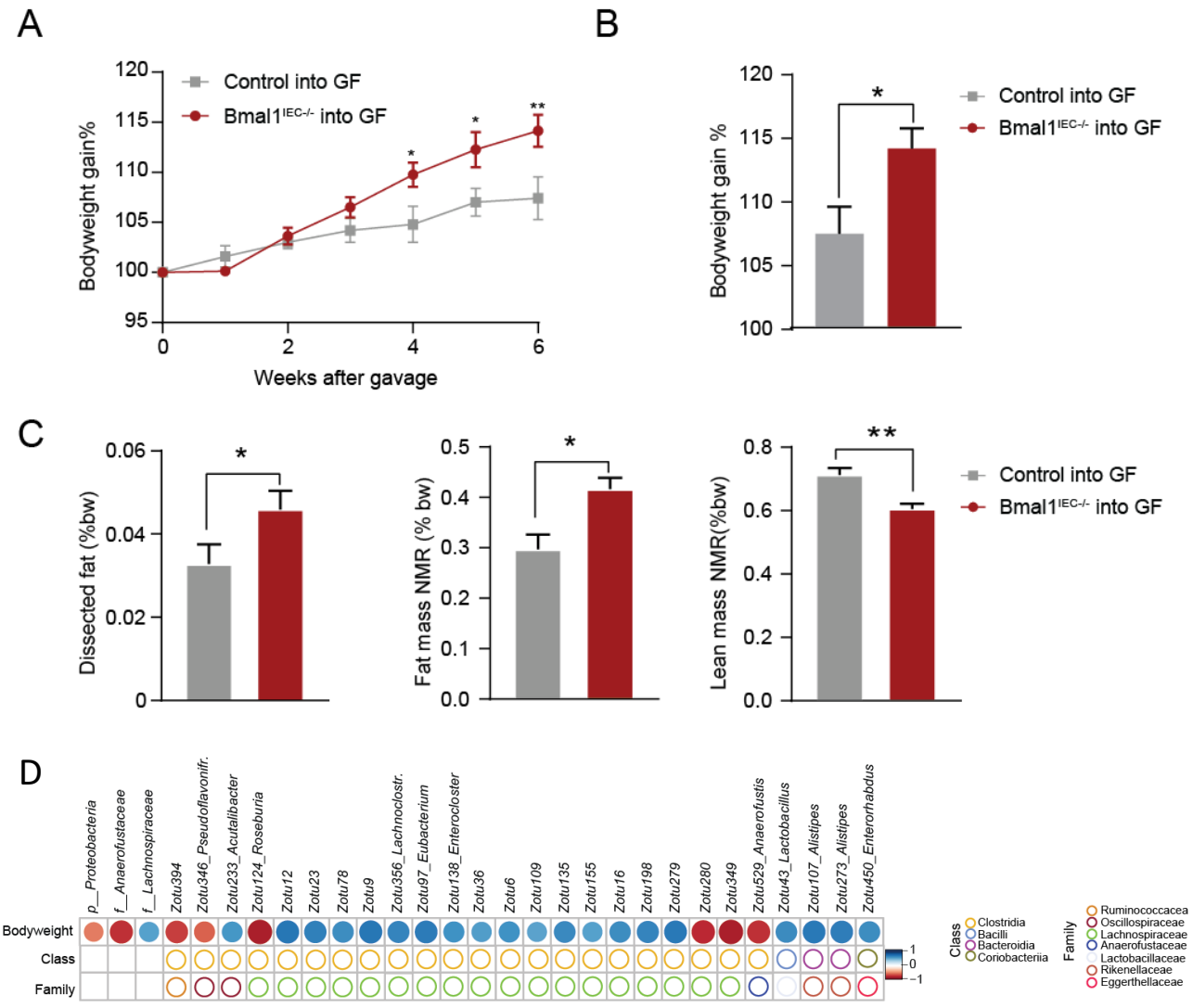

Figure 23 Mice receiving intestinal clock-deficient microbiota exhibit increased weight gain and fat mass.
(A) Total body weight gain **(B)** quantified after 6 weeks of gavage. **(C)** Dissected fat mass and total fat mass/lean mass measured by NMR. **(D)** Significant **S**pearman correlation coefficient (p-value ≤ 0.05 and R ≤ − 0.5; red or R ≥ 0.5; blue) between body weight and bacterial taxa at phyla, family, and zOTU level. * p<0.05, ** p<0.01.

In addition to the observed obese phenotype, jejunum and colon density were significantly decreased, indicative of immune activation in *Bmal1*$^{IEC-/-}$ recipient mice **(Figure 24A)**. Interestingly, the transfer of arrhythmic microbiota led to alterations in immune cell recruitment to the lamina propria. Fluorescence-activated cell sorting (FACS) analysis demonstrated a decrease in T-cell ($CD3^+CD4^+$, $CD3^+CD8^+$) recruitment patterns at CT13 in both the jejunum ($p=0.08$) and colon ($p<0.05$) **(Figure 24B).** These findings align with similar trends observed in *Bmal1*$^{IEC-/-}$ mice under SPF conditions **(Supplementary Figure 11A,B**), showing decreased jejunal T-cell recruitment and significantly increased concentration of complement 3 in fecal supernatant**,** providing further evidence for the role of intestinal clock-controlled microbiota in modulating gut immune regulation.

Moreover, the increase in weight and fat mass in these mice was accompanied by changes in immune cell populations within the adipose tissue. T-cell sub-populations ($CD3^+CD4^+$, $CD3^+CD8^+$) exhibited an increase in the eWAT of *Bmal1*$^{IEC-/-}$ microbial recipients **(Figure 24C)**. However, immune cell recruitment to other peripheral organs, including the mesenteric lymph nodes and spleen, as indicators for systemic inflammation remained unchanged between recipients **(Figure 24C)**. Notably, overall intestinal histology scores in both the colon and jejunum remained unaffected upon transfer of the *Bmal1*$^{IEC-/-}$ derived microbiome **(Figure 24D)**.

These findings collectively highlight the importance of the intestinal clock in maintaining the rhythmic microbial composition and function, which is crucial for balancing host metabolism. The dysregulation observed in immune cell recruitment suggests a potential link between disrupted circadian rhythms in the gut and immune dysfunction, as further investigated in the study by Niu et al. (Niu, 2023).

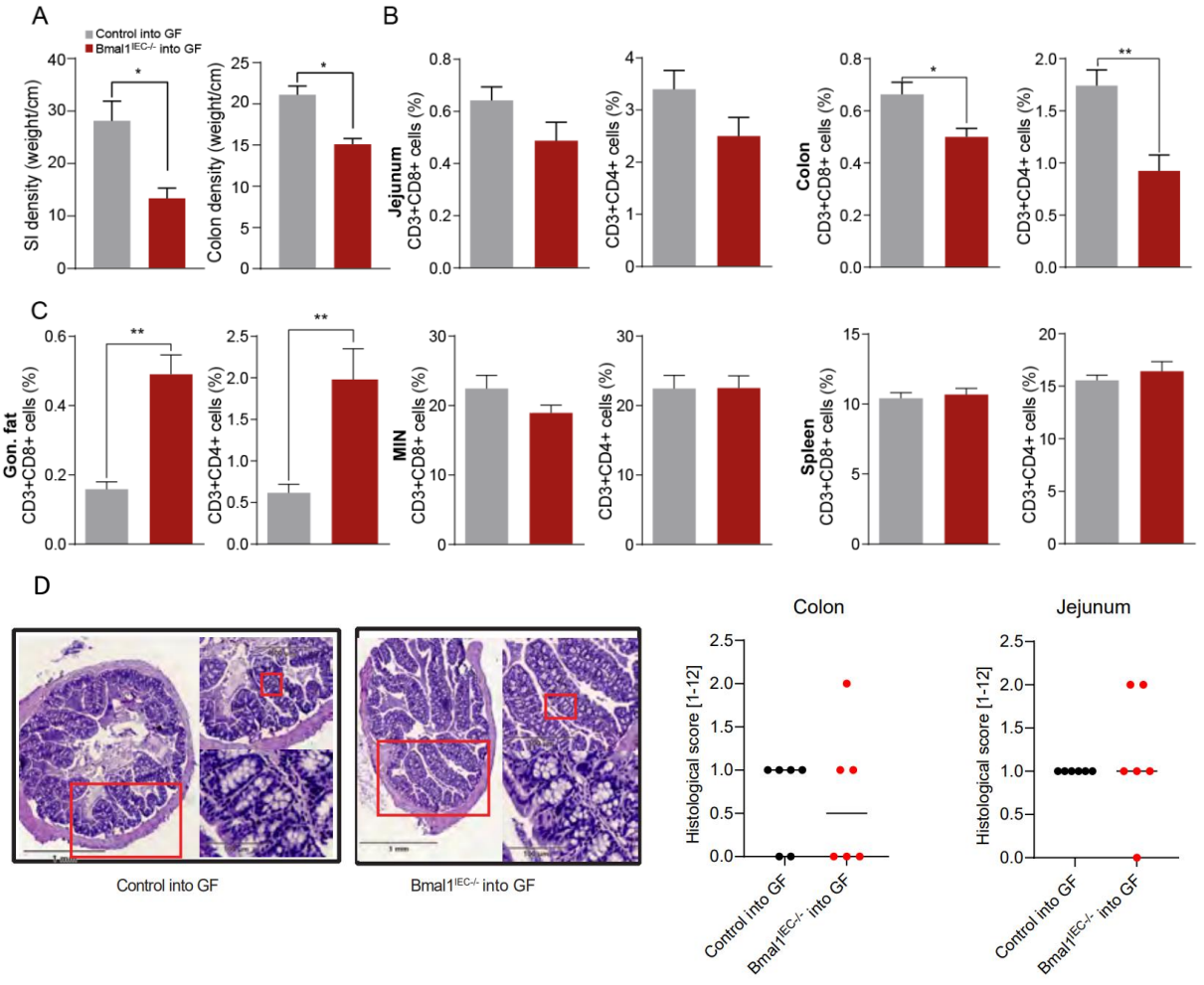

Figure 24 Decreased intestinal T-cell recruitment upon transfer of intestinal clock-deficient microbiome.
(A) Dissected intestinal density (weight/cm) after 6 weeks of transfer in recipient mice. **(B)** Frequency of CD3+CD8+ and CD3+CD4+ immune cell population in jejunum and colon as well as in **(C)** gonadal fat, mesenteric lymph nodes (Mln) and spleen. **(D)** H&E staining of proximal colon cross-section along with the histological scoring of proximal colon and jejunum of germ-free mice after receiving control or *Bmal1*$^{IEC-/-}$ derived cecal microbiota. * p<0.05, **p<0.01 (Mann-Whitney U test, two-sided).

4.8 Westernized dietary feeding results in metabolic abnormalities in intestinal clock-deficient mice

Building upon the observations within this study, highlighting the essential role of a functional intestinal clock in metabolism, specifically in relation to carbohydrates and lipids, an 8-week dietary experimental study was conducted. Mice from both genotypes were subjected to different diets, including a high-fat diet (HFD, 48% kcal palm oil), a western diet (WD, HFD + 30% sucrose water), and a purified control diet (CD) for comparison **(Figure 25A).**

When mice lacking the intestinal clock were exposed to a fiber-depleted CD, a slight decrease in body weight gain was observed, although this difference was not statistically significant (**Figure 25B).** Despite observing alterations in the lipid-relevant transcriptome, there were no significant differences in body weight between the different genotypes upon HFD intervention **(Figure 25C).** To account for slight body weight differences (~1.5g) observed between genotypes exposed to the CD, weight gain under HFD was normalized to the weight gain under CD for each mouse. This normalization allowed for the determination of the specific effect of the additional fat load on body weight gain. Accordingly, HFD-fed *Bmal1*$^{IEC-/-}$ mice exhibited slightly higher body weight gain (p=0.08) compared to controls **(Figure 25E).** Interestingly, *Bmal1*$^{IEC-/-}$ mice revealed a further significant increase in body weight gain when subjected to HFD along with an additional sugar load, reflecting a westernized diet (WD) **(Figure 25D).** Specifically, the supplementary sucrose intake led to a 5% increase in body weight gain in *Bmal1*$^{IEC-/-}$ mice compared to those on HFD alone **(Figure 25F).** The sugar supplementation resulted in an increase in energy intake and a decrease in energy secretion, leading to higher assimilation efficiency for both genotypes compared to both HFD and CD **(Figure 25G).** Under WD conditions, no difference was observed in total assimilation efficiency between genotypes, although the amount of fecal production and, consequently, total energy excretion was significantly increased in *Bmal1*$^{IEC-/-}$ mice compared to controls **(Figure 25G).**

Furthermore, the normalized weight of dissected organs, including SI density, cecum, and pancreas, differed between genotypes under WD-feeding but not under HFD conditions **(Figure 25H)**. For example, WD-fed *Bmal1*$^{IEC-/-}$ mice have a decreased pancreatic weight compared to their controls. Additionally, during an oral glucose tolerance test (OGTT), there was a tendency towards higher total circulating glucose (AUC) in fasted WD-fed *Bmal1*$^{IEC-/-}$ mice, although it did not reach statistical significance **(Figure 25I).**

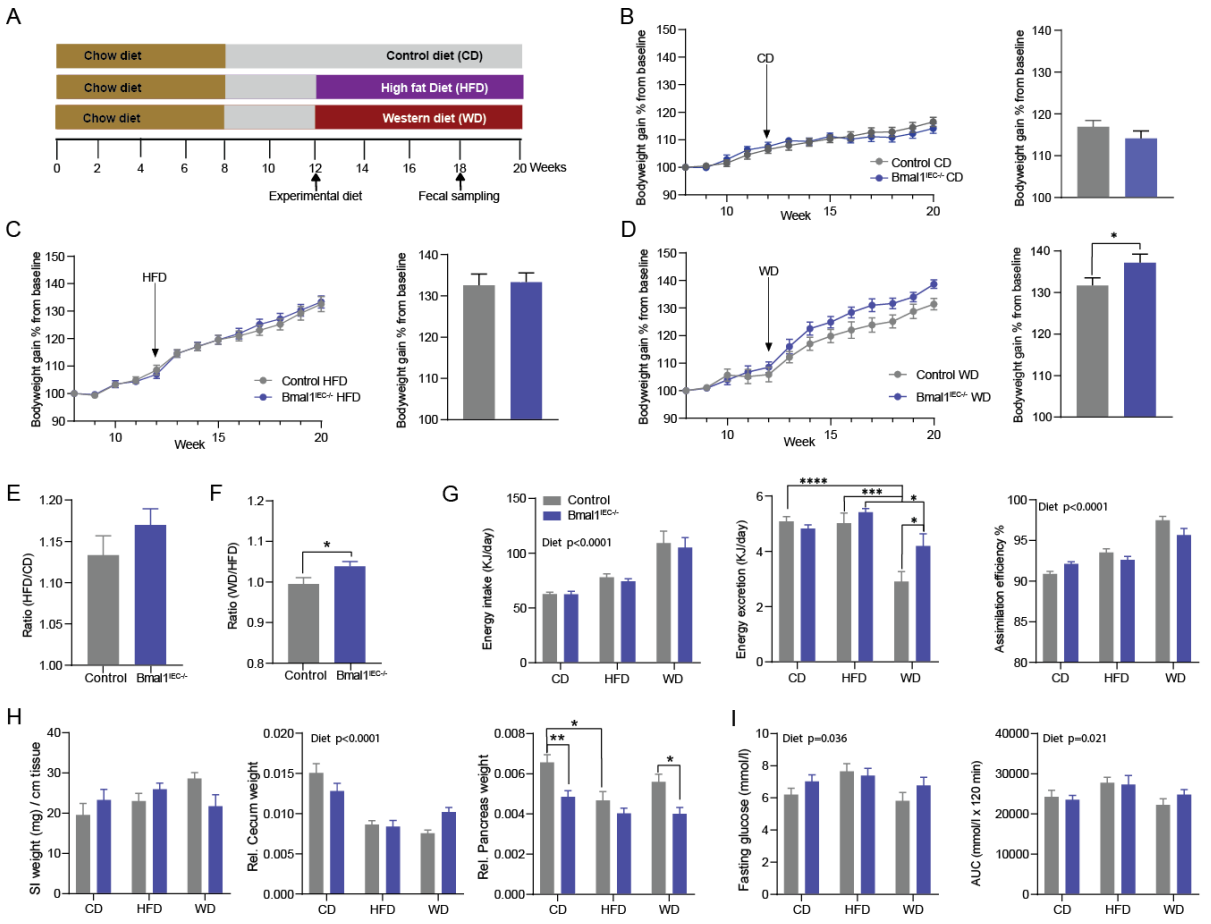

Figure 25 Western diet intervention promotes body weight gain in intestinal clock-deficient mice.
(A) Schematic diagram of experimental paradigm. **(B)** Body weight gain and it's quantification of control diet fed mice, **(C)** HFD fed mice and **(D)** Western diet fed mice. **(E)** Body weight gain of HFD fed mice, normalized to CD. **(F)** Body weight gain of WD fed mice normalized to HFD conditions. **(G)** Energy intake, excretion and total assimilation efficiency under CD, HFD and WD conditions. **(H)** Dissected organ weight (SI density, cecum, pancreas) relative to body weight after 8 weeks of HFD or WD feeding. **(I)** Fasting glucose and total area under the curve (AUC) after glucose tolerance test. Data are represented by mean ± SEM. Significance was calculated with two-sided Mann-Whitney U test or Two-way ANOVA. * p<0.05, ** p<0.01, *** p<0.001, **** p<0.0001.

High-caloric diets have been shown to influence the expression of clock genes in various peripheral tissues (Eckel-Mahan et al., 2013). To assess the functionality of the intestinal clock under different dietary interventions, the expression of clock genes at CT13 in jejunum tissue was compared between the different genotypes exposed to each dietary condition. Surprisingly, both genotypes in all purified dietary conditions (CD, HFD, WD) exhibited a decrease in clock gene expression compared to fiber-rich chow conditions **(Figure 26A).** However, while circadian time differences between CT1 and CT13 were still evident in control mice, no such time difference was detected in *Bmal1*$^{IEC-/-}$ mice **(Figure 26B).** Additionally, in chow-fed mice, an increase in *Rev-Erba* expression was observed at CT13, whereas CD- and HFD-fed mice exhibited higher expression at CT1, suggesting a potential circadian phase shift **(Figure 26B).** These results indicate an altered, yet functional, intestinal circadian clock in control mice upon purified dietary intake, whereas the clock function remained abolished in *Bmal1*$^{IEC-/-}$ mice. WD-

fed mice were solely sampled at CT13, which limited the examination of time differences in clock gene expression.

It is noteworthy that both genotypes exhibited upregulation of genes involved in intestinal carbohydrate absorption under WD compared to HFD, such as *Glut5* and *Sglt1*, responsible for fructose and glucose/galactose transport, respectively **(Figure 26C).** This suggests an adaptive response to the increased availability of dietary sugars. However, reduced expression levels of carbohydrate transport genes were detected in *Bmal1*$^{IEC-/-}$ mice compared to their controls, suggesting a reduced response to the high-sugar load **(Figure 26C).**

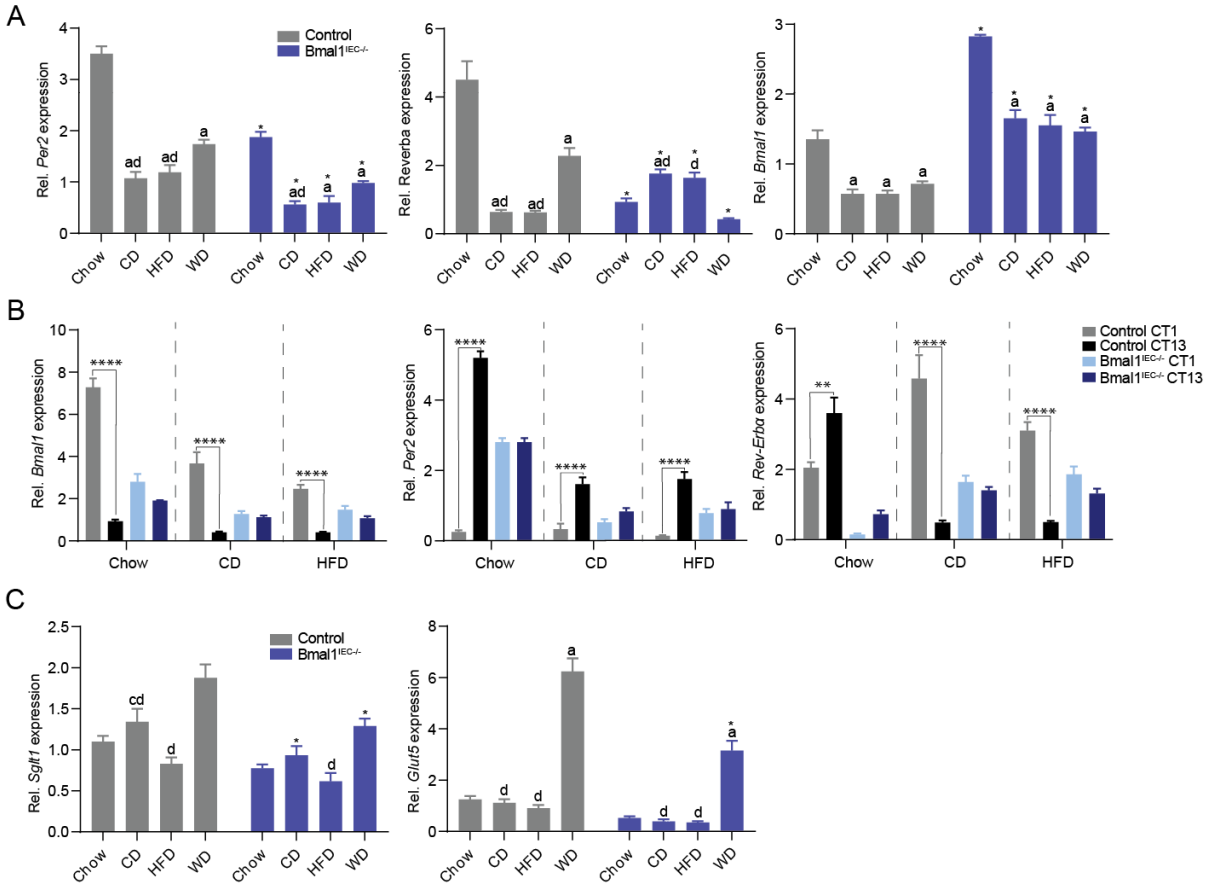

Figure 26 Fiber depletion affects intestinal clock functioning.
(A) Relative *Per2, Rev-Erbα* and *Bmal1* gene expression measured at CT13. **(B)** Relative gene expression of *Bmal1, Per2* and *Rev-Erbα* at CT1 and CT13 for Chow, CD and HFD. **(C)** Relative *Sglt1* and *Glut5* hexose transporter expression was measured at CT13. A,C: * means significant difference between genotypes, letters mean significant difference between diet within genotype with a=chow, b=CD, c=HFD, D=WD. B; ** p<0.01, **** p<0.0001 (Two-way ANOVA).

4.9 Westernized dietary feeding results in genotype-dependent alterations in microbial community but not rhythmicity.

Gut microbial communities play a crucial role in regulating host energy homeostasis (Wang, 2020). To investigate the differences in microbial profiles and community diversity between genotypes and dietary conditions, 16S amplicon sequencing of fecal content was conducted. Mice fed a WD exhibited distinct clustering based on their gut microbial composition, while no strong clustering patterns were observed for mice on a CD or HFD **(Figure 27A)**. However, beta-diversity analysis revealed significant differences in microbial diversity between diets and genotypes within diets **(Supplementary Figure 12)**. WD feeding resulted in a decreased species richness, which was even more pronounced in mice lacking an intestinal clock **(Figure 27B).** Furthermore, under a high-caloric diet, *Bmal1*$^{IEC-/-}$ mice exhibited reduced species diversity compared to their controls (HFD; p=0.02, WD; p=0.06) **(Figure 27B).**

At the phylum level, a two-way ANOVA demonstrated significant differences in Bacteroidetes, Firmicutes, Proteobacteria, and Actinobacteriota relative abundance levels **(Figure 27C, Supplementary Figure 13A).** Particularly, Proteobacteria was upregulated in WD-fed *Bmal1*$^{IEC-/-}$ mice compared to their controls **(Figure 27C).** Additionally, the relative abundance of Firmicutes in WD-fed intestinal clock-deficient mice was decreased **(Figure 27C).**

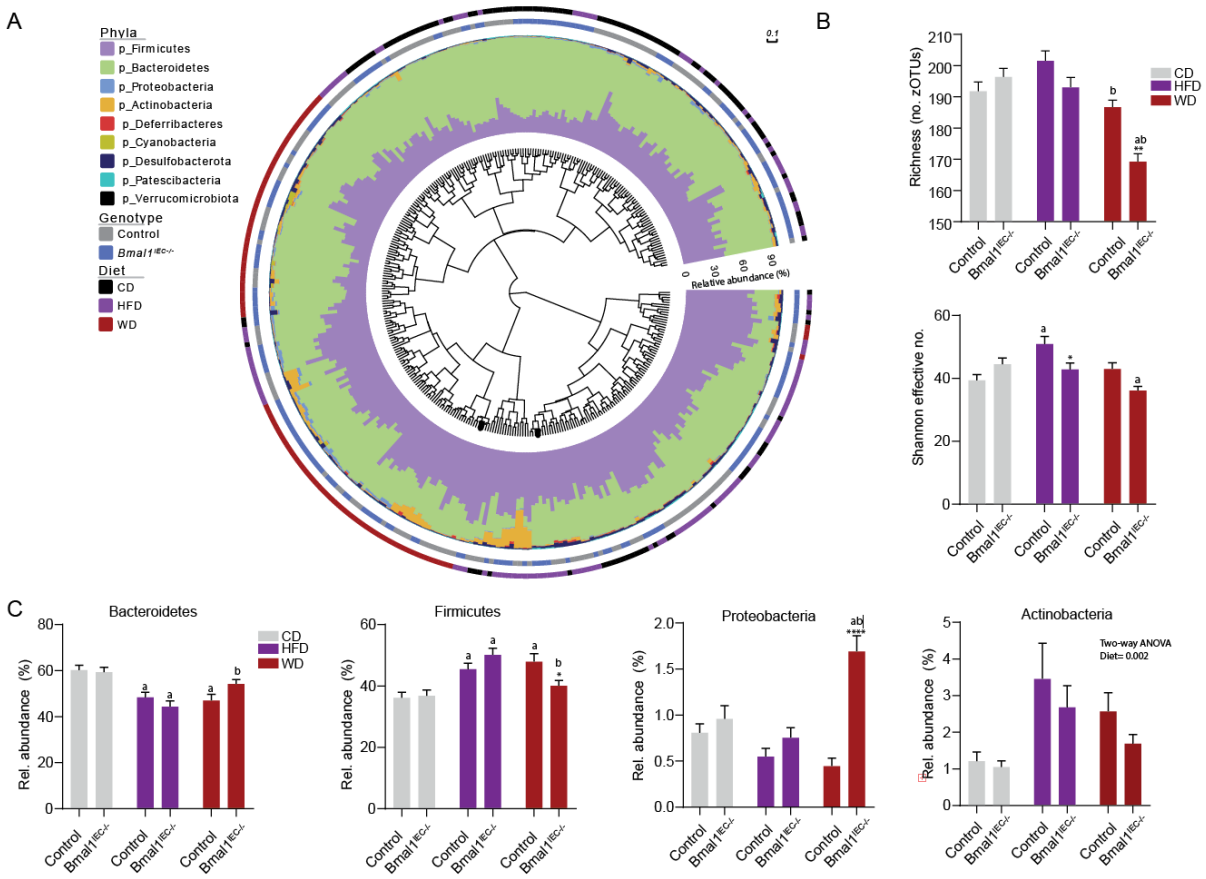

Figure 27 Intestinal clock deficiency results in microbial alterations upon westernized diet feeding.
(A) Phylogenetic tree showing similarities between microbiota profiles based on generalized UniFrac distances between different mice represented by the individual branches. Phyla composition is depicted by stacked bar plots in the first inner circle. Followed by genotype and diet in the outer circle. **(B)** Alpha-diversity (Richness and Shannon effective). **(C)** Relative abundance (%) of significant altered phyla Bacteroidetes, Firmicutes, Proteobacteria and Actinobacteria. Data are represented by mean ± SEM. Significance was calculated with a Two-way ANOVA. * p<0.05, ** p<0.01, **** p<0.0001. * means significant difference between genotypes, letters mean significant difference between diet within genotype with a=CD, b=HFD, c=WD.

Conducting relative abundance differential analyses at the zOTU level showed the downregulation of zOTUs belonging to the *Muribaculaceae* family in *Bmal1*$^{IEC-/-}$ mice across all the dietary conditions compared to control mice **(Figure 28A)**. Furthermore, the total abundance of the *Muribaculaceae* family was reduced upon high-caloric diets, with the highest suppression observed in WD-fed mice. Interestingly, this effect was even more pronounced in the absence of a functional clock **(Figure 28B, Supplementary Figure 13B).** On the contrary, *Bmal1*$^{IEC-/-}$ mice fed WD exhibited a significant increase in the relative abundance of *Parasuterella,* which showed a positive correlation with body weight, while the abundance of *Muribaculaceae* showed a negative correlation with body weight **(Figure 28 A,B)**. These findings support the notion that changes in the abundance of intestinal clock-controlled bacterial taxa are associated with energy homeostasis. During WD, microbial alterations resulted in a

significant upregulation of total SCFAs, BCFAs, and lactate, while the fecal concentrations of primary, conjugated, and secondary BAs were significantly reduced in *Bmal1*$^{IEC-/-}$ mice **(Figure 28 C,D,E).** These results indicate that the intestinal clock plays a role in WD-induced obesity by influencing microbial functioning.

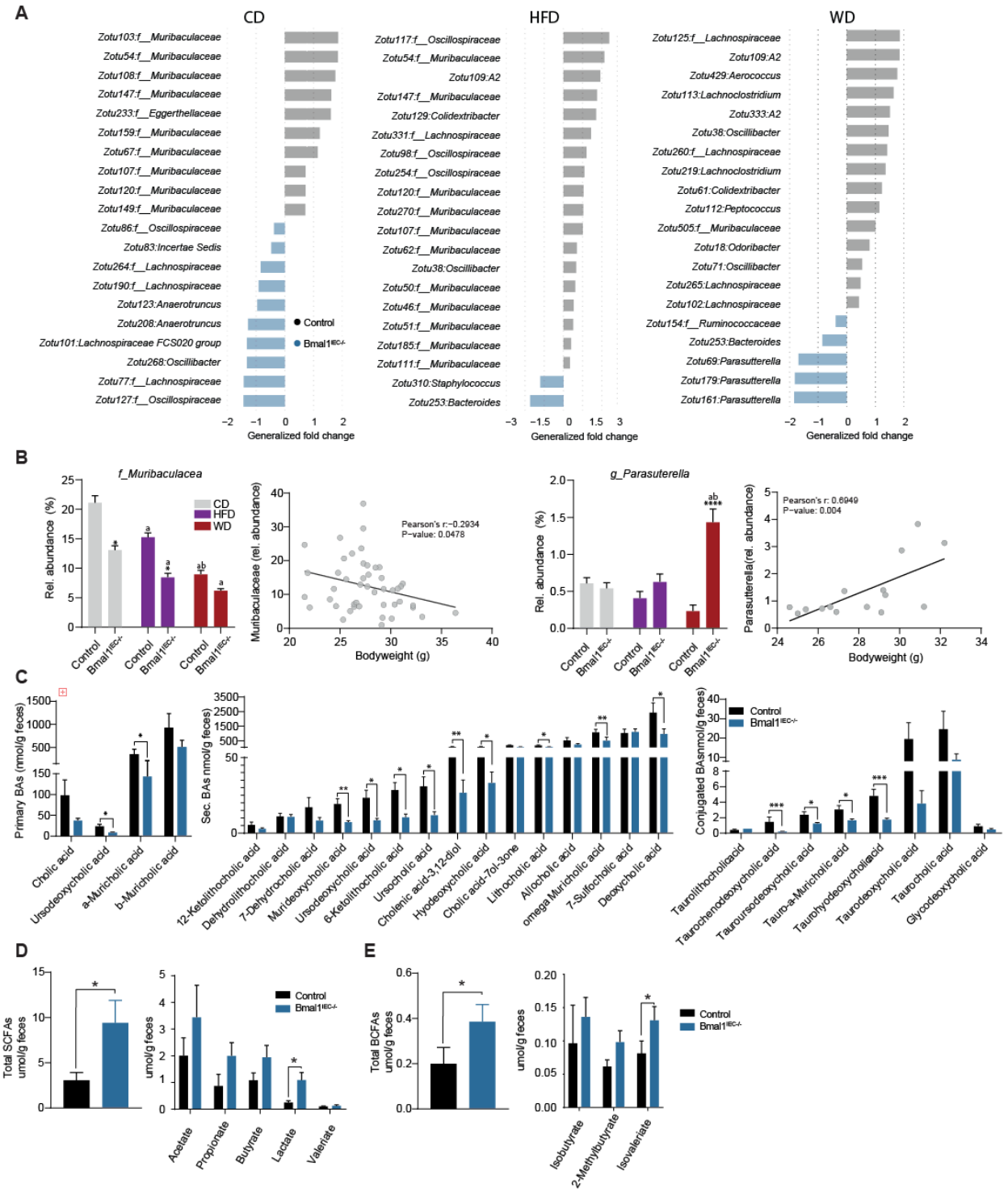

Figure 28 *Parasuterella* is positively associated with western diet-induced obesity upon intestinal clock deficiency. (A) Generalized fold change of zOTUs between control and *Bmal1*$^{IEC-/-}$ mice in all dietary conditions. (B) Relative abundance plots of positive and negative correlated taxonomies with body weight. (C) Fecal bile acid, (D) short-chain fatty acid and (E) branched-chain fatty acid concentrations. Data are represented by mean ± SEM. Significance was calculated with a Two-way ANOVA. * $p<0.05$, **** $p<0.0001$. * Means significant difference between genotypes, letters mean significant difference between diet within genotype with a=CD, b=HFD.

Literature has reported a dampening of microbial rhythms upon HFD interventions (Leone et al., 2015; Zarrinpar et al., 2014). Additionally, this study previously showed that the development of obesity occurs upon arrhythmic microbial transfer, potentially explaining the observed weight gain in WD-fed *Bmal1*$^{IEC-/-}$ mice. Therefore, the circadian microbial rhythmicity in all purified diets and both genotypes was assessed. Surprisingly, all purified diets exhibited a significant reduction in microbial rhythmicity on all taxonomic levels, irrespective of genotype. Consequently, the number of rhythmic zOTUs was comparably low (<8%) in both genotypes **(Figure 29 A,B).** Out of the 390 zOTUs measured, intestinal clock dysfunction only resulted in arrhythmicity of a total of 8 zOTUs in CD-fed mice, 15 zOTUs upon HFD feeding, and 18 zOTUs upon WD feeding **(Figure 29 A,B).** Several arrhythmic zOTUs were also differentially abundant between genotypes **(Figure 29A, Figure 29 C,D,E).** Examples include *Anaerotruncus* and a member of the *Ruminococcaceae* family in CD-fed mice **(Figure 29C)**, *Oscillibacter* and *Blautia* in HFD-fed mice **(Figure 29D),** and *Oscillibacter, Paludicola* and members of the *Lachnospiraceae* family in WD-fed mice **(Figure 29E)**. The remaining zOTUs (~ 360) remained arrhythmic in both control and *Bmal1*$^{IEC-/-}$ mice.

Taken together, these findings suggest that intestinal clock dysfunction promotes diet-induced body weight gain by influencing host and microbial fat and sugar metabolism. Importantly, this effect was additive to the role of the intestinal clock in balancing the host's metabolism by driving the rhythmicity of the microbiota.

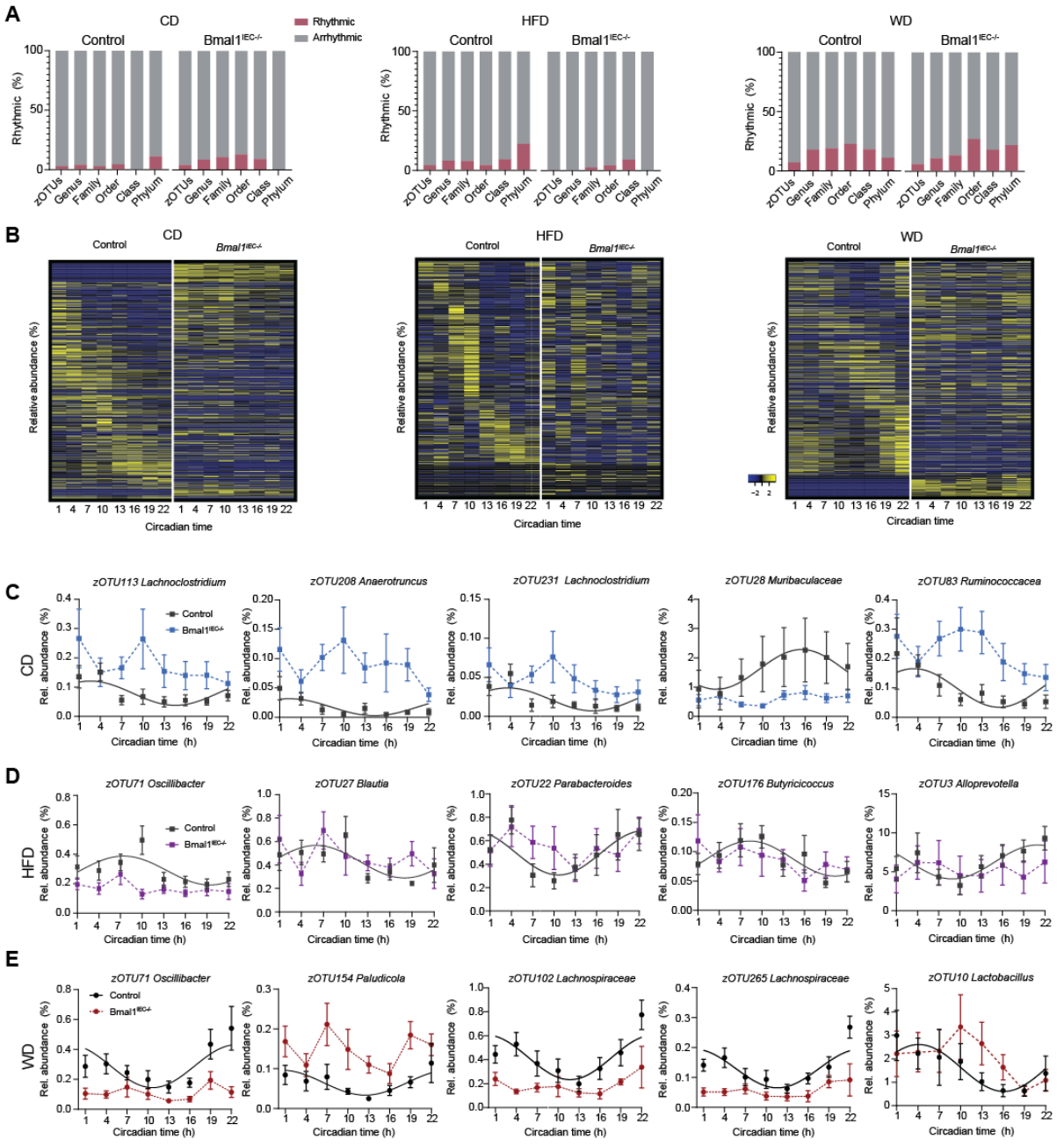

Figure 29 Fiber-deprived purified diets abolish microbial rhythmicity.
(A) Rhythmicity percentage of all taxonomies identified by JTK_Cyle. **(B)** Heatmap depicting relative abundance of all zOTUs. **(C)** Examples of zOTUs losing rhythmicity in *Bmal1*$^{IEC-/-}$ mice upon a control diet (CD), **(D)** high-fat diet (HFD), and **(E)** western diet (WD). Significant rhythms (cosine-wave regression, p-value ≤ 0.05) are illustrated with fitted cosine-wave curves; data points connected by dotted lines indicate no significant cosine fit curves (p-value > 0.05) and thus no rhythmicity.

4.10 Lack of fermentable fiber suppresses microbial rhythmicity

Previous studies have primarily focused on the suppression of microbial rhythmicity in purified HFDs compared to chow diets, which are typically high in fermentable fiber (P.J, 2008; Pellizzon & Ricci, 2018). However, it is essential to acknowledge that the purified HFDs used in these studies are fiber-depleted, potentially confounding the interpretation of the results. Building upon these observations, the aim was to investigate the specific role of dietary fiber in microbial rhythmicity in addition to dietary fat content.

To address this, the same cohort of control mice and intestinal clock-deficient mice were exposed to a series of dietary interventions, including a fiber-rich chow diet with an unknown but highly variable fermentable-fiber composition (>13% fiber), a low-fermentable fiber CD (5% cellulose), and a high-fermentable fiber supplemented CD (CFi, 13.6% mixture of oat fibers, inulin, pectin, and lignocellulose) **(Figure 30A)**. These diets were designed to have similar fat content (∼5%) while differing in their percentage of digestible fiber **(Figure 30B)**. Fecal samples were collected over a 24-hour period after two weeks of each diet intervention **(Figure 30A).**

Analysis of beta-diversity revealed distinct clustering patterns based on the different diets, as visualized in the phylogenetic tree **(Figure 30C).** Furthermore, GUniFrac analyses demonstrated differences in microbial composition between genotypes within each dietary condition (chow p=0.065, CD p=0.001, CFi p=0.001) **(Figure 30 D,E)**. Additionally, alpha-diversity measurements showed that the diet impacted microbial diversity in both genotypes, which was correlated with the amount of fermentable fiber present, with the lowest species richness observed in CD-fed mice **(Figure 30F).** Of note, body weight remained unaltered between genotypes and dietary interventions **(Supplementary Figure 14).**

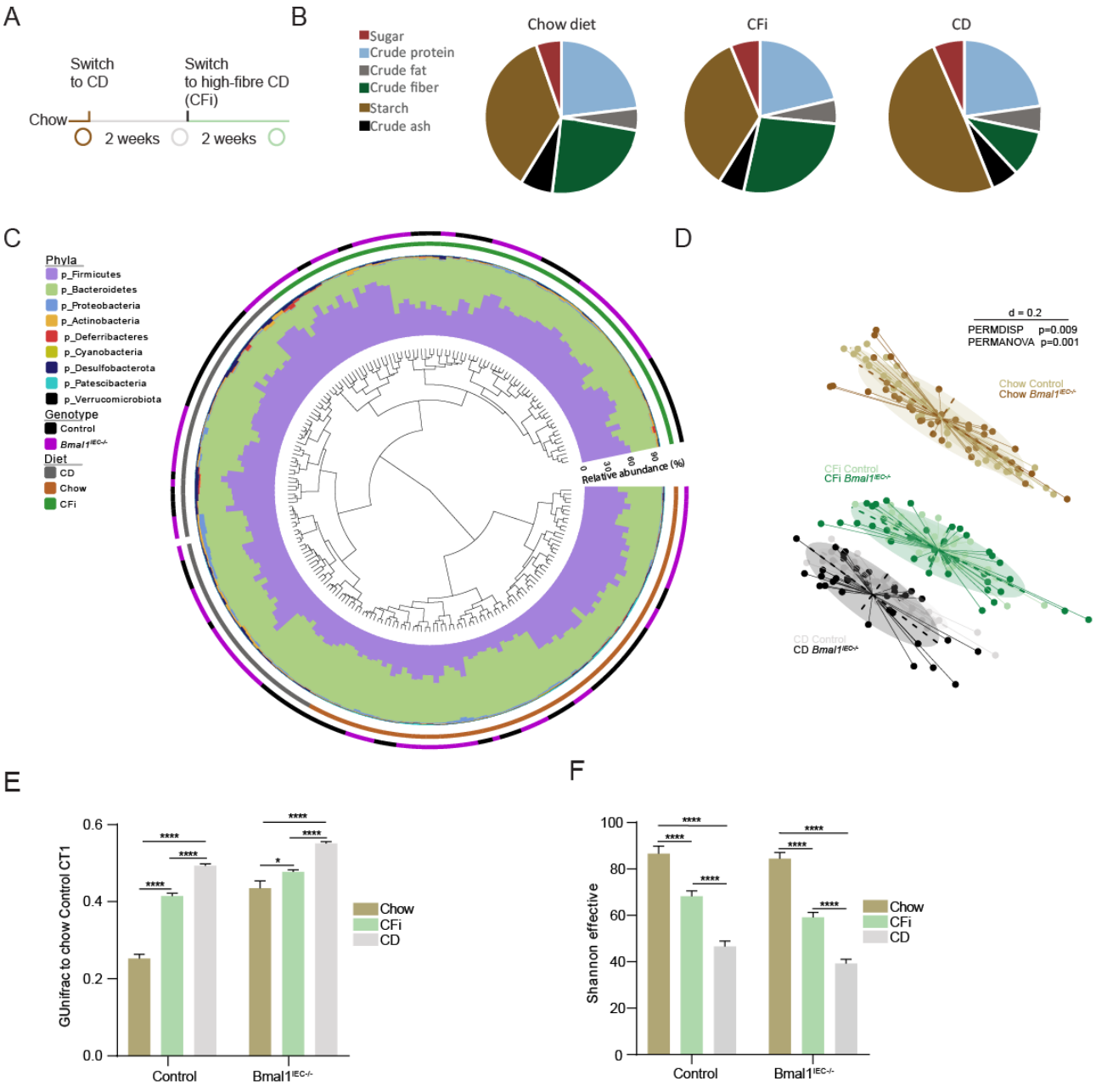

Figure 30 Fiber-dependent alterations in microbial communities'
(A) Schematic illustration of experimental design. The circle indicates a 24-hour fecal sampling time point. **(B)** Pie-charts indicating nutrient content of diets (% of total). **(C)** Dendogram reflecting beta-diversity of fecal microbiota based on generalized UniFrac distances between individual mice' microbiota. Individual taxonomic composition at the phylum level is shown as stacked bar plots around the dendogram. Stripes in the outer part indicate diet; first ring and genotype; second ring. **(D)** Beta-diversity within and between dietary groups, illustrated by MDS plot based on generalized UniFrac distances (GUniFrac) distances of fecal microbiota. **(E)** GUniFrac quantification to the average of chow control CT1 samples. **(F)** Average Alpha-diversity (Shannon). *p<0.05, ****p<0.0001 (Two-way ANOVA).

16S rRNA sequencing over time revealed distinct levels of circadian rhythmicity at all taxonomic levels among the different fiber dietary conditions. Control mice fed chow exhibited the highest levels of rhythmicity, followed by CFi, while the lowest rhythmicity was observed in mice subjected to the low-fiber CD conditions **(Figure 31 A,C)**. These findings strongly indicate that microbial rhythmicity is indeed dependent on dietary fiber. Notably, the dominant phases of oscillating zOTUs differed between chow (CT10 and CT22) and CFi (CT14-16) diets **(Figure 31D)**. Consistent with previous results described under long-term chow dietary conditions, the absence of the intestinal clock led to a 40% reduction in the number of oscillating zOTUs **(Figure 31 B,E,F)**.

Importantly, although similar genotype differences in microbial rhythmicity were observed under fiber-rich CFi, these differences were diminished after two weeks of low-fermentable fiber CD conditions **(Figure 31 A-F)**. Specifically, in the absence of fermentable fiber, a noteworthy suppression of microbiota rhythmicity was observed in control mice, leading to a low level of microbial rhythmicity in both genotypes (zOTUs: 15% control, 7% *Bmal1*$^{IEC-/-}$) **(Figure 31 C,E).** For instance, highly abundant phyla such as Firmicutes and Bacteroidetes exhibited circadian rhythms in control mice under Chow and CFi conditions, but these rhythms were absent under CD **(Supplementary Figure 15).** Similarly, the robust rhythmicity of several families controlled by the intestinal clock and involved in fiber fermentation, including *Lachnospiraceae, Ruminococcaceae,* and *Oscillospiraceae*, as well as several zOTUs such as *Colidextibacter*, *Bacteroides, Alistipes* and *Parabacteroides,* was completely lost in control mice under CD conditions, aligning with the results obtained from *Bmal1*$^{IEC-/-}$ mice **(Figure 31 G,H, Table 8)**.

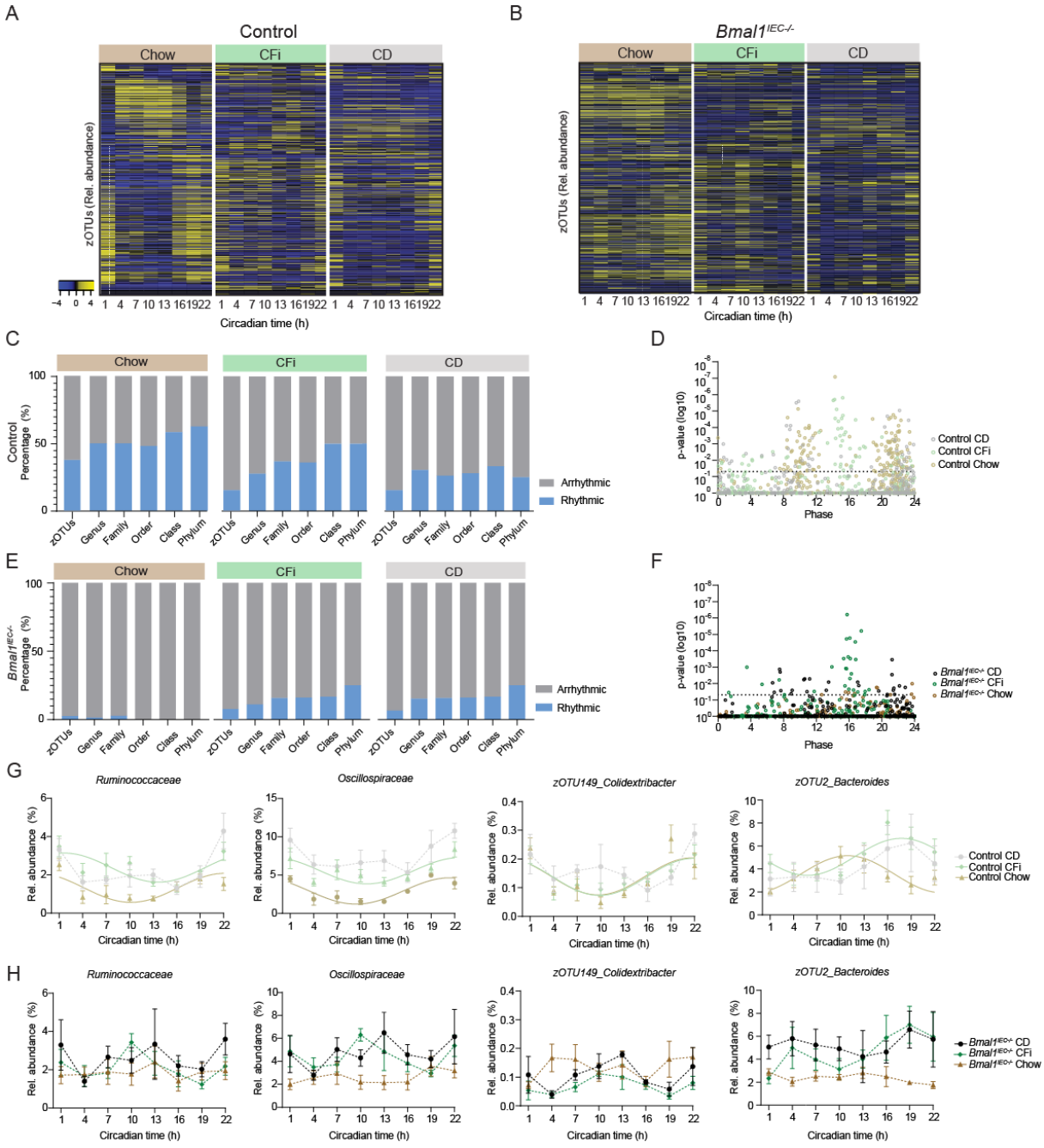

Figure 31 Circadian intestinal clock-controlled microbial rhythmicity is fiber dependent.
(A) Heatmap depicting the relative abundance of zOTUs in control and **(B)** *Bmal1*$^{IEC-/-}$ mice. Data are ordered by the peak phase in chow. Legend represents relative abundance where yellow means high and blue low abundance. **(C)** Bar graph representing the percentage of rhythmic (blue) and arrhythmic (grey) taxa in control mice. **(D)** Significance (Bonferroni adj. p-value JTK) and amplitude of rhythmic and arrhythmic zOTUs and their phase distribution in control mice. **(E)** Same as C for *Bmal1*$^{IEC-/-}$ mice and their **(F)** quantification of phase and p-value as described in D. **(G)** Circadian profiles of taxa in control mice and **(H)** *Bmal1*$^{IEC-/-}$ mice. Significant rhythms (cosine-wave regression, p-value ≤ 0.05) are illustrated with fitted cosine-wave curves; data points connected by dotted lines indicate no significant cosine fit curves (p-value > 0.05) and thus no rhythmicity.

Table 9 Taxonomic classification of fiber-dependent zOTUs.
zOTUs depicted show an overlap in rhythmicity between Chow and CFi fed mice, but remained arrhythmic in CD fed mice.

zOTU	*Adj. p-Chow*	*Adj. p CFi*	*Adj. p CD*	*Phyla*	*Family*	*Genera*
Zotu1	0.001	0.022	1	Bacteroidetes	*Bacteroidaceae*	*Bacteroides*
Zotu2	0.045	0.001	1	Bacteroidetes	*Bacteroidaceae*	*Bacteroides*
Zotu15	0.000	0.001	0.176	Bacteroidetes	*Muribaculaceae*	-
Zotu194	0.000	0.000	1	Bacteroidetes	*Muribaculaceae*	-
Zotu69	0.000	0.025	1	Bacteroidetes	*Muribaculaceae*	-
Zotu78	0.000	0.025	0.091	Bacteroidetes	*Muribaculaceae*	-
Zotu80	0.000	0.018	0.789	Bacteroidetes	*Muribaculaceae*	-
Zotu82	0.000	0.000	1	Bacteroidetes	*Muribaculaceae*	-
Zotu20	0.005	0.022	0.134	Bacteroidetes	*Prevotellaceae*	*Prevotellaceae UCG-001*
Zotu10	0.000	0.015	1	Bacteroidetes	*Rikenellaceae*	*Alistipes*
Zotu18	0.003	0.017	1	Bacteroidetes	*Rikenellaceae*	*Alistipes*
Zotu221	0.026	0.000	0.391	Bacteroidetes	*Rikenellaceae*	*Alistipes*
Zotu123	0.013	0.002	1	Bacteroidetes	*Tannerellaceae*	*Parabacteroides*
Zotu133	0.038	0.006	0.789	Bacteroidetes	*Tannerellaceae*	*Parabacteroides*
Zotu162	0.002	0.002	1	Bacteroidetes	*Tannerellaceae*	*Parabacteroides*
Zotu41	0.005	0.002	0.407	Bacteroidetes	*Tannerellaceae*	*Parabacteroides*
Zotu94	0.000	0.000	1	Bacteroidetes	*Tannerellaceae*	*Parabacteroides*
Zotu96	0.030	0.005	1	Firmicutes	*Lachnospiraceae*	-
Zotu107	0.000	0.006	1	Firmicutes	*Lachnospiraceae*	*Lachnoclostridium*
Zotu202	0.010	0.045	0.082	Firmicutes	*Lachnospiraceae*	*Lachnospiraceae FCS020 group*
Zotu68	0.000	0.022	0.192	Firmicutes	*Oscillospiraceae*	-
Zotu149	0.000	0.007	0.552	Firmicutes	*Oscillospiraceae*	*Colidextribacter*
Zotu192	0.019	0.000	1	Firmicutes	*Peptococcaceae*	*Peptococcus*
Zotu168	0.026	0.022	1	Firmicutes	*Ruminococcaceae*	-
Zotu232	0.001	0.006	1	Proteobacteria	-	-

The findings presented in this study collectively emphasize the crucial role of dietary fiber in governing microbial rhythmicity and their ability to enhance the amplitude of the intestinal clock. Additionally, the necessity of a functional intestinal clock for maintaining host metabolic homeostasis was demonstrated. Based on these discoveries, the hypothesis was that supplementing fiber in a high-caloric but fiber-depleted dietary situation, commonly observed in Western dietary patterns, could improve the metabolic response in control mice.

To test this hypothesis, HFD (48% kcal palm oil) was supplemented with a physiologically relevant concentration of the fermentable fiber inulin (9.4%). Inulin was previously found to impact peripheral clocks (Cheng et al., 2020). Contrary to our hypothesis, this supplementation did not lead to changes in body weight nor clock gene expression compared to HFD alone in control mice **(Figure 32 A,B).** Of note, an increase in pancreatic weight in control mice but not *Bmal1*$^{IEC-/-}$ mice was observed upon inulin supplementation **(Figure 32C).** Both genotypes revealed increased intestinal length of both the jejunum and colon segments, as well as an increased cecum weight upon inulin supplementation. However, the mass of fat deposits and the relative weights of other organs, including the liver, spleen, and MLNs, remained unaltered **(Figure 32C).** These results suggest that inulin alone, at the given concentrations and durations of the study, is insufficient to counteract the metabolic abnormalities induced by the HFD.

In summary, these findings underscore the significance of a mixture of fermentable fiber in regulating intestinal clock-controlled microbial oscillations and their impact on body weight. Moreover, they emphasize the importance of using an appropriate control diet when comparing microbial abundances and oscillations with purified interventional diets in metabolic studies.

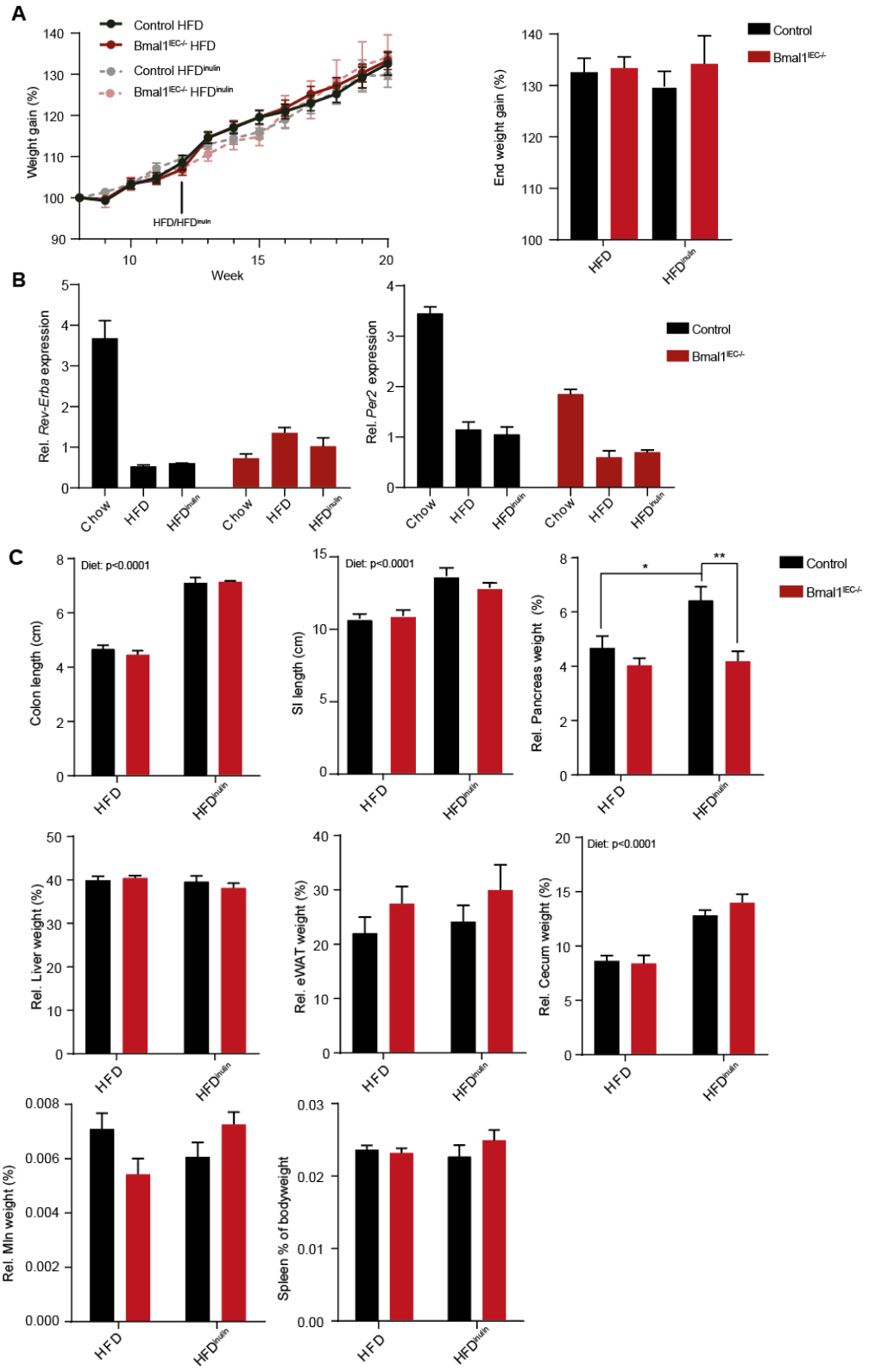

Figure 32 Inulin-enriched high-fat diet intervention does not improve body weight compared to HFD alone.
(A) Body weight gain of mice fed a high-fat diet (HFD) or a high-fat diet enriched with inulin (HFD^{inulin}) and their quantification at sacrifice (w20). **(B)** Clock gene expression at CT13 of chow, HFD and HFD^{inulin} fed mice. **(C)** Dissected organ and fat-pad weight relative to body weight and intestinal segment length. Significance was calculated with two-way ANOVA. * p<0.05, ** p<0.01.

5. Discussion

The circadian system plays a pivotal role in maintaining metabolic homeostasis by regulating various aspects such as energy balance, lipid homeostasis, and food intake patterns (Brubaker & Martchenko, 2022). This study aimed to investigate the involvement of the peripheral intestinal clock in metabolic regulation, specifically focusing on its interactions with the gut microbiome and its impact on carbohydrate and lipid metabolism. These findings shed light on the crucial role of the intestinal clocks in modulating circadian microbial rhythmicity and emphasize how dysregulation of this axis can contribute to metabolic disorders, including obesity. Furthermore, the disruption of the intestinal clock leads to disturbances in carbohydrate metabolism when exposed to a Western diet. This disruption is thought to be mediated by the intestinal clock control of rhythmic carbohydrate and lipid-relevant transcriptome. Additionally, this study highlights the importance of fermentable fiber in regulating intestinal clock functionality, the oscillations of the gut microbiota, and its potential implication in promoting metabolic health.

5.1 The role of the intestinal clock in regulating microbial rhythmicity and function

Previous research has established the existence of diurnal rhythmicity in microbial abundance and functionality (Leone et al., 2015; Liang et al., 2015; Reitmeier et al., 2020; Voigt et al., 2014; Zarrinpar et al., 2014). Building upon this knowledge, this study provides compelling evidence that the majority of microbial taxa exhibit rhythmicity in relative and quantitative abundance even in the absence of external timing cues, suggesting the presence of endogenous circadian mechanism within the host or the bacteria themselves.

Given the close relationship between the gut microbiota and intestinal epithelial cells (IECs), it was hypothesized that the intestinal clock could influence microbial circadian rhythms. To investigate this, mice with a specific deficiency of the *Bmal1* gene in IECs were used, referred to as *Bmal1*$^{IEC-/-}$ mice. The findings provide compelling evidence for the substantial contribution of the intestinal clock in shaping the circadian patterns of the microbiota. Over 50% of the rhythmic fecal and cecal microbial zero-radius operational taxonomic units (zOTUs) lost their rhythmicity in mice lacking a functional intestinal clock.

Several taxa, including *Odoribacter, Oscillibacter, Eubacterium, Bacteroides, Lactobacillus, Clostridium, Desulfovibrio, Ruminococcus, Agathobaculum,* and *Pseudoflavonifractor,* lost their rhythmicity in the absence of IEC-specific *Bmal1*. Many of these taxa were previously found to be regulated by rhythmic food intake, which serves as a prominent *Zeitgeber* for microbial rhythmicity (Leone et al., 2015; Thaiss

et al., 2014; Zarrinpar et al., 2014). However, despite exhibiting rhythmic food intake behavior, the *Bmal1*$^{IEC-/-}$ mice displayed a significant reduction in rhythmicity among these taxonomic families, indicating that rhythmic food intake is not the sole driver of microbial rhythmicity. This is in accordance with a study demonstrating sustained cecal microbial rhythmicity upon continuous intravenous parenteral nutrition (Leone et al., 2015). Moreover, taxa found to be arrhythmic in *Bmal1*$^{IEC-/-}$ mice, such as *Lactobacillus* and members of the *Lachnospiraceae* family, have previously been documented to lose their rhythmicity in mice lacking *Bmal1* or *Per1/2* tissue-wide (Liang et al., 2015; Thaiss et al., 2014), highlighting the importance of the IEC-clock in generating rhythmicity within these bacterial groups.

Of note, our analyses revealed a significant difference in the number of oscillating zOTUs between fecal and cecal content. Specifically, a higher number of oscillating zOTUs in fecal content was observed compared to cecal content. The reduced rhythmicity observed in cecal content can be attributed to several factors, including slower transit time, lower frequency of exposure to dietary substrates, and distinct interactions with the host, such as antimicrobial peptide production as well as immune modulation. These factors are well-known regulators of the microbiome (Donaldson et al., 2020). It is worth noting that the differences in sampling methods employed in this study could also contribute to the observed variations in microbial rhythmicity. Fecal sampling allows for non-invasive and frequent sampling from the same mouse over time (every 3-hours). In contrast, cecal samples were collected every 4 hours at sacrifice from different mice, resulting in larger variability within time points and a smaller sample size for statistical analyses. Nevertheless, most of the intestinal clock-controlled taxa in cecum content overlapped with the fecal microbiota. These intestinal clock-controlled taxa play diverse roles within the gut ecosystem. For example, *Odoribacter* and *Ruminococcus* are involved in carbohydrate metabolism and fiber fermentation, while *Bacteroidetes* and *Lactobacillus* possess the ability to metabolize proteins (Biddle, 2013; Carr et al., 2002; Gerard, 2013; Tailford et al., 2015; Tennoune et al., 2022). Accordingly, the loss of rhythmicity in these taxa upon intestinal clock deficiency suggests potential disruptions in their metabolic activities.

Based on predicted metagenome analyses, intestinal clock-controlled bacteria were strongly associated with ‘carbohydrate metabolism’, ‘amino acid biosynthesis’, and ‘nucleoside and nucleotide biosynthesis’. Cecal metabolomics analyses demonstrated significant alterations in metabolites related to taurine and bile acid metabolism. Furthermore, disruption of rhythmicity was observed in metabolites involved in pathways related to ‘starch and sucrose metabolism’, ‘galactose metabolism’, and the ‘biosynthesis of branched-chain amino acids (BCAAs)’. Additionally, increased levels of fecal and cecal microbial-produced branched-chain fatty acids (BCFAs), valeric acid, and secondary bile acids (BAs) were observed in mice lacking a functional intestinal clock. BCFAs are produced by bacteria such

as *Clostridium* and *Bacteroides* during the fermentation of BCAAs (Aguirre et al., 2016; Smith & Macfarlane, 1996). The elevated levels of BCFAs suggest a shift in bacterial metabolism from carbohydrates to protein fermentation (Hald et al., 2016; Pieper et al., 2012). Notably, the arrhythmicity as well as accumulation of BCAAs and specific secondary BAs, including deoxycholic acids (DCAs) and hyodeoxycholic acids (HDCAs), has been linked to metabolic disorders such as obesity and type 2 diabetes (Haeusler et al., 2013; McCormack et al., 2013; Reitmeier et al., 2020; Yoshimoto et al., 2013; Zheng et al., 2021). Furthermore, alterations in taurine-conjugated bile acids, including tauroursodeoxycholic acid (TUDCA), were observed in *Bmal1*$^{IEC-/-}$ mice. TUDCA has been found to improve insulin sensitivity in obese mice and humans (Kars et al., 2010; Ozcan et al., 2006). The loss of circadian rhythmicity in TUDCA and other bile acids indicates potential disruptions in bile acid metabolism and their associated health benefits. These findings provide compelling evidence supporting the critical role of the intestinal clock in regulating microbial metabolism. The disruption of microbial and metabolite rhythms observed in the absence of the intestinal clock reinforces the hypothesis that a functional IEC clock is essential for maintaining GI and metabolic health.

Mechanisms by which the intestinal clock regulates microbiota rhythms likely involve local interactions between the epithelium and microbes, immune functions, antimicrobial peptide production, and mucus secretion, all of which have previously been documented to display diurnal oscillations **(Figure 32)** (Frazier et al., 2022; Kuang et al., 2019; Mukherji et al., 2013; Wang et al., 2017). Our study demonstrated that the clock in intestinal epithelial cells plays an essential role in regulating mucus production. Mucus acts as a protective barrier in the gut and facilitates bidirectional communication between microbes and the host. For instance, mucus can influence microbial composition by providing bacteria with mucin glycans that they can use as an energy course (Koropatkin et al., 2012). This, in turn, affects the abundance of other microbial taxa through cross-feeding interactions (Schroeder, 2019). Furthermore, the intestinal clock's control of the secretion of metabolites, including BAs, can directly impact gut bacteria's growth, metabolism, and composition (Wahlstrom et al., 2016).

Moreover, slight alterations in intestinal morphology were observed, including an increase in jejunum length and colon density, as well as a shift in small intestinal permeability following intestinal *Bmal1* deletion. In addition, RNA-sequencing analyses revealed changes in genes related to nutrient absorption and immune regulation. The rhythmic patterns of nutrient availability and immune response, driven by the intestinal clock, may create selective pressures that shape the diurnal fluctuation in the microbiota composition (Zheng, Ratiner, et al., 2020). For example, arrhythmicity and dampened amplitude of the hexose transporter genes can affect the availability of glucose and fructose within the gut lumen (Onuma et al., 2022), thereby influencing the composition and metabolism of the gut microbiota, as these are primary carbon sources for various microbial taxa found

to be altered between *Bmal1*$^{IEC-/-}$ mice and their controls (Aguirre et al., 2016). In addition, the absence of the intestinal clock led to the downregulation of several genes involved in T-cell immunity. Although *Bmal1*$^{IEC-/-}$ mice do not develop intestinal inflammatory disorders, a reduction in lymphocyte subpopulations was observed, including CD4+ and CD8+ T-cells, in the small intestine, along with upregulated fecal levels of complement factor 3. These findings suggest a shift in the immune response towards innate immunity dominance. This imbalance could potentially disrupt the finely-tuned interaction between the host immune system and the gut microbiota, leading to altered immune responses and subsequent changes in microbial composition. It is important to note that these interpretations are based on our findings and are speculative. Further studies are required to fully elucidate the precise mechanisms underlying the intestinal clock control of microbial composition.

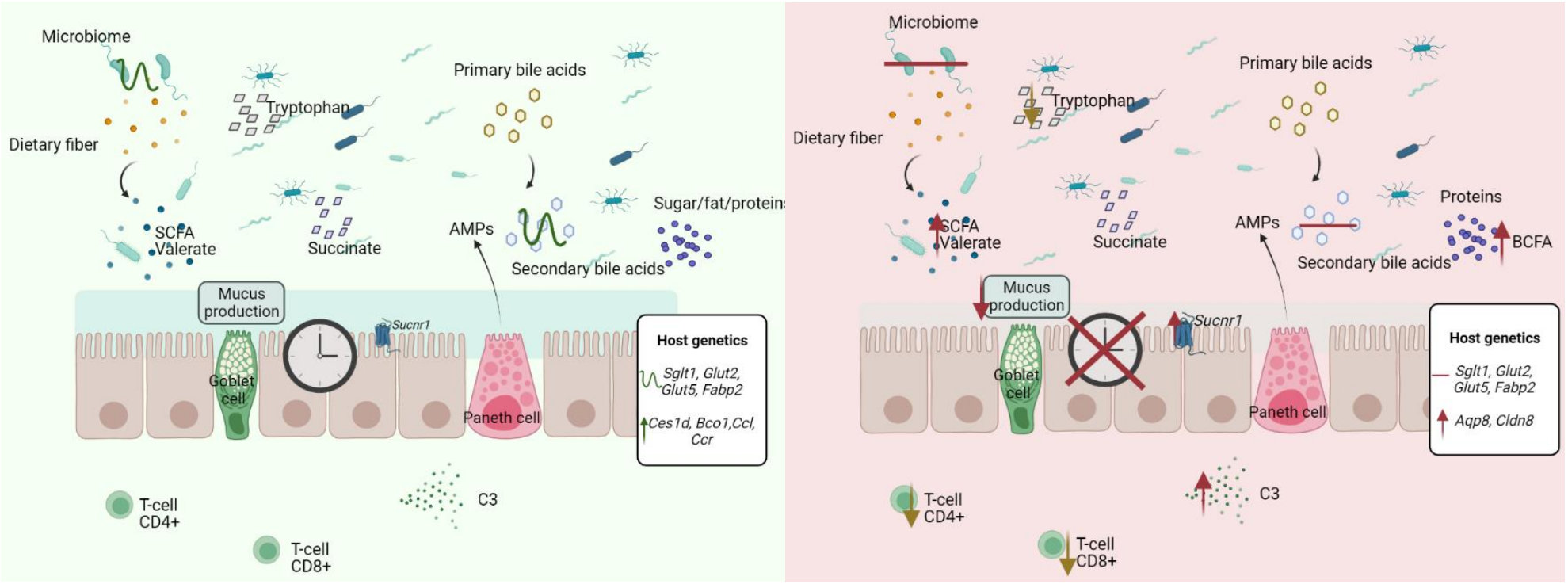

Figure 33 Summary of altered (microbiota-derived) metabolites, host genetics, and their consequences on immune regulation in intestinal clock-deficient mice.
(Left) The circadian clock of intestinal epithelial cells (IECs) plays a crucial role in maintaining the rhythmicity of the gut microbiome, which reciprocally supports IECs through the production of beneficial nutrient fermentation by-products such as short-chain fatty acids (SCFAs), lactate, bile-acids, indoles, and branched-chain fatty acids (BCFAs). These metabolites enhance cellular energy production, regulate gut motility, and promote metabolic flexibility. Furthermore, the mucus layer provides a protective barrier between the gut lumen and epithelial cells. The genetic makeup of the host also influences the composition of the microbiota and the immune response. Metabolic interactions between IECs and microbial metabolites are instrumental in regulating the recruitment and differentiation of immune cells in the intestinal mucosa. Conversely, immune cell-derived factors, including cytokines, can affect the functioning of IECs by targeting metabolism. Disruption of the intestinal clock (right) results in an arrhythmic microbiome, altered microbial metabolite concentrations, and reduced mucus production by the goblet cells. Consequently, immune-cell recruitment patterns are compromised, and complement factor 3 (C3) levels are upregulated. Host genetics, including hexose transporter genes have been shown to be arrhythmic; while the expression levels of *Sucnr1, Aqp8* and *Cldn8* are upregulated. These changes indicate dysregulation in nutrient transport and ion channel functions, capable of altering microbial composition. AMPs (anti-microbial peptides); *Sglt1* sodium-glucose cotransporter isoform 1; *Glut2/5* Glucose transporter; *Fabp2* fatty acid binding protein 2; *Aqp8* Aquaporin 8; *Cldn8* Claudin 8; *Ces1d* Carboxylesterase 1d; *Bco1* Beta-Carotene Oxygenase 1; *Ccl* C-C Motif Chemokine Ligand; *Ccr* C-C Motif Chemokine Receptor.

5.2 Implications of intestinal clock-controlled microbiota on metabolic and immune health.

Recent research has highlighted the functional connection between microbiota arrhythmicity and the development of conditions such as obesity and type 2 diabetes (T2D) (Reitmeier et al., 2020). In this study, intestinal clock disruption leads to arrhythmicity of specific bacterial species associated with metabolic health, including Proteobacteria, *Muribaculacea,* and *Lachnospiraceae* (Janssen & Kersten, 2017; Lagkouvardos et al., 2019). Moreover, untargeted metabolomics analysis revealed that approximately 30% of the circadian cecal metabolome lost its rhythmicity in *Bmal1*$^{IEC-/-}$ mice, particularly affecting metabolites involved in lipid and carbohydrate metabolism. Key pathways related to 'galactose metabolism', 'biosynthesis of unsaturated fatty acids', and 'starch and sucrose metabolism' were under the control of the intestinal clock. Of note, similar pathways were disturbed by the arrhythmic microbiome in T2D patients (Reitmeier et al., 2020). These findings underscore the critical role of a functional intestinal clock in preserving the rhythmicity of the microbiome, which in turn is essential for maintaining optimal host metabolism.

Cecal microbial transfer experiments were conducted from intestinal clock-deficient donors to germ-free wild-type mice to demonstrate the physiological relevance of intestinal clock-controlled microbiota. Results revealed that the transfer of arrhythmic microbiota and associated metabolites into recipient mice led to an obese phenotype, as evidenced by a significant increase in body weight and fat mass. This aligns with previous studies that reported metabolic alterations in recipient mice following the transfer of microbiota obtained from mice undergoing circadian disruption (Altaha, 2022; Thaiss et al., 2014). Interestingly, most of the microbial families, such as *Muribaculacea* and *Lachnospiraceae,* which lost rhythmicity in intestinal clock-deficient donor mice, also exhibited similar patterns in the recipients. Consequently, the abundance of microbial metabolites, including SCFAs and BAs, which are critical in carbohydrate and fatty acid metabolism (den Besten et al., 2013), depended on the donor genotype. *Bmal1*$^{IEC-/-}$ recipients displayed an increase in microbial energy harvest from SCFAs, while levels of bacterial-derived secondary BAs, such as hyodeoxycholic acid (HDCA) known to reduce body weight gain and improve glucose metabolism (Makki et al., 2023), were significantly reduced.

Furthermore, the development of obesity following the transfer of arrhythmic microbiota was accompanied by an increase in T-cell recruitment in the adipose tissue, suggesting the involvement of immune cells in metabolic dysfunction. In addition, recipient mice that received microbiota from intestinal clock-deficient mice exhibited small-intestinal and colonic shortening, as well as suppressed CD4+ and CD8+ T-cell recruitment to the lamina propria. Similar alterations in intestinal parameters

were observed in the specific-pathogen-free donors, indicating the direct influence of the arrhythmic microbiota on the intestinal immune response (Zheng, Liwinski, et al., 2020; Zheng et al., 2021). Mechanisms likely involved specific microbial-produced metabolites. For example, both *Bmal1*$^{IEC-/-}$ donor and recipient mice exhibit upregulated levels of ketolitocholic acid and BCFAs, which are both capable of modulating the adaptive immune cell population (Song et al., 2020).

While intestinal clock deficiency led to microbial arrhythmicity, changes in the overall composition of the microbiota were also observed. Therefore, it is plausible that the physiological alterations observed in recipients following microbiota transfer could be attributed to changes in microbial composition rather than solely rhythmicity. Nonetheless, these findings underscore the importance of intestinal clock-controlled bacteria and bacterial-derived metabolites in the regulation of obesity and shed light on the complex interplay between the intestinal circadian clock, the microbiome, and metabolic health. In addition, these findings provide initial evidence that intestinal clock-controlled gut bacteria are essential for maintaining balanced intestinal immune homeostasis and likely influence the immune response to pathogens, infections, and inflammation.

5.3 Impact of the intestinal clock on host metabolism under western diet conditions

Dysfunctions in the global circadian clock have been associated with metabolic abnormalities in humans, and studies using mouse models have revealed the importance of tissue-specific circadian clocks in overall metabolism. For example, lack of the circadian clock in the liver, adipose tissue, muscle, and pancreas led to disrupted energy homeostasis, as well as lipid and carbohydrate metabolism (Onuma et al., 2022; Pan et al., 2016; Paschos et al., 2012; Wada et al., 2018; Yu et al., 2021).

In this study, additional evidence is presented highlighting the role of the peripheral intestinal clock in regulating host metabolism, specifically through the microbiome. *Bmal1* deficiency in IECs led to increased body weight gain in mice exposed to a westernized diet (WD), consisting of a high-fat diet (HFD) and a high-sucrose solution (30%). Notably, mice exhibited reduced pancreatic weights and slightly elevated fasting glucose levels, reminiscent of diabetes (Garcia et al., 2017). Mechanisms likely include the role of the jejunal clock in regulating key metabolic genes involved in carbohydrate and lipid metabolism. In particular, the intestinal clock was found to regulate the circadian expression of hexose transporters, including *Glut5, Glut2,* and *Sglt1,* involved in the uptake of fructose, glucose, and galactose, as well as genes *Fabp2* and *Dgat2* implicated in intestinal fat absorption (Onuma et al., 2022; Yu et al., 2021). Upon WD conditions, the expression levels of *Glut5* and *Sglt1* in the jejunum were significantly suppressed in *Bmal1*$^{IEC-/-}$ mice compared to their controls, indicative of sugar

malabsorption (Soleimani & Alborzi, 2011). These findings collectively demonstrate that dysfunction of the jejunal clock exacerbates metabolic abnormalities under conditions of abnormal dietary sucrose and fat levels.

Interestingly, HFD alone did not increase body weight gain in *Bmal1*$^{IEC-/-}$ mice. Contrasting findings have been reported in previous studies, where a lack of intestinal *Bmal1* was shown to protect against HFD-induced obesity (Yu et al., 2021). Differences in the metabolic phenotype of the same mouse model between studies may be attributed to various experimental conditions, such as the amount and type of fat and the feeding duration. Reduced weight gain under HFD was found when *Bmal1*$^{IEC-/-}$ mice received 60% cholesterol-rich lard fat for a duration of 10 weeks (Yu et al., 2021), whereas in our study, 8 weeks of 48% low-cholesterol palm oil was fed. Similar inconsistencies in body weight were observed in chow-fed whole-body *Bmal1* knockout models (Lamia et al., 2008; McDearmon et al., 2006). Therefore, the comparability between studies may be impacted by additional factors influencing the host's metabolism, including the microbial ecosystem, which has been reported to vary dramatically between facilities (Parker, 2018). Indeed, the body weight of microbiome-depleted germ-free (GF) *Bmal1*$^{IEC-/-}$ mice was undistinguishable from controls, whereas specific-pathogen-free (SPF) microbial-rich mice developed a housing-dependent increased body weight, highlighting the importance of specific intestinal clock-controlled microbiota for host metabolism.

5.4 Modulation of microbial rhythmicity by dietary fiber and implications for metabolic health

One surprising finding of this study is the suppressed microbial rhythmicity in control mice upon CD, HFD, and WD feeding. Notably, a significant difference in microbial rhythmicity between control and *Bmal1*$^{IEC-/-}$ mice was only observed under fiber-rich diets, including chow and fermentable fiber-supplemented CD (CFi), whereas this genotype difference was almost absent under CD, HFD, and WD conditions. These findings confirm results from previous studies, demonstrating the suppression of microbial rhythms upon HFD (Leone et al., 2015; Zarrinpar et al., 2014). Important to note is that these conclusions were based on a comparison between high-caloric purified dietary conditions and fiber-rich chow-fed control conditions. Given the fact that in our study CD fed mice showed an equal suppression of microbial rhythmicity as HFD, our results clearly demonstrate that the absence of fiber, rather than an increase in fat content, reduces the amount of bacterial oscillations. Therefore, quantification of microbial rhythmicity under controlled experimental dietary conditions needs to be compared to a suitable purified control diet rather than chow diets, which lack standardization across vendors and seasons (Morrison et al., 2020; Pellizzon & Ricci, 2018; Tuganbaev et al., 2020). To

properly investigate host health, independent of variations in microbial richness or rhythmicity, results from this study suggest the use of standardized purified diets enriched with fermentable fibers.

The dampening of microbial rhythmicity under fiber-depleted diets in control mice may result from altered intestinal clock functioning. Specifically, the intestinal clock gene *Rev-Erba* exhibited a changed time-dependency at its circadian peak under fiber-depleted diets compared to a fiber-rich chow diet. Accordingly, prior reports showed phase shifts in peripheral clock gene expression in Per2::Luc mice fed rapidly fermentable cellobiose fibers compared to cellulose, which is resistant to microbial fermentation, indicating crosstalk between peripheral clock genes and fermentable fiber intake (Marques et al., 2017; Tahara et al., 2018). Additionally, the core intestinal clock genes *Bmal1* and *Per2* showed dampened expression compared to chow conditions, although these clock genes peak at slightly different circadian time points. Further experiments including additional circadian time points are needed to differentiate between phase shifts and suppression of the circadian amplitude of these genes.

Nevertheless, given that the intestinal clock drives microbial rhythmicity, our results suggest that the suppressed microbial rhythmicity observed in control mice fed fiber-depleted high-caloric diets (HFD and WD) was likely due to changes in intestinal clock mechanisms. Thus, stabilizing intestinal clock function during HFD feeding could potentially restore microbial oscillations and improve metabolic homeostasis. In line with this hypothesis, time-restricted feeding with HFD has been shown to stabilize peripheral clock gene expression, increase microbial rhythmicity, and result in reduced weight gain compared to ad libitum feeding (Leone et al., 2015; Zarrinpar et al., 2014). In addition, previous studies showed the capability of prebiotics, including inulin, in regulating circadian gene expression, thereby attenuating circadian misalignment brought on by altered light-dark cycles in mice as well as ameliorating HFD-induced obesity (Cheng et al., 2020; Li, 2023). In this study, HFD was supplemented with 9% inulin, a fermentable fiber, aiming to stabilize peripheral clock gene expression in control mice. Although the enrichment of HFD with inulin resulted in a slight reduction in body weight gain and gonadal fat pad mass compared to HFD alone, these changes did not reach statistical significance. Moreover, intestinal clock gene expression remained unaltered compared to HFD alone. Of note, only CT13 was measured within those mice, and more time points are needed to make a firm conclusion. These findings highlight the need for further research to explore the effect of targeting the intestinal clock on microbial rhythmicity and metabolic disorders. Strategies involving a mixture of fermentable fibers, higher concentrations, a longer intervention duration, or RF with fiber-rich diets are warranted to target the intestinal clock more effectively.

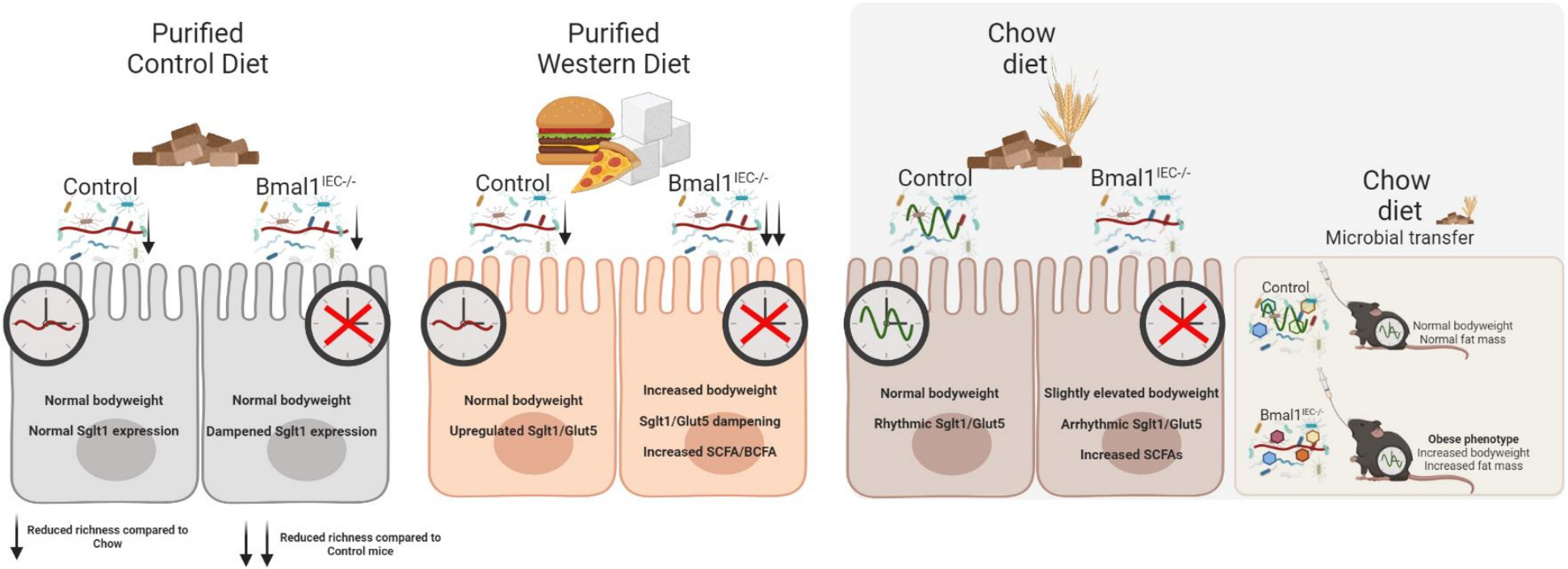

Figure 34 Summary of results from dietary intervention studies on mice with intestinal clock deficiency.
This figure illustrates the key findings obtained from dietary intervention studies conducted on mice with intestinal clock deficiency. Summarizing the dietary effects on body weight, microbiota (richness rhythmicity, metabolites), and hexose transporter expression in control and *Bmal1*$^{IEC-/-}$ mice. When mice were fed a purified control diet, no significant differences in body weight or microbial rhythmicity were observed between the two genotypes. However, the expression of hexose transporters was reduced in *Bmal1*$^{IEC-/-}$ mice compared to controls. In contrast, when the mice were subjected to a high-fat high-sugar purified western diet, the intestinal clock-deficient mice exhibited significant weight gain and a decrease in microbial richness compared to their control counterparts. Furthermore, alterations in microbial-produced metabolites and hexose transporter genes were observed between the two genotypes. Interestingly, all purified diets, including the control diet and western diet, led to a significant reduction in microbial richness and rhythmicity compared to the high-fiber chow conditions. Under chow-fed conditions, the intestinal clock-deficient mice displayed a significant suppression of microbial rhythmicity, arrhythmic hexose transporter genes, and increased concentrations of branched-chain fatty acids (BCFAs). Notably, when the microbiota derived from chow-fed *Bmal1*$^{IEC-/-}$ mice were transferred to germ-free mice, it resulted in an obese phenotype characterized by increased body weight and fat mass compared to the transfer of microbiota derived from control mice.

6. Conclusion and perspective

Taken together, this study provides compelling evidence for the significant role of the peripheral circadian clock, located specifically in intestinal epithelial cells, in maintaining metabolic homeostasis. Our findings demonstrate that the intestinal clock regulates energy homeostasis through two distinct mechanisms, namely by regulating fat and sugar metabolism, as well as circadian microbial rhythmicity. Moreover, the crucial role of dietary fiber in the circadian regulation of the microbiota has been discovered, thereby establishing a novel link between diet, microbial rhythmicity, the intestinal clock, and host metabolism.

Moving forward, there are several exciting avenues for further exploration in this field. First and foremost, the mechanistic underpinnings of how the intestinal clock interacts with the temporal dynamics of the gut microbiota to regulate metabolism warrant further investigation. While this study has suggested some key players, there is still much to uncover. As most of the rhythmicity is observed in the fecal content, a multi-omics characterization of colonic tissue from both control and intestinal clock-deficient mice might shed light on several mediators.

Furthermore, translating these findings into clinical applications and therapeutic interventions is a crucial next step. Developing strategies to manipulate the intestinal clock-microbiota-diet axis to promote metabolic health holds tremendous potential. This could involve the use of targeted probiotics, prebiotics, or fecal microbial transplantation to modulate the composition and function of the gut microbiota in a time-dependent manner. Additionally, designing dietary interventions with mixed-fermentable fibers or timed-restricted feeding, with the goal of promoting peripheral clock gene expression and microbial rhythmicity, could be explored as a means to prevent or treat metabolic disorders.

In conclusion, the intricate relationship between the intestinal clock, gut microbiota, and host metabolic functioning has far-reaching implications for our understanding and management of metabolic health. The results presented here provide a foundation for further exploration. By unraveling the role of the peripheral intestinal clock, we move closer to uncovering novel therapeutic strategies for combating obesity and related metabolic disorders.

Supplements

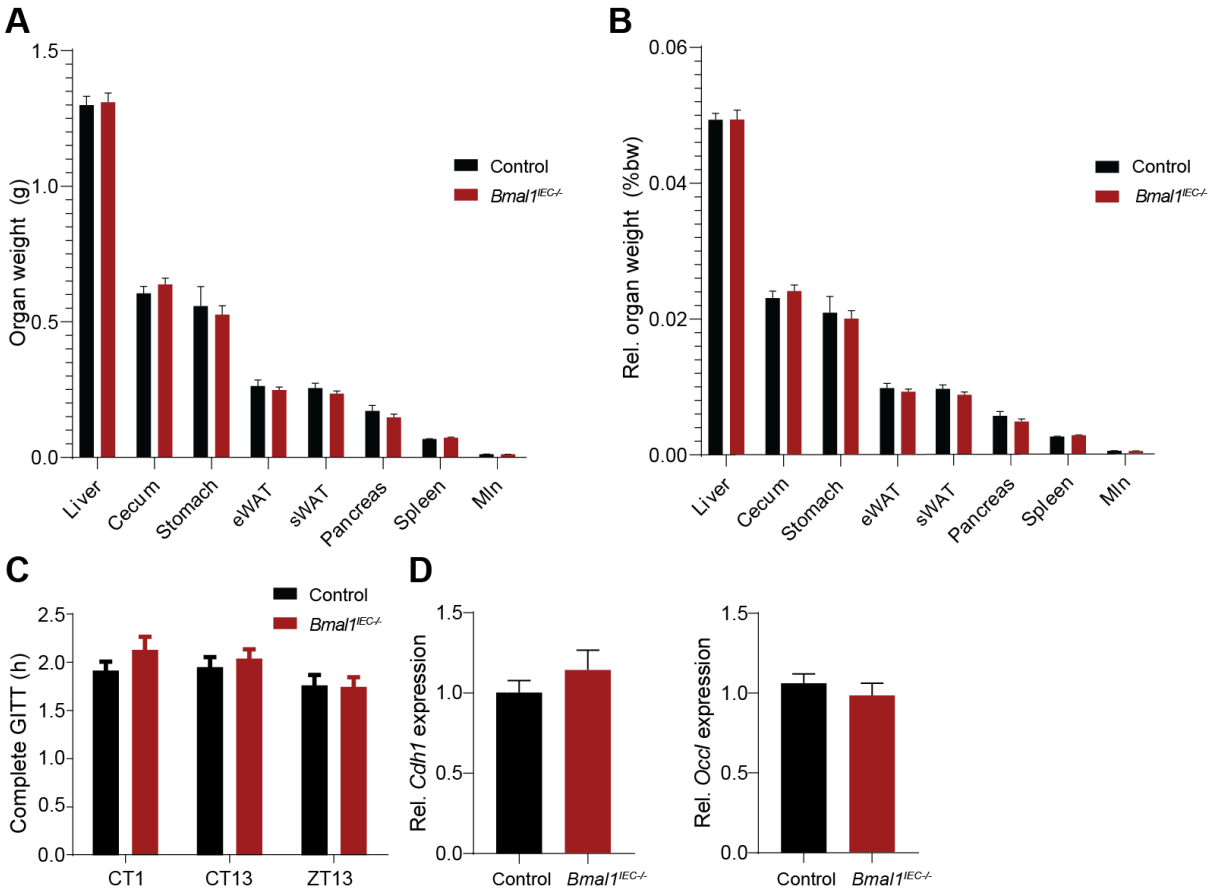

Supplementary Figure 1 Dissected organ weights, total intestinal transit time and barrier markers remain unaltered upon intestinal *Bmal1* ablation.
(A) Organ weight and **(B)** relative organ weight normalized to total body weight and **(C)** total gastrointestinal transit time (GITT) measured through oral gavage of carmine red as well as **(D)** jejunal barrier markers measured through qPCR of control and *Bmal1*$^{IEC-/-}$ mice.

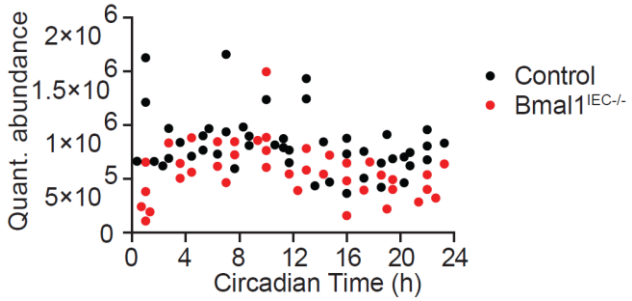

Supplementary Figure 2 Intestinal clock deficiency does not affect circadian 16s copy number.
16S copy number over time, measured with the use of spike-in analyses, of control and *Bmal1*$^{IEC-/-}$ mice.

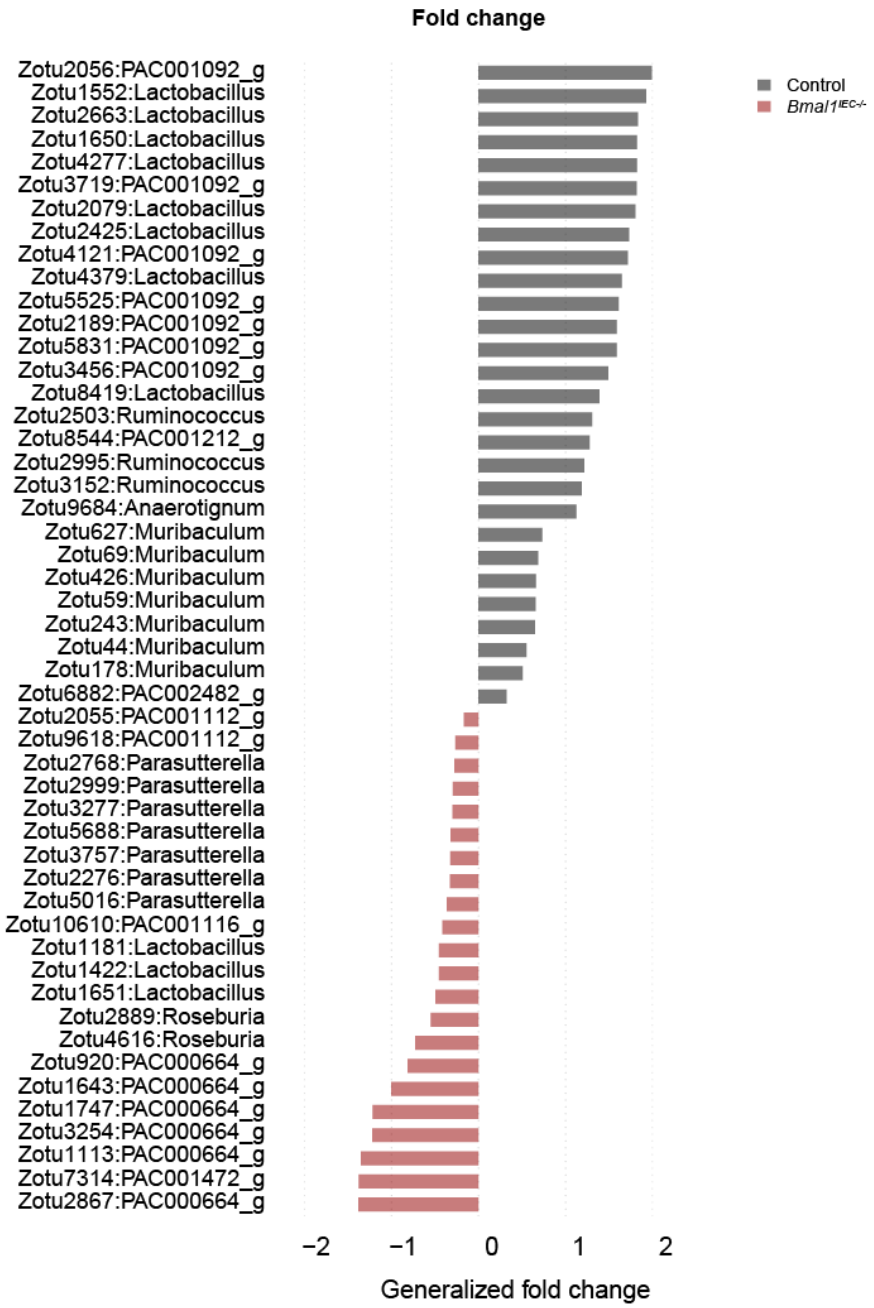

Supplementary Figure 3 Overall fecal zOTU abundance differences between control and *Bmal1*$^{IEC-/-}$ mice.
Generalized (Log2) fold change of the quantitative abundances of fecal zOTUs showing significant difference between *Bmal1*$^{IEC-/-}$ and control mice.

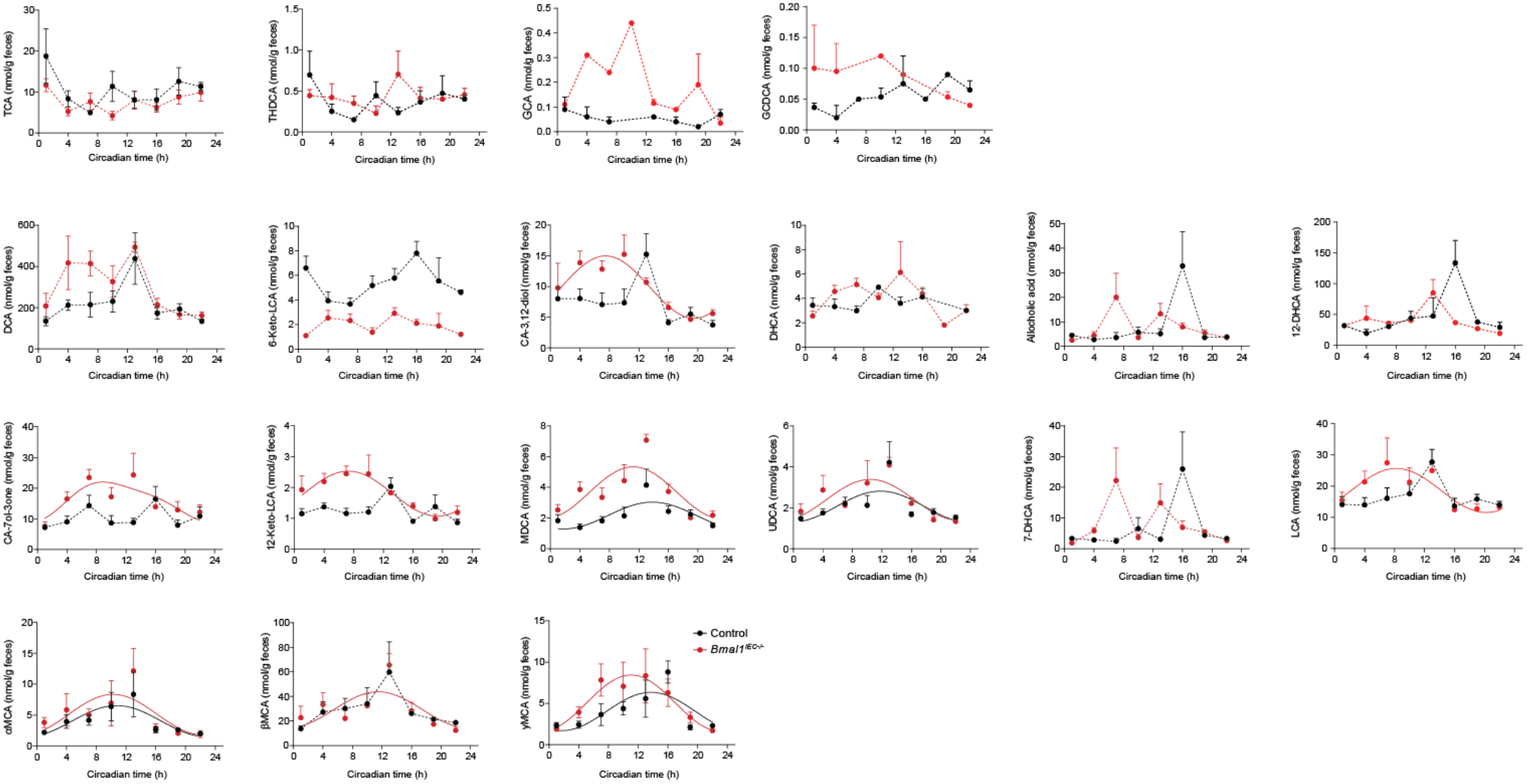

Supplementary Figure 4 Circadian fecal bile acid profiles. Fecal bile acid concentrations measured in feces with the use over the circadian day in control and Significant rhythms (cosine-wave regression, p-value ≤ 0.05) are illustrated with fitted cosine-wave curves; data points connected by dotted lines indicate no significant cosine fit curves (p-value > 0.05) and thus no rhythmicity.

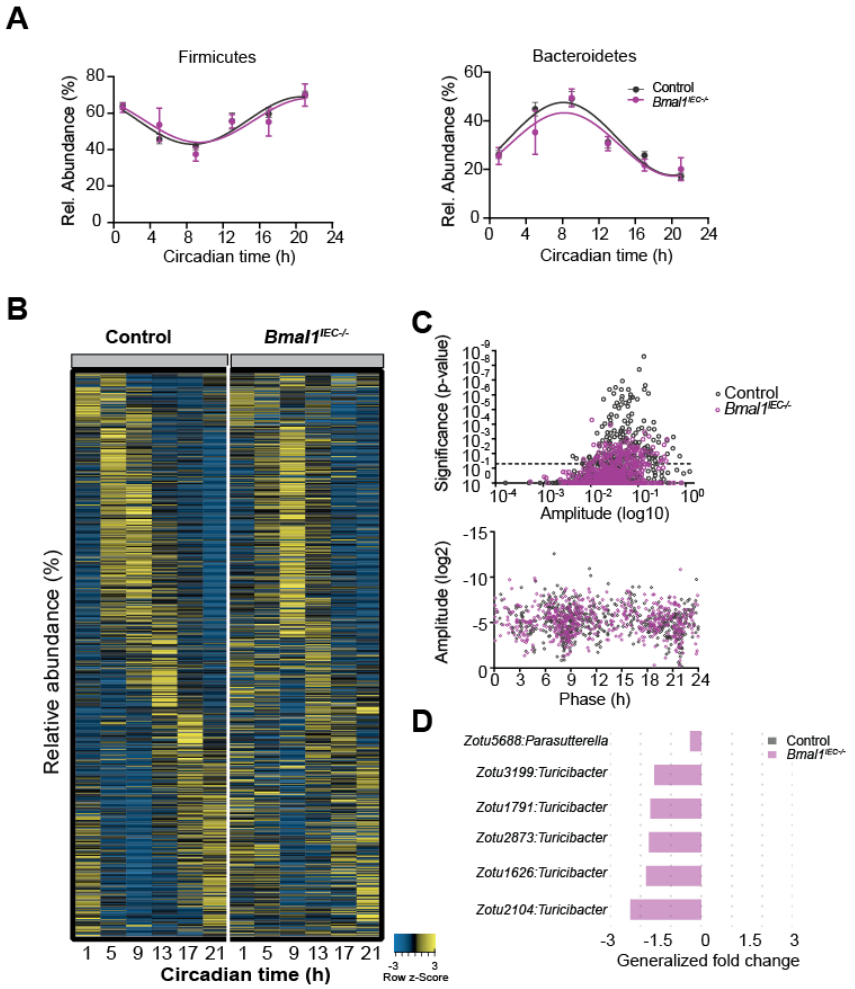

Supplementary Figure 5 Cecal relative abundance analyses.
(A) Circadian profiles of relative abundance of Firmicutes and Bacteroidetes. Significant rhythms (cosine-wave regression, p-value ≤ 0.05) are illustrated with fitted cosine-wave curves. **(B)** Heatmap depicting the relative abundance of 580 zOTUs over time. p-value, amplitude and phase plotted for all measured zOTUs. **(D)** Generalized (Log2) fold change of the quantitative abundances of cecal zOTUs showing significant difference between *Bmal1*$^{IEC-/-}$ and control mice. Purple color indicates increase abundance in the *Bmal1*$^{IEC-/-}$ samples.

A

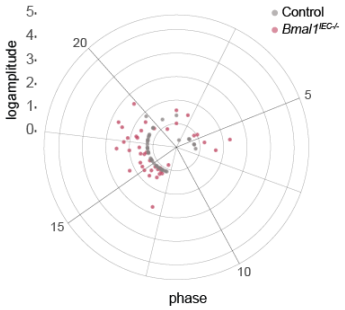

B

KEGG	Adj. p -value
Non-alcoholic fatty liver disease	9.25E -04
Diabetic cardiomyopathy	1.68E -03
Prion disease	4.50E -03
Amyotrophic lateral sclerosis	1.25E -02
Parkinson disease	1.95E -02
Oxidative phosphoryation	2.51E -02
Retrograde endocannabionoid signaling	2.57E -02
Huntington disease	2.57E -02
Hepatitis C	2.67E -02
Alzheimer disease	3.98E -02

C

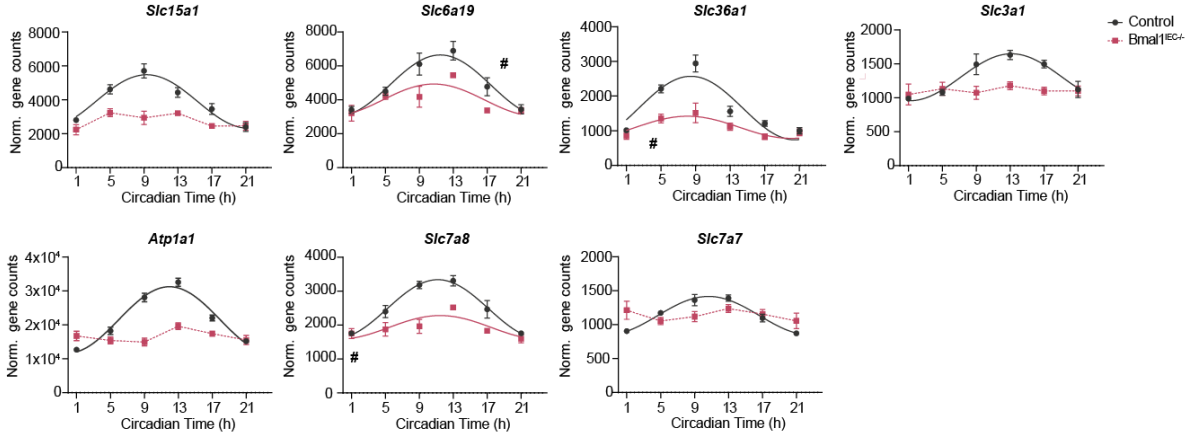

Supplementary Figure 6 Gain of rhythmicity in genes involved in oxidative phosphorylation in *Bmal1*$^{IEC-/-}$ mice.
(A) Polar plot of genes gaining rhythmicity in *Bmal1*$^{IEC-/-}$ mice compared to their controls and their **(B)** gene set enrichment analyses. **(C)** Genes involved in protein metabolism loosing/changing rhythmicity in in *Bmal1*$^{IEC-/-}$ mice compared to their controls. Significant rhythms (cosine-wave regression, p-value ≤ 0.05) are illustrated with fitted cosine-wave curves; data points connected by dotted lines indicate no significant cosine fit curves (p-value > 0.05) and thus no rhythmicity.

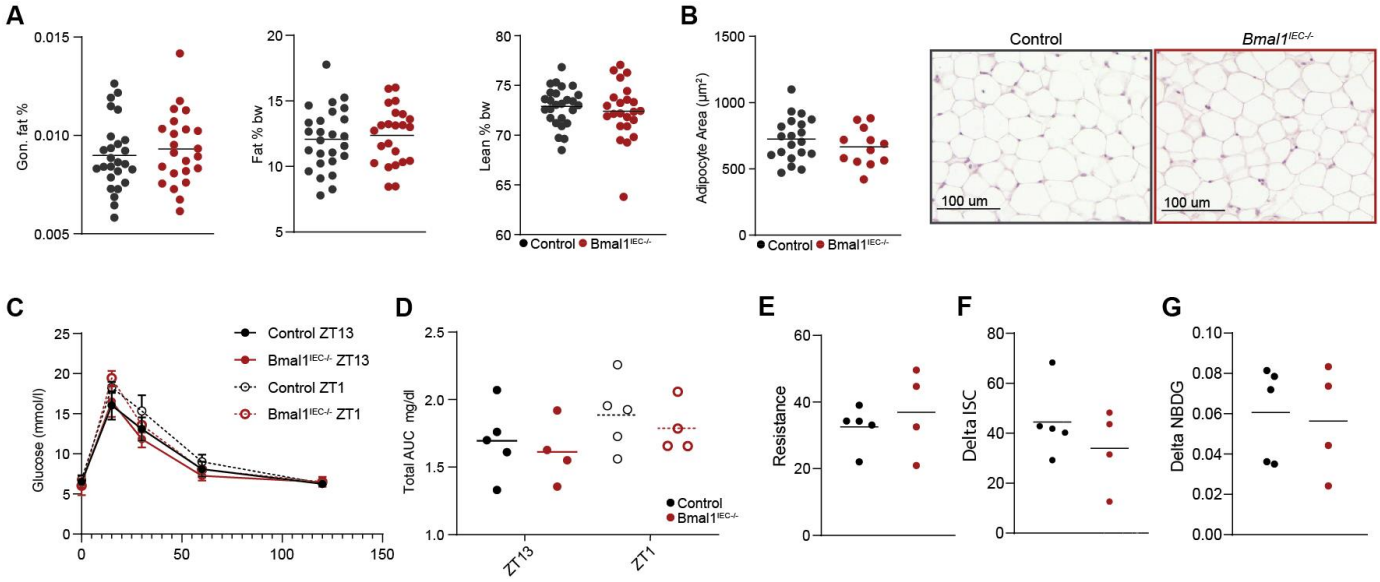

Supplementary Figure 7 Metabolic parameters in chow-fed *Bmal1*$^{IEC-/-}$ mice remained unaltered compared to controls. **(A)** Gonadal dissected fat mass and total fat and lean-mass measured by nuclear-magnetic resonance. **(B)** H&E staining of gonadal fat pads and their adipocyte area quantification. **(C)** Oral-glucose tolerance test (OGTT) measured at ZT1 and ZT13. **(D**) Total area under the curve (AUC) of OGTT. **(E)** Base-line Resistance and **(F)** current measured with Ussing chamber after the addition of 10 mM glucose. **(G)** Total fluorescent glucose uptake (2-NBDG) of jejunal tissues, measured with Ussing chamber.

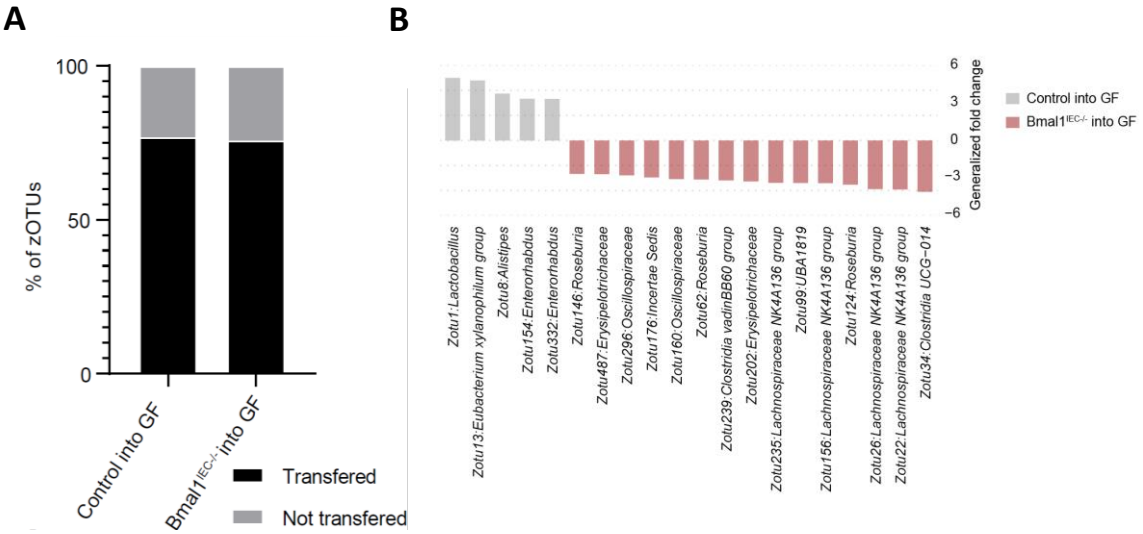

Supplementary Figure 8 Transfer efficiency of control and *Bmal1*$^{IEC-/-}$ cecal microbiota into germ-free host. **(A)** Transfer efficiency of mouse cecal donor microbiota into GF recipient mice based on zOTUs prevalence. **(B)** zOTU differential abundance analyses between control and *Bmal1*$^{IEC-/-}$ recipient mice

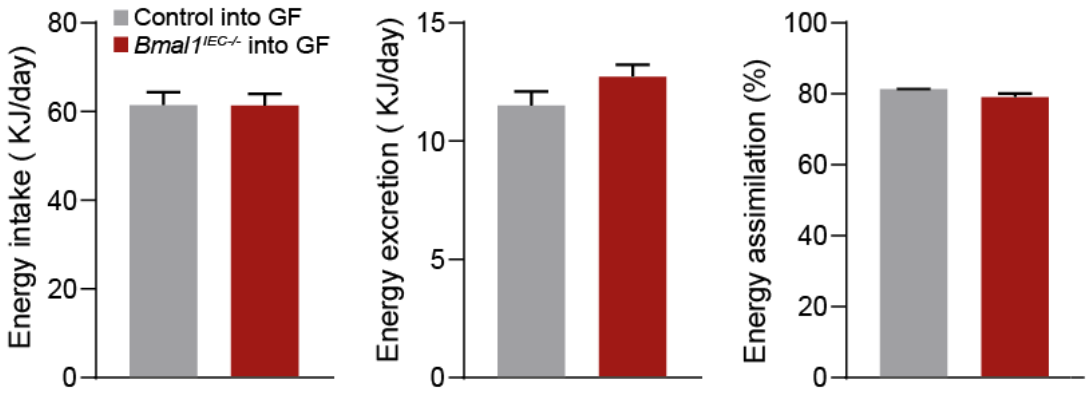

Supplementary Figure 9 Energy intake, excretion and total assimilation remains unaltered between recipient mice. Energy intake, excretion and total energy assimilation measured in control and *Bmal1*$^{IEC-/-}$ recipient mice with the use of BOMB-calorimetry.

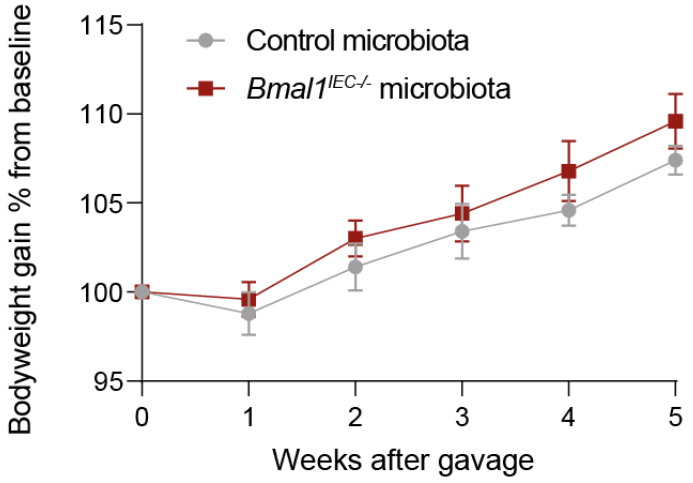

Supplementary Figure 10 Transfer of arrhythmic microbiota induces body weight gain in antibiotic treated mice. Body weight gain measured in antibiotic treated control mice gavaged with either control or *Bmal1*$^{IEC-/-}$ cecal microbiota.

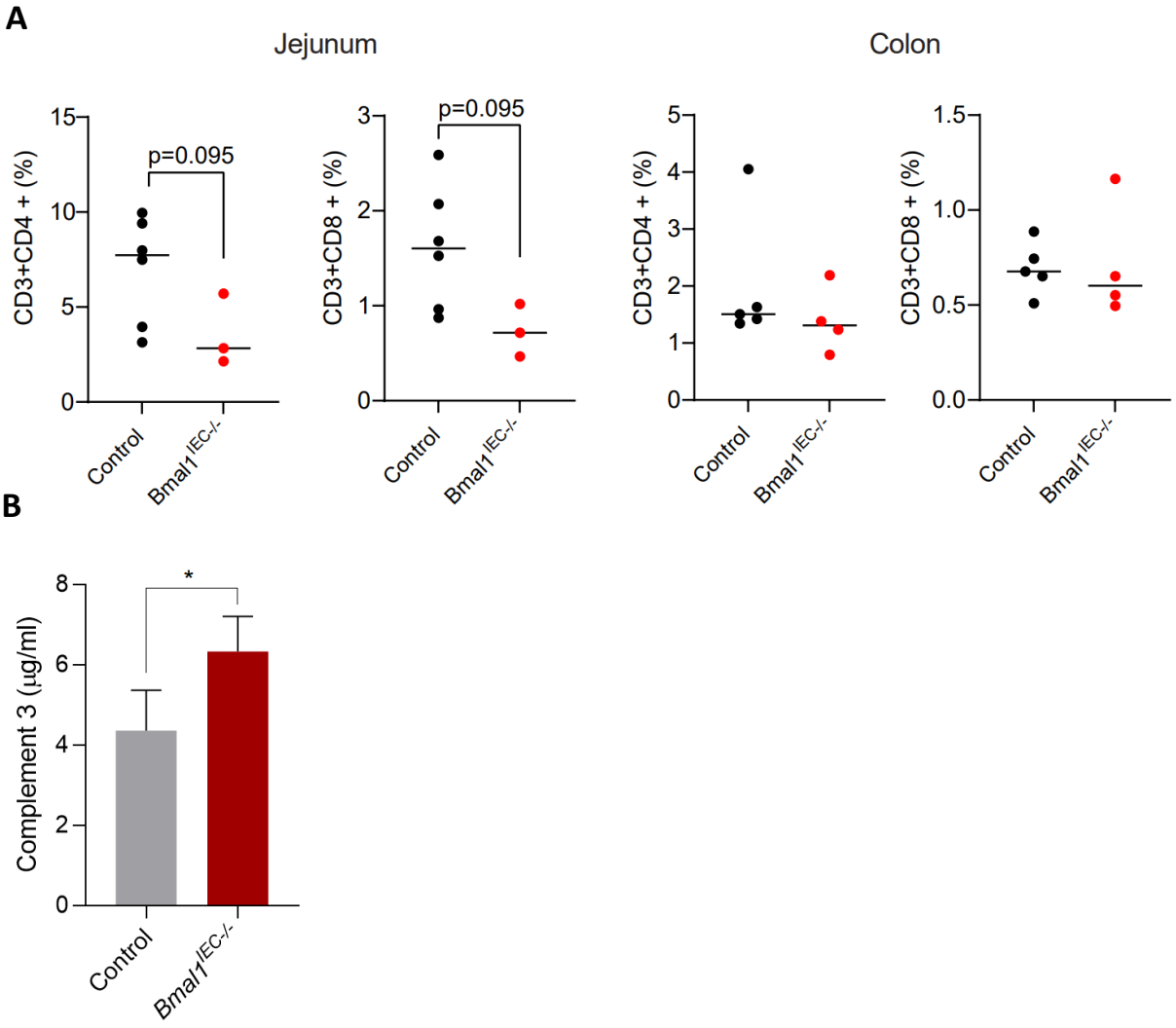

Supplementary Figure 11 Immune parameters in specific pathogen free mice.
(A) Frequency of jejunum lamina propria CD3+CD4+, CD3+CD8+ T-cells measured in SPF (donor) control and *Bmal1*$^{IEC-/-}$ mice.
(B) Complement 3 in fecal supernatant.

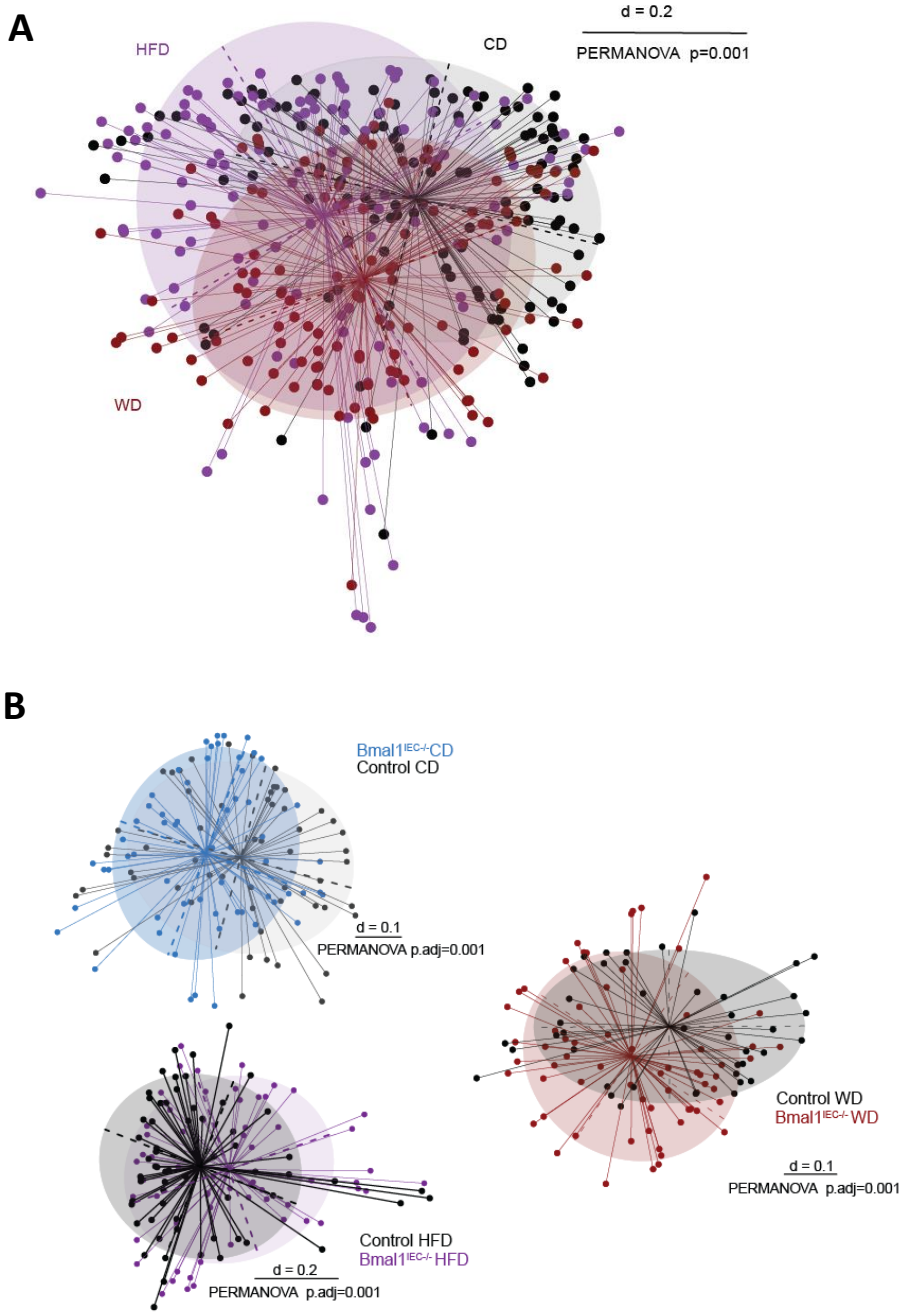

Supplementary Figure 12 Microbial composition significantly differs between genotypes and diets.
(A) MDS plots showing Beta-diversity between diets and **(B)** within-diets between genotypes. Each dot represents one sample. CD: control diet, WD: western diet. HFD: high-fat diet.

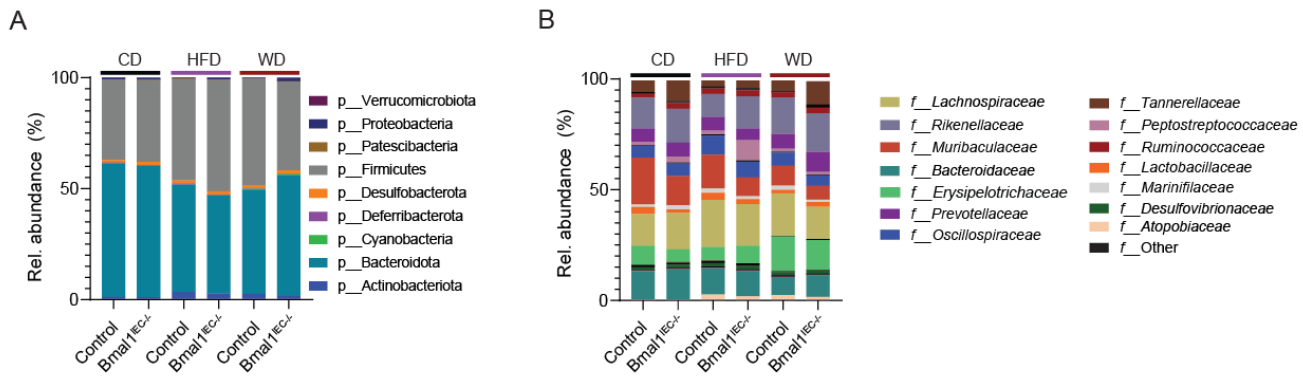

Supplementary Figure 13 Average taxonomic overview on Phyla and Family level.
(A) Relative abundance of phyla and **(B)** highly abundant families in both control and *Bmal1*$^{IEC-/-}$ mice in all three diets (CD=control diet, HFD= high-fat diet, WD= western diet).

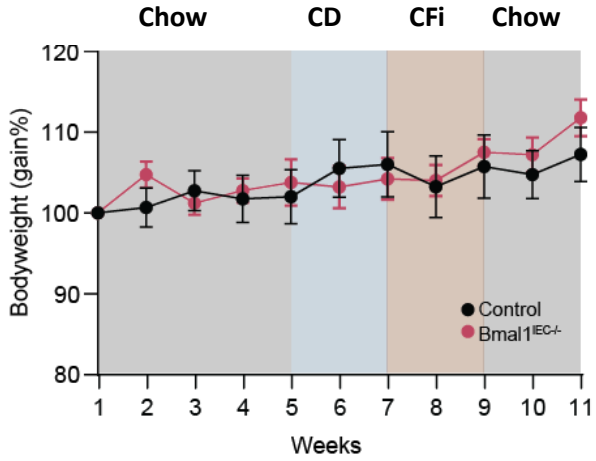

Supplementary Figure 14 Body weight upon dietary fiber interventions. Body weight gain measured over time after chow, control diet (CD), fiber-supplemented control diet (CFi) dietary interventions in control and *Bmal1*$^{IEC-/-}$ mice. P=0.06 at week 11.

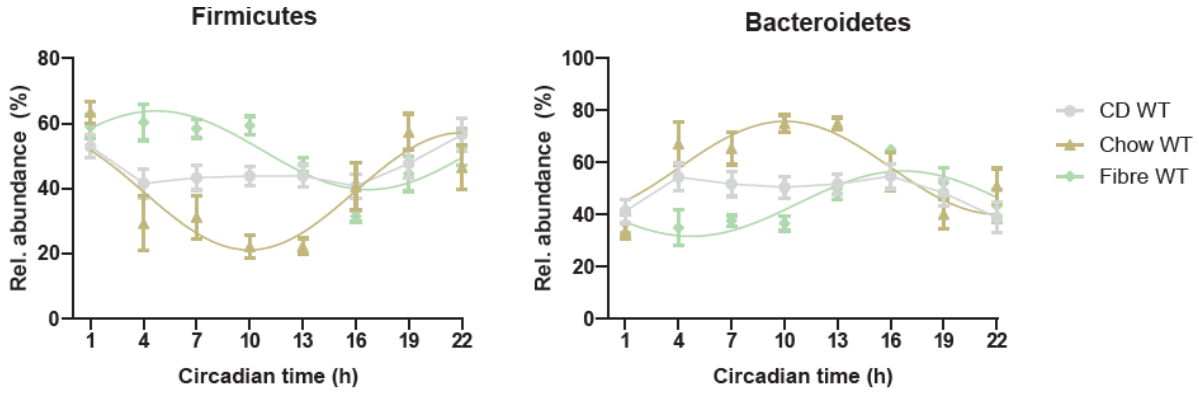

Supplementary Figure 15 Fiber dependent rhythms in the major phyla Firmicutes and Bacteroidetes.
Significant rhythms (cosine-wave regression, p-value ≤ 0.05) are illustrated with fitted cosine-wave curves; data points connected by dotted lines indicate no significant cosine fit curves (p-value > 0.05) and thus no rhythmicity. CD=control diet, Fiber=fiber supplemented control diet.

Supplementary Table 1 Overlap intestinal clock-controlled zOTUs measured in cecal and fecal content.
A total of 42 zOTUs oscillate in both cecal and fecal content of control mice, but not *Bmal1*$^{IEC-/-}$ mice. P-values are calculated with the use of JTK_Cycle

zOTU	Adj. p-Feces	Adj. p cecum	Phyla	Family	Genera	zOTU	Adj. p-Feces	Adj. p cecum	Phyla	Family	Genera
Zotu1149	0.0057	0.0001	Bacteroidetes	*Muribaculaceae*	*PAC001068_g*	Zotu6304	0.0000	0.0060	Firmicutes	*Lachnospiraceae*	*Frisingicoccus*
Zotu1488	0.0166	0.0000	Bacteroidetes	*Muribaculaceae*	*PAC001074_g*	Zotu7431	0.0141	0.0082	Firmicutes	*Lachnospiraceae*	*PAC001043_g*
Zotu3183	0.0028	0.0264	Firmicutes	*Lachnospiraceae*	*Clostridium_g24*	Zotu6146	0.0002	0.0264	Firmicutes	*Ruminococcaceae*	*Agathobaculum*
Zotu16705	0.0000	0.0264	Firmicutes	*Lachnospiraceae*	*PAC000692_g*	Zotu5378	0.0113	0.0150	Firmicutes	*Ruminococcaceae*	*Agathobaculum*
Zotu597	0.0021	0.0013	Bacteroidetes	*Muribaculaceae*	*PAC001068_g*	Zotu2791	0.0000	0.0096	Firmicutes	*Ruminococcaceae*	*Eubacterium_g8*
Zotu5052	0.0005	0.0011	Bacteroidetes	*Odoribacteraceae*	*Odoribacter*	Zotu3890	0.0000	0.0043	Firmicutes	*Ruminococcaceae*	*Eubacterium_g8*
Zotu3323	0.0018	0.0096	Firmicutes	*Lachnospiraceae*	*Clostridium_g24*	Zotu6392	0.0000	0.0037	Firmicutes	*Ruminococcaceae*	*Oscillibacter*
Zotu4392	0.0001	0.0082	Firmicutes	*Lachnospiraceae*	*Clostridium_g24*	Zotu7688	0.0141	0.0302	Firmicutes	*Ruminococcaceae*	*Oscillibacter*
Zotu4575	0.0000	0.0150	Firmicutes	*Lachnospiraceae*	*Clostridium_g24*	Zotu8047	0.0000	0.0096	Firmicutes	*Ruminococcaceae*	*Oscillibacter*
Zotu4461	0.0000	0.0370	Firmicutes	*Lachnospiraceae*	*Eubacterium_g17*	Zotu7905	0.0013	0.0051	Firmicutes	*Ruminococcaceae*	*Oscillibacter*
Zotu3448	0.0015	0.0324	Firmicutes	*Lachnospiraceae*	*KE159538_g*	Zotu7167	0.0001	0.0051	Firmicutes	*Ruminococcaceae*	*Oscillibacter*
Zotu3966	0.0046	0.0173	Bacteroidetes	*Odoribacteraceae*	*Odoribacter*	Zotu38611	0.0001	0.0150	Firmicutes	*Ruminococcaceae*	*Pseudoflavonifractor*
Zotu2534	0.0035	0.0112	Firmicutes	*Lachnospiraceae*	*KE159538_g*	Zotu5975	0.0034	0.0448	Firmicutes	*Ruminococcaceae*	*Pseudoflavonifractor*
Zotu5382	0.0006	0.0140	Firmicutes	*Lachnospiraceae*	*KE159538_g*	Zotu8628	0.0000	0.0173	Firmicutes	*Ruminococcaceae*	*Pseudoflavonifractor*
Zotu7639	0.0092	0.0448	Bacteroidetes	*Muribaculaceae*	*PAC001112_g*	Zotu2995	0.0188	0.0000	Firmicutes	*Ruminococcaceae*	*Ruminococcus*
Zotu2679	0.0000	0.0130	Bacteroidetes	*Muribaculaceae*	*Unclassified*	Zotu2503	0.0000	0.0000	Firmicutes	*Ruminococcaceae*	*Ruminococcus*
Zotu3829	0.0227	0.0026	Bacteroidetes	*Odoribacteraceae*	*Odoribacter*	Zotu3152	0.0064	0.0000	Firmicutes	*Ruminococcaceae*	*Ruminococcus*
Zotu11077	0.0137	0.0394	Firmicutes	*Lachnospiraceae*	*PAC001116_g*	Zotu4702	0.0005	0.0000	Firmicutes	*Ruminococcaceae*	*Ruminococcus*
Zotu6210	0.0029	0.0173	Firmicutes	*Lachnospiraceae*	*Clostridium_g24*	Zotu6054	0.0008	0.0013	Proteobacteria	*Desulfovibrionaceae*	*Desulfovibrio*
Zotu5956	0.0424	0.0215	Firmicutes	*Lachnospiraceae*	*KE159538_g*	Zotu2638	0.0003	0.0002	Proteobacteria	*Desulfovibrionaceae*	*Desulfovibrio*
Zotu5959	0.0003	0.0130	Firmicutes	*Lachnospiraceae*	*PAC001372_g*	Zotu3607	0.0008	0.0001	Proteobacteria	*Desulfovibrionaceae*	*Desulfovibrio*

Supplementary Table 2 List of zOTUs uniquely rhythmic in cecal content of control mice but not *Bmal1*$^{IEC-/-}$ mice.
P-values are calculated with the use of JTK_Cycle. The 18 zOTUs displayed do not reveal rhythmicity in fecal content of both genotypes.

zOTU	Adj. p-Feces	Adj. p cecum	Phyla	Family	Genera	zOTU	Adj. p-Feces	Adj. p cecum	Phyla	Family	Genera
Zotu1004	0.1283	0.0104	Bacteroidetes	*Muribaculaceae*	*PAC002400_g*	Zotu3085	1.0000	0.0043	Bacteroidetes	*Rikenellaceae*	*Alistipes*
Zotu1094	0.0825	0.0029	Bacteroidetes	*Muribaculaceae*	*PAC002400_g*	Zotu1218	0.5935	0.0150	Firmicutes	*Lachnospiraceae*	*PAC001090_g*
Zotu1676	0.1220	0.0040	Bacteroidetes	*Muribaculaceae*	*PAC002400_g*	Zotu1225	0.5591	0.0173	Firmicutes	*Lachnospiraceae*	*PAC001090_g*
Zotu2105	0.1606	0.0051	Bacteroidetes	*Muribaculaceae*	*PAC002400_g*	Zotu1705	0.4461	0.0448	Firmicutes	*Lachnospiraceae*	*PAC001090_g*
Zotu2956	0.3685	0.0448	Bacteroidetes	*Muribaculaceae*	*PAC000198_g*	Zotu2146	1.0000	0.0173	Firmicutes	*Lachnospiraceae*	*PAC001090_g*
Zotu3016	0.3847	0.0394	Bacteroidetes	*Muribaculaceae*	*PAC000198_g*	Zotu2234	0.8695	0.0448	Firmicutes	*Lachnospiraceae*	*PAC001090_g*
Zotu553	0.0741	0.0012	Bacteroidetes	*Muribaculaceae*	*PAC002400_g*	Zotu3417	0.8538	0.0264	Firmicutes	*Lachnospiraceae*	*PAC001090_g*
Zotu734	0.1646	0.0215	Bacteroidetes	*Muribaculaceae*	*PAC002400_g*	Zotu3795	0.1814	0.0150	Firmicutes	*Lachnospiraceae*	*KE159538_g*
Zotu2000	1.0000	0.0026	Bacteroidetes	*Rikenellaceae*	*Alistipes*	Zotu5744	0.3528	0.0247	Firmicutes	*Lachnospiraceae*	*PAC001516_g*

Supplementary Table 3 A list of zOTUs uniquely rhythmic in fecal content of control mice but not *Bmal1*$^{IEC-/-}$ mice.
P-values are calculated with the use of JTK_Cycle. A total of 160 zOTUs displayed do not reveal rhythmicity in cecal content of both genotypes.

zOTU	Adj. p-Feces	Adj. p cecum	Phyla	Family	Genera	zOTU	Adj. p-Feces	Adj. p cecum	Phyla	Family	Genera
Zotu4907	0.0411	1.0000	Bacteroidetes	*Bacteroidaceae*	*Bacteroides*	Zotu410	0.0015	0.2021	Firmicutes	*Lachnospiraceae*	*KE159538_g*
Zotu1680	0.0040	0.3651	Bacteroidetes	*Muribaculaceae*	*PAC001112_g*	Zotu4180	0.0000	1.0000	Firmicutes	*Lachnospiraceae*	*LLKB_g*
Zotu5200	0.0001	0.0695	Bacteroidetes	*Muribaculaceae*	*Muribaculaceae_unclassified*	Zotu4194	0.0066	1.0000	Firmicutes	*Lachnospiraceae*	*PAC001091_g*
Zotu5800	0.0326	1.0000	Bacteroidetes	*Muribaculaceae*	*PAC001692_g*	Zotu4197	0.0000	0.5710	Firmicutes	*Lachnospiraceae*	*PAC000692_g*
Zotu6075	0.0004	1.0000	Bacteroidetes	*Muribaculaceae*	*PAC001692_g*	Zotu4233	0.0029	0.3487	Firmicutes	*Lachnospiraceae*	*KE159538_g*
Zotu879	0.0388	0.4388	Bacteroidetes	*Muribaculaceae*	*PAC001068_g*	Zotu4257	0.0356	0.1636	Firmicutes	*Lachnospiraceae*	*PAC000664_g*
Zotu8825	0.0008	1.0000	Bacteroidetes	*Muribaculaceae*	*PAC001692_g*	Zotu4276	0.0002	0.4388	Firmicutes	*Lachnospiraceae*	*PAC001092_g*
Zotu1131	0.0227	0.5710	Bacteroidetes	*Odoribacteraceae*	*Odoribacter*	Zotu4302	0.0000	0.0935	Firmicutes	*Lachnospiraceae*	*PAC000664_g*
Zotu421	0.0436	0.3018	Bacteroidetes	*Odoribacteraceae*	*Odoribacter*	Zotu4409	0.0000	0.0831	Firmicutes	*Lachnospiraceae*	*PAC001372_g*
Zotu543	0.0326	0.6215	Bacteroidetes	*Odoribacteraceae*	*Odoribacter*	Zotu4420	0.0001	0.9636	Firmicutes	*Lachnospiraceae*	*KE159571_g*
Zotu798	0.0411	0.5239	Bacteroidetes	*Odoribacteraceae*	*Odoribacter*	Zotu443	0.0092	0.2240	Firmicutes	*Lachnospiraceae*	*KE159538_g*
Zotu1117	0.0335	1.0000	Bacteroidetes	*Rikenellaceae*	*Alistipes*	Zotu4441	0.0075	0.5963	Firmicutes	*Lachnospiraceae*	*KE159538_g*
Zotu1160	0.0264	1.0000	Bacteroidetes	*Rikenellaceae*	*Alistipes*	Zotu4706	0.0005	0.4798	Firmicutes	*Lachnospiraceae*	*PAC001092_g*

Zotu159	0.0001	1.0000	Bacteroidetes	*Rikenellaceae*	*Alistipes*	Zotu4755	0.0213	0.1636	Firmicutes	*Lachnospiraceae*	*Roseburia*
Zotu1974	0.0161	1.0000	Bacteroidetes	*Rikenellaceae*	*Alistipes*	Zotu5048	0.0050	0.6753	Firmicutes	*Lachnospiraceae*	*PAC001092_g*
Zotu287	0.0000	1.0000	Bacteroidetes	*Rikenellaceae*	*Alistipes*	Zotu531	0.0000	0.4388	Firmicutes	*Lachnospiraceae*	*PAC000664_g*
Zotu447	0.0001	1.0000	Bacteroidetes	*Rikenellaceae*	*Alistipes*	Zotu5310	0.0089	0.5239	Firmicutes	*Lachnospiraceae*	*PAC001092_g*
Zotu64	0.0001	1.0000	Bacteroidetes	*Rikenellaceae*	*Alistipes*	Zotu5838	0.0078	0.3487	Firmicutes	*Lachnospiraceae*	*KE159538_g*
Zotu73	0.0001	1.0000	Bacteroidetes	*Rikenellaceae*	*Alistipes*	Zotu587	0.0050	0.1820	Firmicutes	*Lachnospiraceae*	*KE159538_g*
Zotu84	0.0000	0.8586	Bacteroidetes	*Rikenellaceae*	*Alistipes*	Zotu5906	0.0002	1.0000	Firmicutes	*Lachnospiraceae*	*PAC001092_g*
Zotu4388	0.0475	1.0000	Firmicutes	*Christensenellaceae*	*PAC001360_g*	Zotu5925	0.0000	0.2240	Firmicutes	*Lachnospiraceae*	*PAC001372_g*
Zotu3987	0.0188	0.6215	Firmicutes	*Clostridiale*	*Clostridiales*	Zotu5953	0.0005	0.4798	Firmicutes	*Lachnospiraceae*	*PAC001092_g*
Zotu4482	0.0151	1.0000	Firmicutes	*Clostridiale*	*Clostridiales*	Zotu6113	0.0151	1.0000	Firmicutes	*Lachnospiraceae*	*LLKB_g*
Zotu4557	0.0045	0.7937	Firmicutes	*Clostridiales*	*Clostridiales*	Zotu6332	0.0002	1.0000	Firmicutes	*Lachnospiraceae*	*LLKB_g*
Zotu5706	0.0006	1.0000	Firmicutes	*Clostridiales*	*Clostridiales*	Zotu665	0.0166	0.1728	Firmicutes	*Lachnospiraceae*	*KE159538_g*
Zotu5724	0.0156	1.0000	Firmicutes	*Clostridiales*	*Clostridiales*	Zotu695	0.0003	0.4388	Firmicutes	*Lachnospiraceae*	*PAC000664_g*
Zotu10420	0.0005	0.9273	Firmicutes	*Lachnospiraceae*	*Clostridium_g21*	Zotu6968	0.0012	0.3487	Firmicutes	*Lachnospiraceae*	*KE159538_g*
Zotu11052	0.0109	1.0000	Firmicutes	*Lachnospiraceae*	*PAC001165_g*	Zotu7017	0.0000	0.3322	Firmicutes	*Lachnospiraceae*	*PAC000664_g*
Zotu1113	0.0377	1.0000	Firmicutes	*Lachnospiraceae*	*PAC000664_g*	Zotu7106	0.0000	1.0000	Firmicutes	*Lachnospiraceae*	*LLKB_g*
Zotu11534	0.0019	0.8929	Firmicutes	*Lachnospiraceae*	*Acetatifactor*	Zotu7176	0.0001	1.0000	Firmicutes	*Lachnospiraceae*	*PAC000664_g*
Zotu11687	0.0064	1.0000	Firmicutes	*Lachnospiraceae*	*PAC002039_g*	Zotu7230	0.0000	0.8261	Firmicutes	*Lachnospiraceae*	*KE159571_g*
Zotu1195	0.0017	0.2737	Firmicutes	*Lachnospiraceae*	*KE159538_g*	Zotu7308	0.0002	0.0509	Firmicutes	*Lachnospiraceae*	*Clostridium_g24*
Zotu12010	0.0008	0.4006	Firmicutes	*Lachnospiraceae*	*PAC001228_g*	Zotu7466	0.0000	0.1636	Firmicutes	*Lachnospiraceae*	*Acetatifactor*
Zotu12668	0.0000	1.0000	Firmicutes	*Lachnospiraceae*	*Anaerotignum*	Zotu747	0.0075	0.2021	Firmicutes	*Lachnospiraceae*	*KE159538_g*
Zotu1444	0.0017	0.5018	Firmicutes	*Lachnospiraceae*	*KE159538_g*	Zotu7580	0.0004	0.2478	Firmicutes	*Lachnospiraceae*	*PAC001524_g*
Zotu1468	0.0037	1.0000	Firmicutes	*Lachnospiraceae*	*PAC001091_g*	Zotu7595	0.0007	0.3018	Firmicutes	*Lachnospiraceae*	*PAC001092_g*
Zotu15047	0.0001	0.3322	Firmicutes	*Lachnospiraceae*	*Clostridium_g21*	Zotu7648	0.0000	1.0000	Firmicutes	*Lachnospiraceae*	*LLKB_g*
Zotu15142	0.0166	1.0000	Firmicutes	*Lachnospiraceae*	*Anaerotignum*	Zotu7703	0.0015	1.0000	Firmicutes	*Lachnospiraceae*	*Clostridium_g21*
Zotu16259	0.0031	0.8261	Firmicutes	*Lachnospiraceae*	*Anaerotignum*	Zotu7714	0.0102	0.5710	Firmicutes	*Lachnospiraceae*	*Clostridium_g21*
Zotu17079	0.0177	0.5474	Firmicutes	*Lachnospiraceae*	*KE159571_g*	Zotu7957	0.0124	0.1176	Firmicutes	*Lachnospiraceae*	*Lachnospira*
Zotu1747	0.0002	1.0000	Firmicutes	*Lachnospiraceae*	*PAC000664_g*	Zotu8041	0.0001	1.0000	Firmicutes	*Lachnospiraceae*	*LLKB_g*
Zotu17734	0.0083	0.3651	Firmicutes	*Lachnospiraceae*	*Clostridium_g24*	Zotu8099	0.0000	0.4388	Firmicutes	*Lachnospiraceae*	*PAC001138_g*
Zotu18027	0.0001	0.3651	Firmicutes	*Lachnospiraceae*	*PAC001199_g*	Zotu8106	0.0137	1.0000	Firmicutes	*Lachnospiraceae*	*PAC001092_g*
Zotu182	0.0000	0.6215	Firmicutes	*Lachnospiraceae*	*PAC000664_g*	Zotu8241	0.0001	0.1820	Firmicutes	*Lachnospiraceae*	*PAC001372_g*
Zotu1951	0.0000	0.2478	Firmicutes	*Lachnospiraceae*	*Eubacterium_g17*	Zotu8654	0.0029	1.0000	Firmicutes	*Lachnospiraceae*	*PAC001092_g*
Zotu1978	0.0388	1.0000	Firmicutes	*Lachnospiraceae*	*KE159605_g*	Zotu8722	0.0156	0.7937	Firmicutes	*Lachnospiraceae*	*Clostridium_g21*
Zotu2077	0.0400	1.0000	Firmicutes	*Lachnospiraceae*	*KE159605_g*	Zotu8964	0.0010	0.4388	Firmicutes	*Lachnospiraceae*	*PAC001372_g*

Zotu2126	0.0213	1.0000	Firmicutes	*Lachnospiraceae*	*PAC001091_g*	Zotu9075	0.0316	1.0000	Firmicutes	*Lachnospiraceae*	*Eubacterium_g17*
Zotu2264	0.0000	0.2737	Firmicutes	*Lachnospiraceae*	*PAC000692_g*	Zotu91	0.0000	0.7327	Firmicutes	*Lachnospiraceae*	*PAC000664_g*
Zotu2270	0.0000	1.0000	Firmicutes	*Lachnospiraceae*	*KE159571_g*	Zotu920	0.0003	1.0000	Firmicutes	*Lachnospiraceae*	*PAC000664_g*
Zotu2288	0.0000	1.0000	Firmicutes	*Lachnospiraceae*	*LLKB_g*	Zotu95	0.0000	0.7937	Firmicutes	*Lachnospiraceae*	*PAC000664_g*
Zotu2289	0.0008	0.1820	Firmicutes	*Lachnospiraceae*	*KE159571_g*	Zotu9560	0.0029	0.4388	Firmicutes	*Lachnospiraceae*	*Anaerotignum*
Zotu2351	0.0014	0.0831	Firmicutes	*Lachnospiraceae*	*Eubacterium_g17*	Zotu9684	0.0008	1.0000	Firmicutes	*Lachnospiraceae*	*Anaerotignum*
Zotu2353	0.0000	0.5474	Firmicutes	*Lachnospiraceae*	*Eubacterium_g17*	Zotu9715	0.0092	0.5963	Firmicutes	*Lachnospiraceae*	*Clostridium_g21*
Zotu2363	0.0289	1.0000	Firmicutes	*Lachnospiraceae*	*PAC001091_g*	Zotu1552	0.0015	1.0000	Firmicutes	*Lactobacillaceae*	*Lactobacillus*
Zotu2543	0.0000	1.0000	Firmicutes	*Lachnospiraceae*	*KE159571_g*	Zotu1650	0.0034	1.0000	Firmicutes	*Lactobacillaceae*	*Lactobacillus*
Zotu2584	0.0000	0.4388	Firmicutes	*Lachnospiraceae*	*PAC000692_g*	Zotu2079	0.0030	1.0000	Firmicutes	*Lactobacillaceae*	*Lactobacillus*
Zotu2644	0.0016	0.5710	Firmicutes	*Lachnospiraceae*	*KE159571_g*	Zotu2425	0.0036	1.0000	Firmicutes	*Lactobacillaceae*	*Lactobacillus*
Zotu271	0.0000	0.5710	Firmicutes	*Lachnospiraceae*	*PAC000664_g*	Zotu2663	0.0280	1.0000	Firmicutes	*Lactobacillaceae*	*Lactobacillus*
Zotu2748	0.0000	0.4006	Firmicutes	*Lachnospiraceae*	*KE159571_g*	Zotu4277	0.0070	1.0000	Firmicutes	*Lactobacillaceae*	*Lactobacillus*
Zotu2762	0.0002	1.0000	Firmicutes	*Lachnospiraceae*	*KE159571_g*	Zotu4379	0.0032	1.0000	Firmicutes	*Lactobacillaceae*	*Lactobacillus*
Zotu3040	0.0001	0.9636	Firmicutes	*Lachnospiraceae*	*Eubacterium_g17*	Zotu10559	0.0019	0.2021	Firmicutes	*Ruminococcaceae*	*Pseudoflavonifractor*
Zotu3108	0.0000	1.0000	Firmicutes	*Lachnospiraceae*	*LLKB_g*	Zotu13555	0.0000	0.1315	Firmicutes	*Ruminococcaceae*	*Pseudoflavonifractor*
Zotu316	0.0000	0.6215	Firmicutes	*Lachnospiraceae*	*PAC000664_g*	Zotu15322	0.0050	0.1468	Firmicutes	*Ruminococcaceae*	*PAC001402_g*
Zotu3168	0.0449	1.0000	Firmicutes	*Lachnospiraceae*	*Roseburia*	Zotu15422	0.0200	1.0000	Firmicutes	*Ruminococcaceae*	*Pseudoflavonifractor*
Zotu3225	0.0003	0.0653	Firmicutes	*Lachnospiraceae*	*Eubacterium_g17*	Zotu3578	0.0000	0.3651	Firmicutes	*Ruminococcaceae*	*Oscillibacter*
Zotu3237	0.0099	0.4593	Firmicutes	*Lachnospiraceae*	*KE159538_g*	Zotu4065	0.0000	0.7937	Firmicutes	*Ruminococcaceae*	*Oscillibacter*
Zotu3254	0.0027	1.0000	Firmicutes	*Lachnospiraceae*	*PAC000664_g*	Zotu4371	0.0011	0.4388	Firmicutes	*Ruminococcaceae*	*Oscillibacter*
Zotu3291	0.0000	0.8261	Firmicutes	*Lachnospiraceae*	*KE159571_g*	Zotu4591	0.0022	0.2240	Firmicutes	*Ruminococcaceae*	*Oscillibacter*
Zotu3313	0.0000	0.4798	Firmicutes	*Lachnospiraceae*	*KE159571_g*	Zotu4998	0.0031	0.6215	Firmicutes	*Ruminococcaceae*	*Oscillibacter*
Zotu3431	0.0000	1.0000	Firmicutes	*Lachnospiraceae*	*PAC000692_g*	Zotu5141	0.0040	0.1820	Firmicutes	*Ruminococcaceae*	*Oscillibacter*
Zotu3560	0.0005	0.6215	Firmicutes	*Lachnospiraceae*	*KE159538_g*	Zotu5420	0.0048	0.6753	Firmicutes	*Ruminococcaceae*	*Oscillibacter*
Zotu3591	0.0061	0.2021	Firmicutes	*Lachnospiraceae*	*PAC001372_g*	Zotu6205	0.0021	0.0653	Firmicutes	*Ruminococcaceae*	*Oscillibacter*
Zotu3633	0.0000	0.4593	Firmicutes	*Lachnospiraceae*	*KE159571_g*	Zotu6695	0.0015	0.1176	Firmicutes	*Ruminococcaceae*	*Pseudoflavonifractor*
Zotu3682	0.0066	0.7040	Firmicutes	*Lachnospiraceae*	*KE159571_g*	Zotu6728	0.0001	0.2478	Firmicutes	*Ruminococcaceae*	*Pseudoflavonifractor*
Zotu3748	0.0000	1.0000	Firmicutes	*Lachnospiraceae*	*LLKB_g*	Zotu6972	0.0007	1.0000	Firmicutes	*Ruminococcaceae*	*PAC001778_g*
Zotu3782	0.0001	0.3322	Firmicutes	*Lachnospiraceae*	*PAC000664_g*	Zotu4248	0.0002	0.0831	Proteobacteria	*Desulfovibrionaceae*	*Desulfovibrio*
Zotu4004	0.0177	0.4197	Firmicutes	*Lachnospiraceae*	*KE159538_g*	Zotu8248	0.0046	1.0000	Saccharibacteria	*Saccharimonas_f*	*PAC000677_g*

List of Figures

Figure 1 Mammalian circadian clock mechanism 3
Figure 2 Rhythmic gastrointestinal functions..... 7
Figure 3 Diurnal carbohydrate absorption in the intestine..... 11
Figure 4 FACS gating strategy. 37
Figure 5 Confirmed deletion of *Bmal1* in intestinal tissue sections of *Bmal1*$^{IEC-/-}$ mice 43
Figure 6 Mice with intestinal specific *Bmal1* deletion do not exhibit a circadian phenotype 44
Figure 7 Slight alterations in jejunal parameters in *Bmal1*$^{IEC-/-}$ mice 45
Figure 8 Intestinal *Bmal1* deletion results in arrhythmicity of major phyla 47
Figure 9 The intestinal clock regulates fecal microbial rhythmicity 48
Figure 10 The intestinal clock mainly regulates the rhythmicity of the families *Lachnospiraceae, Ruminococcaceae* and *Muribaculaceae*. 49
Figure 11 Bacterial alterations in intestinal clock-deficient mice results in altered fecal branched-chain fatty acids and valeric acid concentrations 51
Figure 12 Bacterial alterations in intestinal clock deficient mice results in altered fecal secondary bile acid concentrations 52
Figure 13 Intestinal clock controlled bacteria show significant correlations with bile acid concentrations..... 53
Figure 14 The intestinal clock controls rhythmicity of the cecal microbiota 56
Figure 15 Functional pathways in the cecal microbiota controlled by the intestinal clock 57
Figure 16 Untargeted metabolomics reveals the role of the intestinal clock in host metabolism 59
Figure 17 Intestinal clock-regulated genes are involved in metabolic and immune homeostasis 61
Figure 18 The intestinal clock regulates the rhythmic transcriptome relevant for carbohydrate and lipid metabolism..... 64
Figure 19 Body weight elevation upon intestinal clock-deficiency is microbiota dependent. 64
Figure 20 Significant difference in Beta-diversity between recipient mice 66
Figure 21 Maintained arrhythmicity upon transfer of *Bmal1*$^{IEC-/-}$ derived microbiota into a germfree host 67
Figure 22 Arrhythmic microbial patterns and metabolite alterations upon *Bmal1*$^{IEC-/-}$ microbial transfer 68
Figure 23 Mice receiving intestinal clock-deficient microbiota exhibit increased weight gain and fat mass..... 69
Figure 24 Decreased intestinal T-cell recruitment upon transfer of intestinal clock-deficient microbiome 71

Figure 25 Western diet intervention promotes body weight gain in intestinal clock-deficient mice... 73
Figure 26 Fiber depletion affects intestinal clock functioning. 74
Figure 27 Intestinal clock deficiency results in microbial alterations upon westernized diet feeding . 76
Figure 28 *Parasuterella* is positively associated with western diet-induced obesity upon intestinal clock deficiency 78
Figure 29 Fiber-deprived purified diets abolish microbial rhythmicity..... 79
Figure 30 Fiber-dependent alterations in microbial communities'..... 81
Figure 31 Circadian intestinal clock-controlled microbial rhythmicity is fiber dependent 83
Figure 32 Inulin enriched high-fat diet intervention does not improve body weight compared to HFD alone. 86
Figure 33 Summary of altered (microbiota-derived) metabolites, host genetics and their consequences to immune regulation in intestinal clock-deficient mice 91
Figure 34 Summary of results from dietary intervention studies on mice with intestinal clock deficiency 96

List of Tables

Table 1 Overview of papers using intestinal specific *Bmal1* deficient mouse models 22
Table 2 Dietary composition 25
Table 3 OGTT area under the curve analyses..... 27
Table 4 Dehydrating and paraffin embedding 30
Table 5 Deparaffinization, rehydration and H&E staining..... 30
Table 6 cDNA synthesis protocol..... 31
Table 7 Primer sequences and UPL probe numbers used for qRT-PCR analysis..... 32
Table 8 FACS antibodies 36
Table 9 Taxonomic classification of fiber-dependent zOTUs. 84

List of Supplementary Figures

Supplementary Figure 1 Dissected organ weights, total intestinal transit time and barrier markers remain unaltered upon intestinal *Bmal1* ablation 98
Supplementary Figure 2 Intestinal clock deficiency does not affect circadian 16s copy number 98
Supplementary Figure 3 Overall fecal zOTU abundance differences between control and *Bmal1*$^{IEC-/-}$ mice 99
Supplementary Figure 4 Circadian fecal bile acid profiles 100
Supplementary Figure 5 Cecal relative abundance analyses 101
Supplementary Figure 6 Gain of rhythmicity in genes involved in oxidative phosphorylation in *Bmal1*$^{IEC-/-}$ mice 102
Supplementary Figure 7 Metabolic parameters in chow-fed *Bmal1*$^{IEC-/-}$ mice remained unaltered compared to controls 103
Supplementary Figure 8 Transfer efficiency of control and *Bmal1*$^{IEC-/-}$ cecal microbiota into germ-free host 103
Supplementary Figure 9 Energy intake, excretion and total assimilation remains unaltered between recipient mice 104
Supplementary Figure 10 Transfer of arrhythmic microbiota induces body weight gain in antibiotic treated mice 104
Supplementary Figure 11 Immune parameters in specific pathogen free mice 105
Supplementary Figure 12 Microbial composition significantly differs between genotypes and diets 106
Supplementary Figure 13 Average taxonomic overview on Phyla and Family level 107
Supplementary Figure 14 Body weight upon dietary fiber interventions 107
Supplementary Figure 15 Fiber dependent rhythms in the major phyla Firmicutes and Bacteroidetes 107

List of Supplementary Tables

Supplementary Table 1 Overlap intestinal clock-controlled zOTUs measured in cecal and fecal content 108

Supplementary Table 2 List of zOTUs uniquely rhythmic in cecal content of control mice but not *Bmal1*$^{IEC-/-}$ mice. 109

Supplementary Table 3 A list of zOTUs uniquely rhythmic in fecal content of control mice but not *Bmal1*$^{IEC-/-}$ mice 109

Abbreviations

2-NBDG	[2-(N-(7-Nitrobenz-2-oxa-1,3-diazol-4-yl)Amino)-2-Deoxyglucose]-glucose
7-sulfo-CA	7-Sulfocholic acid
Abca1	ATP Binding Cassette Subfamily A Member 1)
Acat2	Acetyl-CoA Acetyltransferase 2
Agpat	Acylglycerol-3-Phosphate O-Acyltransferase
ANOVA	Analyses of variance
Apo	Apolipoprotein
AUC	Area under the curve
BA	Bile acid
BCAA	Branched-chain amino acids
BCFA	Branched-chain fatty acids
Bco1	Beta-Carotene Oxygenase 1
Bmal1	Brain and Muscle Arnt-Like1
Bmal1$^{fl/fl}$	Control mice
Bmal1$^{IEC-/-}$	Intestinal clock deficient mice
$CaCl_2$	Calcium Chloride
CCG	Clock-controlled genes
CD	Control diet
CD3/4/8	Cluster of differentiation
Cd36	Platelet Glycoprotein 4
Cd3d	CD3 Delta Subunit Of T-Cell Receptor Complex
CDCA	Chenodeoxycholic acid
cDNA	Complementary DNA
Ces1d	Carboxylesterase 1d
CFi	Fermentable-fiber enriched control diet
CK1	Casein kinase 1
CLOCK	Circadian locomotor output cycles kaput
c-Myc	MYC Proto-Oncogene
Cry	Cryptochrome
CT	Circadian time
Cyp3a44	Cytochrome P450 Family 3 Subfamily A Member 44
Dbp	D-Box Binding PAR BZIP Transcription Factor
DD	Constant darkness
Dgat2	Diacylglycerol O-Acyltransferase 2
dH_2O	distilled water
DNA	Deoxyribonucleic acid
dNTP	Deoxynucleotide
DPX	Di-N-Butyl Phthalate in Xylene
DTT	Dithiothreitol

E	energy
E-box	enhancer box
EDTA	Ethylenediaminetetraacetic acid
Ef1α	Elongation Factor 1 Alpha
ELISA	Enzyme-linked immunosorbent assay
EtOH	Ethanol
eWAT	Epididymal white adipose tissue
FABP	Fatty acid binding protein
FACS	Fluorescence-activated cell sorting
FC	Fold change
FFAR	Free fatty acid receptor
FITC	Fluorescein sodium salt
GCA	Glycohcolic acid
gDNA	genomic deoxyribonucleic acid
GF	Germ-free
GI	Gastrointestinal
Gip	Glucose–dependent insulinotrophic polypeptide
GITT	Gastrointestinal transit time
Glp-1	Glucagon-like peptide 1
Glut	Glucose transporter
GO	Gene ontology
GSEA	Gene-set enrichment analyses
H&E	Hematoxylin & Eosin
H_2O	Water
HDAC	Histone deacetylase
HDCA	Hyodeoxycholic acid
HFD	High fat diet
HFD^{inulin}	Inulin enriched high-fat diet
HILIC	Hydrophilic Interaction Liquid Chromatography
IEC	Intestinal epithelial cell
IL	Interleukin
Ilc3	Group 3 innate lymphoid cell
JTK	Jonckheere-Terpstra-Kendall algorithm
KCL	Potassium chloride
keto-LCA	Keto-litocholic acid
kJ	Kilojoules
LCA	Litocholic acid
LC-MS	Liquid chromatography-Mass spectrometry
LD	Light-dark
Lgr5	Leucine Rich Repeat Containing G Protein-Coupled Receptor 5
MCA	Muricholic acid
MDCA	Murideoxycholic acid
MDS	Multidimensional Scaling

MgCl2	Magnesium Chloride
MLN	Mesenteric lymph nodes
mRNA	Messenger ribonucleic acid
MS/MS	Tandem mass spectrometry
Mtp	Microsomal triglyceride transporter protein
n.s.	Not significant
Na_2HPO_4	Disodium hydrogen phosphate
Nacl	Natirum chloride
NaH_2PO_4	Sodium dihydrogen phosphate
$NaHCO_3$	Sodium Bicarbonate
Nfil3	Nuclear Factor, Interleukin 3 Regulated
NMR	Nuclear Magnetic Resonance
O_2	Oxygen
OGTT	Oral glucose tolerance test
PA	Procrustes analyses
PAS-AB	Periodic acid Schiff-alcian blue
PCA	Principal component analyses
Pept1	Peptide transporter 1
Per	Period
PERMANOVA	permutational multivariate analysis of variance
PICRUST	Phylogenetic Investigation of Communities by Reconstruction of Unobserved States
PYY	Peptide YY
qPCR	Quantitative Polymerase Chain Reaction
Reg3y	Regenerating islet-derived protein 3 gamma
Rev-Erb	Nuclear receptor subfamily 1 group D member 1
RF	Restricted feeding
ROR	Retinoic acid receptor related orphan receptors
RP	Reversed phase
rRNA	Ribosomal ribonucleic acid
RT	Resistance
Scd1	Stearoyl-CoA desaturase 1
SCFA	Short chain fatty acid
Scl13a1	Solute Carrier Family 13 Member 1
SCN	Suprachiasmatic nucleus
Sglt1	Sodium-glucose cotransporter 1
SI	Small intestine
SPF	Specific pathogen free
Stat3	Signal Transducer And Activator Of Transcription 3
Sucnr1	Succinate Receptor 1
sWAT	Subcutaneous white adipose tissue
T2D	Type 2 diabetes
TCDCA	Taurochenodeoxycholic acid

TDCA	Taurodeoxycholic acid
Th17	T-helper 17
TLR	Toll like receptor
Tnf	Tumor necrosis factor
TTL	Transcription translational auto regulatory feedback loop
TUDCA	Tauroursodeoxycholic acid
TαMCA	Tauro-α-muricholic acid
UPL	Universal Probe Library
UPLC	Ultra high performance liquid chromatography
WD	Westernized diet
zOTU	Zero-radius operational taxonomic unit
ZT	Zeitgeber time

References

Adusumilli, R., & Mallick, P. (2017). Data Conversion with ProteoWizard msConvert. *Methods Mol Biol*, *1550*, 339-368. https://doi.org/10.1007/978-1-4939-6747-6_23

Aguirre, M., Eck, A., Koenen, M. E., Savelkoul, P. H., Budding, A. E., & Venema, K. (2016). Diet drives quick changes in the metabolic activity and composition of human gut microbiota in a validated in vitro gut model. *Res Microbiol*, *167*(2), 114-125. https://doi.org/10.1016/j.resmic.2015.09.006

Altaha, B. (2022). Genetic and environmental circadian disruption induce weight gain through changes in the gut microbiome. *Mol Metab*. https://doi.org/10.1016/j.molmet.2022.101628

Amara, J., Saliba, Y., Hajal, J., Smayra, V., Bakhos, J. J., Sayegh, R., & Fares, N. (2019). Circadian Rhythm Disruption Aggravates DSS-Induced Colitis in Mice with Fecal Calprotectin as a Marker of Colitis Severity. *Digestive Diseases and Sciences*, *64*(11), 3122-3133. https://doi.org/10.1007/s10620-019-05675-7

Amir, M., Chaudhari, S., Wang, R., Campbell, S., Mosure, S. A., Chopp, L. B., Lu, Q., Shang, J., Pelletier, O. B., He, Y., Doebelin, C., Cameron, M. D., Kojetin, D. J., Kamenecka, T. M., & Solt, L. A. (2018). REV-ERBalpha Regulates T(H)17 Cell Development and Autoimmunity. *Cell Rep*, *25*(13), 3733-3749 e3738. https://doi.org/10.1016/j.celrep.2018.11.101

Arble, D. M., Bass, J., Laposky, A. D., Vitaterna, M. H., & Turek, F. W. (2009). Circadian timing of food intake contributes to weight gain. *Obesity (Silver Spring)*, *17*(11), 2100-2102. https://doi.org/10.1038/oby.2009.264

Arumugam, M., Raes, J., Pelletier, E., Le Paslier, D., Yamada, T., Mende, D. R., Fernandes, G. R., Tap, J., Bruls, T., Batto, J. M., Bertalan, M., Borruel, N., Casellas, F., Fernandez, L., Gautier, L., Hansen, T., Hattori, M., Hayashi, T., Kleerebezem, M., . . . Bork, P. (2011). Enterotypes of the human gut microbiome. *Nature*, *473*(7346), 174-180. https://doi.org/10.1038/nature09944

Aschoff, J. (1951). Die 24-Stunden-Periodik Der Maus Unter Konstanten Umgebungsbedingungen. *Naturwissenschaften*, *38*(21), 506-507. https://doi.org/Doi 10.1007/Bf00628863

Aschoff, J. (1954). Zeitgeber Der Tierischen Tagesperiodik. *Naturwissenschaften*, *41*(3), 49-56. https://doi.org/Doi 10.1007/Bf00634164

Aschoff, J. (1965). Circadian Rhythms in Man. *Science*, *148*(3676), 1427-1432. https://doi.org/10.1126/science.148.3676.1427

Aschoff, J., & Wever, R. (1962). Spontanperiodik Des Menschen Bei Ausschluss Aller Zeitgeber. *Naturwissenschaften*, *49*(15), 337-&. <Go to ISI>://WOS:A19628852B00001

Auwerda, J. J., Bac, D. J., & Schouten, W. R. (2001). Circadian rhythm of rectal motor complexes. *Dis Colon Rectum*, *44*(9), 1328-1332. https://doi.org/10.1007/BF02234793

Bachem, A., Makhlouf, C., Binger, K. J., de Souza, D. P., Tull, D., Hochheiser, K., Whitney, P. G., Fernandez-Ruiz, D., Dahling, S., Kastemuller, W., Jonsson, J., Gressier, E., Lew, A. M., Perdomo, C., Kupz, A., Figgett, W., Mackay, F., Oleshansky, M., Russ, B. E., . . . Bedoui, S. (2019). Microbiota-Derived Short-Chain Fatty Acids Promote the Memory Potential of Antigen-Activated CD8(+) T Cells. *Immunity*, *51*(2), 285-+. https://doi.org/10.1016/j.immuni.2019.06.002

Backhed, F., Ley, R. E., Sonnenburg, J. L., Peterson, D. A., & Gordon, J. I. (2005). Host-bacterial mutualism in the human intestine. *Science*, *307*(5717), 1915-1920. https://doi.org/10.1126/science.1104816

Balsalobre, A., Damiola, F., & Schibler, U. (1998). A serum shock induces circadian gene expression in mammalian tissue culture cells. *Cell*, *93*(6), 929-937. https://doi.org/10.1016/s0092-8674(00)81199-x

Barattini, P., Larsen, K. R., Moore, J. G., & Dayton, M. T. (1993). Circadian rhythm of pepsin efflux in the fasting rat stomach. *Chronobiology International*, *10*(6), 403-409. https://doi.org/10.3109/07420529309059716

Barclay, J. L., Shostak, A., Leliavski, A., Tsang, A. H., Johren, O., Muller-Fielitz, H., Landgraf, D., Naujokat, N., van der Horst, G. T., & Oster, H. (2013). High-fat diet-induced hyperinsulinemia

and tissue-specific insulin resistance in Cry-deficient mice. *Am J Physiol Endocrinol Metab*, *304*(10), E1053-1063. https://doi.org/10.1152/ajpendo.00512.2012

Beli, E., Prabakaran, S., Krishnan, P., Evans-Molina, C., & Grant, M. B. (2019). Loss of Diurnal Oscillatory Rhythms in Gut Microbiota Correlates with Changes in Circulating Metabolites in Type 2 Diabetic db/db Mice. *Nutrients*, *11*(10). https://doi.org/10.3390/nu11102310

Bertalanffy, F. D. (1960). Mitotic rates and renewal times of the digestive tract epithelia in the rat. *Acta Anat (Basel)*, *40*, 130-148. https://doi.org/10.1159/000141580

Biddle, A. (2013). Untangling the Genetic Basis of Fibrolytic Specialization by Lachnospiraceae and Ruminococcaceae in Diverse Gut Communities. *Diversity*, *5*, 627-640.

Bolger, A. M., Lohse, M., & Usadel, B. (2014). Trimmomatic: a flexible trimmer for Illumina sequence data. *Bioinformatics*, *30*(15), 2114-2120. https://doi.org/10.1093/bioinformatics/btu170

Bray, M. S., Ratcliffe, W. F., Grenett, M. H., Brewer, R. A., Gamble, K. L., & Young, M. E. (2013). Quantitative analysis of light-phase restricted feeding reveals metabolic dyssynchrony in mice. *Int J Obes (Lond)*, *37*(6), 843-852. https://doi.org/10.1038/ijo.2012.137

Brooks, J. F., 2nd, Behrendt, C. L., Ruhn, K. A., Lee, S., Raj, P., Takahashi, J. S., & Hooper, L. V. (2021). The microbiota coordinates diurnal rhythms in innate immunity with the circadian clock. *Cell*, *184*(16), 4154-4167 e4112. https://doi.org/10.1016/j.cell.2021.07.001

Brown, K., Abbott, D. W., Uwiera, R. R. E., & Inglis, G. D. (2018). Removal of the cecum affects intestinal fermentation, enteric bacterial community structure, and acute colitis in mice. *Gut Microbes*, *9*(3), 218-235. https://doi.org/10.1080/19490976.2017.1408763

Brubaker, P. L., & Martchenko, A. (2022). Metabolic Homeostasis: It's All in the Timing. *Endocrinology*, *163*(1). https://doi.org/10.1210/endocr/bqab199

Bunger, M. K., Walisser, J. A., Sullivan, R., Manley, P. A., Moran, S. M., Kalscheur, V. L., Colman, R. J., & Bradfield, C. A. (2005). Progressive arthropathy in mice with a targeted disruption of the Mop3/Bmal-1 locus. *Genesis*, *41*(3), 122-132. https://doi.org/10.1002/gene.20102

Bunger, M. K., Wilsbacher, L. D., Moran, S. M., Clendenin, C., Radcliffe, L. A., Hogenesch, J. B., Simon, M. C., Takahashi, J. S., & Bradfield, C. A. (2000). Mop3 is an essential component of the master circadian pacemaker in mammals. *Cell*, *103*(7), 1009-1017. https://doi.org/Doi 10.1016/S0092-8674(00)00205-1

Burholt, D. R., Etzel, S. L., Schenken, L. L., & Kovacs, C. J. (1985). Digestive-Tract Cell-Proliferation and Food-Consumption Patterns of Ha Icr Mice. *Cell and Tissue Kinetics*, *18*(4), 369-386. https://doi.org/DOI 10.1111/j.1365-2184.1985.tb00668.x

Carr, F. J., Chill, D., & Maida, N. (2002). The lactic acid bacteria: a literature survey. *Crit Rev Microbiol*, *28*(4), 281-370. https://doi.org/10.1080/1040-840291046759

Chambers, E. S., Preston, T., Frost, G., & Morrison, D. J. (2018). Role of Gut Microbiota-Generated Short-Chain Fatty Acids in Metabolic and Cardiovascular Health. *Curr Nutr Rep*, *7*(4), 198-206. https://doi.org/10.1007/s13668-018-0248-8

Chandrashekaran, M. K. (1998). Biological rhythms research: A personal account. *Journal of Biosciences*, *23*(5), 545-555. https://doi.org/Doi 10.1007/Bf02709165

Chapnik, N., Rozenblit-Susan, S., Genzer, Y., & Froy, O. (2016). Differential effect of fructose on fat metabolism and clock gene expression in hepatocytes vs. myotubes. *Int J Biochem Cell Biol*, *77*(Pt A), 35-40. https://doi.org/10.1016/j.biocel.2016.05.019

Chassaing, B., Miles-Brown, J., Pellizzon, M., Ulman, E., Ricci, M., Zhang, L., Patterson, A. D., Vijay-Kumar, M., & Gewirtz, A. T. (2015). Lack of soluble fiber drives diet-induced adiposity in mice. *Am J Physiol Gastrointest Liver Physiol*, *309*(7), G528-541. https://doi.org/10.1152/ajpgi.00172.2015

Chen, X., Yu, F., Guo, X., Su, C., Li, S. S., & Wu, B. (2021). Clock gene Bmal1 controls diurnal rhythms in expression and activity of intestinal carboxylesterase 1. *J Pharm Pharmacol*, *73*(1), 52-59. https://doi.org/10.1093/jpp/rgaa035

Cheng, H., & Leblond, C. P. (1974). Origin, differentiation and renewal of the four main epithelial cell types in the mouse small intestine. . *Am J Anat*, *141*(4), 537-561. https://doi.org/10.1002/aja.1001410407

Cheng, W. Y., Lam, K. L., Pik-Shan Kong, A., & Chi-Keung Cheung, P. (2020). Prebiotic supplementation (beta-glucan and inulin) attenuates circadian misalignment induced by shifted light-dark cycle in mice by modulating circadian gene expression. *Food Res Int*, *137*, 109437. https://doi.org/10.1016/j.foodres.2020.109437

Cherbut, C., Ferrier, L., Roze, C., Anini, Y., Blottiere, H., Lecannu, G., & Galimiche, J. P. (1998). Short-chain fatty acids modify colonic motility through nerves and polypeptide YY release in the rat. *American Journal of Physiology-Gastrointestinal and Liver Physiology*, *275*(6), G1415-G1422. https://doi.org/DOI 10.1152/ajpgi.1998.275.6.G1415

Corella, D., Asensio, E. M., Coltell, O., Sorli, J. V., Estruch, R., Martinez-Gonzalez, M. A., Salas-Salvado, J., Castaner, O., Aros, F., Lapetra, J., Serra-Majem, L., Gomez-Gracia, E., Ortega-Azorin, C., Fiol, M., Espino, J. D., Diaz-Lopez, A., Fito, M., Ros, E., & Ordovas, J. M. (2016). CLOCK gene variation is associated with incidence of type-2 diabetes and cardiovascular diseases in type-2 diabetic subjects: dietary modulation in the PREDIMED randomized trial. *Cardiovasc Diabetol*, *15*, 4. https://doi.org/10.1186/s12933-015-0327-8

Costello, H. M., Crislip, G. R., Cheng, K. Y., Lynch, I. J., Juffre, A., Bratanatawira, P., McKee, A., Thelwell, R. S., Mendez, V. M., Wingo, C. S., Douma, L. G., & Gumz, M. L. (2023). Adrenal-Specific KO of the Circadian Clock Protein BMAL1 Alters Blood Pressure Rhythm and Timing of Eating Behavior. *Function (Oxf)*, *4*(2), zqad001. https://doi.org/10.1093/function/zqad001

Dalby, M. J., Ross, A. W., Walker, A. W., & Morgan, P. J. (2017). Dietary Uncoupling of Gut Microbiota and Energy Harvesting from Obesity and Glucose Tolerance in Mice. *Cell Rep*, *21*(6), 1521-1533. https://doi.org/10.1016/j.celrep.2017.10.056

Damiola, F., Le Minh, N., Preitner, N., Kornmann, B., Fleury-Olela, F., & Schibler, U. (2000). Restricted feeding uncouples circadian oscillators in peripheral tissues from the central pacemaker in the suprachiasmatic nucleus. *Genes Dev*, *14*(23), 2950-2961. https://doi.org/10.1101/gad.183500

Davidson, A. J., Poole, A. S., Yamazaki, S., & Menaker, M. (2003). Is the food-entrainable circadian oscillator in the digestive system? *Genes Brain and Behavior*, *2*(1), 32-39. https://doi.org/DOI 10.1034/j.1601-183X.2003.00005.x

de Mairan, J. (1729). Observation botanique. *Hist. Acad. Roy. Sci*, 35-36.

Deane, A. M., Nguyen, N. Q., Stevens, J. E., Fraser, R. J., Holloway, R. H., Besanko, L. K., Burgstad, C., Jones, K. L., Chapman, M. J., Rayner, C. K., & Horowitz, M. (2010). Endogenous glucagon-like peptide-1 slows gastric emptying in healthy subjects, attenuating postprandial glycemia. *J Clin Endocrinol Metab*, *95*(1), 215-221. https://doi.org/10.1210/jc.2009-1503

den Besten, G., van Eunen, K., Groen, A. K., Venema, K., Reijngoud, D. J., & Bakker, B. M. (2013). The role of short-chain fatty acids in the interplay between diet, gut microbiota, and host energy metabolism. *Journal of Lipid Research*, *54*(9), 2325-2340. https://doi.org/10.1194/jlr.R036012

Deota, S., Lin, T. R. Y., Chaix, A., Williams, A., Le, H. P., Calligaro, H., & Ramasamy, R. (2023). Diurnal transcriptome landscape of a multi-tissue response to time-restricted feeding in mammals. *Cell Metabolism*, *35*(1), 150-+. https://doi.org/10.1016/j.cmet.2022.12.006

Dobin, A., Davis, C. A., Schlesinger, F., Drenkow, J., Zaleski, C., Jha, S., Batut, P., Chaisson, M., & Gingeras, T. R. (2013). STAR: ultrafast universal RNA-seq aligner. *Bioinformatics*, *29*(1), 15-21. https://doi.org/10.1093/bioinformatics/bts635

Donaldson, G. P., Chou, W. C., Manson, A. L., Rogov, P., Abeel, T., Bochicchio, J., Ciulla, D., Melnikov, A., Ernst, P. B., Chu, H., Giannoukos, G., Earl, A. M., & Mazmanian, S. K. (2020). Spatially distinct physiology of Bacteroides fragilis within the proximal colon of gnotobiotic mice. *Nat Microbiol*, *5*(5), 746-756. https://doi.org/10.1038/s41564-020-0683-3

Douglas, G. M., Maffei, V. J., Zaneveld, J. R., Yurgel, S. N., Brown, J. R., Taylor, C. M., Huttenhower, C., & Langille, M. G. I. (2020). PICRUSt2 for prediction of metagenome functions. *Nat Biotechnol*, *38*(6), 685-688. https://doi.org/10.1038/s41587-020-0548-6

Douris, N., Kojima, S., Pan, X., Lerch-Gaggl, A. F., Duong, S. Q., Hussain, M. M., & Green, C. B. (2011). Nocturnin regulates circadian trafficking of dietary lipid in intestinal enterocytes. *Curr Biol*, *21*(16), 1347-1355. https://doi.org/10.1016/j.cub.2011.07.018

Duane, W. C., Levitt, D. G., Mueller, S. M., & Behrens, J. C. (1983). Regulation of bile acid synthesis in man. Presence of a diurnal rhythm. *J Clin Invest*, *72*(6), 1930-1936. https://doi.org/10.1172/JCI111157

Durinck, S., Spellman, P. T., Birney, E., & Huber, W. (2009). Mapping identifiers for the integration of genomic datasets with the R/Bioconductor package biomaRt. *Nat Protoc*, *4*(8), 1184-1191. https://doi.org/10.1038/nprot.2009.97

Eckel-Mahan, K. L., Patel, V. R., de Mateo, S., Orozco-Solis, R., Ceglia, N. J., Sahar, S., Dilag-Penilla, S. A., Dyar, K. A., Baldi, P., & Sassone-Corsi, P. (2013). Reprogramming of the Circadian Clock by Nutritional Challenge. *Cell*, *155*(7), 1464-1478. https://doi.org/10.1016/j.cell.2013.11.034

Edgar, R. C. (2010). Search and clustering orders of magnitude faster than BLAST. *Bioinformatics*, *26*(19), 2460-2461. https://doi.org/10.1093/bioinformatics/btq461

Edgar, R. C. (2016). UNOISE2: improved error-correction for Illumina 16S and ITS amplicon sequencing *bioRxiv*.

Edgar, R. C. (2018). Updating the 97% identity threshold for 16S ribosomal RNA OTUs. *Bioinformatics*, *34*(14), 2371-2375. https://doi.org/10.1093/bioinformatics/bty113

Edgar, R. C., Haas, B. J., Clemente, J. C., Quince, C., & Knight, R. (2011). UCHIME improves sensitivity and speed of chimera detection. *Bioinformatics*, *27*(16), 2194-2200. https://doi.org/10.1093/bioinformatics/btr381

Eelderink-Chen, Z., Bosman, J., Sartor, F., Dodd, A. N., Kovacs, A. T., & Merrow, M. (2021). A circadian clock in a nonphotosynthetic prokaryote. *Sci Adv*, *7*(2). https://doi.org/10.1126/sciadv.abe2086

Elliott, R. M., Morgan, L. M., Tredger, J. A., Deacon, S., Wright, J., & Marks, V. (1993). Glucagon-Like Peptide-1(7-36)Amide and Glucose-Dependent Insulinotropic Polypeptide Secretion in Response to Nutrient Ingestion in Man - Acute Postprandial and 24-H Secretion Patterns. *Journal of Endocrinology*, *138*(1), 159-166. https://doi.org/DOI 10.1677/joe.0.1380159

Esmaeilniakooshkghazi, A., George, S. P., Biswas, R., & Khurana, S. (2020). Mouse intestinal tuft cells express advillin but not villin. *Sci Rep*, *10*(1), 8877. https://doi.org/10.1038/s41598-020-65469-0

Eum, S. Y., Schurhoff, N., Teglas, T., Wolff, G., & Toborek, M. (2023). Circadian disruption alters gut barrier integrity via a ss-catenin-MMP-related pathway. *Mol Cell Biochem*, *478*(3), 581-595. https://doi.org/10.1007/s11010-022-04536-8

Fang, J., Wang, H., Zhou, Y., Zhang, H., Zhou, H., & Zhang, X. (2021). Slimy partners: the mucus barrier and gut microbiome in ulcerative colitis. *Exp Mol Med*, *53*(5), 772-787. https://doi.org/10.1038/s12276-021-00617-8

Fawad, J. A., Luzader, D. H., Hanson, G. F., Moutinho, T. J., Jr., McKinney, C. A., Mitchell, P. G., Brown-Steinke, K., Kumar, A., Park, M., Lee, S., Bolick, D. T., Medlock, G. L., Zhao, J. Y., Rosselot, A. E., Chou, C. J., Eshleman, E. M., Alenghat, T., Hong, C. I., Papin, J. A., & Moore, S. R. (2022). Histone Deacetylase Inhibition by Gut Microbe-Generated Short-Chain Fatty Acids Entrains Intestinal Epithelial Circadian Rhythms. *Gastroenterology*, *163*(5), 1377-1390 e1311. https://doi.org/10.1053/j.gastro.2022.07.051

Fonken, L. K., Lieberman, R. A., Weil, Z. M., & Nelson, R. J. (2013). Dim Light at Night Exaggerates Weight Gain and Inflammation Associated With a High-Fat Diet in Male Mice. *Endocrinology*, *154*(10), 3817-3825. https://doi.org/10.1210/en.2013-1121

Fonken, L. K., Workman, J. L., Walton, J. C., Weil, Z. M., Morris, J. S., Haim, A., & Nelson, R. J. (2010). Light at night increases body mass by shifting the time of food intake. *Proceedings of the National Academy of Sciences of the United States of America*, *107*(43), 18664-18669. https://doi.org/10.1073/pnas.1008734107

Frazier, K., Kambal, A., Zale, E. A., Pierre, J. F., Hubert, N., Miyoshi, S., Miyoshi, J., Ringus, D. L., Harris, D., Yang, K., Carroll, K., Hermanson, J. B., Chlystek, J. S., Overmyer, K. A., Cham, C. M., Musch,

M. W., Coon, J. J., Chang, E. B., & Leone, V. A. (2022). High-fat diet disrupts REG3gamma and gut microbial rhythms promoting metabolic dysfunction. *Cell Host & Microbe*, *30*(6), 809-823 e806. https://doi.org/10.1016/j.chom.2022.03.030

Furukawa, M., Kawamoto, T., Noshiro, M., Honda, K. K., Sakai, M., Fujimoto, K., Honma, S., Honma, K., Hamada, T., & Kato, Y. (2005). Clock gene expression in the submandibular glands. *J Dent Res*, *84*(12), 1193-1197. https://doi.org/10.1177/154405910508401219

Furuya, S., & Yugari, Y. (1974). Daily rhythmic change of L-histidine and glucose absorptions in rat small intestine in vivo. *Biochim Biophys Acta*, *343*(3), 558-564. https://doi.org/10.1016/0304-4165(74)90274-8

Gälman, C., Angelin, B., & Rudling, M. (2005). Bile Acid Synthesis in Humans Has a Rapid Diurnal Variation That Is Asynchronous With Cholesterol Synthesis. *Gastroenterology*, *129*(5), 1445-1453.

Garcia, T. S., Rech, T. H., & Leitao, C. B. (2017). Pancreatic size and fat content in diabetes: A systematic review and meta-analysis of imaging studies. *PLoS One*, *12*(7), e0180911. https://doi.org/10.1371/journal.pone.0180911

Gaudier, E., Rival, M., Buisine, M. P., Robineau, I., & Hoebler, C. (2009). Butyrate Enemas Upregulate Muc Genes Expression but Decrease Adherent Mucus Thickness in Mice Colon. *Physiological Research*, *58*(1), 111-119. https://doi.org/10.33549/physiolres.931271

Gentile, C. L. W., T.L. . (2018). The gut microbiota at the intersection of diet and human health. *Science*, *362*(6416), 776-780. https://doi.org/https://doi.org/10.1126/science.aau5812.

Gerard, P. (2013). Metabolism of cholesterol and bile acids by the gut microbiota. *Pathogens*, *3*(1), 14-24. https://doi.org/10.3390/pathogens3010014

Gil-Lozano, M., Wu, W. K., Martchenko, A., & Brubaker, P. L. (2016). High-Fat Diet and Palmitate Alter the Rhythmic Secretion of Glucagon-Like Peptide-1 by the Rodent L-cell. *Endocrinology*, *157*(2), 586-599. https://doi.org/10.1210/en.2015-1732

Godinho-Silva, C., Domingues, R. G., Rendas, M., Raposo, B., Ribeiro, H., da Silva, J. A., Vieira, A., Costa, R. M., Barbosa-Morais, N. L., Carvalho, T., & Veiga-Fernandes, H. (2019). Light-entrained and brain-tuned circadian circuits regulate ILC3s and gut homeostasis. *Nature*, *574*(7777), 254-258. https://doi.org/10.1038/s41586-019-1579-3

Godon, J. J., Zumstein, E., Dabert, P., Habouzit, F., & Moletta, R. (1997). Molecular microbial diversity of an anaerobic digestor as determined by small-subunit rDNA sequence analysis. *Environ. Microbiol.* , *63*, 2802-2813.

Gonzalez-Blazquez, R., Alcala, M., Fernandez-Alfonso, M. S., Villa-Valverde, P., Viana, M., Gil-Ortega, M., & Somoza, B. (2020). Relevance of control diet choice in metabolic studies: impact in glucose homeostasis and vascular function. *Sci Rep*, *10*(1), 2902. https://doi.org/10.1038/s41598-020-59674-0

Goo, R. H., Moore, J. G., Greenberg, E., & Alazraki, N. P. (1987). Circadian variation in gastric emptying of meals in humans. *Gastroenterology*, *93*(3), 515-518. https://doi.org/10.1016/0016-5085(87)90913-9

Govindarajan, K., MacSharry, J., Casey, P. G., Shanahan, F., Joyce, S. A., & Gahan, C. G. (2016). Unconjugated Bile Acids Influence Expression of Circadian Genes: A Potential Mechanism for Microbe-Host Crosstalk. *PLoS One*, *11*(12), e0167319. https://doi.org/10.1371/journal.pone.0167319

Grimaldi, B., Bellet, M. M., Katada, S., Astarita, G., Hirayama, J., Amin, R. H., Granneman, J. G., Piomelli, D., Leff, T., & Sassone-Corsi, P. (2010). PER2 controls lipid metabolism by direct regulation of PPARgamma. *Cell Metab*, *12*(5), 509-520. https://doi.org/10.1016/j.cmet.2010.10.005

Groschwitz, K. R., & Hogan, S. P. (2009). Intestinal barrier function: Molecular regulation and disease pathogenesis. *Journal of Allergy and Clinical Immunology*, *124*(1), 3-20. https://doi.org/10.1016/j.jaci.2009.05.038

Grosjean, E., Simonneaux, V., & Challet, E. (2023). Reciprocal Interactions between Circadian Clocks, Food Intake, and Energy Metabolism. *Biology-Basel*, *12*(4). https://doi.org/ARTN 539

10.3390/biology12040539
Haeusler, R. A., Astiarraga, B., Camastra, S., Accili, D., & Ferrannini, E. (2013). Human Insulin Resistance Is Associated With Increased Plasma Levels of 12a-Hydroxylated Bile Acids. *Diabetes*, *62*(12), 4184-4191. https://doi.org/10.2337/db13-0639
Hald, S., Schioldan, A. G., Moore, M. E., Dige, A., Laerke, H. N., Agnholt, J., Knudsen, K. E. B., Hermansen, K., Marco, M. L., Gregersen, S., & Dahlerup, J. F. (2016). Effects of Arabinoxylan and Resistant Starch on Intestinal Microbiota and Short-Chain Fatty Acids in Subjects with Metabolic Syndrome: A Randomised Crossover Study. *PLoS One*, *11*(7). https://doi.org/ARTN e015922310.1371/journal.pone.0159223
Harfmann, B. D., Schroder, E. A., Kachman, M. T., Hodge, B. A., Zhang, X., & Esser, K. A. (2016). Muscle-specific loss of Bmal1 leads to disrupted tissue glucose metabolism and systemic glucose homeostasis. *Skelet Muscle*, *6*, 12. https://doi.org/10.1186/s13395-016-0082-x
Hatori, M. V., C., Zarrinpar, A., DiTacchio, L., Bushong, E. A., Gill, S., Leblanc, M., Chaix, A., Joens, M., Fitzpatrick, J. A., Ellisman, m. H., & Panda, S. (2012). Time-restricted feeding without reducing caloric intake prevents metabolic diseases in mice fed a high-fat diet. *15*(6), 848-860.
Heyde, I., & Oster, H. (2019). Differentiating external zeitgeber impact on peripheral circadian clock resetting. *Sci Rep*, *9*(1), 20114. https://doi.org/10.1038/s41598-019-56323-z
Hirota, T., Okano, T., Kokame, K., Shirotani-Ikejima, H., Miyata, T., & Fukada, Y. (2002). Glucose down-regulates Per1 and Per2 mRNA levels and induces circadian gene expression in cultured Rat-1 fibroblasts. *Journal of Biological Chemistry*, *277*(46), 44244-44251. https://doi.org/10.1074/jbc.M206233200
Hoogerwerf, W. A., Hellmich, H. L., Cornelissen, G., Halberg, F., Shahinian, V. B., Bostwick, J., Savidge, T. C., & Cassone, V. M. (2007). Clock gene expression in the murine gastrointestinal tract: endogenous rhythmicity and effects of a feeding regimen. *Gastroenterology*, *133*(4), 1250-1260. https://doi.org/10.1053/j.gastro.2007.07.009
Hoogerwerf, W. A., Shahinian, V. B., Cornelissen, G., Halberg, F., Bostwick, J., Timm, J., Bartell, P. A., & Cassone, V. M. (2010). Rhythmic changes in colonic motility are regulated by period genes. *Am J Physiol Gastrointest Liver Physiol*, *298*(2), G143-150. https://doi.org/10.1152/ajpgi.00402.2009
Hoogerwerf, W. A., Sinha, M., Conesa, A., Luxon, B. A., Shahinian, V. B., Cornelissen, G., Halberg, F., Bostwick, J., Timm, J., & Cassone, V. M. (2008). Transcriptional profiling of mRNA expression in the mouse distal colon. *Gastroenterology*, *135*(6), 2019-2029. https://doi.org/10.1053/j.gastro.2008.08.048
Houghton, S. G., Zarroug, A. E., Duenes, J. A., Fernandez-Zapico, M. E., & Sarr, M. G. (2006). The diurnal periodicity of hexose transporter mRNA and protein levels in the rat jejunum: role of vagal innervation. *Surgery*, *139*(4), 542-549. https://doi.org/10.1016/j.surg.2005.09.002
Hughes, M. E., DiTacchio, L., Hayes, K. R., Vollmers, C., Pulivarthy, S., Baggs, J. E., Panda, S., & Hogenesch, J. B. (2009). Harmonics of circadian gene transcription in mammals. *PLoS Genet*, *5*(4), e1000442. https://doi.org/10.1371/journal.pgen.1000442
Hughes, M. E., Hogenesch, J. B., & Kornacker, K. (2010). JTK_CYCLE: an efficient nonparametric algorithm for detecting rhythmic components in genome-scale data sets. *J Biol Rhythms*, *25*(5), 372-380. https://doi.org/10.1177/0748730410379711
Iwashina, I., Mochizuki, K., Inamochi, Y., & Goda, T. (2011). Clock genes regulate the feeding schedule-dependent diurnal rhythm changes in hexose transporter gene expressions through the binding of BMAL1 to the promoter/enhancer and transcribed regions. *J Nutr Biochem*, *22*(4), 334-343. https://doi.org/10.1016/j.jnutbio.2010.02.012
Izumo, M., Pejchal, M., Schook, A. C., Lange, R. P., Walisser, J. A., Sato, T. R., Wang, X., Bradfield, C. A., & Takahashi, J. S. (2014). Differential effects of light and feeding on circadian organization of peripheral clocks in a forebrain Bmal1 mutant. *Elife*, *3*. https://doi.org/10.7554/eLife.04617
Janssen, A. W., & Kersten, S. (2017). Potential mediators linking gut bacteria to metabolic health: a critical view. *J Physiol*, *595*(2), 477-487. https://doi.org/10.1113/JP272476

Jochum, S. B., Engen, P. A., Shaikh, M., Naqib, A., Wilber, S., Raeisi, S., Zhang, L., Song, S., Sanzo, G., Chouhan, V., Ko, F., Post, Z., Tran, L., Ramirez, V., Green, S. J., Khazaie, K., Hayden, D. M., Brown, M. J., Voigt, R. M., . . . Swanson, G. R. (2022). Colonic Epithelial Circadian Disruption Worsens Dextran Sulfate Sodium-Induced Colitis. *Inflamm Bowel Dis*. https://doi.org/10.1093/ibd/izac219

Jud, C., Schmutz, I., Hampp, G., Oster, H., & Albrecht, U. (2005). A guideline for analyzing circadian wheel-running behavior in rodents under different lighting conditions. *Biol Proced Online*, *7*, 101-116. https://doi.org/10.1251/bpo109

Kaczmarek, J. L., Musaad, S. M., & Holscher, H. D. (2017). Time of day and eating behaviors are associated with the composition and function of the human gastrointestinal microbiota. *Am J Clin Nutr*, *106*(5), 1220-1231. https://doi.org/10.3945/ajcn.117.156380

Karpowicz, P., Zhang, Y., Hogenesch, J. B., Emery, P., & Perrimon, N. (2013). The circadian clock gates the intestinal stem cell regenerative state. *Cell Rep*, *3*(4), 996-1004. https://doi.org/10.1016/j.celrep.2013.03.016

Kars, M., Yang, L., Gregor, M. F., Mohammed, B. S., Pietka, T. A., Finck, B. N., Patterson, B. W., Horton, J. D., Mittendorfer, B., Hotamisligil, G. S., & Klein, S. (2010). Tauroursodeoxycholic Acid may improve liver and muscle but not adipose tissue insulin sensitivity in obese men and women. *Diabetes*, *59*(8), 1899-1905. https://doi.org/10.2337/db10-0308

Katakura, K., Lee, J., Rachmilewitz, D., Li, G., Eckmann, L., & Raz, E. (2005). Toll-like receptor 9-induced type I IFN protects mice from experimental colitis. *J Clin Invest*, *115*(3), 695-702. https://doi.org/10.1172/JCI22996

Kawai, M., Kinoshita, S., Yamazaki, M., Yamamoto, K., Rosen, C. J., Shimba, S., Ozono, K., & Michigami, T. (2019). Intestinal clock system regulates skeletal homeostasis. *Jci Insight*, *4*(5). https://doi.org/10.1172/jci.insight.121798

Kellow, J. E., Borody, T. J., Phillips, S. F., Tucker, R. L., & Haddad, A. C. (1986). Human interdigestive motility: variations in patterns from esophagus to colon. *Gastroenterology*, *91*(2), 386-395. https://doi.org/10.1016/0016-5085(86)90573-1

Kervezee, L., Kosmadopoulos, A., & Boivin, D. B. (2020). Metabolic and cardiovascular consequences of shift work: The role of circadian disruption and sleep disturbances. *Eur J Neurosci*, *51*(1), 396-412. https://doi.org/10.1111/ejn.14216

Kim, S. H., Cho, B. H., Kiyono, H., & Jang, Y. S. (2017). Microbiota-derived butyrate suppresses group 3 innate lymphoid cells in terminal ileal Peyer's patches. *Sci Rep*, *7*(1), 3980. https://doi.org/10.1038/s41598-017-02729-6

Ko, F. C., Jochum, S. B., Wilson, B. M., Adra, A., Patel, N., Lee, H., Wilber, S., Shaikh, M., Forsyth, C., Keshavarzian, A., Swanson, G. R., & Sumner, D. R. (2023). Colon epithelial cell-specific Bmal1 deletion impairs bone formation in mice. *Bone*, *168*, 116650. https://doi.org/10.1016/j.bone.2022.116650

Kohsaka, A., Laposky, A. D., Ramsey, K. M., Estrada, C., Joshu, C., Kobayashi, Y., Turek, F. W., & Bass, J. (2007). High-fat diet disrupts behavioral and molecular circadian rhythms in mice. *Cell Metab*, *6*(5), 414-421. https://doi.org/10.1016/j.cmet.2007.09.006

Kombala, C. J., Agrawal, N., Sveistyte, A., Karatsoreos, I. N., Van Dongen, H. P. A., & Brandvold, K. R. (2023). Profiling rhythmicity of bile salt hydrolase activity in the gut lumen with a rapid fluorescence assay. *Org Biomol Chem*, *21*(19), 4028-4038. https://doi.org/10.1039/d2ob02257e

Korn, T., Bettelli, E., Oukka, M., & Kuchroo, V. K. (2009). IL-17 and Th17 Cells. *Annu Rev Immunol*, *27*, 485-517. https://doi.org/10.1146/annurev.immunol.021908.132710

Koropatkin, N. M., Cameron, E. A., & Martens, E. C. (2012). How glycan metabolism shapes the human gut microbiota. *Nature Reviews Microbiology*, *10*(5), 323-335. https://doi.org/10.1038/nrmicro2746

Kuang, Z., Wang, Y. H., Li, Y., Ye, C. Q., Ruhn, K. A., Behrendt, C. L., Olson, E. N., & Hooper, L. V. (2019). The intestinal microbiota programs diurnal rhythms in host metabolism through histone deacetylase 3. *Science*, *365*(6460), 1428-+. https://doi.org/10.1126/science.aaw3134

Kumar, D., Wingate, D., & Ruckebusch, Y. (1986). Circadian variation in the propagation velocity of the migrating motor complex. *Gastroenterology*, *91*(4), 926-930. https://doi.org/10.1016/0016-5085(86)90696-7

Kumar, S. S., G., Li, M. K., C., & Tamura, K. (2018). MEGA X: molecular evolutionary genetics analysis across computing platforms. *Mol. Biol. Evol.*, *35*, 1547-1549.

Kyoko, O. O., Kono, H., Ishimaru, K., Miyake, K., Kubota, T., Ogawa, H., Okumura, K., Shibata, S., & Nakao, A. (2014). Expressions of tight junction proteins Occludin and Claudin-1 are under the circadian control in the mouse large intestine: implications in intestinal permeability and susceptibility to colitis. *PLoS One*, *9*(5), e98016. https://doi.org/10.1371/journal.pone.0098016

Labrecque, N., & Cermakian, N. (2015). Circadian Clocks in the Immune System. *Journal of Biological Rhythms*, *30*(4), 277-290. https://doi.org/10.1177/0748730415577723

Lagkouvardos, I., Fischer, S., Kumar, N., & Clavel, T. (2017). Rhea: a transparent and modular R pipeline for microbial profiling based on 16S rRNA gene amplicons. *PeerJ*, *5*, e2836. https://doi.org/10.7717/peerj.2836

Lagkouvardos, I., Lesker, T. R., Hitch, T. C. A., Galvez, E. J. C., Smit, N., Neuhaus, K., Wang, J., Baines, J. F., Abt, B., Stecher, B., Overmann, J., Strowig, T., & Clavel, T. (2019). Sequence and cultivation study of Muribaculaceae reveals novel species, host preference, and functional potential of this yet undescribed family. *Microbiome*, *7*(1), 28. https://doi.org/10.1186/s40168-019-0637-2

Lamia, K. A., Storch, K. F., & Weitz, C. J. (2008). Physiological significance of a peripheral tissue circadian clock. *Proceedings of the National Academy of Sciences of the United States of America*, *105*(39), 15172-15177. https://doi.org/10.1073/pnas.0806717105

Langmead, B., & Salzberg, S. L. (2012). Fast gapped-read alignment with Bowtie 2. *Nat Methods*, *9*(4), 357-359. https://doi.org/10.1038/nmeth.1923

Laposky, A., Easton, A., Dugovic, C., Walisser, J., Bradfield, C., & Turek, F. (2005). Deletion of the mammalian circadian clock gene BMAL1/Mop3 alters baseline sleep architecture and the response to sleep deprivation. *Sleep*, *28*(4), 395-409. https://doi.org/DOI 10.1093/sleep/28.4.395

Laurin, M., Everett, M. L., & Parker, W. (2011). The cecal appendix: one more immune component with a function disturbed by post-industrial culture. *Anat Rec (Hoboken)*, *294*(4), 567-579. https://doi.org/10.1002/ar.21357

Leblond, C. P., & Stevens, C. E. (1948). The constant renewal of the intestinal epithelium in the albino rat. *Anat Rec*, *100*(3), 357-377. https://doi.org/10.1002/ar.1091000306

Lee, C. C., Liang, F., Lee, I. C., Lu, T. H., Shan, Y. Y., Jeng, C. F., Zou, Y. F., Yu, H. T., & Chen Alen, S. K. (2022). External light-dark cycle shapes gut microbiota through intrinsically photosensitive retinal ganglion cells. *EMBO Rep*, *26*(6). https://doi.org/10.15252/embr.202052316

Lei, W., Ren, W., Ohmoto, M., Urban, J. F., Jr., Matsumoto, I., Margolskee, R. F., & Jiang, P. (2018). Activation of intestinal tuft cell-expressed Sucnr1 triggers type 2 immunity in the mouse small intestine. *Proc Natl Acad Sci U S A*, *115*(21), 5552-5557. https://doi.org/10.1073/pnas.1720758115

Leone, V., Gibbons, S. M., Martinez, K., Hutchison, A. L., Huang, E. Y., Cham, C. M., Pierre, J. F., Heneghan, A. F., Nadimpalli, A., Hubert, N., Zale, E., Wang, Y. W., Huang, Y., Theriault, B., Dinner, A. R., Musch, M. W., Kudsk, K. A., Prendergast, B. J., Gilbert, J. A., & Chang, E. B. (2015). Effects of Diurnal Variation of Gut Microbes and High-Fat Feeding on Host Circadian Clock Function and Metabolism. *Cell Host & Microbe*, *17*(5), 681-689. https://doi.org/10.1016/j.chom.2015.03.006

Levy, M., Kolodziejczyk, A. A., Thaiss, C. A., & Elinav, E. (2017). Dysbiosis and the immune system. *Nat Rev Immunol*, *17*(4), 219-232. https://doi.org/10.1038/nri.2017.7

Lewis, K., Lutgendorff, F., Phan, V., Soderholm, J. D., Sherman, P. M., & McKay, D. M. (2010). Enhanced Translocation of Bacteria Across Metabolically Stressed Epithelia is Reduced by

Butyrate. *Inflammatory Bowel Diseases*, *16*(7), 1138-1148. https://doi.org/10.1002/ibd.21177

Li, H., Handsaker, B., Wysoker, A., Fennell, T., Ruan, J., Homer, N., Marth, G., Abecasis, G., Durbin, R., & Genome Project Data Processing, S. (2009). The Sequence Alignment/Map format and SAMtools. *Bioinformatics*, *25*(16), 2078-2079. https://doi.org/10.1093/bioinformatics/btp352

Li, J., Zhao, F., Wang, Y., Chen, J., Tao, J., Tian, G., Wu, S., Liu, W., Cui, Q., Geng, B., Zhang, W., Weldon, R., Auguste, K., Yang, L., Liu, X., Chen, L., Yang, X., Zhu, B., & Cai, J. (2017). Gut microbiota dysbiosis contributes to the development of hypertension. *Microbiome*, *5*(1), 14. https://doi.org/10.1186/s40168-016-0222-x

Li, X., Chen, P., Zhang, Y., Shen, S., Li, K. (2023). Intervention time modified the effect of inulin on high-fat diet-induced obesity and gut microbial disorders. *Food Frontiers*, *4*(2), 933-944. https://doi.org/https://doi.org/10.1002/fft2.243

Liang, X., Bushman, F. D., & FitzGerald, G. A. (2015). Rhythmicity of the intestinal microbiota is regulated by gender and the host circadian clock. *Proceedings of the National Academy of Sciences of the United States of America*, *112*(33), 10479-10484. https://doi.org/10.1073/pnas.1501305112

Liao, Y., Smyth, G. K., & Shi, W. (2014). featureCounts: an efficient general purpose program for assigning sequence reads to genomic features. *Bioinformatics*, *30*(7), 923-930. https://doi.org/10.1093/bioinformatics/btt656

Lindberg, G., Iwarzon, M., & Hammarlund, B. (1996). 24-hour ambulatory electrogastrography in healthy volunteers. *Scand J Gastroenterol*, *31*(7), 658-664. https://doi.org/10.3109/00365529609009146

Liu, X., Ma, Y., Yu, Y., Zhang, W., Shi, J., Zhang, X., Dai, M., Wang, Y., Zhang, H., Zhang, J., Shen, J., Zhang, F., Song, M., & Wang, J. (2023). Gut microbial methionine impacts circadian clock gene expression and reactive oxygen species level in host gastrointestinal tract. *Protein Cell*, *14*(4), 309-313. https://doi.org/10.1093/procel/pwac021

Liu, X. J., Yu, R., Zhu, L. R., Hou, X. H., & Zou, K. F. (2017). Bidirectional Regulation of Circadian Disturbance and Inflammation in Inflammatory Bowel Disease. *Inflammatory Bowel Diseases*, *23*(10), 1741-1751. https://doi.org/10.1097/Mib.0000000000001265

Livak, K. J., & Schmittgen, T. D. (2001). Analysis of relative gene expression data using real-time quantitative PCR and the 2(-Delta Delta C(T)) Method. *Methods*, *25*(4), 402-408. https://doi.org/10.1006/meth.2001.1262

Love, M. I., Huber, W., & Anders, S. (2014). Moderated estimation of fold change and dispersion for RNA-seq data with DESeq2. *Genome Biol*, *15*(12), 550. https://doi.org/10.1186/s13059-014-0550-8

Luzader, D., Moutinho, T. J., Mitchell, P., Papin, J., Hong, C., & Moore, S. (2018). Gut Microbial Metabolites Modulate the Amplitude and Phase of Per2 and Bmal1 Circadian Rhythms in Intestinal Epithelial Cells and Organoids. *Gastroenterology*, *154*(6), S67-S67. <Go to ISI>://WOS:000450011100192

Ma, K., Xiao, R., Tseng, H. T., Shan, L., Fu, L., & Moore, D. D. (2009). Circadian dysregulation disrupts bile acid homeostasis. *PLoS One*, *4*(8), e6843. https://doi.org/10.1371/journal.pone.0006843

Madison, B. B., Dunbar, L., Qiao, X. T., Braunstein, K., Braunstein, E., & Gumucio, D. L. (2002). Cis elements of the villin gene control expression in restricted domains of the vertical (crypt) and horizontal (duodenum, cecum) axes of the intestine. *Journal of Biological Chemistry*, *277*(36), 33275-33283. https://doi.org/10.1074/jbc.M204935200

Makki, K., Brolin, H., Petersen, N., Henricsson, M., Christensen, D. P., Khan, M. T., Wahlstrom, A., Bergh, P. O., Tremaroli, V., Schoonjans, K., Marschall, H. U., & Backhed, F. (2023). 6alpha-hydroxylated bile acids mediate TGR5 signalling to improve glucose metabolism upon dietary fiber supplementation in mice. *Gut*, *72*(2), 314-324. https://doi.org/10.1136/gutjnl-2021-326541

Marcheva, B., Ramsey, K. M., Buhr, E. D., Kobayashi, Y., Su, H., Ko, C. H., Ivanova, G., Omura, C., Mo, S., Vitaterna, M. H., Lopez, J. P., Philipson, L. H., Bradfield, C. A., Crosby, S. D., JeBailey, L.,

Wang, X., Takahashi, J. S., & Bass, J. (2010). Disruption of the clock components CLOCK and BMAL1 leads to hypoinsulinaemia and diabetes. *Nature*, *466*(7306), 627-631. https://doi.org/10.1038/nature09253

Marques, F. Z., Nelson, E., Chu, P. Y., Horlock, D., Fiedler, A., Ziemann, M., Tan, J. K., Kuruppu, S., Rajapakse, N. W., El-Osta, A., Mackay, C. R., & Kaye, D. M. (2017). High-Fiber Diet and Acetate Supplementation Change the Gut Microbiota and Prevent the Development of Hypertension and Heart Failure in Hypertensive Mice. *Circulation*, *135*(10), 964-977. https://doi.org/10.1161/CIRCULATIONAHA.116.024545

Martchenko, A., Martchenko, S. E., Biancolin, A. D., & Brubaker, P. L. (2020). Circadian Rhythms and the Gastrointestinal Tract: Relationship to Metabolism and Gut Hormones. *Endocrinology*, *161*(12). https://doi.org/10.1210/endocr/bqaa167

Martchenko, A., Oh, R. H., Wheeler, S. E., Gurges, P., Chalmers, J. A., & Brubaker, P. L. (2018). Suppression of circadian secretion of glucagon-like peptide-1 by the saturated fatty acid, palmitate. *Acta Physiologica*, *222*(4). https://doi.org/ARTN e1300710.1111/apha.13007

Martchenko, S. E. (2021). L-cell Arntl is required for rhythmic glucagonlike peptide-1 secretion and maintenance of intestinal homeostasis. *Molecular Metabolism*. https://doi.org/https://doi.org/10.1016/j.molmet.2021.101340

Martchenko, S. E., Martchenko, A., Cox, B. J., Naismith, K., Waller, A., Gurges, P., Sweeney, M. E., Philpott, D. J., & Brubaker, P. L. (2020). Circadian GLP-1 Secretion in Mice Is Dependent on the Intestinal Microbiome for Maintenance of Diurnal Metabolic Homeostasis. *Diabetes*, *69*(12), 2589-2602. https://doi.org/10.2337/db20-0262

Matsu-Ura, T., Dovzhenok, A., Aihara, E., Rood, J., Le, H., Ren, Y., Rosselot, A. E., Zhang, T., Lee, C., Obrietan, K., Montrose, M. H., Lim, S., Moore, S. R., & Hong, C. I. (2016). Intercellular Coupling of the Cell Cycle and Circadian Clock in Adult Stem Cell Culture. *Mol Cell*, *64*(5), 900-912. https://doi.org/10.1016/j.molcel.2016.10.015

McCarthy, J. J., Andrews, J. L., McDearmon, E. L., Campbell, K. S., Barber, B. K., Miller, B. H., Walker, J. R., Hogenesch, J. B., Takahashi, J. S., & Esser, K. A. (2007). Identification of the circadian transcriptome in adult mouse skeletal muscle. *Physiol Genomics*, *31*(1), 86-95. https://doi.org/10.1152/physiolgenomics.00066.2007

McCormack, S. E., Shaham, O., McCarthy, M. A., Deik, A. A., Wang, T. J., Gerszten, R. E., Clish, C. B., Mootha, V. K., Grinspoon, S. K., & Fleischman, A. (2013). Circulating branched-chain amino acid concentrations are associated with obesity and future insulin resistance in children and adolescents. *Pediatr Obes*, *8*(1), 52-61. https://doi.org/10.1111/j.2047-6310.2012.00087.x

McDearmon, E. L., Patel, K. N., Ko, C. H., Walisser, J. A., Schook, A. C., Chong, J. L., Wilsbacher, L. D., Song, E. J., Hong, H. K., Bradfield, C. A., & Takahashi, J. S. (2006). Dissecting the functions of the mammalian clock protein BMAL1 by tissue-specific rescue in mice. *Science*, *314*(5803), 1304-1308. https://doi.org/10.1126/science.1132430

Menaker, M., & Wisner, S. (1983). Temperature-compensated circadian clock in the pineal of Anolis. *Proc Natl Acad Sci U S A*, *80*(19), 6119-6121. https://doi.org/10.1073/pnas.80.19.6119

Mistlberger, R. E., & Skene, D. J. (2004). Social influences on mammalian circadian rhythms: animal and human studies. *Biological Reviews*, *79*(3), 533-556. https://doi.org/10.1017/S1464793103006353

Mohawk, J. A., Green, C. B., & Takahashi, J. S. (2012). Central and peripheral circadian clocks in mammals. *Annu Rev Neurosci*, *35*, 445-462. https://doi.org/10.1146/annurev-neuro-060909-153128

Moore, R. Y. (1996). Entrainment pathways and the functional organization of the circadian system. *Prog Brain Res*, *111*, 103-119. https://doi.org/10.1016/s0079-6123(08)60403-3

Moore, S. R., Pruszka, J., Vallance, J., Aihara, E., Matsuura, T., Montrose, M. H., Shroyer, N. F., & Hong, C. I. (2014). Robust circadian rhythms in organoid cultures from PERIOD2::LUCIFERASE mouse small intestine. *Dis Model Mech*, *7*(9), 1123-1130. https://doi.org/10.1242/dmm.014399

Morrison, K. E., Jasarevic, E., Howard, C. D., & Bale, T. L. (2020). It's the fiber, not the fat: significant effects of dietary challenge on the gut microbiome. *Microbiome*, *8*(1), 15. https://doi.org/10.1186/s40168-020-0791-6

Mota, M. C., Silva, C. M., Balieiro, L. C. T., Fahmy, W. M., & Crispim, C. A. (2017). Social jetlag and metabolic control in non-communicable chronic diseases: a study addressing different obesity statuses. *Sci Rep*, *7*(1), 6358. https://doi.org/10.1038/s41598-017-06723-w

Mukherji, A., Kobiita, A., Ye, T., & Chambon, P. (2013). Homeostasis in intestinal epithelium is orchestrated by the circadian clock and microbiota cues transduced by TLRs. *Cell*, *153*(4), 812-827. https://doi.org/10.1016/j.cell.2013.04.020

Nauck, M. A., Niedereichholz, U., Ettler, R., Holst, J. J., Orskov, C., Ritzel, R., & Schmiegel, W. H. (1997). Glucagon-like peptide 1 inhibition of gastric emptying outweighs its insulinotropic effects in healthy humans. *Am J Physiol*, *273*(5), E981-988. https://doi.org/10.1152/ajpendo.1997.273.5.E981

Ni, Y., Yu, G., Chen, H., Deng, Y., Wells, P. M., Steves, C. J., Ju, F., & Fu, J. (2020). M2IA: a web server for microbiome and metabolome integrative analysis. *Bioinformatics*, *36*(11), 3493-3498. https://doi.org/10.1093/bioinformatics/btaa188

Niu, Y. (2023). *Targeting the intestinal circadian clock by meal timing ameliorates gastrointestinal inflammation*.

Oishi, K., Atsumi, G., Sugiyama, S., Kodomari, I., Kasamatsu, M., Machida, K., & Ishida, N. (2006). Disrupted fat absorption attenuates obesity induced by a high-fat diet in Clock mutant mice. *FEBS Lett*, *580*(1), 127-130. https://doi.org/10.1016/j.febslet.2005.11.063

Onuma, S., Kinoshita, S., Shimba, S., Ozono, K., Michigami, T., & Kawai, M. (2022). The Lack of Bmal1, a Core Clock Gene, in the Intestine Decreases Glucose Absorption in Mice. *Endocrinology*, *163*(9). https://doi.org/10.1210/endocr/bqac119

Ozcan, U., Yilmaz, E., Ozcan, L., Furuhashi, M., Vaillancourt, E., Smith, R. O., Gorgun, C. Z., & Hotamisligil, G. S. (2006). Chemical chaperones reduce ER stress and restore glucose homeostasis in a mouse model of type 2 diabetes. *Science*, *313*(5790), 1137-1140. https://doi.org/10.1126/science.1128294

P.J, T. (2008). Diet-Induced Obesity Is Linked to Marked but Reversible Alterations in the Mouse Distal Gut Microbiome. *Cell Host & Microbe*, *3*(4), 213-223.

Pagel, R., Bar, F., Schroder, T., Sunderhauf, A., Kunstner, A., Ibrahim, S. M., Autenrieth, S. E., Kalies, K., Konig, P., Tsang, A. H., Bettenworth, D., Divanovic, S., Lehnert, H., Fellermann, K., Oster, H., Derer, S., & Sina, C. (2017). Circadian rhythm disruption impairs tissue homeostasis and exacerbates chronic inflammation in the intestine. *FASEB J*, *31*(11), 4707-4719. https://doi.org/10.1096/fj.201700141RR

Pan, X., Bradfield, C. A., & Hussain, M. M. (2016). Global and hepatocyte-specific ablation of Bmal1 induces hyperlipidaemia and enhances atherosclerosis. *Nat Commun*, *7*, 13011. https://doi.org/10.1038/ncomms13011

Pan, X. Y., & Hussain, M. M. (2007). Diurnal transcriptional regulation of microsomal triglyceride transfer protein and plasma lipid levels. *Arteriosclerosis Thrombosis and Vascular Biology*, *27*(6), E123-E123. <Go to ISI>://WOS:000246714600497

Pan, X. Y., & Hussain, M. M. (2009). Clock is important for food and circadian regulation of macronutrient absorption in mice. *Journal of Lipid Research*, *50*(9), 1800-1813. https://doi.org/10.1194/jlr.M900085-JLR200

Pan, X. Y., Terada, T., Irie, M., Saito, H., & Inui, K. (2002). Diurnal rhythm of H+-peptide cotransporter in rat small intestine. *American Journal of Physiology-Gastrointestinal and Liver Physiology*, *283*(1), G57-G64. https://doi.org/10.1152/ajpgi.00545.2001

Pan, X. Y., Terada, T., Okuda, M., & Inui, K. I. (2004). The diurnal rhythm of the intestinal transporters SGLT1 and PEPT1 is regulated by the feeding conditions in rats. *Journal of Nutrition*, *134*(9), 2211-2215. https://doi.org/DOI 10.1093/jn/134.9.2211

Panda, S., Antoch, M. P., Miller, B. H., Su, A. I., Schook, A. B., Straume, M., Schultz, P. G., Kay, S. A., Takahashi, J. S., & Hogenesch, J. B. (2002). Coordinated transcription of key pathways in the

mouse by the circadian clock. *Cell*, *109*(3), 307-320. https://doi.org/10.1016/s0092-8674(02)00722-5

Pang, Z., Chong, J., Zhou, G., de Lima Morais, D. A., Chang, L., Barrette, M., Gauthier, C., Jacques, P. E., Li, S., & Xia, J. (2021). MetaboAnalyst 5.0: narrowing the gap between raw spectra and functional insights. *Nucleic Acids Res*, *49*(W1), W388-W396. https://doi.org/10.1093/nar/gkab382

Papantoniou, K., Devore, E. E., Massa, J., Strohmaier, S., Vetter, C., Yang, L., Shi, Y., Giovannucci, E., Speizer, F., & Schernhammer, E. S. (2018). Rotating night shift work and colorectal cancer risk in the nurses' health studies. *International Journal of Cancer*, *143*(11), 2709-2717. https://doi.org/10.1002/ijc.31655

Pardini, L., Kaeffer, B., Trubuil, A., Bourreille, A., & Galmiche, J. P. (2005). Human intestinal circadian clock: expression of clock genes in colonocytes lining the crypt. *Chronobiology International*, *22*(6), 951-961. https://doi.org/10.1080/07420520500395011

Parkar, S. G., Kalsbeek, A., & Cheeseman, J. F. (2019). Potential Role for the Gut Microbiota in Modulating Host Circadian Rhythms and Metabolic Health. *Microorganisms*, *7*(2). https://doi.org/10.3390/microorganisms7020041

Parker, K. D. (2018). Microbiome Composition in Both Wild-Type and Disease Model Mice Is Heavily Influenced by Mouse Facility. *Front. Microbiol.*, *9*.

Paschos, G. K., Ibrahim, S., Song, W. L., Kunieda, T., Grant, G., Reyes, T. M., Bradfield, C. A., Vaughan, C. H., Eiden, M., Masoodi, M., Griffin, J. L., Wang, F., Lawson, J. A., & Fitzgerald, G. A. (2012). Obesity in mice with adipocyte-specific deletion of clock component Arntl. *Nat Med*, *18*(12), 1768-1777. https://doi.org/10.1038/nm.2979

Paulose, J. K., Wright, J. M., Patel, A. G., & Cassone, V. M. (2016). Human Gut Bacteria Are Sensitive to Melatonin and Express Endogenous Circadian Rhythmicity. *PLoS One*, *11*(1), e0146643. https://doi.org/10.1371/journal.pone.0146643

Pelikan, A., Herzel, H., Kramer, A., & Ananthasubramaniam, B. (2022). Venn diagram analysis overestimates the extent of circadian rhythm reprogramming. *FEBS J*, *289*(21), 6605-6621. https://doi.org/10.1111/febs.16095

Pellizzon, M. A., & Ricci, M. R. (2018). The common use of improper control diets in diet-induced metabolic disease research confounds data interpretation: the fiber factor. *Nutr Metab (Lond)*, *15*, 3. https://doi.org/10.1186/s12986-018-0243-5

Pendergast, J. S., Branecky, K. L., Yang, W., Ellacott, K. L., Niswender, K. D., & Yamazaki, S. (2013). High-fat diet acutely affects circadian organisation and eating behavior. *Eur J Neurosci*, *37*(8), 1350-1356. https://doi.org/10.1111/ejn.12133

Peng, L. Y., Li, Z. R., Green, R. S., Holzman, I. R., & Lin, J. (2009). Butyrate Enhances the Intestinal Barrier by Facilitating Tight Junction Assembly via Activation of AMP-Activated Protein Kinase in Caco-2 Cell Monolayers. *Journal of Nutrition*, *139*(9), 1619-1625. https://doi.org/10.3945/jn.109.104638

Penny, H. A., Domingues, R. G., Krauss, M. Z., Melo-Gonzalez, F., Lawson, M. A. E., Dickson, S., Parkinson, J., Hurry, M., Purse, C., Jegham, E., Godinho-Silva, C., Rendas, M., Veiga-Fernandes, H., Bechtold, D. A., Grencis, R. K., Toellner, K. M., Waisman, A., Swann, J. R., Gibbs, J. E., & Hepworth, M. R. (2022). Rhythmicity of intestinal IgA responses confers oscillatory commensal microbiota mutualism. *Sci Immunol*, *7*(75), eabk2541. https://doi.org/10.1126/sciimmunol.abk2541

Pickel, L., Lee, J. H., Maughan, H., Shi, I. Q., Verma, N., Yeung, C., Guttman, D., & Sung, H. K. (2022). Circadian rhythms in metabolic organs and the microbiota during acute fasting in mice. *Physiol Rep*, *10*(14), e15393. https://doi.org/10.14814/phy2.15393

Pieper, R., Kroger, S., Richter, J. F., Wang, J., Martin, L., Bindelle, J., Htoo, J. K., von Smolinski, D., Vahjen, W., Zentek, J., & Van Kessel, A. G. (2012). Fermentable Fiber Ameliorates Fermentable Protein-Induced Changes in Microbial Ecology, but Not the Mucosa! Response, in the Colon of Piglets. *Journal of Nutrition*, *142*(4), 661-667. https://doi.org/10.3945/jn.111.156190

Pilgrim, C., Erb, W., & Maurer, W. (1963). Diurnal Fluctuations in the Numbers of DNA Synthesizing Nuclei in Various Mouse Tissues. *Nature*, *199*, 863. https://doi.org/10.1038/199863a0

Pittendrigh, C. S. (1954). On Temperature Independence in the Clock System Controlling Emergence Time in Drosophila. *Proc Natl Acad Sci U S A*, *40*(10), 1018-1029. https://doi.org/10.1073/pnas.40.10.1018

Polidarova, L., Sladek, M., Sotak, M., Pacha, J., & Sumova, A. (2011). Hepatic, Duodenal, and Colonic Circadian Clocks Differ in their Persistence under Conditions of Constant Light and in their Entrainment by Restricted Feeding. *Chronobiology International*, *28*(3), 204-215. https://doi.org/10.3109/07420528.2010.548615

Polidarova, L., Sotak, M., Sladek, M., Pacha, J., & Sumova, A. (2009). Temporal Gradient in the Clock Gene and Cell-Cycle Checkpoint Kinase Wee1 Expression along the Gut. *Chronobiology International*, *26*(4), 607-620. https://doi.org/Pii 91121205310.1080/07420520902924889

Pomaznoy, M., Ha, B., & Peters, B. (2018). GOnet: a tool for interactive Gene Ontology analysis. *BMC Bioinformatics*, *19*(1), 470. https://doi.org/10.1186/s12859-018-2533-3

Preuss, F., Tang, Y. M., Laposky, A. D., Arble, D., Keshavarzian, A., & Turek, F. W. (2008). Adverse effects of chronic circadian desynchronization in animals in a "challenging" environment. *American Journal of Physiology-Regulatory Integrative and Comparative Physiology*, *295*(6), R2034-R2040. https://doi.org/10.1152/ajpregu.00118.2008

Rao, S. S., Sadeghi, P., Beaty, J., Kavlock, R., & Ackerson, K. (2001). Ambulatory 24-h colonic manometry in healthy humans. *Am J Physiol Gastrointest Liver Physiol*, *280*(4), G629-639. https://doi.org/10.1152/ajpgi.2001.280.4.G629

Reiter, S., Dunkel, A., Metwaly, A., Panes, J., Salas, A., Haller, D., & Hofmann, T. (2021). Development of a Highly Sensitive Ultra-High-Performance Liquid Chromatography Coupled to Electrospray Ionization Tandem Mass Spectrometry Quantitation Method for Fecal Bile Acids and Application on Crohn's Disease Studies. *J Agric Food Chem*, *69*(17), 5238-5251. https://doi.org/10.1021/acs.jafc.1c00769

Reitmeier, S., Kiessling, S., Clavel, T., List, M., Almeida, E. L., Ghosh, T. S., Neuhaus, K., Grallert, H., Linseisen, J., Skurk, T., Brandl, B., Breuninger, T. A., Troll, M., Rathmann, W., Linkohr, B., Hauner, H., Laudes, M., Franke, A., Le Roy, C. I., . . . Haller, D. (2020). Arrhythmic Gut Microbiome Signatures Predict Risk of Type 2 Diabetes. *Cell Host & Microbe*, *28*(2), 258-272 e256. https://doi.org/10.1016/j.chom.2020.06.004

Rensing, L., & Ruoff, P. (2002). Temperature effect on entrainment, phase shifting, and amplitude of circadian clocks and its molecular bases. *Chronobiology International*, *19*(5), 807-864. https://doi.org/10.1081/Cbi-120014569

Repouskou, A., & Prombona, A. (2016). c-MYC targets the central oscillator gene Per1 and is regulated by the circadian clock at the post-transcriptional level. *Biochimica Et Biophysica Acta-Gene Regulatory Mechanisms*, *1859*(4), 541-552. https://doi.org/10.1016/j.bbagrm.2016.02.001

Rhoads, D. B., Rosenbaum, D. H., Unsal, H., Isselbacher, K. J., & Levitsky, L. L. (1998). Circadian periodicity of intestinal Na+/glucose cotransporter 1 mRNA levels is transcriptionally regulated. *Journal of Biological Chemistry*, *273*(16), 9510-9516. https://doi.org/DOI 10.1074/jbc.273.16.9510

Richter, C. P. (1922). *A behavioristic study of the activity of the rat*. Williams & Wilkins Company. http://hdl.loc.gov/loc.gdc/scd0001.00054921330

Rudic, R. D., McNamara, P., Curtis, A. M., Boston, R. C., Panda, S., Hogenesch, J. B., & Fitzgerald, G. A. (2004). BMAL1 and CLOCK, two essential components of the circadian clock, are involved in glucose homeostasis. *PLoS Biol*, *2*(11), e377. https://doi.org/10.1371/journal.pbio.0020377

Saito, H., Terada, T., Shimakura, J., Katsura, T., & Inui, K. (2008). Regulatory mechanism governing the diurnal rhythm of intestinal H+/peptide cotransporter 1 (PEPT1). *Am J Physiol Gastrointest Liver Physiol*, *295*(2), G395-402. https://doi.org/10.1152/ajpgi.90317.2008

Saito, M., Murakami, E., & Suda, M. (1976). Circadian rhythms in disaccharidases of rat small intestine and its relation to food intake. *Biochim Biophys Acta*, *421*(1), 177-179. https://doi.org/10.1016/0304-4165(76)90181-1

Salgado-Delgado, R., Angeles-Castellanos, M., Saderi, N., Buijs, R. M., & Escobar, C. (2010). Food intake during the normal activity phase prevents obesity and circadian desynchrony in a rat model of night work. *Endocrinology*, *151*(3), 1019-1029. https://doi.org/10.1210/en.2009-0864

Sanchez, H. N., Moroney, J. B., Gan, H. Q., Shen, T., Im, J. L., Li, T. B., Taylor, J. R., Zan, H., & Casali, P. (2020). B cell-intrinsic epigenetic modulation of antibody responses by dietary fiber-derived short-chain fatty acids. *Nature Communications*, *11*(1). https://doi.org/ARTN 6010.1038/s41467-019-13603-6

Scheer, F. A., Hilton, M. F., Mantzoros, C. S., & Shea, S. A. (2009). Adverse metabolic and cardiovascular consequences of circadian misalignment. *Proc Natl Acad Sci U S A*, *106*(11), 4453-4458. https://doi.org/10.1073/pnas.0808180106

Scheving, L. A. (2000). Biological clocks and the digestive system. *Gastroenterology*, *119*(2), 536-549. https://doi.org/DOI 10.1053/gast.2000.9305

Scheving, L. A., Yeh, Y. C., Tsai, T. H., & Scheving, L. E. (1980). Circadian phase-dependent stimulatory effects of epidermal growth factor on deoxyribonucleic acid synthesis in the duodenum, jejunum, ileum, caecum, colon, and rectum of the adult male mouse. *Endocrinology*, *106*(5), 1498-1503. https://doi.org/10.1210/endo-106-5-1498

Scheving, L. E., Scheving, L. A., Tsai, T. H., & Pauly, J. E. (1984). Effect of Fasting on Circadian Rhythmicity in Deoxyribonucleic-Acid Synthesis of Several Murine Tissues. *Journal of Nutrition*, *114*(11), 2160-2166. https://doi.org/DOI 10.1093/jn/114.11.2160

Schibler, U. (2003). Peripheral circadian oscillators in mammals: time and food. *J Biol Rhythms*.

Schroeder, B. O. (2019). Fight them or feed them: how the intestinal mucus layer manages the gut microbiota. *Gastroenterology Report*, *7*(1), 3-12. https://doi.org/10.1093/gastro/goy052

Schugar, R. C., Gliniak, C. M., Osborn, L. J., Massey, W., Sangwan, N., Horak, A., Banerjee, R., Orabi, D., Helsley, R. N., Brown, A. L., Burrows, A., Finney, C., Fung, K. K., Allen, F. M., Ferguson, D., Gromovsky, A. D., Neumann, C., Cook, K., McMillan, A., . . . Brown, J. M. (2022). Gut microbe-targeted choline trimethylamine lyase inhibition improves obesity via rewiring of host circadian rhythms. *Elife*, *11*. https://doi.org/10.7554/eLife.63998

Segers, A., & Depoortere, I. (2021). Circadian clocks in the digestive system. *Nat Rev Gastroenterol Hepatol*, *18*(4), 239-251. https://doi.org/10.1038/s41575-020-00401-5

Segers, A., Desmet, L., Sun, S., Verbeke, K., Tack, J., & Depoortere, I. (2020). Night-time feeding of Bmal1(-/-) mice restores SCFA rhythms and their effect on ghrelin. *Journal of Endocrinology*, *245*(1), 155-164. https://doi.org/10.1530/Joe-20-0011

Segers, A., Desmet, L., Thijs, T., Verbeke, K., Tack, J., & Depoortere, I. (2019). The circadian clock regulates the diurnal levels of microbial short-chain fatty acids and their rhythmic effects on colon contractility in mice. *Acta Physiologica*, *225*(3). https://doi.org/ARTN e1319310.1111/apha.13193

Shimba, S., Ishii, N., Ohta, Y., Ohno, T., Watabe, Y., Hayashi, M., Wada, T., Aoyagi, T., & Tezuka, M. (2005). Brain and muscle Arnt-like protein-1 (BMAL1), a component of the molecular clock, regulates adipogenesis. *Proc Natl Acad Sci U S A*, *102*(34), 12071-12076. https://doi.org/10.1073/pnas.0502383102

Silva, F. A., de Souza, E. L., Queiroga, R., Voss, G. B., Pintado, M. M. E., & Vasconcelos, M. A. S. (2022). A fibre and phenolic-rich flour from Isabel grape by-products with stimulatory effects on distinct probiotics and beneficial impacts on human colonic microbiota in vitro. *Lett Appl Microbiol*, *75*(2), 249-260. https://doi.org/10.1111/lam.13723

Sladek, M., Rybova, M., Jindrakova, Z., Zemanova, Z., Polidarova, L., Mrnka, L., O'Neill, J., Pacha, J., & Sumova, A. (2007). Insight into the circadian clock within rat colonic epithelial cells. *Gastroenterology*, *133*(4), 1240-1249. https://doi.org/10.1053/j.gastro.2007.05.053

Smith, C. A., Want, E. J., O'Maille, G., Abagyan, R., & Siuzdak, G. (2006). XCMS: processing mass spectrometry data for metabolite profiling using nonlinear peak alignment, matching, and identification. *Anal Chem*, *78*(3), 779-787. https://doi.org/10.1021/ac051437y

Smith, E. A., & Macfarlane, G. T. (1996). Enumeration of human colonic bacteria producing phenolic and indolic compounds: effects of pH, carbohydrate availability and retention time on dissimilatory aromatic amino acid metabolism. *J Appl Bacteriol*, *81*(3), 288-302. https://doi.org/10.1111/j.1365-2672.1996.tb04331.x

Soleimani, M., & Alborzi, P. (2011). The role of salt in the pathogenesis of fructose-induced hypertension. *Int J Nephrol*, *2011*, 392708. https://doi.org/10.4061/2011/392708

Song, X., Sun, X., Oh, S. F., Wu, M., Zhang, Y., Zheng, W., Geva-Zatorsky, N., Jupp, R., Mathis, D., Benoist, C., & Kasper, D. L. (2020). Microbial bile acid metabolites modulate gut RORgamma(+) regulatory T cell homeostasis. *Nature*, *577*(7790), 410-415. https://doi.org/10.1038/s41586-019-1865-0

Song, Z., Cai, Y., Lao, X., Wang, X., Lin, X., Cui, Y., Kalavagunta, P. K., Liao, J., Jin, L., Shang, J., & Li, J. (2019). Taxonomic profiling and populational patterns of bacterial bile salt hydrolase (BSH) genes based on worldwide human gut microbiome. *Microbiome*, *7*(1), 9. https://doi.org/10.1186/s40168-019-0628-3

Sookoian, S., Gemma, C., Gianotti, T. F., Burgueno, A., Castano, G., & Pirola, C. J. (2008). Genetic variants of Clock transcription factor are associated with individual susceptibility to obesity. *Am J Clin Nutr*, *87*(6), 1606-1615. https://doi.org/10.1093/ajcn/87.6.1606

Stephan, F. K., & Zucker, I. (1972). Circadian rhythms in drinking behavior and locomotor activity of rats are eliminated by hypothalamic lesions. *Proc Natl Acad Sci U S A*, *69*(6), 1583-1586. https://doi.org/10.1073/pnas.69.6.1583

Stevenson, N. R., Sitren, H. S., & Furuya, S. (1980). Circadian Rhythmicity in Several Small Intestinal Functions Is Independent of Use of the Intestine. *American Journal of Physiology*, *238*(3), G203-G207. https://doi.org/DOI 10.1152/ajpgi.1980.238.3.G203

Stokes, K., Cooke, A., Chang, H. N., Weaver, D. R., Breault, D. T., & Karpowicz, P. (2017). The Circadian Clock Gene BMAL1 Coordinates Intestinal Regeneration. *Cellular and Molecular Gastroenterology and Hepatology*, *4*(1), 95-114. https://doi.org/10.1016/j.jcmgh.2017.03.011

Stokes, K., Nunes, M., Trombley, C., Flores, D. E. F. L., Wu, G., Taleb, Z., Alkhateeb, A., Banskota, S., Harris, C., Love, O. P., Khan, W. I., Rueda, L., Hogenesch, J. B., & Karpowicz, P. (2021). The Circadian Clock Gene, Bmal1, Regulates Intestinal Stem Cell Signaling and Represses Tumor Initiation. *Cellular and Molecular Gastroenterology and Hepatology*, *12*(5), 1847-1872. https://doi.org/10.1016/j.jcmgh.2021.08.001

Stokkan, K. A., Yamazaki, S., Tei, H., Sakaki, Y., & Menaker, M. (2001). Entrainment of the circadian clock in the liver by feeding. *Science*, *291*(5503), 490-493. https://doi.org/10.1126/science.291.5503.490

Stunkard, A. J., & Allison, K. C. (2003). Two forms of disordered eating in obesity: binge eating and night eating. *Int J Obes Relat Metab Disord*, *27*(1), 1-12. https://doi.org/10.1038/sj.ijo.0802186

Subramanian, B., Gao, S., Lercher, M. J., Hu, S., & Chen, W. H. (2019). Evolview v3: a webserver for visualization, annotation, and management of phylogenetic trees. *Nucleic Acids Res*, *47*(W1), W270-W275. https://doi.org/10.1093/nar/gkz357

Summa, K. C., Voigt, R. M., Forsyth, C. B., Shaikh, M., Cavanaugh, K., Tang, Y., Vitaterna, M. H., Song, S., Turek, F. W., & Keshavarzian, A. (2013). Disruption of the Circadian Clock in Mice Increases Intestinal Permeability and Promotes Alcohol-Induced Hepatic Pathology and Inflammation. *PLoS One*, *8*(6), e67102. https://doi.org/10.1371/journal.pone.0067102

Sun, S., Hanzawa, F., Kim, D., Umeki, M., Nakajima, S., Sakai, K., Ikeda, S., Mochizuki, S., & Oda, H. (2019). Circadian rhythm-dependent induction of hepatic lipogenic gene expression in rats fed a high-sucrose diet. *Journal of Biological Chemistry*, *294*(42), 15206-15217. https://doi.org/10.1074/jbc.RA119.010328

Sun, S., Hanzawa, F., Umeki, M., Matsuyama, Y., Nishimura, N., Ikeda, S., Mochizuki, S., & Oda, H. (2019). Impacts of high-sucrose diet on circadian rhythms in the small intestine of rats. *Chronobiology International*, *36*(6), 826-837. https://doi.org/10.1080/07420528.2019.1592185

Tahara, Y., Yamazaki, M., Sukigara, H., Motohashi, H., Sasaki, H., Miyakawa, H., Haraguchi, A., Ikeda, Y., Fukuda, S., & Shibata, S. (2018). Gut Microbiota-Derived Short Chain Fatty Acids Induce Circadian Clock Entrainment in Mouse Peripheral Tissue. *Scientific Reports*, *8*. https://doi.org/ARTN 139510.1038/s41598-018-19836-7

Tailford, L. E., Crost, E. H., Kavanaugh, D., & Juge, N. (2015). Mucin glycan foraging in the human gut microbiome. *Front Genet*, *6*, 81. https://doi.org/10.3389/fgene.2015.00081

Takahashi, J. S. (2017). Transcriptional architecture of the mammalian circadian clock. *Nat Rev Genet*, *18*(3), 164-179. https://doi.org/10.1038/nrg.2016.150

Tavakkolizadeh, A., Ramsanahie, A., Levitsky, L. L., Zinner, M. J., Whang, E. E., Ashley, S. W., & Rhoads, D. B. (2005). Differential role of vagus nerve in maintaining diurnal gene expression rhythms in the proximal small intestine. *J Surg Res*, *129*(1), 73-78. https://doi.org/10.1016/j.jss.2005.05.023

Teng, F., Goc, J., Zhou, L., Chu, C., Shah, M. A., Eberl, G., & Sonnenberg, G. F. (2019). A circadian clock is essential for homeostasis of group 3 innate lymphoid cells in the gut. *Science Immunology*, *4*(40). https://doi.org/ARTN eaax1215

10.1126/sciimmunol.aax1215

Tennoune, N., Andriamihaja, M., & Blachier, F. (2022). Production of Indole and Indole-Related Compounds by the Intestinal Microbiota and Consequences for the Host: The Good, the Bad, and the Ugly. *Microorganisms*, *10*(5). https://doi.org/10.3390/microorganisms10050930

Thaiss, C. A., Levy, M., Korem, T., Dohnalova, L., Shapiro, H., Jaitin, D. A., David, E., Winter, D. R., Gury-BenAri, M., Tatirovsky, E., Tuganbaev, T., Federici, S., Zmora, N., Zeevi, D., Dori-Bachash, M., Pevsner-Fischer, M., Kartvelishvily, E., Brandis, A., Harmelin, A., . . . Elinav, E. (2016). Microbiota Diurnal Rhythmicity Programs Host Transcriptome Oscillations. *Cell*, *167*(6), 1495-1510 e1412. https://doi.org/10.1016/j.cell.2016.11.003

Thaiss, C. A., Zeevi, D., Levy, M., Zilberman-Schapira, G., Suez, J., Tengeler, A. C., Abramson, L., Katz, M. N., Korem, T., Zmora, N., Kuperman, Y., Biton, I., Gilad, S., Harmelin, A., Shapiro, H., Halpern, Z., Segal, E., & Elinav, E. (2014). Transkingdom control of microbiota diurnal oscillations promotes metabolic homeostasis. *Cell*, *159*(3), 514-529. https://doi.org/10.1016/j.cell.2014.09.048

Thu Le, H. P., Nakamura, Y., Oh-Oka, K., Ishimaru, K., Nakajima, S., & Nakao, A. (2017). The frequency of Th17 cells in the small intestine exhibits a day-night variation dependent on circadian clock activity. *Biochem Biophys Res Commun*, *490*(2), 290-295. https://doi.org/10.1016/j.bbrc.2017.06.038

Thuring, E. M., Hartmann, C., Schwietzer, Y. A., & Ebnet, K. (2023). TMIGD1: Emerging functions of a tumor supressor and adhesion receptor. *Oncogene*. https://doi.org/10.1038/s41388-023-02696-5

Thursby, E., & Juge, N. (2017). Introduction to the human gut microbiota. *Biochem J*, *474*(11), 1823-1836. https://doi.org/10.1042/BCJ20160510

Tourlousse, D. M., Yoshiike, S., Ohashi, A., Matsukura, S., Noda, N., & Sekiguchi, Y. (2017). Synthetic spike-in standards for high-throughput 16S rRNA gene amplicon sequencing. *Nucleic Acids Res*, *45*(4), e23. https://doi.org/10.1093/nar/gkw984

Tsugawa, H., Cajka, T., Kind, T., Ma, Y., Higgins, B., Ikeda, K., Kanazawa, M., VanderGheynst, J., Fiehn, O., & Arita, M. (2015). MS-DIAL: data-independent MS/MS deconvolution for comprehensive metabolome analysis. *Nat Methods*, *12*(6), 523-526. https://doi.org/10.1038/nmeth.3393

Tuganbaev, T., Mor, U., Bashiardes, S., Liwinski, T., Nobs, S. P., Leshem, A., Dori-Bachash, M., Thaiss, C. A., Pinker, E. Y., Ratiner, K., Adlung, L., Federici, S., Kleimeyer, C., Moresi, C., Yamada, T., Cohen, Y., Zhang, X., Massalha, H., Massasa, E., . . . Elinav, E. (2020). Diet Diurnally Regulates

Small Intestinal Microbiome-Epithelial-Immune Homeostasis and Enteritis. *Cell*, *182*(6), 1441-1459 e1421. https://doi.org/10.1016/j.cell.2020.08.027

Turek, F. W., Joshu, C., Kohsaka, A., Lin, E., Ivanova, G., McDearmon, E., Laposky, A., Losee-Olson, S., Easton, A., Jensen, D. R., Eckel, R. H., Takahashi, J. S., & Bass, J. (2005). Obesity and metabolic syndrome in circadian Clock mutant mice. *Science*, *308*(5724), 1043-1045. https://doi.org/10.1126/science.1108750

Vener, K. J., Szabo, S., & Moore, J. G. (1989). The effect of shift work on gastrointestinal (GI) function: a review. *Chronobiologia*, *16*(4), 421-439. https://www.ncbi.nlm.nih.gov/pubmed/2697524

Voigt, R. M., Forsyth, C. B., Green, S. J., Mutlu, E., Engen, P., Vitaterna, M. H., Turek, F. W., & Keshavarzian, A. (2014). Circadian disorganization alters intestinal microbiota. *PLoS One*, *9*(5), e97500. https://doi.org/10.1371/journal.pone.0097500

Voigt, R. M., Summa, K. C., Forsyth, C. B., Green, S. J., Engen, P., Naqib, A., Vitaterna, M. H., Turek, F. W., & Keshavarzian, A. (2016). The Circadian Clock Mutation Promotes Intestinal Dysbiosis. *Alcoholism-Clinical and Experimental Research*, *40*(2), 335-347. https://doi.org/10.1111/acer.12943

Wada, T., Ichihashi, Y., Suzuki, E., Kosuge, Y., Ishige, K., Uchiyama, T., Makishima, M., Nakao, R., Oishi, K., & Shimba, S. (2018). Deletion of Bmal1 Prevents Diet-Induced Ectopic Fat Accumulation by Controlling Oxidative Capacity in the Skeletal Muscle. *Int J Mol Sci*, *19*(9). https://doi.org/10.3390/ijms19092813

Wahlstrom, A., Sayin, S. I., Marschall, H. U., & Backhed, F. (2016). Intestinal Crosstalk between Bile Acids and Microbiota and Its Impact on Host Metabolism. *Cell Metabolism*, *24*(1), 41-50. https://doi.org/10.1016/j.cmet.2016.05.005

Walker, W. H., 2nd, Walton, J. C., DeVries, A. C., & Nelson, R. J. (2020). Circadian rhythm disruption and mental health. *Transl Psychiatry*, *10*(1), 28. https://doi.org/10.1038/s41398-020-0694-0

Wang, B. (2020). A High-Fat Diet Increases Gut Microbiota Biodiversity and Energy Expenditure Due to Nutrient Difference. *Nutrients 12*(10).

Wang, Q., Robinette, M. L., Billon, C., Collins, P. L., Bando, J. K., Fachi, J. L., Secca, C., Porter, S. I., Saini, A., Gilfillan, S., Solt, L. A., Musiek, E. S., Oltz, E. M., Burris, T. P., & Colonna, M. (2019). Circadian rhythm-dependent and circadian rhythm-independent impacts of the molecular clock on type 3 innate lymphoid cells. *Sci Immunol*, *4*(40). https://doi.org/10.1126/sciimmunol.aay7501

Wang, Y., Osterbur, D. L., Megaw, P. L., Tosini, G., Fukuhara, C., Green, C. B., & Besharse, J. C. (2001). Rhythmic expression of Nocturnin mRNA in multiple tissues of the mouse. *BMC Dev Biol*, *1*, 9. https://doi.org/10.1186/1471-213x-1-9

Wang, Y. H., Kuang, Z., Yu, X. F., Ruhn, K. A., Kubo, M., & Hooper, L. V. (2017). The intestinal microbiota regulates body composition through NFIL3 and the circadian clock. *Science*, *357*(6354), 913-+. https://doi.org/10.1126/science.aan0677

Warden, C. H., & Fisler, J. S. (2008). Comparisons of diets used in animal models of high-fat feeding. *Cell Metab*, *7*(4), 277. https://doi.org/10.1016/j.cmet.2008.03.014

Wei, T. (2021). *R package 'corrplot': VIsualization of a correlation matrix*. https://github.com/taiyun/corrplot

Weiss, A. S., Burrichter, A. G., Durai Raj, A. C., von Strempel, A., Meng, C., Kleigrewe, K., Munch, P. C., Rossler, L., Huber, C., Eisenreich, W., Jochum, L. M., Going, S., Jung, K., Lincetto, C., Hubner, J., Marinos, G., Zimmermann, J., Kaleta, C., Sanchez, A., & Stecher, B. (2022). In vitro interaction network of a synthetic gut bacterial community. *ISME J*, *16*(4), 1095-1109. https://doi.org/10.1038/s41396-021-01153-z

Welsh, D. K., Yoo, S. H., Liu, A. C., Takahashi, J. S., & Kay, S. A. (2004). Bioluminescence imaging of individual fibroblasts reveals persistent, independently phased circadian rhythms of clock gene expression. *Curr Biol*, *14*(24), 2289-2295. https://doi.org/10.1016/j.cub.2004.11.057

Wever, R. (1975). The circadian multi-oscillatory system of man. *Int J Chronobiol*, *3*(1), 19-55. https://www.ncbi.nlm.nih.gov/pubmed/1193771

Wishart, D. S., Tzur, D., Knox, C., Eisner, R., Guo, A. C., Young, N., Cheng, D., Jewell, K., Arndt, D., Sawhney, S., Fung, C., Nikolai, L., Lewis, M., Coutouly, M. A., Forsythe, I., Tang, P., Shrivastava, S., Jeroncic, K., Stothard, P., . . . Querengesser, L. (2007). HMDB: the Human Metabolome Database. *Nucleic Acids Res*, *35*(Database issue), D521-526. https://doi.org/10.1093/nar/gkl923

Woon, P. Y., Kaisaki, P. J., Braganca, J., Bihoreau, M. T., Levy, J. C., Farrall, M., & Gauguier, D. (2007). Aryl hydrocarbon receptor nuclear translocator-like (BMAL1) is associated with susceptibility to hypertension and type 2 diabetes. *Proc Natl Acad Sci U S A*, *104*(36), 14412-14417. https://doi.org/10.1073/pnas.0703247104

Wu, G., Anafi, R. C., Hughes, M. E., Kornacker, K., & Hogenesch, J. B. (2016). MetaCycle: an integrated R package to evaluate periodicity in large scale data. *Bioinformatics*, *32*(21), 3351-3353. https://doi.org/10.1093/bioinformatics/btw405

Wu, G., Tang, W., He, Y., Hu, J., Gong, S., He, Z., Wei, G., Lv, L., Jiang, Y., Zhou, H., & Chen, P. (2018). Light exposure influences the diurnal oscillation of gut microbiota in mice. *Biochem Biophys Res Commun*, *501*(1), 16-23. https://doi.org/10.1016/j.bbrc.2018.04.095

Xia, Y., Ding, X., Wang, S., & Ren, W. (2023). Circadian orchestration of host and gut microbiota in infection. *Biol Rev Camb Philos Soc*, *98*(1), 115-131. https://doi.org/10.1111/brv.12898

Yamaguchi, M., Kotani, K., Tsuzaki, K., Takagi, A., Motokubota, N., Komai, N., Sakane, N., Moritani, T., & Nagai, N. (2015). Circadian rhythm genes CLOCK and PER3 polymorphisms and morning gastric motility in humans. *PLoS One*, *10*(3), e0120009. https://doi.org/10.1371/journal.pone.0120009

Yamamoto, T., Nakahata, Y., Soma, H., Akashi, M., Mamine, T., & Takumi, T. (2004). Transcriptional oscillation of canonical clock genes in mouse peripheral tissues. *BMC Mol Biol*, *5*, 18. https://doi.org/10.1186/1471-2199-5-18

Yang, S., Liu, A., Weidenhammer, A., Cooksey, R. C., McClain, D., Kim, M. K., Aguilera, G., Abel, E. D., & Chung, J. H. (2009). The role of mPer2 clock gene in glucocorticoid and feeding rhythms. *Endocrinology*, *150*(5), 2153-2160. https://doi.org/10.1210/en.2008-0705

Yassour, M., Lim, M. Y., Yun, H. S., Tickle, T. L., Sung, J., Song, Y. M., Lee, K., Franzosa, E. A., Morgan, X. C., Gevers, D., Lander, E. S., Xavier, R. J., Birren, B. W., Ko, G., & Huttenhower, C. (2016). Sub-clinical detection of gut microbial biomarkers of obesity and type 2 diabetes. *Genome Med*, *8*(1), 17. https://doi.org/10.1186/s13073-016-0271-6

Yin, J., Li, Y., Han, H., Ma, J., Liu, G., Wu, X., Huang, X., Fang, R., Baba, K., Bin, P., Zhu, G., Ren, W., Tan, B., Tosini, G., He, X., Li, T., & Yin, Y. (2020). Administration of Exogenous Melatonin Improves the Diurnal Rhythms of the Gut Microbiota in Mice Fed a High-Fat Diet. *mSystems*, *5*(3). https://doi.org/10.1128/mSystems.00002-20

Yntema, T., Koonen, D. P. Y., & Kuipers, F. (2023). Emerging Roles of Gut Microbial Modulation of Bile Acid Composition in the Etiology of Cardiovascular Diseases. *Nutrients*, *15*(8). https://doi.org/10.3390/nu15081850

Yoo, S. H., Yamazaki, S., Lowrey, P. L., Shimomura, K., Ko, C. H., Buhr, E. D., Siepka, S. M., Hong, H. K., Oh, W. J., Yoo, O. J., Menaker, M., & Takahashi, J. S. (2004). PERIOD2::LUCIFERASE real-time reporting of circadian dynamics reveals persistent circadian oscillations in mouse peripheral tissues. *Proc Natl Acad Sci U S A*, *101*(15), 5339-5346. https://doi.org/10.1073/pnas.0308709101

Yoon, S. H., Ha, S. M., Kwon, S., Lim, J., Kim, Y., Seo, H., & Chun, J. (2017). Introducing EzBioCloud: a taxonomically united database of 16S rRNA gene sequences and whole-genome assemblies. *Int J Syst Evol Microbiol*, *67*(5), 1613-1617. https://doi.org/10.1099/ijsem.0.001755

Yoshida, D., Aoki, N., Tanaka, M., Aoyama, S., & Shibata, S. (2015). The circadian clock controls fluctuations of colonic cell proliferation during the light/dark cycle via feeding behavior in mice. *Chronobiology International*, *32*(8), 1145-1155. https://doi.org/10.3109/07420528.2015.1065415

Yoshimoto, S., Loo, T. M., Atarashi, K., Kanda, H., Sato, S., Oyadomari, S., Iwakura, Y., Oshima, K., Morita, H., Hattori, M., Honda, K., Ishikawa, Y., Hara, E., & Ohtani, N. (2013). Obesity-induced

gut microbial metabolite promotes liver cancer through senescence secretome. *Nature*, *499*(7456), 97-+. https://doi.org/10.1038/nature12347

Young, B. (2006). *Wheater's functional histology : a text and colour atlas* (5th ed.). Churchill Livingstone/Elsevier. Table of contents only http://www.loc.gov/catdir/toc/fy0614/2006280114.html

Yu, F., Wang, Z., Zhang, T., Chen, X., Xu, H., Wang, F., Guo, L., Chen, M., Liu, K., & Wu, B. (2021). Deficiency of intestinal Bmal1 prevents obesity induced by high-fat feeding. *Nat Commun*, *12*(1), 5323. https://doi.org/10.1038/s41467-021-25674-5

Yu, F., Zhang, T., Zhou, C., Xu, H., Guo, L., Chen, M., & Wu, B. (2019). The Circadian Clock Gene Bmal1 Controls Intestinal Exporter MRP2 and Drug Disposition. *Theranostics*, *9*(10), 2754-2767. https://doi.org/10.7150/thno.33395

Yu, X. F., Rollins, D., Ruhn, K. A., Stubblefield, J. J., Green, C. B., Kashiwada, M., Rothman, P. B., Takahashi, J. S., & Hooper, L. V. (2013). T(H)17 Cell Differentiation Is Regulated by the Circadian Clock. *Science*, *342*(6159), 727-730. https://doi.org/10.1126/science.1243884

Zarrinpar, A., Chaix, A., Yooseph, S., & Panda, S. (2014). Diet and feeding pattern affect the diurnal dynamics of the gut microbiome. *Cell Metab*, *20*(6), 1006-1017. https://doi.org/10.1016/j.cmet.2014.11.008

Zbidi, S., Zinoubi, B., Vandewalle, H., & Driss, T. (2016). Diurnal Rhythm of Muscular Strength Depends on Temporal Specificity of Self-Resistance Training. *J Strength Cond Res*, *30*(3), 717-724. https://doi.org/10.1519/JSC.0000000000001144

Zhang, S., Dai, M., Wang, X., Jiang, S. H., Hu, L. P., Zhang, X. L., & Zhang, Z. G. (2020). Signalling entrains the peripheral circadian clock. *Cell Signal*, *69*, 109433. https://doi.org/10.1016/j.cellsig.2019.109433

Zhang, Y. K. J., Guo, G. L., & Klaassen, C. D. (2011). Diurnal variations of mouse plasma and hepatic bile acid concentrations as well as expression of biosynthetic enzymes and transporters. *PLoS One*, *6*(1).

Zheng, D. P., Liwinski, T., & Elinav, E. (2020). Interaction between microbiota and immunity in health and disease. *Cell Research*, *30*(6), 492-506. https://doi.org/10.1038/s41422-020-0332-7

Zheng, D. P., Ratiner, K., & Elinav, E. (2020). Circadian Influences of Diet on the Microbiome and Immunity. *Trends in Immunology*, *41*(6), 512-530. https://doi.org/10.1016/j.it.2020.04.005

Zheng, X. J., Chen, T. L., Zhao, A. H., Ning, Z. C., Kuang, J. L., Wang, S. L., You, Y. J., Bao, Y. Q., Ma, X. J., Yu, H. Y., Zhou, J., Jiang, M., Li, M. C., Wang, J. Y., Ma, X. H., Zhou, S. P., Li, Y. T., Ge, K., Rajani, C., . . . Jia, W. (2021). Hyocholic acid species as novel biomarkers for metabolic disorders. *Nature Communications*, *12*(1). https://doi.org/ARTN 148710.1038/s41467-021-21744-w

Acknowledgements

First, I would like to express my gratitude to my supervisor, Silke Kiessling, for her support throughout my PhD journey. Silke, you gave me the trust to develop my own research project from scratch, and even in the face of numerous disappointing and non-significant experiments, you remained steadfast in your belief in the project and me. The knowledge and principles of chronobiology that I have acquired through you will undoubtedly shape my future as a postdoctoral researcher. I would also like to thank Prof. Dirk Haller, my second supervisor, your contributions during our lab seminars have provided valuable perspectives on the microbial aspects of my project.

Furthermore, I feel incredibly fortunate to have been part of such a great junior chronobiology research group, including Baraa, Yunhui, and Elizaveta. Being part of a small team has resulted in a great friendship with all of you! Without you, I would have had way less 'fun' doing night experiments, collecting 24-h profiles of mice poo. and so on!

I want to express my thanks to the master students who worked alongside me during my PhD - Živa, Johanna, Robert, and Guojing. Your assistance and collaboration have been invaluable, and I have enjoyed working with each of you. In addition, my appreciation goes out to the entire lab team, and in particular Nico, for teaching me how to make 5M solutions and for sharing several after-work beers. I would also like to extend my thanks to the past and present PhD members of the Haller lab, including Janine, Miriam, Lisi, Sandra, Adam, Mo, Kaelin and Stephanie. You made the office and Freising a great environment to be in!

Of course, no PhD journey would have been completed without some stress-relieving activities, and for that, I especially want to thank my friends outside of the lab in both Germany and the Netherlands. Your friendships gave me the perfect opportunities to not work all the time but instead eat great food, travel, talk, drink, climb, hike, or dance!

Felix, I want to express my sincere appreciation for your constant support and willingness to (pretend to) listen, even when I rambled on about topics such as poo, some kind of clocks, mouse sacrifices, and frustrations over non-significant data. Your presence and understanding made coming home after a challenging day all the more comforting.

Lastly, I want to express my deepest love and gratitude to my sister and my parents. Your unwavering support and presence throughout this journey have meant the world to me. It was not easy being away from home, especially during the difficult past year. Although I will remain in Freising for a while longer, I will make sure we will see each other a lot, in good health, in the coming years!

Publications and Presentations

Manuscripts

Peer reviewed

M. Heddes*, B. Altaha*, Y. Niu, S. Reitmeier, K. Kleigrewe, D. Haller and S. Kiessling. *The intestinal clock drives the microbiome to maintain gastrointestinal homeostasis*. Nature Communications. https://doi.org/10.1101/2021.10.18.464061.

* Authors contributed equally to this work.

B. Altaha, M. Heddes, V. Pilorz, Y. Niu, E. Gorbunova, M. Gigl, K. Kleigrewe, H. Oster, D. Haller, S. Kiessling. *Genetic and environmental circadian disruption induce weight gain through changes in the gut microbiome*. Molecular Metabolism. https://doi.org/10.1016/j.molmet.2022.101628.

Manuscript submitted for publication

M. Heddes, Y. Niu, B. Altaha, K. Kleigrewe, C. Meng, D. Haller and S. Kiessling. *The intestinal clock controls host's metabolic response to diet by driving intestinal metabolic functions and the fiber-dependent microbiome.* bioRxiv. https://doi.org/10.1101/2023.04.11.534733

Y. Niu, M. Heddes, B. Altaha, M. Birkner, K. Kleigrewe, C. Meng, D. Haller, S. Kiessling. *Targeting the intestinal circadian clock by meal timing ameliorates gastrointestinal inflammation.* bioRxiv. https://doi.org/10.1101/2023.01.24.525433.

Presentations

2022

Oral- & poster presentation

The Society for Research on Biological Rhythms (SRBR) (Florida, America).

The Intestinal Circadian Clock Drives Microbial Rhythmicity to Maintain Gastrointestinal Homeostasis

Marjolein Heddes, Baraa Altaha, Yunhui Niu, Sandra Reitmeier, Karin Kleigrewe, Dirk Haller, Silke Kiessling.

2021

Oral- & poster presentation

International Conference on Chronobiology (ICC2022) (Virtual).

The intestinal Circadian Clock as the Main Driver of Microbial Rhythmicity

Marjolein Heddes, Baraa Altaha, Yunhui Niu, Sandra Reitmeier, Karin Kleigrewe, Dirk Haller, Silke Kiessling.

2019

Oral- & poster presentation

Chronobiology Training School (Munich, Germany).

Unravelling the Role of the Intestinal Clock in the Interplay between Host Metabolism and the Microbiome

Marjolein Heddes, Baraa Altaha & Silke Kiessling.